Mechanistic basis of shear-dependent cGMP signaling in platelets

Dissertation

der Mathematisch-Naturwissenschaftlichen Fakultät

der Eberhard Karls Universität Tübingen

zur Erlangung des Grades eines

Doktors der Naturwissenschaften

(Dr. rer. nat.)

vorgelegt von

Frank Regler

aus Ingolstadt

Tübingen

2021

Gedruckt mit Genehmigung der Mathematisch-Naturwissenschaftlichen Fakultät der Eberhard Karls Universität Tübingen.

Tag der mündlichen Qualifikation:	22.12.2021
Dekan:	Prof. Dr. Thilo Stehle
1. Berichterstatter:	Prof. Dr. Robert Feil
2. Berichterstatter:	PD Dr. Hannes Schmidt

Table of contents

Zusammenfassung

Cyclisches Guanosin 3'-5'-Monophosphat (cGMP) ist ein intrazellulärer sekundärer Botenstoff, der in zahlreichen physiologischen Prozessen eine wesentliche Rolle spielt. Der cGMP Signalweg dient schon seit mehr als einem Jahrhundert als Ziel von medikamentöser Intervention. Seine enorme Wichtigkeit macht man sich v.a. bei vasokonstriktiven Erkrankungen zu Nutze, da eine Erhöhung von cGMP zu einer Relaxation von Glattmuskelzellen führt. Zu den prominentesten cGMP-modulierenden Pharmaka gehören Sildenafil (Viagra®) für die Behandlung von erektiler Dysfunktion und Riociguat (Adempas®), welches bei pulmonaler Hypertension eingesetzt wird. In Säugetieren sind zwei Typen von Guanylylcyclasen für die Generierung von cGMP verantwortlich: Eine membrangebundene partikuläre Guanylylcyclase (pGC), welche u.a. von natriuretischen Peptiden aktiviert wird, und eine für Stickstoffmonoxid (NO) sensitive Guanylylcyclase (NO-GC). Beide Guanylylcyclasen katalysieren die Umwandlung von 5'GTP zu cGMP, welches an mehrere Effektoren binden und diese aktivieren kann. Häufig wird hierbei die cGMP-abhängige Proteinkinase Typ I (cGKI) aktiviert. Diese vermittelt schlussendlich viele der physiologischen Effekte des cGMP-Signalwegs. In Blutplättchen (Thrombozyten) spielt der NO/NO-GC/cGMP/cGKI-Signalweg eine bedeutende Rolle zur Erhaltung der Hämostase. Im kardiovaskulären System wird von Endothelzellen ständig NO freigesetzt, welches in Blutplättchen die Generierung von cGMP durch die NO-GC und Aktivierung der cGKI zur Folge hat. Dies führt zu einer Inhibierung der Plättchenaggregation und somit wird eine überschießende Aktivierung der Plättchen verhindert und das Thromboserisiko gesenkt.

Unsere Arbeitsgruppe hat bereits gezeigt, dass die NO-induzierte Bildung von cGMP in Blutplättchen von Scherkräften abhängig ist („mechano-cGMP"). Im ersten Teil dieser Arbeit galt es, die mechanistische Basis von mechano-cGMP näher aufzuklären und den Mechanorezeptor zu identifizieren, der die physikalische Scherkraft in ein biochemisches cGMP-Signal umwandelt. Hierfür wurden klassische biochemische Methoden wie Zellfraktionierung, Western Blots, Co-Immunopräzipitationen und Massenspektrometrie mit modernen live-cell-imaging Methoden kombiniert, die es erlauben cGMP-Veränderungen in Echtzeit zu beobachten. Wir nahmen zunächst an, dass sich ein cGMP-Signalkomplex an der Innenseite der Plasmamembran der Blutplättchen befindet, auf den Scherkräfte

einwirken. Um dies zu verifizieren, wurden humane Blutplättchen in Cytosol- und Membranfraktion getrennt. In letzterer wurde nicht nur die Anwesenheit von cGKI und NO-GC detektiert, sondern auch eine physikalische Interaktion dieser beiden Proteine mittels Co-Immunopräzipitation nachgewiesen. Um weitere Komponenten des cGMP-Signalkomplexes, v.a. potenzielle Mechanorezeptoren, zu identifizieren, wurden die Co-Immunopräzipitate der Membranfraktionen mithilfe der Massenspektrometrie analysiert. Hierbei wurden mehrere Integrine nachgewiesen. Integrine spielen eine wichtige Rolle bei der Signalweiterleitung zwischen Zellen und deren Umgebung und wurden auch schon als Mechanorezeptoren beschrieben. Anschließend wurden die Blutplättchen auf einen möglichen funktionellen Zusammenhang zwischen Integrinen und dem cGMP-Signalweg untersucht. Mithilfe von transgenen Mäusen, die einen Förster-Resonanzenergietransfer (FRET)-basierten cGMP-Sensor (cGi500) exprimieren, konnte man beobachten, dass eine Inhibierung der Integrine α_{IIb}, β_3 und β_1 zu einer Verminderung des mechanosensitiven cGMP-Signals führt. Insgesamt weisen diese Daten auf einen membran-assoziierten cGMP-Signalkomplex in Blutplättchen hin, in dem sich sowohl die NO-GC, als auch die cGKI befinden. Zudem fungieren Integrine in diesem Signalkomplex mutmaßlich als Mechanosensor und führen als Antwort auf NO und Scherkräfte zur Bildung von cGMP.

Im zweiten Teil dieser Arbeit wurde auf die pharmakologische Relevanz des mechano-cGMP-Signalwegs in Blutplättchen eingegangen. Hierzu wurde *in vivo* im sog. Cremaster-Modell der Maus die Wirkung des NO-GC-Stimulators Riociguat auf die Thrombusentwicklung untersucht. Es wurde beobachtet, dass unter Gabe von Riociguat Thromben zwar initial ähnlich wuchsen wie unter Kontrollbedingungen, sich jedoch schneller wieder auflösten. Dieser antithrombotische Effekt eines cGMP-erhöhenden Pharmakons könnte einen Vorteil gegenüber den heutzutage gängigen Antikoagulanzien mit sich bringen: Das initiale Wachstum des Thrombus nach einer Gefäßverletzung wird aufgrund geringer Scherkräfte in dieser Phase nicht inhibiert. Sobald jedoch der Thrombus wächst und höhere Scherkräfte auf ihn einwirken, bremst der cGMP-Signalweg das übermäßige Wachstum des Thrombus. Zukünftig könnte der mechano-cGMP-Signalweg bei der Behandlung von kardiovaskulären Erkrankungen wichtig werden, da durch seine pharmakologische Aktivierung sowohl das Blutungs- als auch das Thromboserisiko minimiert werden könnte.

Summary

Cyclic guanosine 3’-5’-monophosphate (cGMP) is an intracellular second messenger which plays a pivotal role in many physiological processes. Drugs elevating cGMP levels have risen to prominence during the past century. The importance of the cGMP signaling pathway as a target for medical interventions is highlighted in the treatment of vasoconstrictive diseases, as increasing cGMP levels leads to relaxation of vascular smooth muscle cells. The most well-known cGMP drugs include Sildenafil (Viagra®) and Riociguat (Adempas®) which are used to treat erectile dysfunction and alleviate pulmonary hypertension, respectively. In mammals, two types of guanylyl cyclases are responsible for the generation of cGMP: A membrane-bound particulate guanylyl cyclase (pGC) which is activated by, e.g., natriuretic peptides, and a nitric oxide (NO)-sensitive guanylyl cyclase (NO-GC). Both types of cyclases transform 5’-GTP to cGMP, which leads to activation of different downstream effectors. Many cGMP-induced physiological effects are mediated by the cGMP-dependent protein kinase type I (cGKI). In platelets (thrombocytes), the NO/NO-GC/cGMP/cGKI signaling pathway plays an important role in hemostasis. In the cardiovascular system, NO is continuously released from endothelial cells into the circulation, leading to activation of NO-GC in platelets, generation of cGMP, activation of cGKI, and inhibition of platelet aggregation. This prevents an excessive activation of platelets and reduces the risk of developing dangerous thrombi.

In a previous study from our working group, it was shown that NO-induced generation of cGMP in platelets is shear-dependent (“mechano-cGMP”). In the first part of this work, we sought to gain insights into the mechanistic basis of mechano-cGMP and identify the mechanoreceptor which converts shear stress, a physical force, into a biochemical cGMP signal. We used classical biochemical methods such as cell fractionation, Western blotting, co-immunoprecipitation, and mass spectrometry, combined with state-of-the-art live-cell imaging approaches that allow for the observation of cGMP signals in real time. We hypothesized that a cGMP signaling complex is present at the inner leaflet of the platelet plasma membrane. To test this hypothesis, we fractionated human platelets into cytosolic and membrane fractions. In the latter, we detected the presence of both the NO-GC and cGKI. Furthermore, we showed a physical interaction between these two proteins at the platelet membrane via co-immunoprecipitation. To identify more components of the

cGMP signalosome, especially potential mechanoreceptors, we analyzed the co-immunoprecipitates of membrane fractions via mass spectrometry and detected several integrins. Integrins are important relays between cells and their environment and have also been described as mechanoreceptors. We therefore tested several integrins for a functional connection to shear-dependent cGMP signaling in platelets. Using platelets from transgenic mice expressing a Förster resonance energy transfer (FRET)-based cGMP biosensor (cGi500), we discovered that inhibition of integrin α_{IIb}, β_3 or β_1 attenuated the mechanosensitive cGMP response. In sum, we have identified a membrane-associated cGMP signaling complex containing the NO-GC and cGKI, with integrins serving as mechanotransducers for shear stress. In the presence of NO and mechanical force, the cGMP signalosome generates cGMP leading to the inhibition of platelet aggregation.

In the second part of this work, we explored the pharmacological relevance of mechano-cGMP in platelets. Using the murine *in vivo* cremaster model, we studied whether the NO-GC stimulator Riociguat affects thrombus development. While Riociguat treatment had no significant effect on initial thrombus growth, it promoted the dissolution of thrombi. Pharmacologically increasing cGMP via drugs to achieve an antithrombotic effect could be advantageous compared to established anticoagulants, as the initial aggregation and sealing process of a vascular lesion is not inhibited due to low shear conditions during this phase. As soon as the developing thrombus grows and platelets in the thrombus are exposed to increasing shear stress, cGMP levels increase and limit thrombus growth. Thus, the mechano-cGMP pathway in platelets may play an important role in the treatment of cardiovascular disease, as its pharmacological activation could minimize both the risk of bleeding and thrombosis.

Acknowledgements

First and foremost, I want to thank Prof. Dr. Robert Feil and Dr. Susanne Feil for giving me the opportunity to work in their lab and to finish my PhD. I am very greatful and feel very fortunate that I was entrusted with this exciting and challenging project and I did my best to repay that trust. The time as a PhD student has taught me many valuable lessons including non-scientific ones and all of them were necessary for me to reach this point. I will forever be grateful for the competent mentoring and supervision that I was given.

Next, I want to thank all the members of the Feil Lab, past and present, for their contribution to the pleasant and professional working atmosphere. It was always enjoyable to come to work and I hope the teamwork and support that I was able to relish will always be a part of this working group.

Thank you to Lai Wen for providing the scientific basis of this work and for trusting me to continue your exciting research.

I would especially like to thank Michael Krämer, Daniel Stehle and Moritz Lehners who supported me from the beginning of my time as a PhD student, where I had to overcome difficult parts of my project. Thank you for always giving me valuable scientific and non-scientific advice and helping me reach the finish line! Thank you Kristina Zaldivia for your priceless platelet advice and help!

Thank you to Angelos Vachaviolos and Jacek Dobrowinski for always encouraging me and making me believe in myself. Angelos, your kind and encouraging words (“just quit”) always motivated me and Jacek, thank you for immediately mentioning my good qualities to Robert (not pertaining to scientific work) during my job interview.

A big thanks must also go to Barbara Birk for her great technical assistance throughout my time in the lab. I also have to express my sincerest gratitude to Moritz Lehners who corrected the first version of my thesis in - according to him - “non-detailed fashion”.

Furthermore, I would like to mention the new generation of team platelet! You were always very motivated, competent and keen to pursue platelet research. With a great project comes great responsibility but I am certain that you, Luba Unger and Daniel Pinto, will guide our platelet project into new heights!

Thank you to my friends outside of work who always helped me maintain a healthy work-life-balance and enduring my more annoying episodes.

My deepest appreciation also goes out to Astrid Große for not only taking care of my experimental mice, but more importantly always looking out after me.

I have to thank my family, especially my parents, who always believed in me and supported me in every part of my life. They always trusted my decisions and career aspirations and never once doubted me. I hope that I have made them proud.

List of figures

List of tables

List of abbreviations

AB	Antibody
ADP	Adenosine diphosphate
APS	Ammoniumpersulfate
AUC	Area under the curve
BNP	B-Type natriuretic peptide
BSA	Bovine serum albumin
cAMP	Cyclic andenosine monophosphate
CFP	Cyan fluorescent protein
cGi500	cGMP indicator with EC50 500 nM
cGKI	cGMP-dependent protein kinase type I
cGMP	Cyclic guanosine monophosphate
CNG	Cyclic nucleotide-gated cation channel
CNP	C-Type natriuretic peptide
Co-IP	Co-immunoprecipitation
Cre	Cyclization recombination
DEA/NO	Diethylamine NONOate
DMSO	Dimethyl sulfoxide
DNA	Deoxyribonucleic acid
dNTP	Deoxynucleoside triphosphate
ECL	Enhanced chemiluminescence
ECM	Extracellular matrix
EDTA	Ethylenediaminetetraacetic acid
ELISA	Enzyme-linked immunosorbent assay
eNOS	Endothelial nitric oxide synthase
ER	Endoplasmic reticulum
FRET	Förster resonance energy transfer
GAPDH	Glyceraldehyde 3-phosphate dehydrogenase
GC	Guanylyl cyclase
GC-A	Guanylyl cyclase A
GC-B	Guanylyl cyclase B
GP	Glycoprotein
GPCR	G-protein coupled receptor
GTP	Guanosine triphosphate
HPLC	High-pressure liquid chromatography
HRP	Horseradish peroxidase
IgG	Immunoglobuline G
iNOS	Inducible nitric oxide synthase
IP	Immunoprecipitation
IP_3	Inositol triphosphate
IP_3R	Inositol triphosphate receptor
IRAG	Inositol 1,4,5-triphosphate-associated cGMP kinase substrate
LC-MS	Liquid chromatography mass spectrometry
loxP	Locus of X-over of P1
LPS	Lipopolysaccharide
MLC	Myosin light chain
MLCK	Myosin light chain kinase

MLCP	Myosin light chain phosphatase
MRP	Multidrug resistant protein
MS	Mass spectrometry
mT	Membrane tdTomato
nNOS	Neuronal nitric oxide synthase
NO	Nitric oxide
NO-GC	Nitric oxide-sensitive guanylyl cyclase
NO-GCβ_1	β_1 subunit of NO-GC
NOS	Nitric oxide synthase
NP40	Nonidet-P40
ODQ	1H-[1,2,4]oxadiazolo[4,3-a]quinoxalin-1-one
ORAI1	Calcium release-activated calcium channel protein 1
PBS	Phosphate-buffered saline
PCR	Polymerase chain reaction
PDE	Phosphodiesterase
PECAM-1	Platelet-endothelial cell adhesion molecule 1
Pf4	Platelet factor 4
pGC	Particulate guanylyl cyclase
PGI2	Prostacyclin
PKC	Protein kinase C
PRP	Platelet-rich plasma
PVDF	Polyvinylidene fluoride
RIA	Radioimmunoassay
ROCK	Rho-associated protein kinase
ROI	Region of interest
SDS	Sodium dodecyl sulfate
SDS-PAGE	Sodium dodecyl sulfate–polyacrylamide gel electrophoresis
SEM	Standard error of the mean
SERCA	Sarco/endoplasmic reticulum Ca^{2+} - ATPase
TBS	Tris-buffered saline
TBS-T	Tris-buffered saline + Tween 20
TEMED	Tetramethylethylenediamine
TxA2	Tromboxane A2
VASP	Vasodilator-stimulated phosphoprotein
VE	Vascular endothelial
VEGFR	Vascular endothelial growth factor receptor
VSMC	Vascular smooth muscle cell
vWF	Von Willebrand factor
YFP	Yellow fluorescent protein
ZET	Magnetron sputtered exciter or emitter for laser use

1. Introduction

1.1 Platelets and their role in hemostasis

Thrombocytes, also known as platelets, are anucleate cell fragments circulating in the blood stream that play a pivotal role in hemostasis. They are derived from megakaryocytes in the bone marrow and have a lifespan of 5 – 11 days after which they are degraded mainly in the spleen [1]. Human blood contains 150,000-400,000 platelets/µl on average, which is why roughly 10^{11} platelets are produced every day in a healthy adult to maintain this platelet count [2]. While platelets have been described to influence other (patho-)physiological processes like cancer [3] and atherosclerosis [4, 5], their main role is to prevent bleeding by formation of hemostatic plugs (thrombi) at a site of endothelial injury. A coagulation cascade is initiated upon platelet adhesion to the exposed collagen in the subendothelial matrix. Platelets first become activated, undergo shape change, and afterwards release the content of their granules [6, 7]. Initial binding of the platelets to the vessel wall is mediated via the collagen receptor glycoprotein (GP) Ia-IIa (integrin $\alpha_2\beta_1$) and GPVI **(Figure 1)** [6]. As platelets are also exposed to shear stress due to the blood flow during this process, this biophysical force also plays an important role in platelet adhesion and activation [8]. In smaller arteries and arterioles, where high shear forces are present, platelet adhesion to the injured vessel wall is mediated by the interaction of von Willebrand factor (vWF), which is mobilized on the collagen, and GPIb-IX-V, a membrane-bound glycoprotein receptor complex [6, 8, 9]. After the activation process of the platelets has been triggered, several intracellular signaling pathways can lead to shape change and granule secretion **(Figure 1)**. When activated, platelets secrete soluble agonists like ADP, Thromboxane A_2 and thrombin, which act on different G-Protein-coupled receptors (GPCRs) **(Figure 1)** [6, 10]. Intracellular calcium is released after platelet activation and the specific platelet signaling pathways all converge eventually to upregulate integrin adhesion receptors to further stabilize platelet adhesion and thrombus growth **(Figure 1)** [6, 10]. The main integrin adhesion receptor in this regard is GPIIb/IIIa (fibrinogen receptor), also called integrin $\alpha_{IIb}\beta_3$, which mediates a further stabilization of the thrombus by cross-linking platelets after binding of vWF and fibrinogen to this receptor **(Figure 1)** [6, 10]. The formed thrombus is also further stabilized by thrombin. Thrombin not only acts as

a strong platelet agonist but also converts fibrinogen to fibrin leading to a stable hemostatic plug consisting of platelet aggregates and a polymerized fibrin mesh [7, 10]. While activation stimuli lead to platelet aggregation, platelets are also subjected to inhibitory stimuli to avoid aberrant vessel occlusion. The two major endogenous platelet inhibitors, nitric oxide (NO) and prostacyclin, are constantly secreted by endothelial cells into the vessel lumen, triggering the cyclic guanosine monophosphate (cGMP) and cyclic adenosine monophosphate (cAMP) signaling pathway in platelets, respectively **(Figure 1)**.

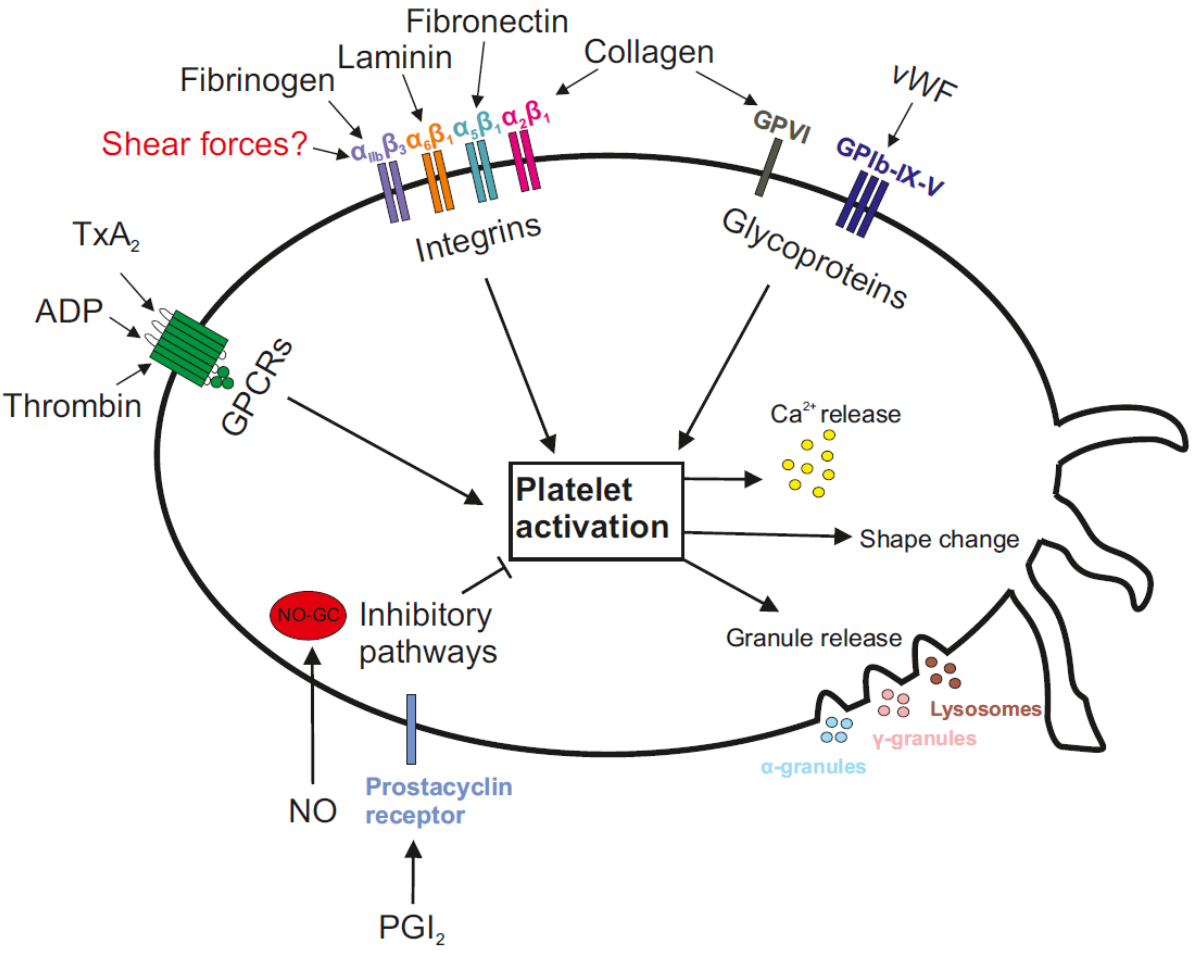

Figure 1. Platelet activation and inhibitory pathways.

Platelets can be activated through several intracellular signaling pathways triggered from external stimuli. Thromboxane A2 (TxA_2), ADP and thrombin can lead to platelet activation via GPCRs (green). Glycoprotein mediated signaling can also lead to platelet activation, for instance after binding of vWF to GPIb-IX-V (blue) or collagen to GPVI (gray). Several types of heterodimeric integrins like $\alpha_{IIb}\beta_3$ (violet), α6β1 (orange), $\alpha_5\beta_1$ (teal) and $\alpha_2\beta_1$ (magenta) are key players of platelet activation after binding of fibrinogen, laminin, fibronectin, or collagen, respectively. Shear forces have also been described to be necessary for platelet activation, also possibly mediated via different integrins. Activation of platelets leads to the release of intracellular calcium (yellow) as well as α-granules (cyan), γ-granules (pink) and lysosome contents (brown). Shape change is a direct consequence of platelet activation. Inhibitory pathways limiting platelet activation are triggered by NO which binds the NO-GC (red) and PGI_2 binding the Prostacyclin receptor (light blue).

Although the main role of platelets is to form a hemostatic plug by aggregation, this process is also tightly regulated to prevent pathophysiology. On the one hand, platelets must plug lesions in the vasculature to prevent blood loss and maintain a healthy circulation. On the other hand, excessive aggregation of platelets and thrombus formation can lead to life-threatening pathological conditions like thrombosis, myocardial infarction and stroke [7]. In the clinics, in order to inhibit platelet aggregation, a wide range of drugs targeting different platelet-activating signaling pathways have been available for a decent amount of time, yet most come with the side-effect of increased bleeding. Thus, studying and understanding the underlying mechanisms that regulate platelet activation and inhibition is not only of great scientific, but also clinical research interest [11].

1.2 Shear stress and the role of integrins in mechanotransduction

Physical forces influence a large variety of physiological processes and functions, for example touch sensation and proprioception [12], bone remodeling [13], lung physiology [14] and kidney morphogenesis [15] among others. As such, every cell and organism has to be able to sense biomechanical stimuli and process them into a biochemical signal in order to adapt to the external environment in the form of a physiological response. Dysregulation of these responses can lead to major human diseases [16]. Responsible for sensing and processing of these stimuli are so-called mechanotransducers. As mechanical stimuli can come in many forms, it is highly probable that they are not sensed in the same manner by one or even a few mechanotransducers across different cell types [16]. Mechanotransduction can be based on conformational changes in mechanosensing proteins after exposure to force. It can lead to opening of membrane channels or altered affinities to binding partners and then alter intracellular signaling and physiological responses [17]. Increased focus has been put on mechanotransduction research as its importance has become more and more apparent.

In the cardiovascular system, mechanotransduction plays a pivotal role in several cell types and in diseases like atherosclerosis [18]. Here, blood flow exerts physical forces in different forms on surrounding cells, thereby influencing their physiological response. For instance, pressure and shear stress created by the blood flow

influence the morphology and physiology of the heart and vasculature [17, 19-21]. Blood flow-induced shear stress has been studied in more detail, particularly in connection to normal vascular function and in atherosclerotic disease models [18]. It has been observed that atherosclerotic lesions are more prevalent at sites of disturbed blood flow where the turbulent flow leads to low or oscillatory shear stress acting on the endothelium [22, 23].

Most of our knowledge on mechanotransduction in the cardiovascular system comes from studies on endothelial cells of the vasculature, while relatively few studies have analyzed the mechanobiology of fibroblasts and vascular smooth muscle cells (VSMCs) [23-25]. Several types of receptors have already been investigated for their mechanosensing properties. For one, cell-matrix and cell-junction forming proteins have been described to be involved in shear-sensing [23]. These include the cell junction protein PECAM-1 [26, 27] and adherens junction proteins like vascular endothelial (VE)-cadherin [28]. Several types of membrane proteins have also been looked at as shear sensors [23]. These include ion channels like potassium channels [29, 30] and calcium release-activated calcium channel protein 1 (ORAI1) [31], tyrosine kinase receptors like vascular endothelial growth factor receptor 2 (VEGFR2) [28], integrins [32], calveolae [33], G-proteins [34] and GPCRs [35, 36]. It is also implied that mechanotransduction can occur via the endothelial actin cytoskeleton [37, 38] and the glycocalyx [25, 39]. Nevertheless, there is a lot of ongoing research deciphering the relevance of these receptors in mechanotransduction as well as their connection to intracellular signaling pathways and ultimately their physiological role.

It can only be assumed that platelets possess similar mechanotransducing mechanisms as described above. As circulating cell fragments, platelets are permanently subjected to the natural environment of blood flow and therefore also hemodynamic forces like shear stress. Shear stress results from frictional forces (shear forces) which are exerted on objects subjected to fluid flow, for example cells on the vessel surface or platelets. It is the product of the shear rate (s^{-1}) and fluid viscosity (η) and is expressed in units of dynes/cm^2 [23]. As a biomechanical force, shear stress is influenced by the following three factors: Blood flow velocity, vessel geometry and fluid viscosity [18]. Since vessels come in different sizes and blood flow is heavily physiologically regulated, the extent of shear stress platelets are

exposed to can vary to a large degree. This makes the identification of mechanosensing mechanisms in platelets important, yet also complex and difficult.

In many cell types, mechanosensitive structures include heterodimeric transmembrane receptors called integrins [32]. They are composed of an α and β subunit and have a relatively large extracellular domain connected to a short cytosolic tail via a single-pass transmembrane domain [40, 41]. Beside their pivotal role in mechanotransduction [32], integrins are key players enabling adhesion to the extracellular matrix (ECM) and cell-cell adhesions [41, 42]. Concerning a potential mechanosensitivity of integrins, it has been shown in vascular endothelial cells that shear stress can regulate the activity of different integrins and that this not only plays a role in regulating vascular integrity, but it also influences the development of atherosclerosis [43-45].

In platelets, integrins play an integral role in mediating initial platelet adhesion to the ECM and driving further platelet aggregation **(Figure 1)**. Platelets express several integrins: $\alpha_{IIb}\beta_3$, $\alpha_5\beta_3$, $\alpha_2\beta_1$, $\alpha_5\beta_1$ and $\alpha_6\beta_1$ [40], with the β_1 integrins playing a supportive role in binding the ECM proteins laminin ($\alpha_6\beta_1$), fibronectin ($\alpha_5\beta_1$) and collagen ($\alpha_2\beta_1$), and $\alpha_{IIb}\beta_3$ being the dominant integrin on the platelet surface binding plasma fibrinogen and acting as a driving force of platelet aggregation [42]. Due to its apparent importance, a lot of scientific focus has been put on integrin $\alpha_{IIb}\beta_3$. Several drugs, for example Abciximab and Tadalafil, have been developed that target integrin $\alpha_{IIb}\beta_3$ to limit thrombosis in acute coronary syndromes [46, 47].

Integrins enable so-called bidirectional signaling via outside-in and inside-out signaling [40, 41, 48]: The intracellular domain activates the ligand binding function of the receptor by inducing a conformational change of the outer part (from low-affinity to high-affinity) from the “inside” (inside-out signaling). The extracellular part of the receptor (in its high affinity state) can interact with ECM ligands from “outside” of the cell, thus, changing signaling patterns on the inner side (outside-in signaling) and leading to cellular responses [49, 50].

As for their mechanosensing properties, a recent study in platelets shows that integrin β_3 serves as a shear sensor which activates outside-in signaling and promotes platelet coagulation [49]. Another study suggests that beside its low-affinity and high-affinity states, integrin $\alpha_{IIb}\beta_3$ has an intermediate affinity state that specifically mediates mechanosignaling and promotes biomechanical platelet

aggregation [51]. Nevertheless, there are still a lot of uncertainties regarding shear-induced integrin signaling in platelets, whether it is the sensing mechanism itself or which signaling pathways are connected to the mechanotransduction process that leads to physiological responses.

Conclusively, biomechanical stimuli such as shear stress have not been fully considered in many studies of platelet biochemistry and physiology and might open new perspectives and options for potential drug development.

1.3 Introduction to cGMP signaling

Cyclic guanosine monophosphate (cGMP) is a key second messenger molecule that regulates a large variety of physiological processes in mammals. First discovered in rat urine in 1963 [52], it rose to prominence due to its importance in regulating cardiovascular homeostasis [53]. cGMP has been described to control processes like cellular growth and contractility, inflammation, sensory transduction, neuronal plasticity and learning, axon bifurcation, platelet activation and many more [53, 54]. It has been shown that altered cGMP signaling due to genetic variants can be associated with a change in blood pressure regulation and an increased risk of cardiovascular disease [55-58]. In the clinics, several drugs targeting the cGMP signaling pathway have been approved for therapeutic use, particularly cGMP elevating drugs treating cardiovascular diseases [11]. Prominent cGMP-elevating drugs include Sildenafil (VIAGRA®) for the treatment of erectile dysfunction, organic nitrates for angina pectoris and Riociguat for the treatment of distinct forms of life-threatening pulmonary hypertension [11].

cGMP can be generated intracellularly by two distinct types of guanylyl cyclases (GCs): Membrane-bound particulate guanylyl cyclases (pGCs) and the NO-sensitive GCs (NO-GCs), formerly referred to as “soluble” GCs. While pGCs are activated by natriuretic peptides, the gaseous molecule NO serves as the driving force of cGMP generation via the NO-GC **(Figure 2)**.

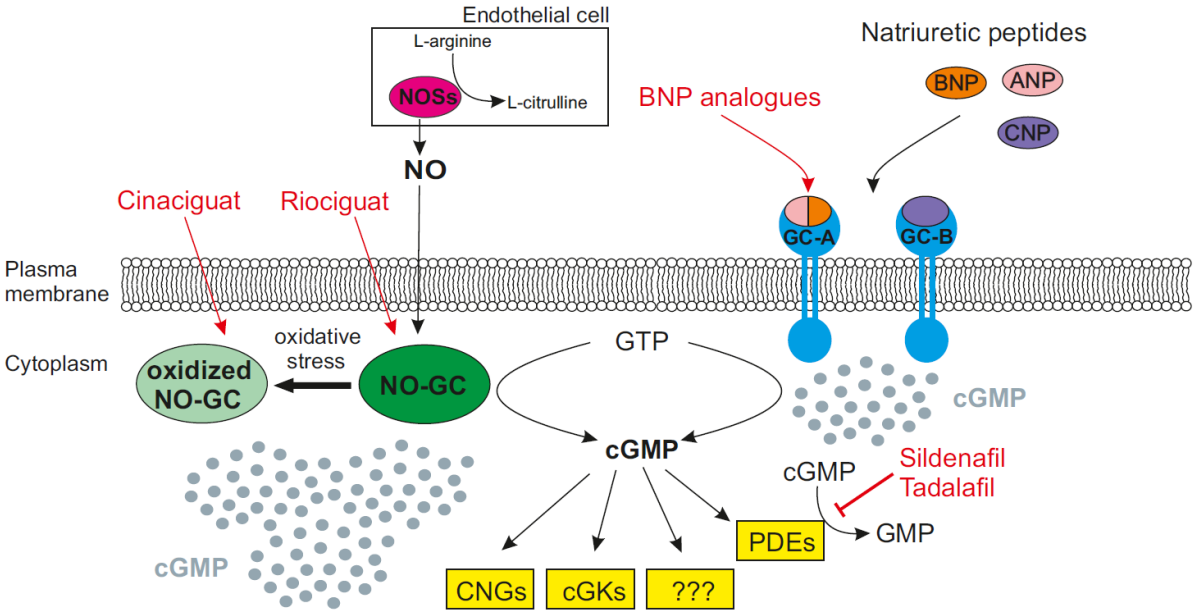

Figure 2. The cGMP signaling pathway.

Two different types of guanylyl cyclases can generate cGMP (gray circles): The NO-GC (formerly referred to as the soluble GC, green circle) and several types of transmembrane particulate guanylyl cyclases, including GC-A and GC-B (blue). The NO-GC is activated by nitric oxide (NO), which is generated by NO synthases (NOSs, magenta circle), e.g., in endothelial cells. NO-GC can be oxidized (light green circle) after which it loses its function. While GC-A is activated by ANP (pink circle) or BNP (orange circle), CNP (purple circle) binds to GC-B. Effectors of cGMP signaling (yellow squares) include cyclic nucleotide-gated channels (CNGs), cGMP-dependent protein kinases (cGKs), phosphodiesterases (PDEs), and possibly other proteins (???). PDEs hydrolyze cGMP to GMP. Different drugs (red) target and modulate the cGMP signaling pathway: While Cinaciguat exclusively stimulates oxidized NO-GC, Riociguat drives cGMP generation by targeting non-oxidized NO-GC. BNP analogues bind to GC-A and Sildenafil as well as Tadalafil can inhibit PDE5-mediated cGMP degradation. Modified from Feil & Kemp-Harper, 2006 [59].

NO is synthesized from L-arginine by enzymes known as NO synthases (NOSs), which include the endothelial NOS (eNOS), neuronal NOS (nNOS), and inducible NOS (iNOS) [60, 61]. Being constitutively expressed in various tissues, nNOS and eNOS can be activated by an increase in intracellular calcium and subsequent calmodulin binding in the nervous system and endothelial cells, respectively [62]. As the name alludes to, the expression of iNOS is inducible upon stimulation with lipopolysaccharide (LPS) or cytokines in cell types such as macrophages, VSMCs and endothelial cells [11, 63].

cGMP binds and activates three main types of downstream effectors: cyclic nucleotide-gated cation channels (CNGs), cGMP-dependent protein kinases (cGKs) and phosphodiesterases (PDEs) [53, 54, 64] **(Figure 2)**. CNGs are important cellular switches that transduce changes of cyclic nucleotides into changes of the membrane potential and intracellular calcium concentration [54]. PDEs lead to the degradation of

not only cGMP but also cAMP [11, 65]. The main cGMP effector in many cells are the cGKs which, for instance, lead to smooth muscle relaxation or inhibition of platelet aggregation [11, 53, 54].

Several approved drugs target the cGMP signaling pathway by increasing cGMP concentrations **(Figure 2)**. For instance, while Riociguat stimulates the NO-sensitive ferrous form (Fe^{2+}) of the NO-GC, the NO-GC activator Cinaciguat targets its NO-insensitive oxidized ferric form (Fe^{3+}) or heme-free state [53, 66]. BNP analogues induce cGMP generation via the pGCs and are explored in the treatment of heart failure [53]. As PDE5 inhibitors such as Sildenafil and Tadalafil reduce the degradation of cGMP, they primarily induce smooth muscle relaxation and are therefore used to treat erectile dysfunction and pulmonary hypertension [53]. Taken together, the cGMP signaling pathway is highly druggable, but many effects elicited by the already approved drugs remain elusive. In the present work, we sought to investigate the effect of modulating the cGMP signaling pathway in platelets and ultimately whether it can be therapeutically targeted to regulate platelet activity and therefore hemostasis or even thrombosis.

1.4 cGMP signaling in platelets: An overview

cGMP is a key regulator of platelet physiology, with NO leading to increased cGMP levels and ultimately to an inhibition of platelet aggregation [67-69]. Physiologically, NO is produced by eNOS in the endothelium and then diffuses into the lumen of the vessel [60], where the excessive aggregation of platelets and therefore a potential occlusion of the vessel must be avoided [70]. The NO-induced elevation of cGMP in platelets inhibits several processes including cytoskeletal remodeling, intracellular calcium release, agonist-induced integrin activation, granule secretion as well as TxA_2 synthesis and release [65, 70-72]. These are all vital processes involved in the mediation of platelet activation, shape change, adhesion, aggregation, and coagulation **(Figure 3)** [70].

After activation by NO or drugs like Riociguat, cGMP is generated in platelets solely by the soluble NO-GC **(Figure 3, red)**, since no particulate guanylyl cyclase has been detected in platelets up to this day. After cGMP generation, three main targets of cGMP signaling are activated: While PDEs and cGMP transporters mediate cGMP

removal, cGMP-dependent protein kinase type I (cGKI) is responsible for the main downstream effects of cGMP.

Cyclic nucleotide levels are negatively regulated by the phosphodiesterases PDE2, PDE3 and PDE5, which catalyze the hydrolysis of one of the phosphodiester bonds of cGMP and cAMP, leading to inactive 5'-GMP and 5'-cAMP, respectively [11, 73, 74]. The main PDE specifically degrading cGMP in platelets is PDE5 [75]. A crosstalk between cGMP and cAMP signaling also exists through the activities of PDE2 and PDE3 **(Figure 3, blue)**. PDE2 is activated by cGMP via allosteric modification, leading to the hydrolysis of both cGMP and cAMP [11, 76]. Conversely, high concentrations of cAMP can also competitively inhibit PDE2-mediated cGMP hydrolysis [76]. PDE3 hydrolyzes cAMP and as this activity can be competitively inhibited by cGMP, PDE3 is also termed the "cGMP-inhibited" PDE [11, 76].

Another form of cGMP removal are cGMP transporters that promote cGMP efflux. In platelets, efflux is most prominently made possible by a member of the multidrug resistance-associated protein (MRP) family, MRP4 [77-81]. While it has been observed that MRP4-mediated cGMP efflux can attenuate cGMP-mediated inhibitory effects in platelets [77], its functional importance has not been held in high regard, especially compared to PDE-mediated cGMP degradation [11].

The main cGMP effector in platelets which mediates downstream effects is the cGKI (discussed in detail in chapter 1.6), a kinase which has been described to phosphorylate several proteins **(Figure 3, orange dots)**. The two main substrates of the cGKI which are highly expressed in platelets are the vasodilator-stimulated phosphoprotein (VASP) and inositol-1,4,5-triphosphate (IP_3) receptor-associated cGMP kinase substrate (IRAG). These substrates have been shown to play a role in inhibiting platelet aggregation [82, 83]. IRAG suppresses intracellular Ca^{2+} release by forming a complex with cGKI and the IP_3 receptor type 1 (IP_3R1) [84, 85], thus preventing the endoplasmic reticulum (ER) from releasing Ca^{2+} which is essential for platelet activation **(Figure 3)**. The other major cGKI substrate in platelets is VASP [86, 87], which is phosphorylated at Ser157 and Ser239 and thereby activated. VASP plays an inhibitory role in actin fiber formation, a necessary process in cytoskeletal remodeling and therefore platelet shape change [87]. VASP phosphorylation is also connected to the inhibition of integrin $\alpha_{IIb}\beta_3$ as it hinders the binding of fibrinogen to integrin $\alpha_{IIb}\beta_3$ [88-90]. Unfortunately, the exac t role of VASP phosphorylation in

hemostasis and thrombosis remains elusive, but its role in inhibiting platelet shape change cannot be ignored [11].

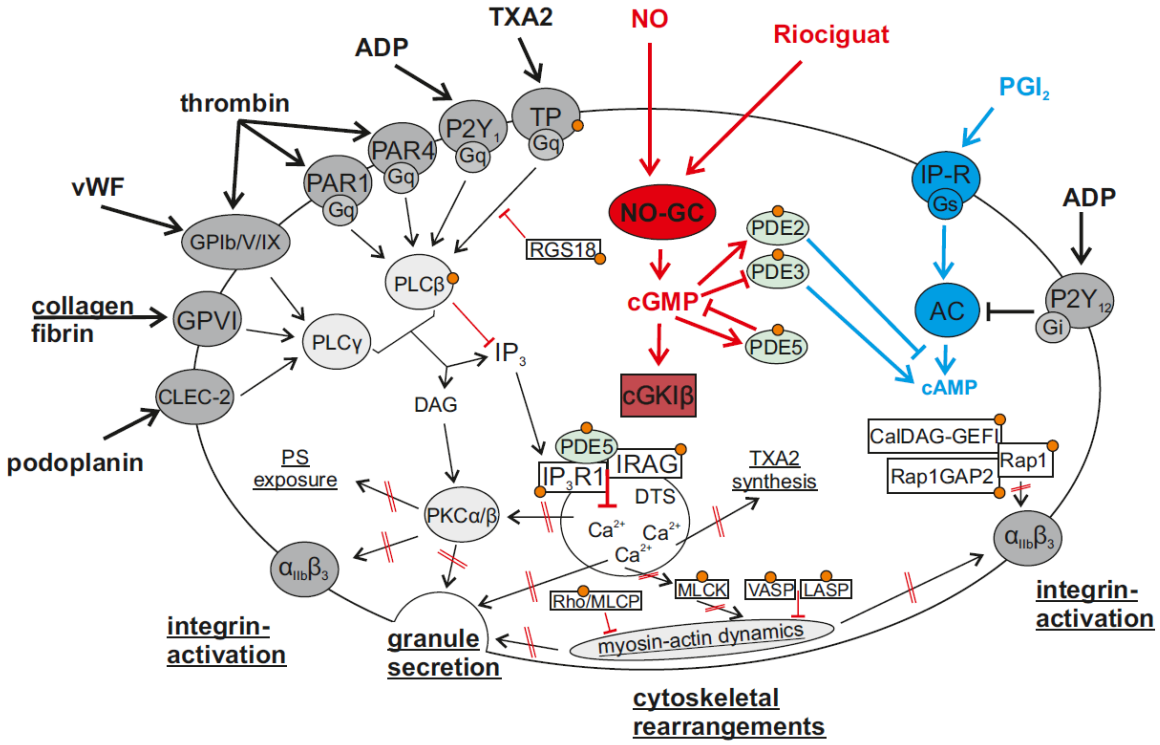

Figure 3. **Regulation of protein phosphorylation and function of human platelets by the cGMP signaling pathway.**

Platelet activation and adhesion is mediated by several soluble platelet agonists (thrombin, ADP, TXA2) and adhesion molecules (collagen, fibrin, vWF, podoplanin). These bind to their specific membrane receptors and initiate signaling cascades driving various platelet responses, for instance integrin $\alpha_{IIb}\beta_3$ activation, granule secretion, regulation of cytoskeletal rearrangements via myosin-actin dynamics and PS exposure. The cGMP signaling pathway inhibits the platelet activation responses depicted by the red blocked arrows. Stimulation of the cGMP signaling pathway via NO or Riociguat mainly leads to inhibition of intracellular Ca^{2+} release via phosphorylation of IRAG and to inhibition of cytoskeletal rearrangements via phosphorylation of VASP. PDE5 reduces intracellular cGMP levels.A crosstalk between the cGMP (red) and cAMP (blue) signaling pathway exists through the regulation of PDE2 and PDE3. PDE2 is activated by cGMP and leads to the hydrolysis of both cGMP and cAMP. PDE3 degrades cAMP, but its activity is competitively inhibited by cGMP. Known phosphorylation targets of cGKI are marked by an orange dot. PLC, phospholipase C; RGS18, regulator of G-protein signaling 18; IP_3R1, inositol1,4,5-triphosphate (IP_3) receptor 1; IRAG, IP_3 receptor-associated cGKI substrate protein; small GTPase system: [CalDAG-GEFI/RASGRP2; Rap1; Rap1GAP2]; actin system: [Rho; MLCP; MLCK; VASP; LASP]; MLCP, myosin light-chain phosphatase; MLCK, myosin light-chain kinase; VASP, vasodilator-stimulated phosphoprotein; LASP, LIM and SH3 protein 1; vWF, von Willebrand factor; TXA2, thromboxane A2; TP, thromboxane receptor; PGI_2, prostacyclin; IP-R, prostacyclin receptor; PS, phosphatidylserine; PKC, protein kinase C; DTS, dense tubular system. Modified from Makhoul et al., 2018 [70].

Other targets that play a role in platelet activation can also be phosphorylated by cGKI [65, 70], most of them connected to GPCR signaling and the effect on integrins, Ca^{2+} release and the cytoskeleton [11, 70]. For example, cGKI phosphorylates the Rho family member of small GTPases Rap1B [91] and also Rap1GAP2 [92], together

playing a role in integrin $\alpha_{IIb}\beta_3$ activation [93]. Regulator of G-protein signaling 18 (RGS18) is a further phosphorylation target of cGKI, which, after being phosphorylated, reduces $G\alpha_q$-signaling, thereby also inhibiting the release of Ca^{2+} from the ER [94]. Another small G-protein which is regulated by cGKI is Rac1, which is controlled by the phosphorylation of ARHGAP17 and ARHGEF6 [95]. cGKI activity reduces levels of Rac1 and in this way also negatively impacts cytoskeletal remodeling and platelet activation [11, 96]. Platelet shape change can also be inhibited by cGKI via phosphorylation of RhoA, which prevents its association with RhoA kinase (ROCK) [97, 98]. Upon phosphorylation by ROCK, the myosin light-chain phosphatase (MLCP) is activated, leading to the dephosphorylation of myosin light-chain (MLC) and therefore to the inhibition of platelet shape change [99]. Also playing a role in this process is the myosin light-chain kinase (MLCK) which is either indirectly regulated by cGMP through the inhibition of Ca^{2+} release or can also be directly phosphorylated and inhibited by cGKI [100].

In vivo, it has been observed that many clinically approved cGMP-elevating drugs, beside their dominant vasodilatory effect, also lead to cGMP generation in platelets and to an inhibition of platelet aggregation [101-104]. Despite the general consensus that the cGMP signaling pathway inhibits platelet aggregation, there have also been studies that describe a stimulatory role of cGMP in platelet activation [105, 106], which has sparked a controversial debate regarding the exact functional role of cGMP in platelets [107, 108].

Taken together, activation of cGKI through cGMP leads to the phosphorylation of several downstream proteins, such as IRAG and VASP, which, in turn, leads to the inhibition of Ca^{2+} release from the ER and the inhibition of cytoskeletal rearrangements **(Figure 3)**. The fact that these two key processes driving platelet activation and aggregation are inhibited by cGKI underline the importance of the cGMP signaling pathway in preventing excessive platelet aggregation.

1.5 NO-GC and its role in cGMP generation in platelets

Platelets generate cGMP solely via the NO-GC. A particulate natriuretic peptide-responsive guanylyl cyclase has not been identified in platelets to date. The NO-GC is a heterodimer consisting of two subunits: An α-subunit and a heme-containing

β-subunit [109, 110]. There are two known functional forms of the heterodimeric NO-GC: The NO-GC2 with an expression confined mostly to the brain, lung and placenta, and the NO-GC1 which can be found in most tissues, especially in the cardiovascular system including in platelets and VSMCs [109, 111-114].

The NO-GC1 consists of the $\alpha_1\beta_1$ and the NO-GC2 of the $\alpha_2\beta_1$ subunits [115]. The β_2 isoform, identified in the kidney, has not been found to form a functional heterodimer [115, 116]. Both subunits are composed of similar domains with the β-subunit providing the heme-binding N-terminus, also called the H-NOX domain [109]. NO can bind the Fe^{2+} of the heme-moiety, form a complex (NO-Fe^{2+}-His-complex) and hereby increase the catalytic activity of the enzyme over 200-fold [11, 117]. Compounds that target the Fe^{2+}-heme can be used to induce cGMP generation, namely several NO-donors and drugs like Riociguat or Vericiguat, which are termed NO-GC stimulators [66].

The importance of the reduced Fe^{2+}-form for NO-binding has to be highlighted since oxidation to Fe^{3+} leads to a strongly reduced sensitivity of the cyclase to NO [118, 119]. Oxidation is either the consequence of oxidative stress, or can be artificially induced by an NO-GC-inhibiting compound, ODQ [119]. The Fe^{3+}-heme can also be specifically targeted by drugs like Cinaciguat, a so-called NO-GC activator, in order to promote cGMP generation from the oxidized form of the enzyme [66]. Several functional analyses of the platelet guanylyl cyclase have been performed that conclude that the NO-GC1 form is the predominant form and as such, platelets from α_2-knockout mice did not significantly differ from control platelets [120]. The NO-GC is also connected to the previously described inhibitory function of cGMP in platelet aggregation. Knocking out the β_1-subunit of the NO-GC [121] or using mutant mice expressing an NO-unresponsive haem-free NO-GC (apo-NO-GC) [122] diminishes the inhibition of platelet aggregation by NO. In the study of Gobel et al. [121], it was also observed that the bleeding time in β_1 knockout mice was decreased. It has to be noted that, in general, studies regarding the exact function of the NO-GC are also complicated by the fact that NO can also trigger NO-GC-independent effects like S-nitrosylation of cysteine residues [123] and that the activity of the NO-GC in platelets can probably also be induced NO-independently, such as with platelet agonists vWF, thrombin and collagen [105, 106].

Considering all this, the exact mechanisms of how the NO-GC is regulated before and during platelet activation, aggregation and thrombosis has not been fully unraveled and understanding these mechanisms is of great importance to uncover the role of cGMP in platelet physiology and pathophysiology.

1.6 Structure of cGMP-dependent protein kinase and its function in platelets

In most cell types, the main effector molecules that exert downstream effects of cGMP are the cGKs. These enzymes belong to the serine/threonine kinase family and are present in a large variety of cell types, tissues and organisms [53, 124]. Many physiological processes are known to be regulated by cGKs, including, but not limited to, the relaxation of VSMCs [125, 126], platelet aggregation [127], angiogenesis [128], the negative inotropic effect of cGMP in the myocardium [129] and long-term potentiation in the hippocampus [130]. Mammals are equipped with two genes that encode different cGKs: *prkg1* for cGKI and *prkg2* for cGKII [131]. In the cardiovascular system, especially in platelets and VSMCs, cGKI is the predominantly present type [11]. The *prkg1* gene encodes two distinct isoforms of cGKI, cGKIα and cGKIβ, which have a different N-terminal domain [124, 132, 133]. Both cGKI and cGKII are homodimers of two identical subunits, which are built from three different domains: The N-terminus, a regulatory domain and the kinase domain [124, 131]. While the N-terminal domain mediates homodimerization, interactions with other proteins, and autoinhibition of the kinase activity in a cGMP-void state, the kinase domain catalyzes the phosphorylation of substrate proteins on the hydroxyl groups of serine or threonine side chains [131]. Two cGMP molecules bind two different cGMP-binding pockets (low and high affinity pockets) in the regulatory domain of the kinase [131]. In total, four cGMP molecules (two per subunit) are therefore necessary to release the catalytic kinase domain from the autoinhibitory N-terminus allowing the kinase to efficiently phosphorylate target proteins **(Figure 4)** [131].

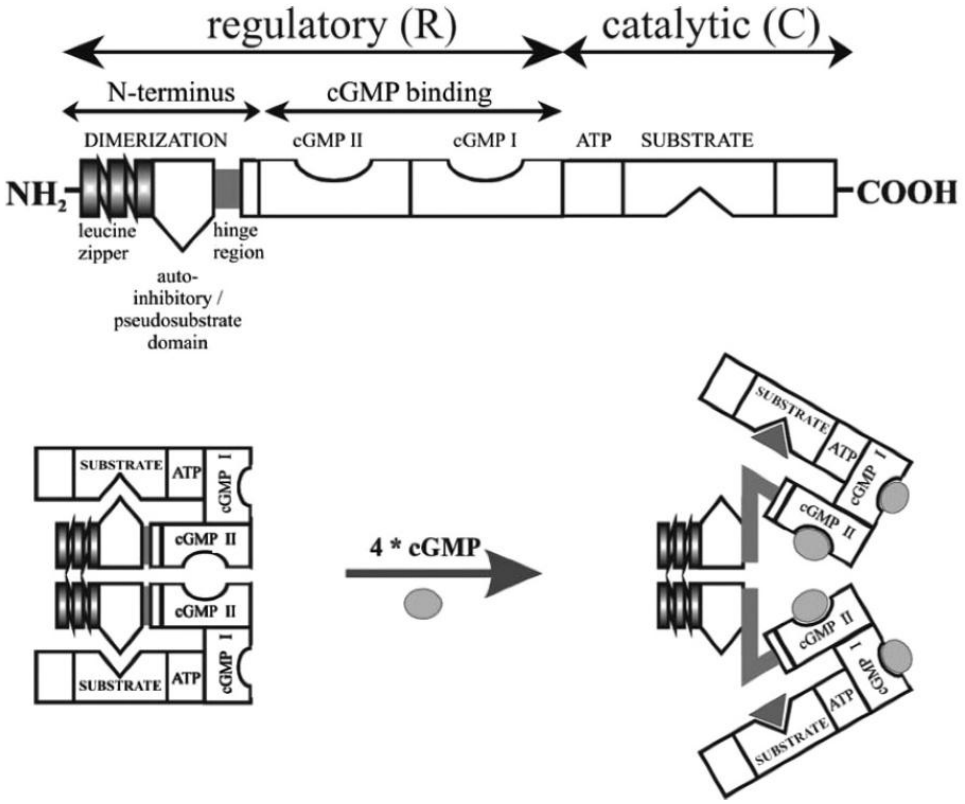

Figure 4. The structure of cGMP-dependent protein kinase I.

cGKs are homodimers with each subunit consisting of three domains (top): (1) The N-terminus which enables dimerization and protein interactions and inhibits kinase activity in a cGMP-free state, (2) the regulatory domain in which two cGMP molecules per subunit can bind two cGMP binding pockets with different affinity, and (3) the catalytic domain which drives the transfer of the γ-phosphate of ATP to the serine or threonine residue of a target protein. When no cGMP is present, the enzyme is in an autoinhibited state (bottom left), where the catalytic domain is bound to the inhibitory domain of the N-terminus. Once 4 molecules of cGMP bind, the catalytic subunit is released (bottom right) and the enzyme can exert its catalytic effect by enabling phosphorylation of target proteins. Taken from Hofmann et al., 2009 [131].

While murine platelets express cGKIβ in large and cGKIα in low amounts, only cGKIβ can be detected in human platelets [82, 84]. Knocking out cGKI in murine platelets led to increased aggregation compared to wild type platelets [127]. Similar to NO-GC-deficient platelets (see 1.5), these findings point towards an inhibitory role of the NO-GC-cGMP-cGKI signaling axis in platelet aggregation. This notion is also supported by *in vivo* observations made in mice deficient in VASP or IRAG, the two main phosphorylation targets of cGKI, which also show diminished inhibition of platelet aggregation [82, 83]. However, the action of cGKI is not limited to VASP and IRAG. Recent phosphoproteome analyses have identified a large number of additional potential phosphorylation targets of cGKI connected to multiple signaling networks [70]. Understanding the connection and function of all these signaling networks is vital to shed light on the exact role of cGKI in platelets.

1.7 Real-time imaging of cGMP with the FRET-based biosensor cGi500

Commonly used methods to measure cGMP concentrations not only in platelets but also in other cells and tissues include the enzyme-linked immunosorbent assay (ELISA) and radioimmunoassay (RIA). These are end-point assays using cell extracts that determine cGMP levels at one defined time point. Therefore, these methods do not provide any spatial information about the cGMP signal at the level of single cells or tissues, and their temporal resolution of is severely limited. Furthermore, since subtle cGMP changes can be confined to distinct subcellular compartments, these specific cGMP concentration changes might not get detected using these common assays [134].

To get around the lack of spatial and temporal resolution, fluorescent biosensors have been developed to observe dynamic changes of signaling molecules in living cells *in vitro* and *in vivo* [135]. In the present study, the genetically encoded Förster resonance energy transfer (FRET)-based biosensor cGi500 **(Figure 5)** has been used to visualize the spatiotemporal dynamics of cGMP signaling [136, 137]. In general, FRET-based sensors consist of chromophores between which energy is transferred via FRET, a phenomenon first described by Theodor Förster in 1948 [138]. The cGi500 sensor, developed by Russwurm et al. [136] and then used for the real-time observation of cGMP changes in transgenic mice [137] is composed of the tandem cGMP-binding domain of cGKI flanked by two fluorophores, cyan fluorescent protein (CFP) and yellow fluorescent protein (YFP). The distance and orientation of the sensor's fluorophores determines whether FRET can take place from CFP (FRET donor) to YFP (FRET acceptor). In the absence of cGMP, due to the close proximity of the two fluorophores, upon excitation of CFP at a wavelength of 445 nm, FRET can occur from CFP to YFP which then emits the transferred energy at a wavelength of 535 nm **(Figure 5, left)**. Once cGMP binds, the sensor conformation is changed leading to a drastic reduction of FRET efficiency due to the increased distance between the fluorophores. Exciting CFP at 445 nm in this case leads to a highly increased emission of CFP at a wavelength of 480 nm and reduced emission of YFP at 535 nm since the energy is not transferred to the YFP fluorophore any longer **(Figure 5, right)**. By tracking FRET efficiency and following the ratio of CFP/YFP

emission (F480/F535), it is possible to observe intracellular cGMP level changes in real-time in any cell, tissue or organism expressing the sensor.

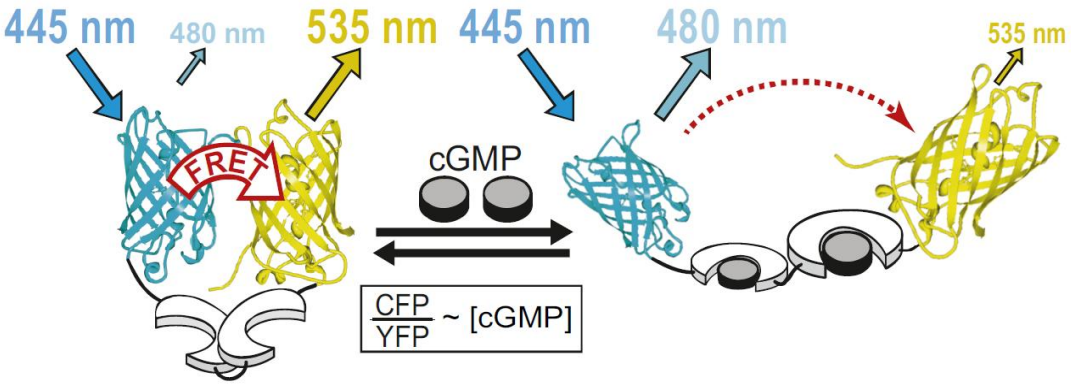

Figure 5. The FRET-based cGMP biosensor cGi500.

The ratiometric cGMP biosensor cGi500 consists of two fluorophores, CFP and YFP, flanking the cGMP-binding domain of bovine cGKI. In the cGMP-free state (left side), the distance and orientation of the fluorophores allows FRET to occur from CFP to YFP with high efficiency. This means that when exciting at a wavelength of 445 nm, due to FRET, a increased emission of YFP at 535 nm becomes observable. Once cGMP is present (right side), the conformation of the sensor changes and thereby drastically diminishes FRET efficiency. In this orientation, upon exciting at a wavelength of 445 nm, YFP emission is reduced and CFP emission at 480 nm increased. The ratio of emission at 480 nm and 535 nm (F480/F535) is then determined and taken as a representation of intracellular cGMP level changes. Adapted from Thunemann et al., 2013 [137].

Transgenic mice expressing this sensor allow us to observe dynamic cGMP level changes in living cells, tissues and even the whole organism. The sensor permits the measurement of dynamic cGMP level changes in single platelets or whole thrombi not only in the *ex vivo* setup, but also in the living mouse under almost native conditions [139, 140]. Considering that a potential transfection of platelets would most probably not lead to a successful expression of the sensor construct, inherent genetic expression remains the most viable method to measure cGMP changes. A further advantage of using sensor-expressing platelets is the fact that it allows for simple real-time visualization of thrombus formation *ex vivo* (flow chamber, see 2.4) and *in vivo* (intravital imaging, see 2.11) by simply detecting YFP fluorescence using a fluorescence microscope.

The cGMP sensor can not only be expressed globally, but also in a cell type-specific manner. The latter is achieved using the Cre/loxP system [141]. This system uses a Cre recombinase, the expression of which can be under control of a respective tissue-specific promoter, which leads to the excision of a gene fragment flanked by

loxP sites. The sophisticated Cre/loxP technology is widely used in mouse genetics as it allows not only spatial, but also temporal control of gene expression [142, 143]. The Cre/loxP recombination system opens many possibilities for our *ex vivo* and also *in vivo* experiments with platelets. A Cre recombinase driven by the platelet-specific Pf4 promoter, can specifically mark megakaryocytes and platelets with the fluorescent sensor through recombination, thus distinguishing them clearly from other unrecombined cells which could still express another fluorescence protein like tdTomato (mT) [136, 137, 144].

1.8 The cGMP signaling cascade as an autoregulatory brake of thrombosis

Although it is generally accepted that the NO-cGMP signaling cascade is an endogenous platelet inhibitor, other reports have also described a stimulatory role of cGMP in platelet activation [105, 106, 145]. Taking this into consideration, the notion that the cGMP signaling pathway might play a biphasic role in platelet activation and inhibition has become more widespread [48, 107, 108, 146]. The problem remains that the underlying molecular mechanisms making the cGMP signaling pathway in platelets important in cardiovascular health and disease have yet to be uncovered in detail [139].

This is in part due to the fact that most of our knowledge of the cGMP signaling pathway in platelets comes from *in vitro* analyses of human and murine platelets which do not completely mimic the *in vivo* situation. Factors that have been described to affect platelet activity *in vivo* such as flow conditions and shear stress [147-149] were not considered in traditional end-point measurements of cGMP via ELISAs or RIAs. Therefore, the results from these experiments are hard to interpret in relation to the *in vivo* situation.

The problems limiting the interpretation of these traditional experiments were circumvented in the publication of Wen et al. in which transgenic cGMP sensor mice were used to study the spatiotemporal dynamics of cGMP signals in real-time under flow conditions [139]. Using murine platelets that express the FRET-based cGMP biosensor cGi500 (see chapter 1.7), it was possible to visualize and monitor cGMP level changes under flow in immobilized, pre-activated platelets. One striking

observation was that cGMP generation in pre-activated platelets in the presence of NO was highly shear-dependent **(Figure 6)** [139]. Thrombi that were formed in a flow chamber (explained in detail in chapter 2.4) generated cGMP **(Figure 6, black trace)** upon superfusion of an NO-donor, in this case DEA/NO. As soon as the flow was halted, the cGMP level dropped back to basal levels, despite the presence of NO, while switching the flow on again resulted in a cGMP increase **(Figure 6, black trace)**. These findings led to the conclusion that NO-induced cGMP generation in platelet thrombi is dependent on fluid shear stress [139].

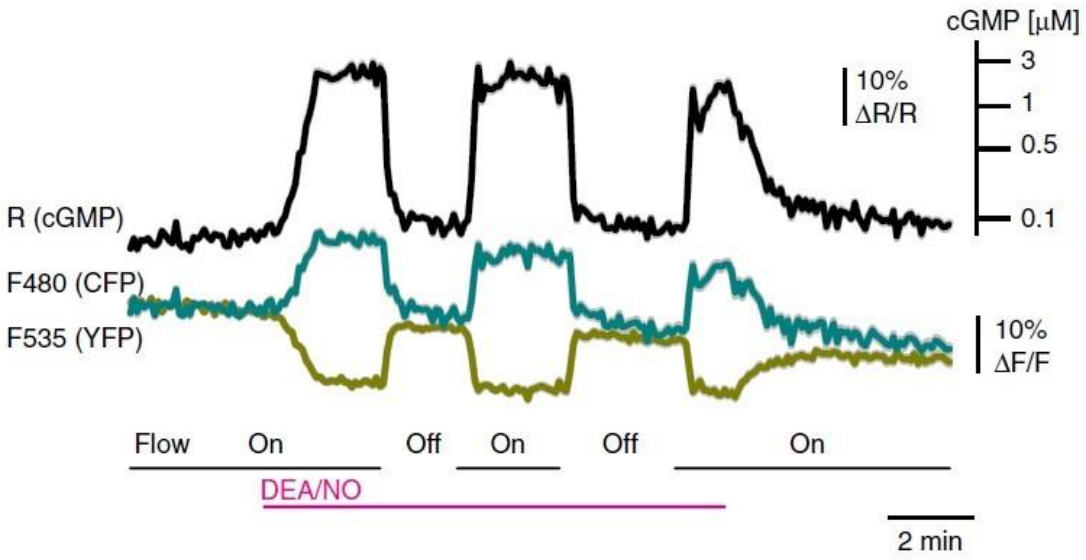

Figure 6. Shear-dependency of NO-induced cGMP signals in platelet thrombi.

Platelet thrombi expressing the FRET-based biosensor cGi500 were generated in a flow chamber and real-time cGMP signals were recorded. The teal and olive traces represent the CFP and YFP emissions of the FRET sensor, respectively. The black trace indicates the ratio change of CFP/YFP emission and therefore depicts relative changes in cGMP levels over time. Upon stimulation of the platelet thrombi with 100 nM DEA/NO (pink) under flow conditions (Flow On), cGMP is generated. After cessation of flow (Flow Off), cGMP levels drop back to basal levels. Repeated introduction and cessation of flow leads to repeated cGMP increases and decreases, respectively. Based on a calibration scale of the cGi500 sensor (upper right), cGMP signals reached levels ≥3 µM Note that the black cGMP peaks were "cut off" at approx.. 3 µM, presumably due to saturation of the cGMP sensor. The shear rate used in this experiment was $500s^{-1}$ and data is shown as mean ± SEM from n = 11 thrombi from 10 independent experiments. Taken from Wen et al., 2018 [139].

Further experiments showed that it is the cGMP synthesis via NO-GC which is the major shear-sensitive component in platelets [139]. Neither inhibition of the efflux of cGMP via MRP4 nor the inhibition of the degradation of cGMP via PDEs affected the flow-dependency of cGMP increases in the presence of NO [139]. Increasing cGMP levels led to a reduction of intracellular calcium concentrations and inverse changes when flow conditions were ceased, leading to the conclusion that cGMP inhibits intracellular calcium release via cGKI and the subsequent phosphorylation of IRAG

[82, 139]. In an intravital imaging setup (explained in detail in chapter 2.11), cGMP levels were also analyzed *in vivo*. Here, it became apparent that after a mechanical or laser-induced injury of a vessel, platelet cGMP signals were stronger in the periphery of the forming thrombus [139]. This is in-line with a model in which growing thrombi are exposed to increased shear forces at their periphery where they then generate more cGMP, which, in turn, leads to the inhibition of thrombus growth **(Figure 7)**. Consistent with this hypothesis, genetic deletion of platelet NO-GC led to significantly increased thrombosis *in vivo*, in particular an increased thrombus dissolution time, indicating that NO-cGMP signaling in platelets is important for limiting and stabilizing thrombus formation *in vivo* [139].

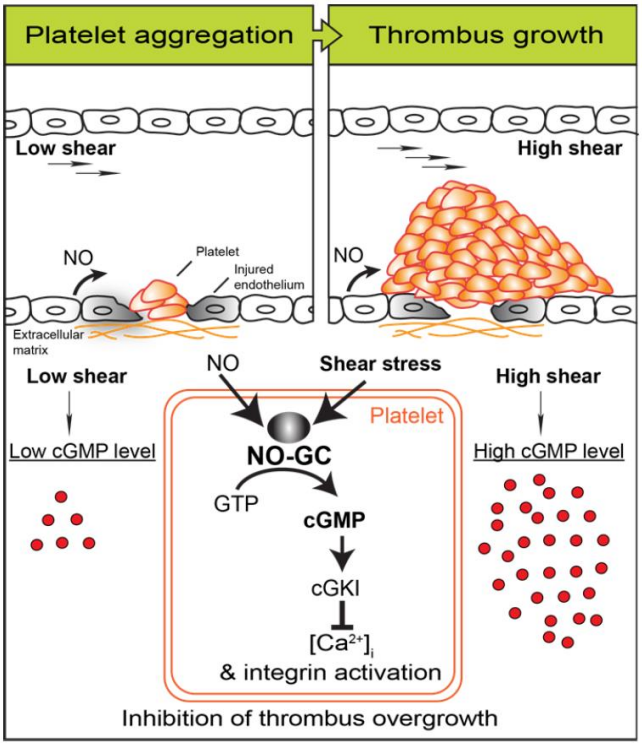

Figure 7. Model of the cGMP signaling cascade acting as a shear-dependent brake of thrombosis.

Upon initial vessel injury and low shear conditions (left side), low cGMP levels are present and platelet aggregation and plug formation is promoted. NO, supplied from the endothelium, and shear stress is necessary to induce cGMP generation via NO-GC. As the size of the growing thrombus increases, platelets become exposed to higher shear forces and in response generate more cGMP (right side). This leads to a downstream activation of the cGMP effector cGKI, which ultimately inhibits intracellular calcium release and integrin activation and therefore limits the overgrowth of the thrombus. Since the initial formation of a hemostatic plug happens under low shear conditions, it is not affected by the shear-dependent NO-cGMP-cGKI signaling cascade. cGMP-based drugs might be invaluable as anti-thrombotics, since they inhibit thrombosis without the side-effect of increased bleeding. Taken from Wen et al., 2018 [139].

Although Wen and colleagues attempted to identify mechanotransducers that could play a role in this mechano-cGMP cascade, the exact mechanism of how shear stress is sensed, transduced and connected to cGMP signaling has yet to be determined [139]. Due to the present data and model, we hypothesized that NO-GC, in a state of enhanced NO sensitivity [150], as well as cGKI localize to the cytoplasmatic side of the platelet plasma membrane where they are assembled into a larger signaling complex and where mechanical forces in the form of shear stress are

converted in to biochemical cGMP signals **(Figure 8)** [139]. This mechanism might be relevant not only in platelets, but also in VSMCs and probably several other cell types.

In the present study, we sought to characterize the elusive platelet cGMP signalosome and unravel the molecular mechanisms behind mechanosensitive cGMP signaling in platelets **(Figure 8)**. Insights into this process might prove to be invaluable, since drugs targeting the cGMP signaling pathway in platelets could serve as effective anti-thrombotics without the disadvantage of an increased risk of bleeding, which generally comes with anti-thrombotics used in the clinics.

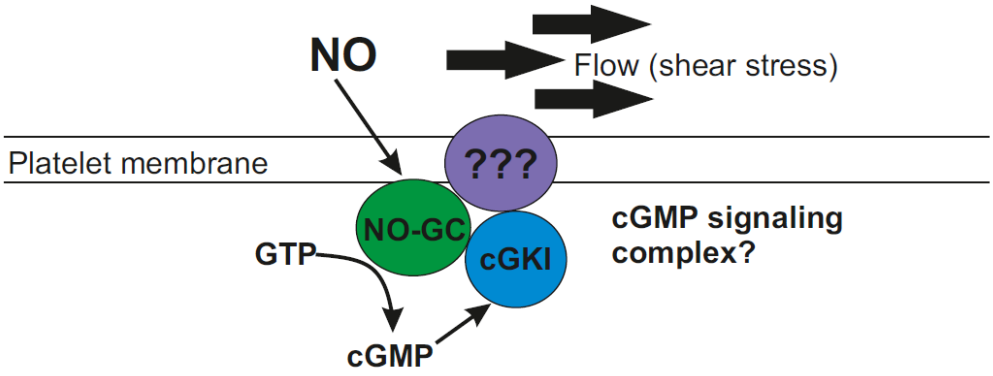

Figure 8. Working hypothesis of a cGMP signaling complex at the platelet membrane.

Platelets are exposed to shear stress at the membrane, where a yet to be identified mechanotransducer (purple) senses the mechanical force and converts it into a biochemical signal. Both NO-GC (green) and cGKI (blue) localize to the inner leaflet of the platelet membrane and together with a mechanotransducer and additional unknown proteins form a cGMP signaling complex. Upon stimulation of the cGMP signalosome by endothelial NO and shear stress, NO-GC generates cGMP, which activates cGKI and ultimately leads to an inhibition of thrombus overgrowth.

1.9 Aim of the work

The main aims of this work were (1) to elucidate the mechanistic basis of the mechano-cGMP signaling pathway in platelets *in vitro* and (2) to investigate the pharmacological relevance of platelet cGMP signaling *in vivo*. Based on the findings of Wen et al. [139] suggesting that NO-cGMP signaling in platelets is highly shear-dependent, it appeared important to dissect the exact mechanism of how shear stress is sensed, transduced and connected to cGMP signaling in platelets. To achieve these goals, we used rather traditional methods of biochemistry combined with transgenic mouse models and innovative methods for real-time imaging of cGMP signals in platelets under flow. Furthermore, the pharmacological relevance of the platelet cGMP signaling pathway was investigated *in vivo* to determine whether drugs altering cGMP levels in platelets can be used to limit thrombosis. To this end, using transgenic mice and an intravital imaging approach in the cremaster muscle, thrombi were generated in small blood vessels and their growth profile was analyzed in the absence and presence of the NO-GC stimulator Riociguat.

2. Materials and methods

2.1 General materials

2.1.1 Common reagents, chemicals, and antibodies

Table 1. Common reagents

Reagent	Company
1 kb plus ladder	Life Technologies
10x Lysis Reaction Buffer S	Bioron
2-mercaptoethanol	Carl Roth
2-propanol	Carl Roth
37% Hydrochloric Acid (HCl)	Carl Roth
Acetic Acid	Sigma-Aldrich
Agarose	Biozym
Ammoniumpersulfate (APS)	Carl Roth
Bovine Serum Albumin (BSA)	Carl Roth
Bromophenol blue	Carl Roth
$CaCl_2$ x 2 H_20	Merck
Citric Acid (anhydrous)	Carl Roth
D-Glucose	Carl Roth
Dimethyl sulfoxide (DMSO)	Carl Roth
dNTPs	Genaxxon
Ethanol	Sigma-Aldrich
Ethylenediaminetetraacetic acid (EDTA)	Carl Roth
Formaldehyde 37%	Chemsolute
Glycerol	Carl Roth
Heparin	Carl Roth
HEPES	Carl Roth
KH_2PO_4	Merck
Methanol	Sigma-Aldrich
$MgSO_4$ x H_2O	Carl Roth
Midori Green	Nippon Genetics
Milk Powder	Carl Roth
Na_2CO_3	Sigma-Aldrich
$Na_2S_2O_3$	Merck
NaH_2PO_4	Carl Roth
$NaHCO_3$	Honeywell
Nonidet P-40	Roche
Polysorbate 20 (Tween)	Carl Roth
Potassium Chloride (KCl)	Carl Roth
Proteinase K	Genaxxon
Rotiphorese Gel 30	Carl Roth
Silver nitrate	Carl Roth

Reagent	Company
SKF Solution	Takeda
Sodium Azide	Merck
Sodium Chloride (NaCl)	Carl Roth
Sodium dodecyl sulfate (SDS)	Carl Roth
Taq-Polymerase	Bioron
TEMED	Carl Roth
Tris-Cl	Carl Roth
tri-Sodium Citrate 2-hydrate	Carl Roth
Trizma (Base)	Sigma-Aldrich
WesternBright Peroxide	Advansta
WesternBright Sirius	Advansta

Table 2. Drugs and further compounds

Compound	Company	Stock
DEA/NO	Enzo	100 mM in 10 mM NaOH
Riociguat	Sigma-Aldrich	10 mM in DMSO
Collagen (fibrillar type I)	Takeda	1 mg/ml
Tirofiban Hydrochloride Monohydrate	Sigma-Aldrich	10 mM in EtOH
cOmplete mini (protease inhibitor)	Roche	1 tablet in 1 ml H_2O
PhosStop (phosphatase inhibitor)	Roche	1 tablet in 1 ml H_2O

Table 3. Common primary antibodies (ABs) for Western Blots

Primary AB	Species	Dilution	Source	ID
PECAM-1	goat	1:500	Santa Cruz	sc-1506
cGKI (DH)	rabbit	1:5000	In house made[151]	
sGCβ_1-2A	rabbit	1:10000	Kind gift from Andreas Friebe	
GAPDH	rabbit	1:1000	Cell Signaling	2118
VASP	rabbit	1:1000	Cell Signaling	3132
PDE5	rabbit	1:20000	Kind gift from Laurinda Jaffe	
MLCK	mouse	1:10000	Sigma Aldrich	M7905
CD41	rabbit	1:3000	Proteintech	24552-1-AP
SERCA3	rabbit	1:1000	Proteintech	13619-1-AP
CD29	rabbit	1:1000	Cell Signaling	DS61W
P-VASP Ser239	rabbit	1:1000	Cell Signaling	3114
CD61	rabbit	1:2000	Proteintech	8309-1-AP

Table 4. Secondary antibodies for Western Blots

Secondary AB	Dilution	Source	ID
α-goat IgG HRP linked	1:5000	Santa Cruz	sc-2020
α-rabbit IgG HRP linked	1:5000	CellSignaling	7074S
α-mouse IgG HRP linked	1:5000	Santa Cruz	sc-2055

Table 5. Common antibodies (FRET measurements)

Primary AB	Species	Dilution	Source	ID	Use
JON/A (PE conj.)	rat	none	emFRET	M023-2	Blocking
$\alpha_{IIb}\beta_3$	rat	none	emFRET	M021-0	Blocking
CD61	arm. hamster	none	BioLegend	104310	Blocking
CD41	rabbit	1:25	Proteintech	24552-1-AP	Blocking
CD29	rabbit	1:25	CellSignaling	DS61W	Blocking
PECAM-1	goat	1:500	Santa Cruz	sc-1506	Blocking

2.1.2 Buffers and solutions

Table 6. Buffers and solutions

ACD Buffer		
tri-Sodium Citrate 2-hydrate	85 mM	25 g/l
Citric Acid (anhydrous)	73 mM	14 g/l
D-Glucose	110 mM	15 g/l
Anode Solution I		
Trizma (Base)		36.3 g
Methanol		200 ml
H_2O		ad 1 l
Anode Solution II		
Trizma (Base)		3.03 g
Methanol		200 ml
H_2O		ad 1 l
Antibody Dilution Buffer		
TBS-T		50 ml
BSA	5% (w/v)	2.5 g
20% NaN_3	0.05% (v/v)	125 µl

Cathode Solution

6-Amino hexanoicacid	5.2 g
Trizma (Base)	3.03 g
Methanol	200 ml
H_2O	ad 1 l
Adjust pH to 7.6 with HCl	

6x DNA Loading Dye

Glycerol	30% (v/v)
10x TE Buffer	10% (v/v)
Bromophenol Blue	0.05% (v/v)
Xylene Cyanol	0.05% (v/v)

Hypotonic Buffer A (stock, pH 7.4)

EDTA	10 mM
NaH_2PO_4	10 mM

Hypotonic Buffer A (working solution)

Hypotonic Buffer A (stock)	4 ml
cOmplete mini (protease inhibitor) stock	500 µl
PhosStop (phosphatase inhibitor) stock	500 µl

Krebs Solution 1	Final (working)	
NaCl	118.4 mM	172.98 g
KCl	3.8 mM	7.09 g
$CaCl_2$ x $2H_2O$ (dissolve separately)	2.5 mM	9.19 g
$MgSO_4$ x H_2O		3.9 g
H_2O		ad 1 l

Krebs Solution 2

$NaHCO_3$	20 mM	42 g
KH_2PO_4	1.2 mM	4.08 g
H_2O	1.2 mM	ad 1 l

Krebs Buffer (working solution)

Krebs Solution 1		200 ml
Krebs Solution 2		200 ml
H_2O		ad 5 l
Keep pH at 7.4, bubble with:	(5% CO_2 in N_2)	

5x NP40

Glycerol	50% (v/v)	1 ml
Nonidet-P40	5% (v/v)	100 µl
Tris-Cl	100 mM	200 µl (1 M stock)
EDTA	750 mM	375 µl (4 M stock)
cOmplete mini (protease inhibitor)		325 µl (1 tablet in 341 µl H_2O)

Phosphate-buffered saline (PBS) (pH 7.4)

NaCl	135 mM	8 g/l
KCl	3 mM	0.2 g/l
NaH_2PO_4	8 mM	1.42 g/l
KH_2PO_4	2 mM	0.24 g/l
H_2O		ad 1 l
adjust pH to 7.4 if necessary		

10x RT (pH 8.0)

KCl	500 mM
Trizma (Base)	100 mM
$MgCl_2$	15 mM
dNTPs	2 mM

5x SDS LoadingDye

Tris (pH 6.8)	3.2 ml (1 M stock)
Glycerol	4 ml
SDS	1.5 g
2-Mercaptoethanol	2.5 ml
Bromophenolblue	10 mg
H_2O	ad 10 ml

10x SDS RunningBuffer

Trizma (Base)	30.2 g/l
Glycine	144 g/l
SDS	10 g/l

5x TBE

Tris-Cl	250 mM	30.29 g/l
Boric Acid	250 mM	15.46 g/l
EDTA	5 mM	10 ml/l from 0.5 M stock
H_2O		ad 10 l

10x TBS

NaCl	1.5 M	87.66 g
Tris-Cl	100 mM	12.11 g
H_2O		ad 1 l
Adjust pH to 8.0 with NaOH		

TBS-T

10x TBS		100 ml
Tween-20	0.10%	1 ml
H_2O		ad 1 l

4x Tris/SDS (pH 8.8)

Trizma (Base)		18.2 g
SDS		0.4 g
H_2O		ad 100 ml
Adjust pH to 8.8 with HCl		

4x Tris/SDS (pH 6.8)

Trizma (Base)		3.02 g
SDS		0.2 g
H_2O		ad 50 ml
Adjust pH to 6.8 with HCl		

10x Tyrode Buffer

$NaHCO_3$	120 mM	10 g/l
Hepes	100 mM	23.8 g/l
NaCl	1.37 M	80 g/l
KCl	27 mM	2 g/l
D-Glucose	55 mM	10 g/l

1x Tyrode Buffer

BSA	0.1%	0.1 g
10 x Tyrode Buffer		10 ml
H_2O		ad 100 ml

2.2 Mouse breeding and genotyping

2.2.1 Maintenance of mouse lines

Mice used in the experiments were housed in the former building of the Interfaculty Institute of Biochemistry at the University of Tübingen, Germany. The mouse lines were bred and kept under the following standard conditions of the animal facility: 20-22 ^{o}C room temperature, a relative humidity of 50-60% and a 12-hour dark and light cycle. Two types of cages were used, depending on the number of mice: Type II cages (Makrolon, 375cm^2) for keeping up to three mice and Type III cages (Makrolon, 820-840 cm^2) for up to eight mice. Standard rodent chow (Ssniff Spezialdiäten GmbH, Soest, Germany) was supplied *ad libitum* with permanent access to tap water. Autoclaved shredded wood chips (Tapvei Estonia OÜ, Harjumaa, Estonia) served as the bedding, while wooden tunnels (Tapvei Estonia OÜ, Harjumaa, Estonia) and tissues were provided as environmental enrichments. For breeding, one or two mature female mice (at least 8 weeks old) were sat together with a mature male mouse (at least 6 weeks old) preferably in the Type II cage of the male. Pregnant female mice were separated from the male and housed in a new Type III cage with extra nesting material (Nestlets, Emiscon-Jung GmbH, Forstinning, Germany) and dedicated breeding chow (Ssniff Spezialdiäten GmbH). 3 weeks after being born, the offspring was separated by gender and an ear tag was punched for later identification of the mice and to gain tissue biopsies for DNA extraction and subsequent genotyping via polymerase chain reaction (PCR) (see 2.2.2 and 2.2.3).

2.2.2 DNA extraction from mouse tissues

Ear tags (from 2.2.1) were used to extract DNA in order to genotype the mice via PCR. The tissue was lysed with PCR lysis buffer **(Table 7)** by incubating over night at 55 ^{o}C. Tissue was then completely dissolved by vortexing and then centrifuged at 11,000 rpm for 7 minutes to gain the DNA-containing supernatant, which was transferred to a new 0.5 ml PCR tube. The DNA and Proteinase K were then denatured at 95 ^{o}C for 15 minutes. Afterwards, the lysate was used for genotyping PCRs (see 2.2.3).

Table 7. Composition of the PCR lysis buffer.

PCR lysis buffer	per sample
10x Reaction buffer S	5 µl
Proteinase K (50 mg/ml)	1 µl
H_2O	44 µl
Total	50 µl

2.2.3 Genotyping PCR

To determine the gene variant, a genotyping PCR was performed using specific primers (see **Table 9**). Since these vary in optimal annealing temperature and produce products of different length, different PCR programs were used **(Table 10)**. Specific nomenclature was used for Cre/loxP mediated gene expression variants **(Table 10)**. While L2 denotes a gene flanked by 2 loxP sites (“flox”), L1 describes the presence of 1 loxP site after Cre-mediated excision of the floxed gene fragment **(Table 10)**. Each PCR reaction consisted of 2 µl of extracted DNA and a PCR master mix **(Table 8)**. At least one positive control for the respective PCR and one negative control using water were included in each run to validate the correct functionality of the PCR and to rule out eventual false positives due to contamination. PCR cycles were run in a thermocycler (Biometra TAdvanced) and upon completion, 5 µl of 6x DNA Loading Dye was added to each sample. A 2% agarose gel containing Midoori Green (8 µl per 200 ml Agarose) was prepared to separate and visualize PCR products. Using 12 µl of each PCR sample and 7 µl of the 1 kb plus ladder, amplified DNA fragments were separated by size by applying a current of 130 V. Bands were visualized using the Bio-Rad ChemiDoc imaging device.

Table 8. Composition of the PCR reaction buffer.

PCR Master mix	per sample
10x RT buffer	2.5 µl
Primer 1 (20 nM)	0.3 µl
Primer 2 (20 nM)	0.3 µl
(Primer 3) (20 nM)	0.3 µl
Taq Polymerase 5 U/µl	0.2 µl
H_2O	ad 23 µl
Total (incl. 2 µl DNA)	25 µl

Table 9. List of primers and their sequences.

Primer	Gene	Sequence (5' to 3')
BB01	R26-mT/cGi500(L2)	CTCTGCTGCCTCCTGGCTTCT
BB02	R26-mT/cGi500(L2)	CGAGGCGGATCACAAGCAATA
BB03	R26-mT/cGi500(L2)	TCAATGGGCGGGGGTCGTT
BB19	NO-GCβ_1	AAGATGCTGAAGGGAAGGATGC
BB20	NO-GCβ_1	CAGCCCAAAGAAACAAGAAGAAAG
BB21	NO-GCβ_1	GATGTGGGATTGTTTCTGAGGA
RF53	cGKI	CCTGGCTGTGATTTCACTCCA
RF118	cGKI	AAATTATAACTTGTCAAATTCTTG
RF125	cGKI	GTCAAGTGACCACTATG
iCre1	Pf4-Cre	GACAGGCAGGCCTTCTCTGAA
iCre2	Pf4-Cre	CTTCTCCACACCAGCTGTGGA

Table 10. List of PCR programs.

Allele	Primers	Product size	PCR Program		
			94 °C	3 min	
R26-mT/	BB01	flox (L2): 250 bp	95 °C	60 sec	
cGi500(L2)	BB02	wt (+): 330 bp	60 °C	45 sec	30x
flox (L2)	BB03		72 °C	60 sec	
wt (+)			72 °C	7 min	
			94 °C	3 min	
NO-GCβ_1	BB19	flox (L2): 720 bp	95 °C	60 sec	
flox (L2)	BB20	wt (+): 680 bp	63 °C	45 sec	30x
wt (+)	BB21		72 °C	60 sec	
			72 °C	7 min	
			95 °C	5 min	
cGKI	RF53	flox (L2): 338 bp	95 °C	10 sec	
flox (L2)	RF118	wt (+): 284 bp	50 °C	30 sec	35x
wt (+)	RF125	KO (L1): 250 bp	72 °C	30 sec	
KO (L1)			72 °C	5 min	
			95 °C	5 min	
iCre	iCre1	tg (tg): 500 bp	95 °C	10 sec	
tg (tg)	iCre2	wt: none	58 °C	30 sec	35x
wt (+)			72 °C	30 sec	
			72 °C	5 min	
			94 °C	3 min	
cGi500(L1)	BB01	L1: 250 bp	95 °C	60 sec	
L1	BB02	wt (+): 330 bp	60 °C	45 sec	30x
wt (+)	BB03		72 °C	60 sec	
			72 °C	7 min	

2.3 Blood sampling

2.3.1 Human blood

Fresh human peripheral blood samples were collected from healthy volunteers free of platelet-affecting drugs for at least 14 days and after they provided written informed consent. 11.25 ml blood was withdrawn slowly using a Safety-Multifly (21g, Sarstedt AG & Co. AG, Nümbrecht, Germany) into 20 ml syringes plugged to a Membrane Adapter (Sarstedt AG & Co. AG, Nümbrecht, Germany) while each syringe was filled with 3.75 ml ACD buffer (Total volume: 15 ml). The blood samples were then slowly transferred to 15 ml falcon tubes and further processed immediately (see 2.5) to avoid platelet activation. All experiments conducted using human blood were in accordance with relevant ethical standards and regulations and approved by the institutional ethics committee (Ethik Kommission an der Medizinischen Fakultät der Eberhard-Karls-Universität und am Universitätsklinikum Tübingen, 141/2018BO2).

2.3.2 Murine blood

Experiments using murine blood were in accordance with relevant ethical regulations and approved by the Regierungspräsidium Tübingen (IB 2/15 and IB 02/20 M). Mice were anesthetized with an intraperitoneal injection of anaesthesia (a mixture of fentanyl (0.05 mg/kg), midazolam (5 mg/kg) and medetomidine (0.05 mg/kg)) or by isofluorane inhalation. Afterwards, at least 1 ml blood was collected from the retroorbital plexus into a tube containing 300 µl of 20 U/ml heparin in PBS. 2 parts of blood were then supplied with 1 part of 1x Tyrode buffer and immediately processed for further experiments (see 2.4). After bleeding, a cervical dislocation was subsequently performed on the mouse.

2.4 Flow chamber FRET measurements

2.4.1 Flow chamber setup

Investigating the role of cGMP in platelets under flow conditions requires them to be in a closed chamber setup where they can be subjected to flow and therefore shear

stress in a controllable manner. To achieve this, a flow chamber setup was constructed **(Figure 9)**. Using this setup and platelets expressing the FRET-based cGMP biosensor cGi500, upon stimulation, it was possible to observe cGMP level changes over time under different flow conditions and treatments of the bound platelets.

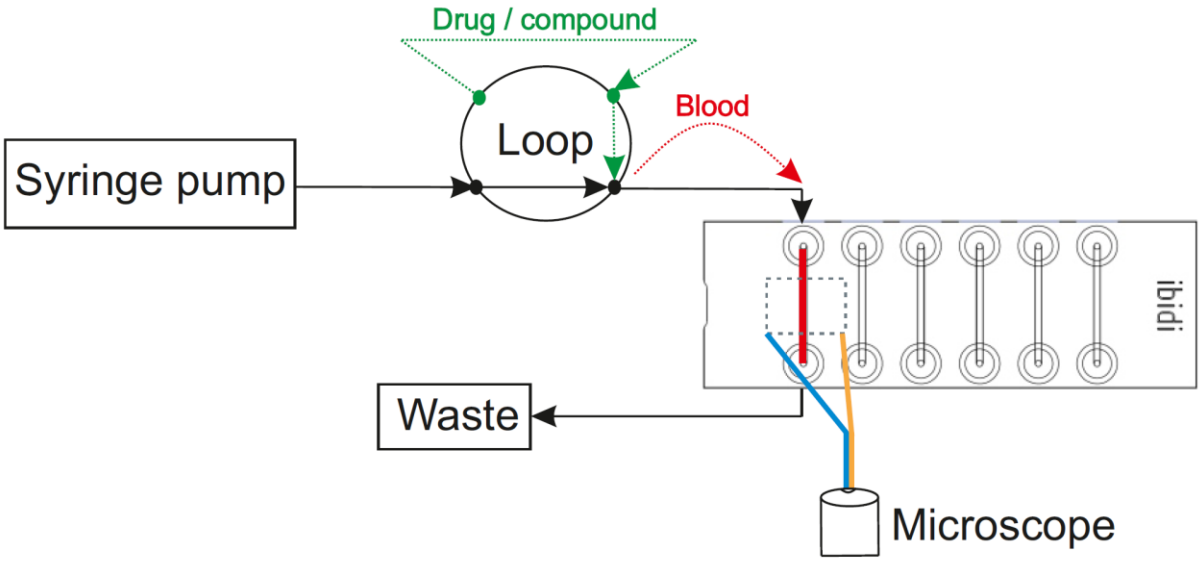

Figure 9. Flow chamber setup for real-time cGMP imaging in thrombi.

Whole blood is perfused through a collagen-coated flow chamber by a syringe pump. A loop can be used to apply any drug or other compound into the running system at any time without disrupting the flow. During perfusion of murine whole blood through the flow chamber, platelets become activated and form thrombi. If they express the FRET-based cGMP biosensor cGi500, an epifluorescence microscope can detect CFP (cyan) and YFP (yellow) emission to measure cGMP changes in real-time in any desired thrombus. Modified from Wen et al., 2018 [139].

Using a 1 ml syringe, flow chambers (ibidi µ-slide VI 0.1) were coated with 40 µl of 200 µg/ml collagen diluted in SKF Solution (isotonic glucose solution) in each chamber and incubated over night at 4 ^{o}C. Each chamber was blocked with 1% BSA in PBS for 20 min before use and then rinsed once with 1x Tyrode. The syringe pump (PHD200, Harvard Apparatus, Holliston, U.S.A.) was set to the correct syringe diameter (20 mm for 20 ml syringe) and a 20 ml syringe filled with 1x Tyrode Buffer was connected. For each chamber, 200 µl murine whole blood (see 2.3.2) was entirely perfused through the chamber (roughly 4 min) at room temperature at a shear rate of 500/s (flow rate setting perfusor: 46.72 µl/min), a value present in larger arteries physiologically [152], to generate thrombi. This flow and corresponding shear rate guaranteed the formation of sufficiently sized thrombi for analysis. The formed

thrombi inside the chamber were then incubated for 20 min at room temperature with 50 µl of antibodies, drugs or vehicle control per chamber to block specific receptors (see **Table 11**, Pre-incubation). After treatment they were continuously superfused with 1x Tyrode at room temperature for up to 15 min at a flow rate of 93.45 µl/min (1000/s shear rate), a shear rate commonly measured in smaller arterioles [152]. In this case, the flow rate was increased due to time constraints. Under these conditions, FRET measurements were performed. The flow was turned off at any point by stopping the perfusor and simultaneously clamping the waste connection to prevent backwards flow. For DEA/NO application, 500 µl 150 nM DEA/NO, which was first pre-diluted in 10 mM NaOH and shortly before application further diluted in 1x Tyrode Buffer, was applied through a loop (0.5 ml) together with the respective antibody, drug or vehicle control **(Table 5, Table 11)**.

Table 11. Drug and antibody dilutions for FRET experiments.

Antibody/drug	**Stock conc.**	**Pre-incubation (50 µl)**	**Perfusion (diluted in 2 ml)**
Tirofiban	10 mM in EtOH	10 µM in 1x Tyrode	10 µM in 2 ml 1x Tyrode
CD29	info n/a	2 µl + 48 µl 1x Tyrode	2 µl in 2 ml 1x Tyrode
CD41	0.5 mg/ml	2 µl + 48 µl 1x Tyrode	2 µl in 2 ml 1x Tyrode
CD61	1 mg/ml	50 µl stock	25 µg/ml
CD41/CD61	0.5 mg/ml	50 µl stock	25 µg/ml
JON/A	info n/a	50 µl stock	50 µl in 2 ml 1x Tyrode
PECAM-1	0.1 mg/ml	20 µl + 30µl 1x Tyrode	20 µl in 2 ml 1x Tyrode

Antibody/drug	**Stock diluted in**
Tirofiban	10 mM in 99% EtOH
CD29	10 mM Hepes, 150 mM NaCl, 100 µg/ml BSA, 50% glycerol
CD41	PBS, 0.1% NaN_3, 50% glycerol
CD61	PBS
CD41/CD61	PBS, 0.1% NaN_3
JON/A	20 mM Tris, 137 mM NaCl, 0.05% BSA, 0.09% NaN_3
PECAM-1	PBS, 0.1% NaN_3

2.4.2 *Ex vivo* flow chamber imaging setup and acquisition

The imaging setup consisted of an inverted microscope (Axiovert 200, Carl Zeiss AG, Oberkochen, Germany), a DualView beam splitter with a dichroic mirror (516 nm) and CFP (480/50 nm) and YFP (535/40 nm) emission filters (Teledyne Photometrics, Tucson, U.S.A.), as well as a CCD camera (Retiga R1, QImaging, Sarasota, U.S.A.). For FRET imaging, a computer-controlled light source (Oligochrome, Till Photonics, Gräfeling, Germany) with an electronic shutter excited CFP through a 445/20 nm excitation filter and was combined with a dichroic mirror (470 nm). The beam splitter (480/50 nm and 535/40 nm emission filters) then separated CFP and YFP emission for simultaneous recording using the CCD camera. The objective used was an LD A-Plan 10x/0.3 (Carl Zeiss AG, Oberkochen, Germany) with additional 1.6x optovar magnification (Carl Zeiss AG, Oberkochen, Germany). Before measuring FRET, a field of view was chosen by looking at the cGi500 fluorescence of the thrombi through the YFP filter set (excitation: 497/16 nm, emission: 535/22 nm). The VisiView software (Visitron Systems, Puchheim, Germany) was used for the entire acquisition process.

Images were acquired every 2 s (total cycle, 1 frame is therefore 2 s) with an exposure time of 300 ms and 2x2 binning up to a maximum duration of 15 min at room temperature.

2.4.3 Analysis of FRET data

After images were recorded using the VisiView software (version 4.0), they were further processed and evaluated offline using FIJI [153], Microsoft Excel (Microsoft Corp.) and Origin Pro 2016 (OriginLab Corp.).

Three individual thrombi and one background region devoid of visible thrombus formation per measurement were defined as regions of interest (ROIs) in FIJI. Mean fluorescence intensities (mean gray values) of the CFP and YFP time-lapse images were determined in all ROIs. The mean gray values were further processed with Microsoft Excel.

In Microsoft Excel, a FRET ratio trace was generated for every individual thrombus. This was done by first subtracting the CFP and YFP background intensities from

mean gray values recorded in the thrombus regions. Afterwards, the CFP/YFP ratio of the background-corrected values was determined. The ratio (R) was then normalized to the baseline at the beginning of each measurement (R_0 = mean of first 50 frames, before first drug application), and changes in cGMP levels were depicted as relative ratio changes ($\Delta R/R_0$). These $\Delta R/R$ traces represent the relative cGMP concentration changes in the selected thrombi normalized to the baseline. An Excel macro automating this procedure was kindly provided by Dr. Martin Thunemann.

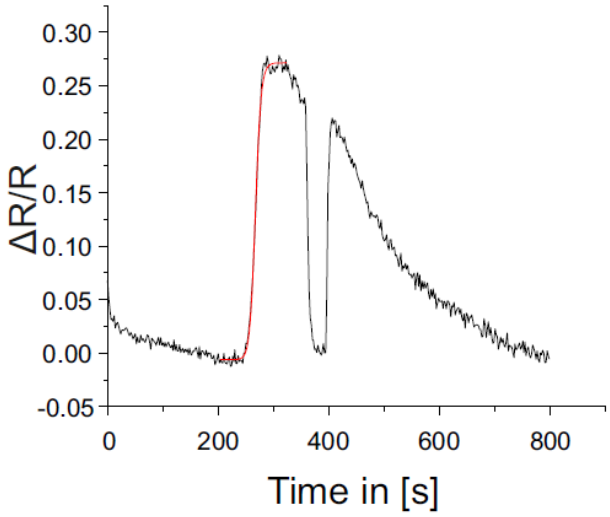

Model	Hill1
Equation	y = START + (END - STAR T) * x^n / (k^n + x^n)
Plot	E
START	-0.00603 ± 0.00123
END	0.27144 ± 0.00138
k	267.08848 ± 0.19144
n	52.87746 ± 1.74644
Reduced Chi-Sqr	3.46654E-5
R-Square (COD)	0.99797
Adj. R-Square	0.99786

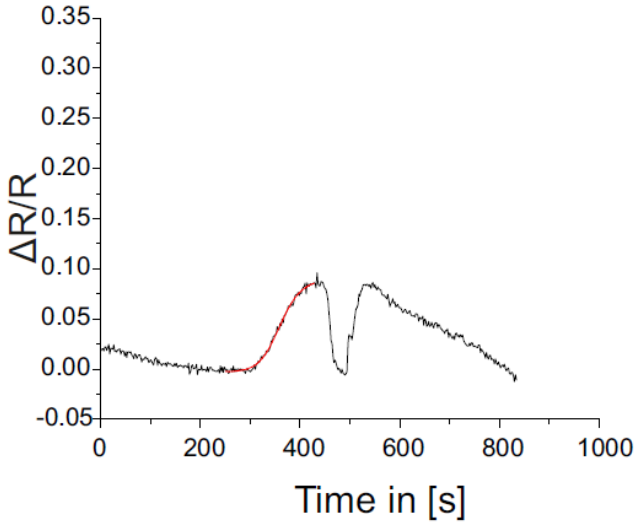

Model	Hill1
Equation	y = START + (END - START) * x^n / (k^n + x^n)
Plot	E
START	-0.0027 ± 5.41625E-4
END	0.09039 ± 0.00132
k	359.94367 ± 0.8672
n	16.87007 ± 0.60173
Reduced Chi-Sqr	5.35825E-6
R-Square (COD)	0.99525
Adj. R-Square	0.99509

Figure 10. Evaluation and determination of cGMP response and speed of cGMP generation.

Presented are representative $\Delta R/R$ traces of control (upper trace) and treated with antibodies or drugs (lower trace). Values were first baseline-corrected and a sigmoidal curve fit was applied from the baseline to the initial NO-induced cGMP peak (red line) using the Hill1 function ($y=START+(END - START)\ x^n/k^n+x^n$). The value n (green) is a representation of the slope of the curve and therefore speed of cGMP generation, while the determined END value (orange) indicates the peak height and the maximum cGMP generation. It has to be noted that the peak height is restricted to the point of sensor saturation, which probably occurs in a range between a $\Delta R/R$ of 0.25 and 0.3.

The ΔR/R values were then imported to OriginPro for further analysis. In a first step, ΔR/R traces were corrected for baseline drift by setting four anchor points: Two before drug application (baseline), one after the return of cGMP levels to baseline (after flow cessation) and one at the end of the measurement. The corrected ratio traces were used for evaluation. Peak height (END value) and slope (n value) of the initial NO-induced cGMP increase were determined after baseline correction using a sigmoidal curve fit according to the Hill1 function **(Figure 10)**. Both the peak height and n values of three different thrombi of each measurement were evaluated to compare the NO-induced maximum cGMP concentration and the generation speed, respectively.

2.5 Fractionation of human platelets

To analyze the cytosolic and membrane fractions of platelets separately, they have to be fractionated first. The fractionation protocol used here was based on the publication of Zabel et al. [150]. In short, platelets were isolated from whole blood, lysed using a hypotonic buffer and shock-freezing in liquid nitrogen, and then fractionated via ultracentrifugation **(Figure 11)**.

The entire fractionation protocol was performed uninterrupted in a time frame of roughly 6 h with up to 6 preparations in parallel:

1. Centrifuge 15 ml sampled human whole blood in 15 ml Falcons (see 2.3.1) at 320 g for 20 min at room temperature. The brake function of the centrifuge has to be turned off so that the blood can be clearly separated into 3 phases: The lower phase will contain the red blood cells, the middle one (small ring) the leukocytes and the upper, clear one the platelet-rich plasma (PRP).
2. Transfer the PRP to new 15 ml falcons while taking care not to include other phases from the preparation.
3. Centrifuge the PRP at 500 g for 12 min. The brake function of the centrifuge can be activated from here.
4. Discard the plasma and resuspend the platelet pellet gained from 15 ml whole blood carefully in 1.8 ml 1x Tyrode Buffer. While resuspending, use a cut pipette tip and pipet slowly to prevent the activation of the platelets.

5. If required, apply treatment to the different platelet suspensions:
   - Add 200 µl 1x Tyrode Buffer
   - Add 200 µl 1x Tyrode Buffer and vortex for 2 min at max. setting
   - Add 200 µl 100 µM DEA/NO in 1x Tyrode (final concentration: 10 µM)
   - Add 200 µl 100 µM DEA/NO and vortex for 2 min at max. setting
6. Centrifuge platelet suspensions at 20,000 g for 1 min at 4 ^{o}C.
7. Discard supernatant and lyse pellets in 250 µl Hypotonic Buffer A (working solution) each by resuspending.
8. Shock-freeze samples in liquid nitrogen and thaw on ice. Repeat this step a total of three times.
9. Centrifuge lysed samples at 1000 g for 2 min at 4 ^{o}C to remove cell debris.
10. Transfer supernatant to ultracentrifugation tubes (Beckmann-Coulter, Brea, U.S.A.).
11. Balance sample pairs exactly using a micro scale by adding Hypotonic Buffer A to match weights (equal eight up to 1 µg).
12. Ultracentrifuge samples at 100,000 g for 1 hour at 4 ^{o}C.
13. Collect supernatant in a new tube. This is the cytosolic fraction.
14. Carefully rinse the solid pellet once with 250 µl Hypotonic Buffer A.
15. Resuspend platelet pellet (membrane fraction) in 250 µl Hypotonic Buffer A by vortexing and pipetting.
16. Add 125 µl 5x NP40 to each sample (final concentration NP40: 1.66x). This is necessary to completely resuspend the membrane fraction by also rigorously vortexing. The same volume of NP40 is then also added to the cytosolic fractions, so that cytosolic and membrane fractions have the same final volume of 375 µl. This makes it easier to compare equal volume fractions in later experiments. Keep the 2:1 mixture of Hypotonic Buffer A (working solution) and 5x NP40 for future determination of protein concentration (see 2.6).
17. Store samples at -20 ^{o}C.

    Expected protein yields (determined using Lowry protein assay, see 2.6): membrane fraction: 0.4 - 0.7 µg/µl, cytosolic fraction: 0.8 - 1.1 µg/µl

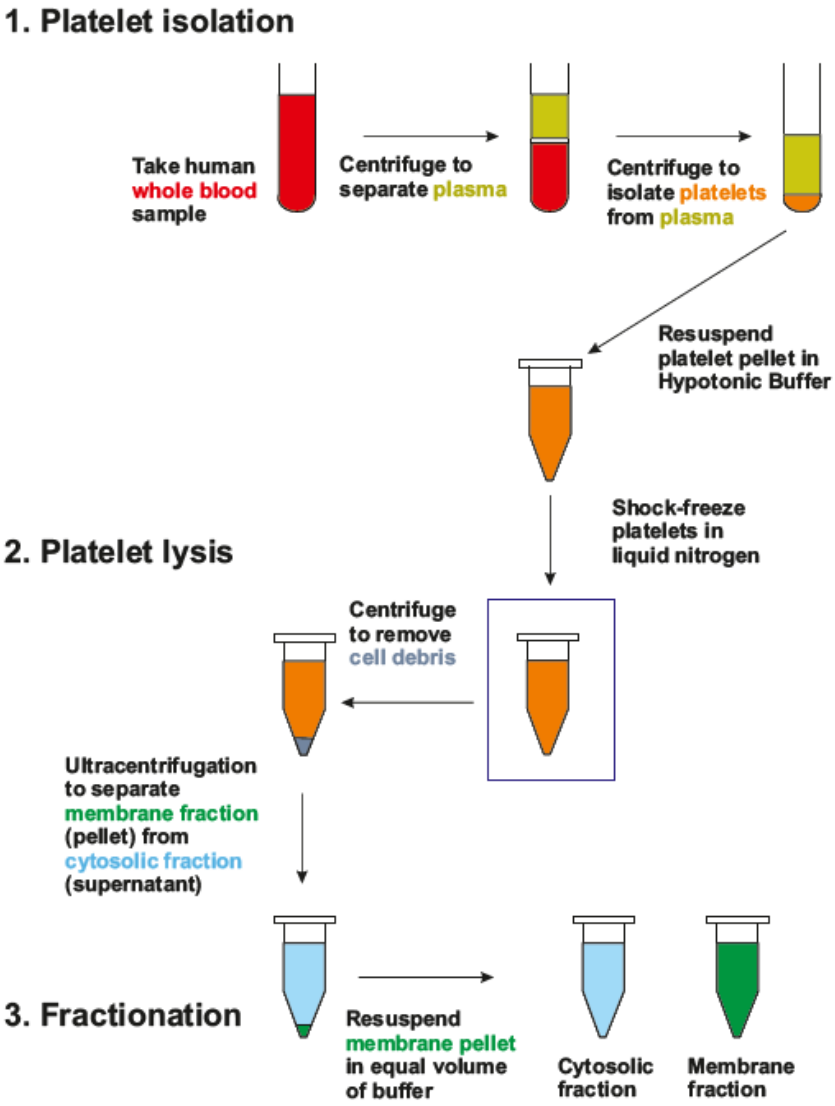

Figure 11. Fractionation of human platelets.

Human peripheral blood is collected and centrifuged to separate it into three phases: The lower phase containing the erythrocytes, a small white ring (called buffy coat) containing the leukocytes, and the upper phase consisting of the platelet-rich plasma. Platelets are then obtained from the plasma via another centrifugation step and resuspended in Hypotonic Buffer A. Platelets are then lysed by shock-freezing and thawing them multiple times. The cell debris is removed via centrifugation and the samples are now ready for the fractionation process. An ultracentrifugation step applying high centrifugal forces (100,000 g) is necessary to separate the platelet membrane from the cytosolic fraction. Both fractions are then diluted in an equal volume of hypotonic buffer and NP40 which allows a simple comparison of equal volume fractions of cytosol and membrane.

2.6 Determination of protein concentration via Lowry assay

The protein concentration of the cytosolic and membrane fraction of the fractionated platelets was determined using the Total Protein Kit (Sigma-Aldrich, St. Louis, U.S.A.). This kit, based on the Lowry method of determining protein content, uses the Peterson's modification. The Lowry protein assay is based on two reactions: In the

first step, the Biuret reaction, peptides with at least 2 peptide bonds form a colored chelate complex with Cu^{2+}-ions in an alkaline solution. In the second reaction the reduced copper ions in turn reduce the Folin-Ciocalteau reagent and a product (blue color) is formed which can be measured colorimetrically. A standard curve using known concentrations of bovine serum albumin (BSA) is used to calculate the protein concentration of the samples. The Lowry assay was performed in the following steps:

1. Prepare samples and standard in desired dilutions (total volume: 100 µl): For the standard curve, use a concentration series of: 12.5, 25, 50, 100 and 200 µg/ml. For cytosolic fractions, use a 1:20 dilution in H_2O and for membrane fractions, use a 1:10 dilution. H_2O and the corresponding relation of the sample buffer (Hypotonic Buffer A and NP40) are used as blank references. Always measure in duplicates.
2. Add 100 µl Lowry's reagent to each sample, vortex and incubate at room temperature for 20 min.
3. Add 50 µl Folin-Ciocalteau reagent to each sample, vortex and incubate at room temperature in the dark for 30 min.
4. Transfer 200µl of each reaction into a 96-well plate. Remove air bubbles using a lighter.
5. Measure optical density in an ELISA reader (Thermo Multiskan EX) at 620 nm.
6. Generate a standard curve of the BSA concentration series and calculate protein concentrations using the best fit line.

2.7 SDS-PAGE and Western Blot

The visualization of specific proteins in samples is commonly done via Western Blot. This is typically preceded by an SDS-PAGE (sodium dodecyl sulphate-polyacrylamide gel electrophoresis) where proteins are separated according to their molecular weight in a polyacrylamide gel. Proteins are then transferred electrophoretically from the gel onto a membrane (PVDF, polyvinylidene fluoride) in a process termed as "blotting". On this membrane, specific antibodies (primary antibodies, see **Table 3**) can bind their respective proteins. To detect the bound antibodies, a secondary antibody linked to an HRP (horseradish peroxidase) is added which binds the Fc part of the primary antibody. When subjecting the HRP

coupled to the secondary antibody to an ECL (enhanced chemiluminescence) solution, light is emitted and detected by a CCD camera (Bio-Rad ChemiDoc, Bio-Rad Laboratories, Inc., Hercules, U.S.A.).

2.7.1 SDS-PAGE

SDS gels were prepared using Bio-Rad's Mini Protean 3 system (Bio-Rad Laboratories, Inc., Hercules, U.S.A.). All gels were poured in the 1.5 mm thick version and 10-well combs were used to form the pockets in which the samples could be loaded. The SDS gel consists of 2 layers with the stacking gel poured on top of the resolving gel. The stacking gel makes sure that the proteins in each sample start the separation process in a straight line by transitioning into the resolving gel at the same time point. While making sure to pour the resolving gel first, the gel composition was as follows:

Table 12. Composition of SDS-polyacrylamide gels

Resolving gel (10%)	**Per gel**	**Stacking gel (4%)**	**Max. 3 gels**
Rotiphorese 30	3.3 ml	Rotiphorese 30	1.3 ml
4x Tris/SDS (pH 8.8)	2.5 ml	4x Tris/SDS (pH 6.8)	2.5 ml
H_2O	4.1 ml	H_2O	6.1 ml
APS (20%)	50 µl	APS	50 µl
TEMED	10 µl	TEMED	20 µl

The two glass plates were assembled in the stand and to check whether the construct is leaky, water was added in the space between the two plates. If it was tight, the resolving gel was poured as quickly as possible after APS and TEMED have been combined up to the lower green border of the stand. 500 µl of 2-propanol was then pipetted on each gel to remove air bubbles and to straighten the gel. After polymerization of the gel (roughly 30 min), the 2-propanol was removed with paper towels and the rest of the chamber was filled with the stacking gel. A comb was inserted into the gel before it polymerized. The gels were then used immediately or stored at 4 ^{o}C by wrapping them in wet paper towels and plastic wrap.

For the electrophoresis step, the gel was placed into the Mini Protean Tetra Vertical Electrophoresis Cell (Bio-Rad Laboratories, Inc., Hercules, U.S.A.) with the shorter glass plate side facing inwards. Both the inner and outer part of the chamber was now filled with 1x SDS Running Buffer. Before loading the samples, they had to be denaturated at 95 ^{o}C together with 1x SDS Loading Dye for 10 minutes. A maximum of 40 µl of sample was then loaded and 3 µl of a protein marker (PageRuler^{TM} Plus Prestained Protein Ladder, Thermo Scientific, Waltham, U.S.A.) was applied in at least one pocket. The electrophoresis cell was then closed and 100 V was applied until the sample transitions into the resolving gel, where the voltage was increased to 130 V.

2.7.2 Western Blot analysis

Once the proteins were separated by their size, they were blotted onto a PVDF membrane. For this, a semi-dry transfer was conducted. For each gel, 4 Whatman filter papers (Hartenstein, Würzburg, Germany) cut in the rough size of the gel were soaked in Anode Solution I, 4 in Anode Solution II and 8 in Cathode Solution. The PVDF membrane (also in the size of the gel) was rinsed in methanol for at least 2 min and shortly in Anode Solution II before use.

The 4 Whatman papers in Anode Solution I were then placed on the Anode of the Transfer chamber (Bio-Rad Laboratories, Inc., Hercules, U.S.A.) and the ones soaked in Anode Solution II were placed on top. On top of these, the PVDF membrane was carefully stacked along with the SDS-gel gently allocated on the membrane. After covering the stack with the 8 Whatman papers from the Cathode Solution, the transfer chamber was closed and for each gel, 60 mA was applied. The blotting process took a total of 80 minutes after which the membrane was taken out and cut at desired heights (judging by the ladder bands) depending on the different proteins one wished to analyze.

The membrane strips were then blocked with 5% milk powder in TBS-T to block unspecific binding of antibodies. After washing the membrane three times for 5 min with TBS-T, the membrane strips were incubated on a rolling shaker over night at 4 ^{o}C in a falcon tube containing the respective primary antibody (table 3) diluted in Antibody Dilution Buffer. The membranes were washed again three times with TBS-T

for 5 min and incubated in the appropriate secondary antibody (table 4) diluted in 1% milk powder in TBS-T for 2 h shaking at room temperature. After another washing step with TBS-T repeated three times for 5 min, the membranes were then developed.

1 part WesternBright Sirius was mixed with 1 part WesternBright Peroxide (1 ml total per gel) and applied onto the membrane parts. Chemiluminescent images were taken by the Bio-Rad ChemiDoc cumulatively in 10 second intervals typically for a total duration of 180 s. For evaluation and image processing, the software FIJI [153] and CorelDRAW were utilized.

2.8 Co-Immunoprecipitation

To investigate possible protein interactions, co-immunoprecipitations (Co-IPs) have proven to be a widely useful biochemical approach. For this, magnetic µMACS™ Protein A MicroBeads (Miltenyi) were used. In this approach **(Figure 12)**, a specific antibody was first designated as a “pulldown” antibody. This antibody is typically against the protein of interest for which interacting proteins are to be determined. The first step of the Co-IP involved binding the pulldown antibody (via its Fc-part) to Protein A. Since Protein A was coupled to the magnetic beads, this construct was used to “precipitate” the bound protein together with its interacting proteins. For this, the cytosolic and membrane fractions of platelets were added to the antibody bound to the magnetic beads. The antibody now bound the specific protein and by applying the fractions to a magnetic column, the protein of interest remained bound to the column together with its interacting partners. After several washing steps, the protein of interest along with interacting proteins was then eluted and further processed. The Co-IP was performed using the following protocol:

1. For one Co-IP, ideally 150 µg protein (0.4 - 0.7 µg/µl) in 1 part 5x NP40 and 2 parts Hypotonic Buffer A should be used. If protein amount does not suffice, the minimum amount is 75 µg of protein. For each Co-IP, a negative control (no pulldown antibody added) should be done in parallel to rule out unspecific precipitates.

2. Pre-clearing of protein samples: Incubate 50 µl µMACS^{TM} Protein A beads with 100-150 µg protein for 1 h on ice to remove proteins that bind unspecifically to beads.
3. Separate the supernatant from the beads using a magnetic separation rack (New England BioLabs) into a new tube. Magnetic beads are discarded.
4. Add 100 µl Protein A beads and 1 µl of the pulldown antibody (0.5 µg/µl) to the pre-cleared protein sample. Incubate this mixture for 2 h on ice while vortexing every 30 min.
5. Equilibrate the magnetic column (Miltenyi) with 200 µl 1x NP40.
   Note: Collect all the subsequent fractions (underlined) in different tubes in order to test precipitation efficiency.
6. Load the mixture of magnetic beads, lysate (and antibody) entirely on the column and collect the initial flowthrough.
7. Load the collected initial flowthrough on the column again to obtain the final Flowthrough fraction.
8. Wash the column with 300 µl 1x NP40 three times to obtain Wash 1 – Wash 3 fractions in three different tubes.
9. Heat 2x and 1x SDS Loading Dye to 95^{o}C. In order to elute the proteins bound to the column, first add 20 µl 2x SDS Loading Dye to each column and wait for 5 min. Then, add 50 µl 1x SDS Loading Dye and collect the Eluate (should have a volume of appox. 70 µl)
10. Store all collected fractions at -20 ^{o}C.

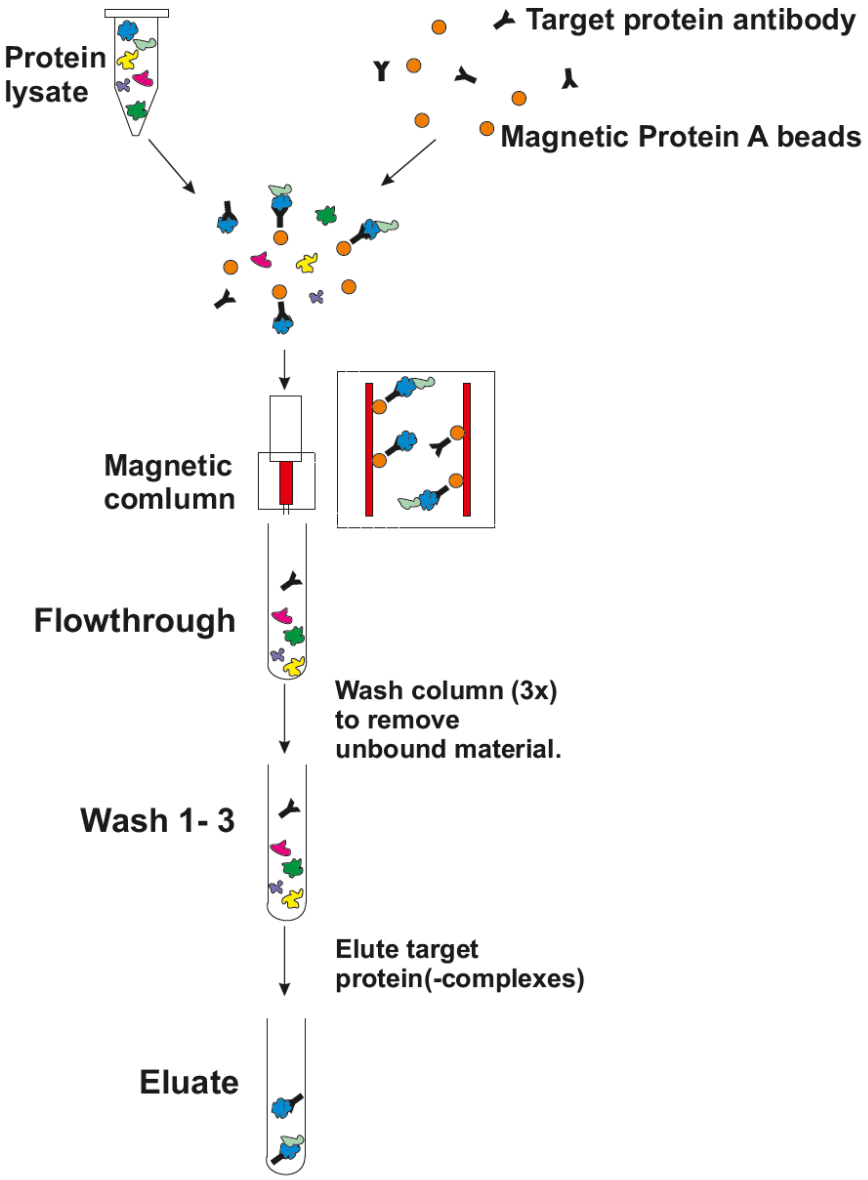

Figure 12. Co-IP principle.

A lysate containing proteins is incubated together with magnetic Protein A beads and an antibody targeting a desired protein. The Fc-part of the antibody binds Protein A which is coupled to magnetic beads, while the antibody also specifically binds the desired protein, linking it and other bound proteins to the beads. These are now applied onto a magnetic column, where the beads with the bound proteins are retained. Other proteins not bound to the column can be found in the flowthrough. The column is now washed three times to further remove unbound proteins. In the elution step, a buffer containing SDS is used to flush out the (co-)immunoprecipitates.

2.9 Silver staining

To check whether the quality of the eluates collected from the Co-IP (2.8) is sufficient for mass spectrometric analysis, a silver staining had to be performed beforehand. With this method, proteins are visualized in an SDS gel. A highly similar pattern of

bands on the SDS-gel was a requirement for further mass spectrometric analysis, as comparing inherently dissimilar samples would not lead to a meaningful result. For this, an SDS-PAGE (2.7) was performed with 7 µl of each membrane eluate (10% volume fraction). After running the SDS-PAGE, the silver staining of the gel is completed according to the following protocol:

Step	Solution	Duration
1. Fixation:	12 ml Acetic Acid	10 min
	40 ml Ethanol	
	50 µl Formaldehyde 37% (lab. hood)	
	ad 100 ml H_2O	
2. Wash	50% Ethanol	3 x 5 min
3. Impregnation	200 µl 10% $Na_2S_2O_3$	1 min
4. Wash	H_2O	3 x 20 sec
5. Silver Incubation	0.2 g $AgNO_3$	20 min
	75 µl Formaldehyde 37%	in the dark
	ad 100 ml H_2O	
6. Wash	H_2O	2 min
7. Develop	12 g Na_2CO_3	controlled
	8 µl $Na_2S_2O_3$	2 x 100 ml
	100 µl Formaldehyde 37%	
	ad 200 ml H_2O	
8. Wash	H_2O	2 x 2 min
9. Stop	40 ml Ethanol	10 min
	12 ml Acetic acid	
	ad 100 ml H_2O	
10. Wash	50% Ethanol	10 min
11. Wash	H_2O	store

The staining was documented using the ChemiDoc Imaging System (Bio-Rad Laboratories, Inc., Hercules, U.S.A.).

2.10 Mass spectrometry (MS)

Mass spectrometric analysis was done in collaboration with Stefan Loroch (AG Sickmann) from the Leibniz-Institut für Analytische Wissenschaften (ISAS) in Dortmund. Due to contaminants like keratin severely disrupting the mass spectrometric analysis, special precautions had to be adhered to: Every single utensil used for this experiment had to be sterilized and a face mask and hair net had to be worn. Since BSA also disturbs the measurement, the Tyrode buffer during the fractionation step for this experiment (see 2.5) had to be prepared without BSA. NP40 also negatively influences the analysis, which is why the columns during the Co-IP step (see 2.8) were equilibrated in 1x NP40 but all subsequent washing steps were performed with PBS only. Elution was performed with a 2x and 1x SDS elution buffer composed of the SDS Loading Dye without bromophenol blue. Only samples that passed quality control were examined further: A sufficient fractionation quality of the membrane fractions had to be confirmed via Western Blot and the silver staining (see 2.9) had to show a highly similar pattern of bands on the gel. All Co-IPs for this experiment were performed using 75 µg protein from membrane fractions from 4 different individuals. Samples from two different individuals were isolated in one preparation, with each individual providing blood for three fractionations (one triplicate per donor). Two samples per individual (pooling if necessary if protein amounts from single preparations were too low) were sent in dry ice for mass spectrometric analysis, with each sample undergoing two immunoprecipitations: One Co-IP with 1 µl pulldown antibody (cGKI) and one negative control without the addition of an antibody.

2.10.1 LC-MS sample preparation

Samples were then prepared for LC-MS at the Leibniz-Institut für Analytische Wissenschaften (ISAS). Cysteines were reduced in 10 mM dithiothreitol, incubated at 56 ^{o}C for 30 min and alkylated in 20 mM iodoacetamide for 30 min at room temperature in the dark. Proteins were precipitated by diluting the sample 1:10 in ice-cold ethanol (-40 ^{o}C) followed by vigorous mixing and incubation at -40 ^{o}C for 1 h. Precipitated proteins were spun down at 20,000g at 4 ^{o}C for 45 min and re-solubilized in 1.5 µl 6 M guanidinium hydrochloride (GuHCl) by mixing vigorously and

repeated freeze-thaw cycles at a temperature of -80 °C. For digestion, samples were diluted 1:20 in 50 mM ammonium bicarbonate and 1 mM $CaCl_2$.100 ng trypsin was added followed by an incubation step at 37 ^{o}C for 12 h. 10% of each sample was subjected to a monolithic column HPLC for digestion quality control [154] and 45% was analyzed by nanoLC-MS.

2.10.2 NanoLC-MS

NanoLC-MS/MS was conducted using a U3000 HPLC online-coupled to an LTQ Orbitrap Velos Pro mass spectrometer (both Thermo Fisher Scientific, Bremen, Germany including all HPLC columns). Samples were loaded onto a trap column (Acclaim PepMap100 C18; 100 µm x 2 cm) in 0.1% TFA at a flow rate of 14 µl/min. After 5 min, the pre-column was switched in-line with the main column (Acclaim PepMap100 C18; 75 µm × 15 cm) and peptides were separated using a 60 min binary gradient ranging from 2.5-30% acetonitrile in presence of 0.1% formic acid at 60°C and a flow rate of 300 nl/min.

The MS was operated in top15 data-dependent acquisition mode starting with a 300-1500 m/z MS scan at a resolution of 60,000, followed by up to 15 MS/MS of the most intense ions with assigned charge states of $z \geq +2$ using collision-induced dissociation. The maximum ion injection times were set to 100 ms for MS and MS/MS to reach automatic gain control target values of 10^6 and 10^4 for MS and MS/MS, respectively. The dynamic exclusion was set to 20 s and the polysiloxane at m/z 371.1012 was used as internal calibrant [155].

2.10.3 Analysis of MS data

Database search was conducted using Mascot 2.6 implemented in Proteome Discoverer 2.2 against Uniprot taxonomy human (October-2017, 20,238 target sequences). Trypsin was used as protease with a maximum of 2 missed cleavages and error tolerances were set to 10 ppm for precursor ions and 0.5 Da for fragment ions. Oxidation of methionine was set as variable and carbamidomethylation of cysteines as fixed modification. The false discovery rate was adjusted to 1% using the Percolator node [156] and only high confident proteins with ≥ 2 unique peptides

were kept. Features were assigned using the Minora feature detector. The protein list was imported into Microsoft Excel, intensities were log2-transformed and candidates were selected if p-values of the paired Student's T-test were ≤ 0.05.

2.11 Intravital imaging of thrombus formation

All intravital cremaster animal experiments fulfilled relevant ethical regulations and were approved by the Regierungspräsidium Tübingen (IB 2/15). The goal of these experiments was to examine whether cGMP level alteration via the drug Riociguat (Bayer AG, Leverkusen, Germany), an NO-GC stimulator, affects thrombus formation *in vivo*. To accomplish this experimentally, the cremaster muscle of an anesthetized mouse (male) was prepared to expose its blood vessels. After a laser-induced injury of an artery, ideally, platelets were activated and formed a thrombus at the site of injury. Thrombus formation and growth was documented in the presence and absence of Riociguat in order to detect a possible effect of the drug on platelet activity.

2.11.1 Cremaster preparation and *in vivo* experimental setup

Imaging of thrombus formation in a vessel in a living mouse has been described previously by Falati et al. [157]. For our *in vivo* experimental setup, the cremaster muscle of a mouse had to be prepared first **(Figure 13)**. Mice expressing the cGi500 sensor in recombined platelets (Cre expression under the Pf4 promoter, Pf4-Cre) and a red membrane-bound mTomato construct in non-recombined cells (Genotype: *R26-mT/cGi500-L2$^{fl/fl}$; Pf4-Cre$^{tg/+}$; NO-GCβ$_1^{+/fl}$*) were used for this experiment. Pf4-Cre-mediated recombination led to the excision of a stop-cassette flanked by loxP sites ("fl") after the mTomato fluorphore, which led to the expression of the cGMP sensor cGi500 solely in platelets and megakaryocytes [139, 140]. As it was planned to compare platelet-specific NO-GCβ$_1$ knockout mice to the respective control mice, we used heterozygous NO-GCβ$_1$ control mice (+/fl) in this experiment.

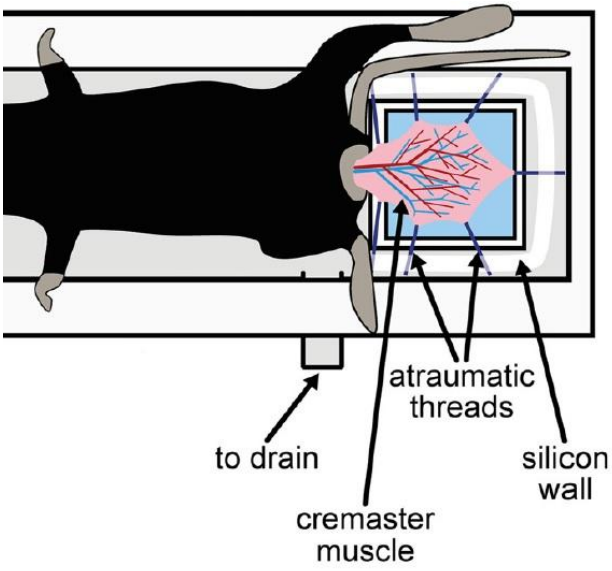

Figure 13.Cremaster muscle intravital imaging setup.

The anesthetized mouse is fixed on the custom-made stage as shown. The cremaster muscle is exteriorized and fixed on a stage (light blue) with atraumatic threads held in place by a silicon wall. A constant superfusion of Krebs Buffer is maintained by dripping the buffer on the exteriorized cremaster muscle at a constant rate (8 ml/min). To maintain a continuous superfusion, the buffer gets drained from the system through a connection at the bottom of the stage. For drug application, the drug dilution is simultaneously superfused into the buffer system at the same rate using a syringe pump (Harvard Instruments). Adapted from Thunemann et al., 2014 [140].

Mice were anesthetized by qualified personnel (Susanne Feil, Michael Böttcher) with a mixture of fentanyl (0.05 mg/kg), midazolam (5 mg/kg) and medetomidine (0.05 mg/kg) which was injected intraperitoneally. The cremaster muscle was then prepared by being laid open, cleared of residual connective tissue, and finally fixed on a custom-built stage so that imaging becomes possible. The body temperature of the mouse was maintained at 37 ^{o}C by heating the stage for the entire duration of the experiment. The exposed cremaster muscle was permanently supplied with a superfusion of Krebs Buffer (working solution) which was constantly bubbled with 95% N_2 and 5% CO_2. To induce thrombus formation, an injury on the outer side of an intact arterial vessel with a diameter of 30-60 µm was inflicted via an ablation laser (see 2.11.2). Arterial vessels were differentiated from venous vessels by determining a distal direction of the blood flow. Injuries were applied at the farthest part of the vessels as soon as it showed the appropriate size and unperturbed blood flow. Further injuries on the same vessel were performed upwards of the blood flow with a minimum distance of about 80-100 µm to the previous injury, as long as blood flow remained unperturbed. The first measurements were performed under control conditions, i.e. DMSO (Riociguat vehicle control) was simultaneously superfused into

the Krebs Buffer using a syringe pump. Both superfusions were set to 8 ml/min. After visualizing the formation of 1-3 thrombi under the control condition, the drug treatment was applied in the same mouse instead of the vehicle control by adding it to the superfusion in the same manner (8 ml/min). After the first application of Riociguat (10 µM in the superfusate of Krebs Buffer), the drug was superfused at the same rate for the remaining duration of the measurement which lasted for roughly 1 – 1.5 h.

2.11.2 *In vivo* imaging setup and data acquisition

The injury of the artery was induced 5 s after the start of acquisition by an ablation laser (Teem Photonics, Meylan, France) at a wavelength of 532 nm for a duration of 4 ms/pixel with an energy of >3 µJ on a spinning disk microscope. The setup consists of an upright Axio Examiner Z1 microscope (Carl Zeiss, Oberkochen, Germany), a Yokogawa CSU-X1 spinning disk confocal scanner, three diode lasers (445 nm, 488 nm and 561 nm) and a CCD camera (Sport Pursuit, Diagnostic Instruments). A 40x magnification water-immersion objective (W Plan-APOCHROMAT 40x/1.0 DIC VIS-IR, Carl Zeiss) was used for all measurements. YFP emission (525/50 nm) was measured after excitation using the 488 nm laser in platelets expressing the cGi500 biosensor. As a YFP fluorophore is part of the sensor, it can handily be used to visualize thrombus formation and development. Non-recombined cells emit an mTomato signal (ZET/405/488/561/635M, excitation using the 561 nm laser) and among other cells, the vessel wall is clearly labeled “red”. The software VisiView (Visitron Systems) was used for data acquisition. A wavelength series covering a bright field (exposure time: 200 ms), a YFP (exposure time: 250 ms) and an mTomato (exposure time: 100 ms) image was recorded (2x2 binning) with images taken every second (1 s total cycle). At least 65 frames (1 min after laser-induced injury) were recorded per measurement, depending on the longevity of the thrombus.

2.11.3 Analysis of cremaster data

Evaluation of the YFP image series was conducted with FIJI [153] based on the publication of Dubois et al. [158]. A region of interest (ROI) was drawn around the formed thrombus using a Z-projection (time-based using mean intensities) and an upstream region was drawn for background subtraction. A threshold value was set by using the mean maximum pixel intensity of the background region of each imageat each time point in order to create a binary mask [158]. The total number of pixels above the threshold value in the ROI covering the thrombus constitutes the size of the thrombus, quantified as the area covered. Thrombus growth profiles over time were generated for each thrombus with control and Riociguat treatment. The median thrombus growth profiles were compared for each condition. Thrombus persistence during the first minute after thrombus formation was determined by first calculating the area covered by thrombi over time in the ROI around the thrombus and normalizing each thrombus to their maximum value of covered area (so that the maximum size had a value of 1). The area under the curve (AUC) of each normalized growth profile curve was then measured with Origin Pro 2016 (OriginLab Corp.) for the first 30 s after injury (5 s – 35 s) and for the subsequent time window of 35 s – 65 s. If the AUC value of the latter time window was equal or higher than 50% of the AUC value of the initial 30 s window, the thrombus was regarded as “stable”, while values below 50% were deemed as “unstable”.

2.12 Statistical analysis

For statistical analysis, the data was first tested for normal distribution. For normal distribution, a two-sample Student’s *t*-test (equal variance) or Welch’s *t*-test (unequal variance) was performed with Bonferroni correction. For non-normally distributed data, a Mann-Whitney *U*-test was conducted. To test a statistical difference between two categorical variables, a χ^2-test was performed. Significance was indicated with asterisks, with * = $p \leq 0.05$, ** = $p \leq 0.01$ and *** = $p \leq 0.001$.

3. Results

3.1 NO-GC and cGKI are localized in the cytosolic and membrane fraction of human platelets

In a previous study, it was shown that cGMP concentrations were increased in the periphery of the thrombus where it is exposed to higher shear forces [139]. Based on the observation that cGMP seems to be generated as a response to elevated shear-stress, our working hypothesis predicted that components of the cGMP signaling cascade localize to the plasma membrane of platelets, where shear stress is sensed. Here, they would interact with a yet to be identified mechanotransducer and form a cGMP signaling complex at the membrane which generates cGMP locally after the exposure, sensing and transduction of shear stress.

While both the NO-GC and cGKI are generally regarded as cytosolic proteins, some studies have already described a membrane localization of cGKI [134] and NO-GC [145, 150, 159], supporting our working hypothesis. To test for a possible localization of cGMP signaling components at the platelet membrane, we fractionated human resting platelets into a cytosolic (C) and membrane (M) fraction **(Figure 14**, for an illustration of the method, see **Figure 11)**. Both fractions were then subjected to Western Blot analysis to determine the localization of cGMP signaling components, specifically cGKI, the β_1 subunit of NO-GC (NO-GCβ_1), PDE5, and VASP. Using marker proteins for cytosol and membrane to determine the fractionation efficiency, the relative localization of the different proteins was then visualized by loading equal volume fractions of cytosolic and membrane fractions **(Figure 14)**.

The separation of the cytosolic from the membrane fraction seemed effective, judging by the absence of the membrane marker PECAM-1 in the cytosolic fraction and the enrichment of the cytosolic marker GAPDH in the cytosol. Despite the enrichment, it has to be noted that in some fractionations, low amounts of GAPDH were also detected in the membrane fraction **(**e.g., **Figure 15)**. While on the one hand this might point towards a suboptimal fractionation efficiency, despite it being regarded as a standard marker of the cytosol, the possible presence of GAPDH at the membrane should not be excluded, as this phenomenon has been observed before [160]. Nevertheless, all analyzed cGMP signaling proteins were not only detected in the

cytosol, but also in the membrane fraction in varying relative quantities **(Figures 14-15)**.

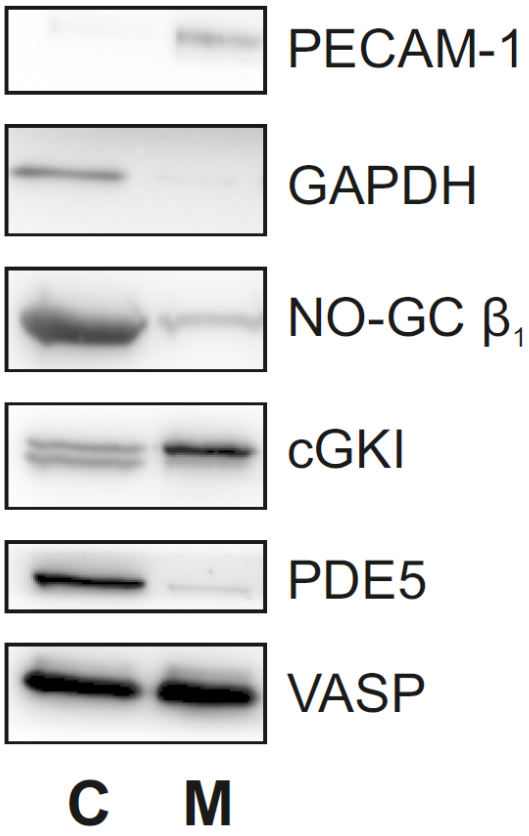

Figure 14. Fractionation of human platelets.

Human resting platelets were fractionated into cytosolic (C) and membrane (M) fractions. Loaded were 29 µl of the final dilution (375 µl) of cytosolic and membrane fractions gained from the preparation of platelets out of 15 ml whole blood. Western Blot analysis revealed the localization of cGMP signaling proteins NO-GCβ_1, cGKI, VASP, and PDE5. While PECAM-1 was used as a membrane marker, GAPDH served as a marker for the cytosol. Since equal volume fractions were loaded, the relative localization of all proteins in each fraction can be observed. The presented blot is representative for n=5 (cGKI), n=3 (PDE5), n=8 (NO-GCβ_1), n=4 (VASP) and n=8 (GAPDH) different experiments.

While VASP and cGKI were detected in roughly equal amounts in the cytosolic and membrane **(Figures 14-15)**, PDE5 was highly enriched in the cytosolic fraction. It also has to be noted that only the cytosolic fraction shows two bands for cGKI **(Figure 14-15)**. Moreover, the observation of others [150, 159] that NO-GCβ_1 is also localized in the membrane fraction was confirmed in our experiments, supporting the notion that a subcellular cGMP signaling complex at the membrane might exist.

Next, we checked whether shear stress or stimulation of the cGMP signaling pathway might alter the localization of the respective proteins. For this, we subjected the platelets to shear stress by vortexing, 10 µM DEA/NO to activate NO-GC, or to a combination of both before lysis, and subsequently compared the relative localization of the proteins via Western Blot analysis **(Figure 15A)**.

A

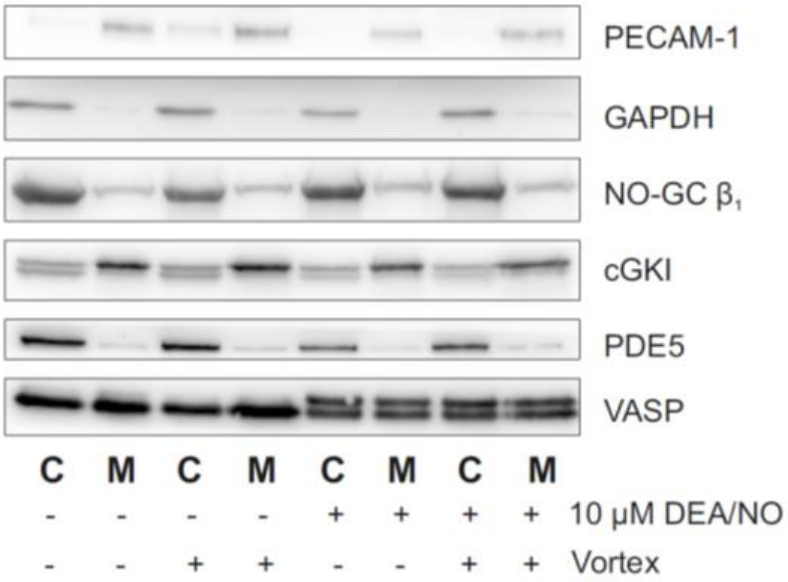

B **NO-GC**

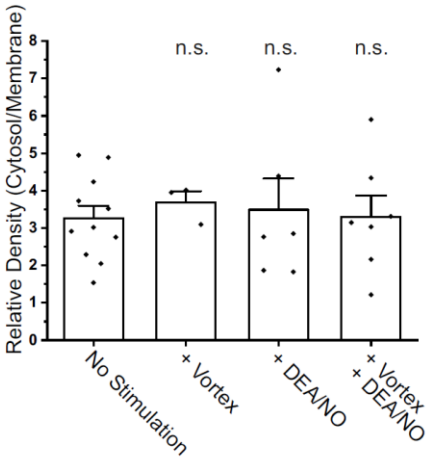

C **cGKI**

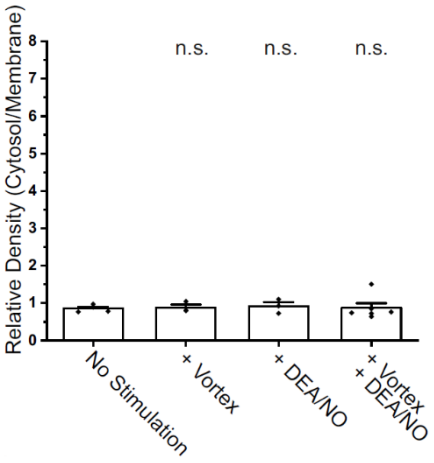

D **VASP**

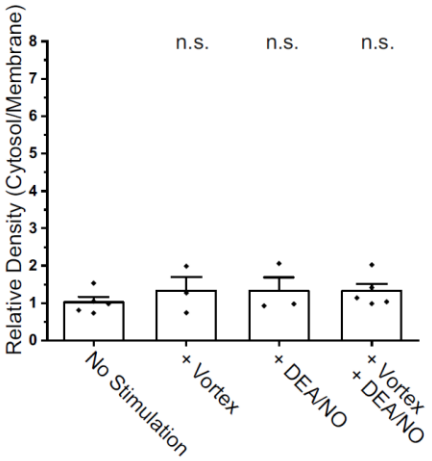

E **PDE5**

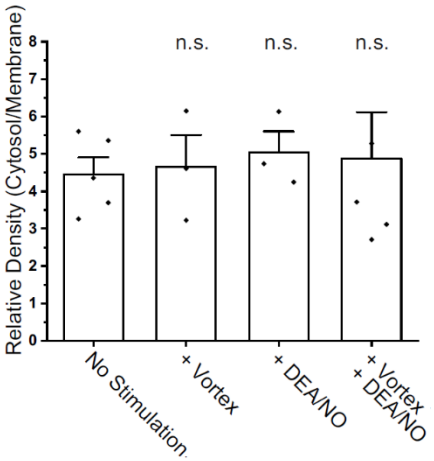

Figure 15. The localization of cGMP signaling components remains unchanged after NO stimulation and shear stress exposure.

(a) Before lysis, human platelets were subjected to 10 µM DEA/NO, shear stress by vortexing, or both for 2 min at room temperature. Loaded were equal volume fractions (29 µl) of the final dilution (375 µl) of cytosolic and membrane fractions gained from the preparation of platelets out of 15 ml whole blood.Stimulation with DEA/NO leads to phosphorylation of VASP, visible as a second band on the Western Blot. **(B)** – **(E)** Quantification of the band densities to determine the relative localization of cGMP signaling proteins NO-GC **(B)**, cGKI **(C)**, VASP **(D)** and PDE5 **(E)**, with n=8 (NO-GCβ_1), n=5 (cGKI), n=4 (VASP) and n=3 (PDE5). Statistical analysis was performed with student's *t*-test with n.s. = non-significant ($p>0.05$), All data is presented as mean + SEM.

Although stimulation with DEA/NO led to VASP phosphorylation, there was no observable change in the localization of cGKI, NO-GCβ_1, VASP or PDE5, as confirmed by the quantifications of the Western Blots **(Figure 15B-E)**. Applying shear stress also did not change the intraplatelet localization of the cGMP signaling components, even when combined with DEA/NO **(Figure 15B-E)**. The quantification data also shows the extent of how abundant specific proteins of the cGMP signaling cascade are in the membrane fraction compared to the cytosol. Both cGKI and VASP seemed to be equally abundant in the cytosol and membrane fraction (relative densities of roughly 1:1), while NO-GC, despite a clear presence in the membrane fraction, was still localized in a roughly 3-4-fold higher amount in the cytosol. PDE5 showed the highest relative cytosolic localization, in a relation of about 4:1 to 5:1. We also checked, whether stimulation of the platelets with DEA/NO and/or shear stress by vortexing prior to lysis change

Taken together, human platelets were successfully fractionated in cytosol and membrane fractions, with NO-GC, cGKI and VASP also being clearly present in the membrane fraction, supporting the possibility of a membrane-bound cGMP signaling complex generating cGMP.

3.2 NO-GC is co-localized with cGKI in the membrane fraction of human platelets

After determining the presence of both cGKI and NO-GCβ_1 in the membrane fraction of human resting platelets, we aimed to see whether not only a co-localization, but an interaction of these cGMP signaling proteins takes place here. For this, we used a Co-IP approach and put our primary focus on NO-GC and cGKI interactors. Unfortunately, a suitable NO-GC antibody for this approach was not available, which is why we were limited to the use of a cGKI pulldown antibody **(Figure 16)**. In this

approach, proteins interacting with cGKI should be co-immunoprecipitated and therefore also detected in the eluate.

First, optimization of the IP procedure was vital to efficiently co-immunoprecipitate and detect proteins interacting with the investigated cGMP protein kinase cGKI (data not shown). For this, different conditions regarding the amount of Protein A beads, pulldown antibody and protein lysate were tested. To visualize the efficiency of the entire IP procedure, especially regarding the cGKI pulldown antibody, equal volume fractions (10%) of each step of the entire Co-IP were loaded on a gel and analyzed via Western Blot **(Figure 16)**. Negative IP controls were conducted without a pulldown antibody to rule out potential unspecific binding to the column. While the flowthrough fraction denotes how much of the loaded lysate, more specifically the cytosolic or the membrane fraction, did not remain on the magnetic column, the following three washing steps remove otherwise weakly or unspecifically bound proteins. Despite the optimization procedures, it was still clearly visible that the efficiency of the IP was very low, as most of the input protein amount **(Figure 16A-B, Flowthrough)** was also found in the flowthrough. The IP of cGKI (and associated proteins) is achieved via the pulldown antibody which is coupled to magnetic Protein A beads. These remain on the column ideally together with all proteins interacting with the cGKI. Elution of the immunoprecipitated cGKI and its interactors then allows us to investigate and visualize whether specific proteins are present in the eluate and therefore interacting with cGKI in the different fractions. The Co-IP approach is also illustrated in **Figure 12**. Even though most of the cGKI proteins did not remain on the column after loading **(Figure 16A-B, Flowthrough)**, there was still precipitated cGKI visible in the eluate of both the cytosolic **(Figure 16A)** and membrane fraction **(Figure 16B)** with the negative control **(Figure 16A-B, lower halves)** excluding unspecific binding of cGKI to the column. To better detect co-immunoprecipitated proteins, a larger volume fraction (50%) was loaded **(Figure 16A-B, right)**. PECAM-1, which has been described to be a mechanotransducer [27, 44, 161] was tested in this experiment for an interaction with cGKI at the membrane, with GAPDH serving as a control for the cytosolic fraction.

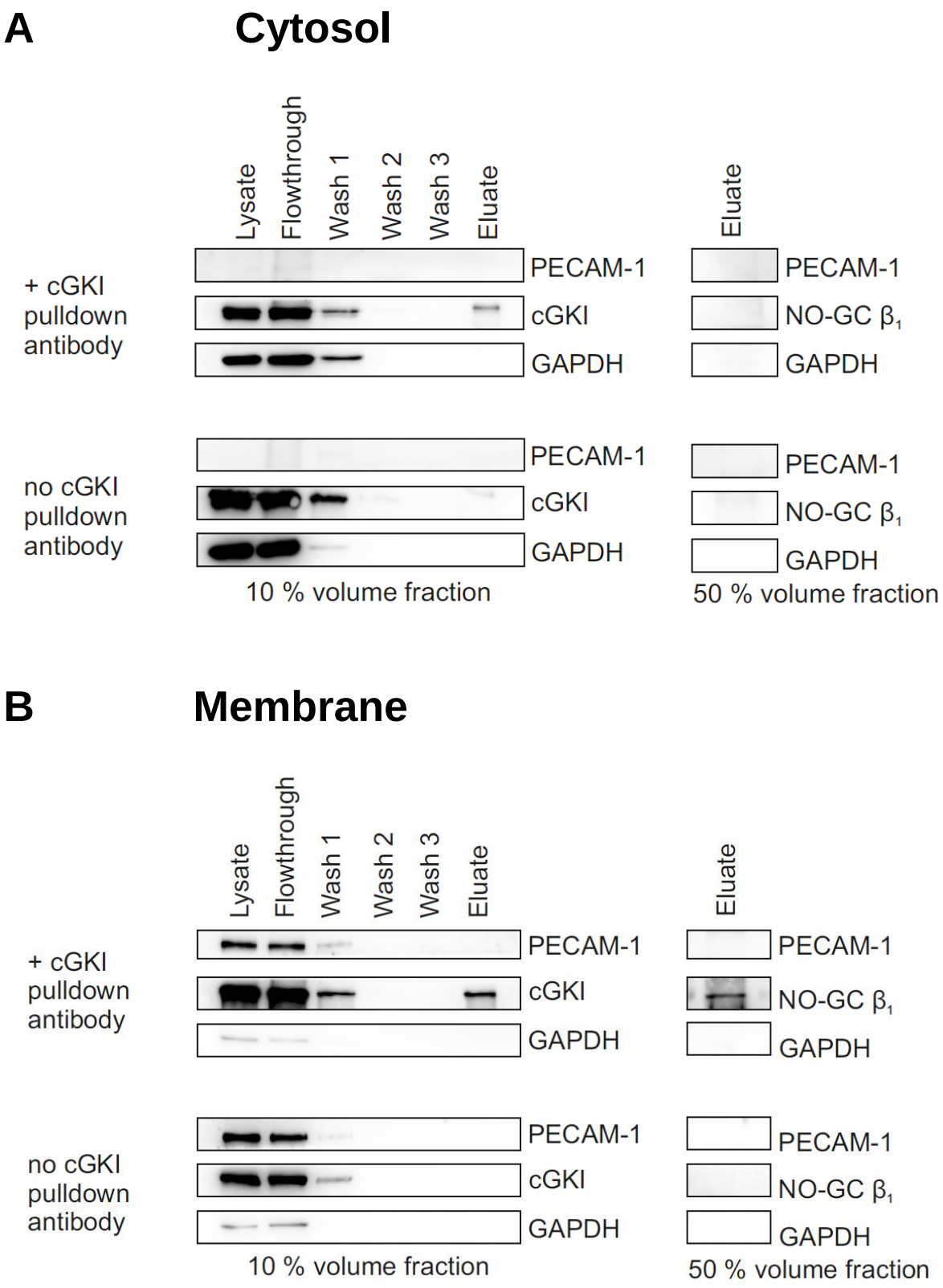

Figure 16. Co-IP of NO-GC and cGKI in the membrane fraction.

Western Blot analysis of the Co-IP of both cytosolic **(A)** and membrane fraction **(B)** of human platelets using a cGKI pulldown antibody. Initial input was 150 µg protein (lysate) from the fractionation procedure of platelets gained from 15 ml whole blood. Equal volume fractions (10%) of each IP step were loaded to enable a relative comparison of the amount of each tested protein (PECAM-1, cGKI, GAPDH) in each step. A larger volume fraction If the eluate (50%, right) was loaded to see a possible Co-IP of NO-GCβ_1, PECAM-1 or GAPDH. Presented blots are representative for n=3 for membrane and n=3 for cytosolic fraction IPs.

While neither membrane-bound PECAM-1 nor GAPDH was detected in any eluate, NO-GC was co-immunoprecipitated with cGKI in the membrane fraction **(Figure 16B)**, but not in the cytosolic fraction **(Figure 16A)**, pointing towards a membrane-restricted interaction (direct or indirect via additional proteins) between NO-GCβ_1 and cGKI. Both the negative immunoprecipitation controls without a pulldown antibody as well as the lack of PECAM-1 and GAPDH in the positive eluates support the notion that the Co-IP of NO-GCβ_1 is not due to an unspecific binding, but rather due to an direct or indirect interaction of the NO-GCβ_1 with the column-bound cGKI.

Taking all the results of this experiment into account, the Co-IP of NO-GC with cGKI hints towards an interaction of these cGMP signaling components specifically at the membrane of platelets, possibly to increase cGMP levels in response to shear stress.

3.3 Integrins physically interact with cGKI at the human platelet membrane

To identify other proteins that potentially interact with cGKI at the membrane of platelets, a discovery-oriented approach that analyzes all interactions in parallel was necessary. We therefore prepared cGKI Co-IP samples of the membrane fraction from human resting platelets for mass spectrometric analysis. The comparison with the Co-IP without the addition of a pulldown antibody serving as a background control allowed us to rule out all unspecifically bound proteins. The Co-IP with the addition of the cGKI pulldown antibody was checked for specifically enriched proteins precipitated with cGKI.

Prior to a mass spectrometric analysis, the Co-IP samples had to be tested for their compatibility. A meaningful mass spectrometric and subsequent statistical analysis requires similarly prepared samples and controls, with as little deviation in terms of protein presence and concentration from each other as possible. For this, a silver staining protocol had to be performed beforehand to test whether all samples show a similar pattern of protein bands after separation via gel electrophoresis **(Figure 17)**.

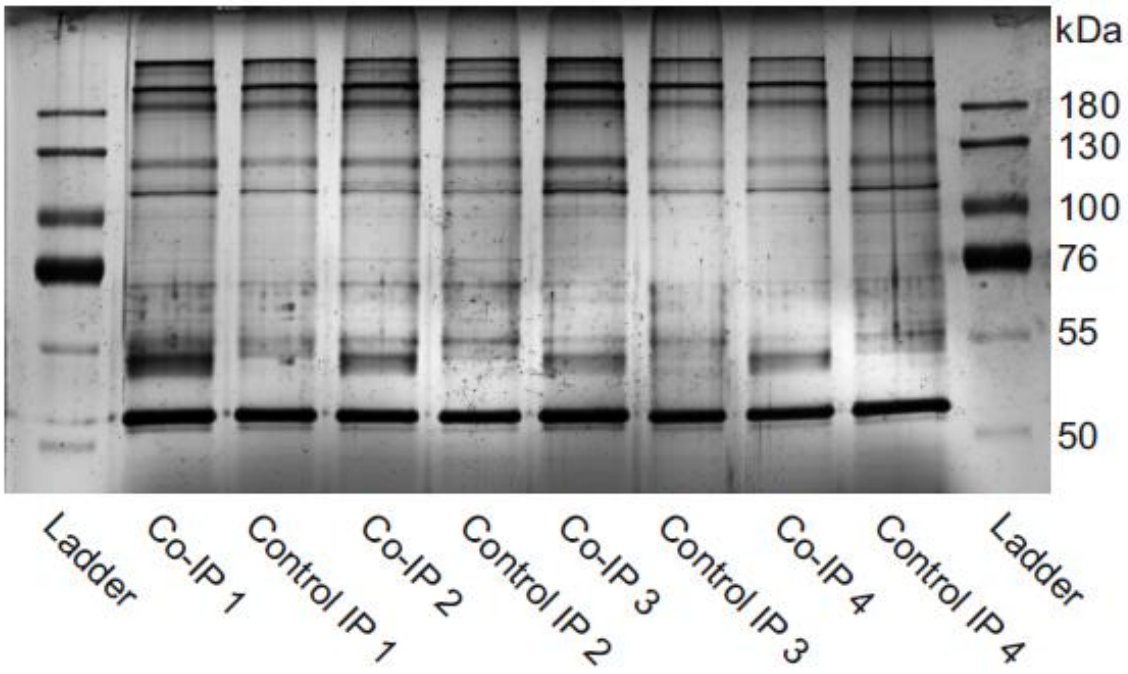

Figure 17. Silver staining of membrane co-immunoprecipitates.

Silver staining of the co-immunoprecipitates gained from the membrane fraction of human platelets using a cGKI pulldown antibody. Loaded were equal volume fractions (29 µl) of the final dilution (375 µl) of membrane fractions gained from the preparation of platelets out of 15 ml whole blood. Co-IP samples performed with a cGKI pulldown antibody are loaded beside the respective control IP which was done without the addition of a pulldown antibody. The samples shown here were gained from two different individuals, each with two pairs of Co-IP and respective control IP. The protein ladder denotes protein sizes.

Several protein bands became visible after the staining, with each sample showing a highly similar pattern **(Figure 17)**. Considering that the control Co-IP (without pulldown antibody) also showed several and even prominent protein bands, it can be said that many proteins bound to the column unspecifically during the Co-IP process which are then eventually eluted. Since both positive Co-IP and the respective control IP showed a highly similar pattern of proteins bands, the negative IP seemed to be a useful control to rule out the background and to specifically check which proteins are enriched in the respective positive Co-IP. The only visible difference between positive Co-IP and negative controls was a band only visible in the positive Co-IP samples located slightly below the 55 kDa ladder band. This band can almost certainly be attributed to the cGKI pulldown antibody (IgG heavy chain at about 50 kDa) which was not added to the control.

In sum, it can be concluded that our Co-IP samples from membrane fractions of human platelets were compatible for mass spectrometric analysis, as they exhibited a similar pattern of (mainly unspecifically) eluted proteins. These were eventually ruled

out after the mass spectrometric analysis using the negative IP samples as the background control. Only the proteins that were enriched in our positive cGKI Co-IPs as compared to the negative control were therefore regarded and further analyzed.

After subjecting our co-immunoprecipitates to mass spectrometric analysis, we identified over 500 proteins in our Co-IP eluates and close to 60 significantly enriched proteins in the positive Co-IP sample compared to the negative control **(Appendix)**. Many of the highly enriched proteins observed are connected to vesicle trafficking (including SNAP23, TAO3, catalase and actin-related protein 2/3 complex). However, we decided to focus on the components of the cGMP signaling pathway **(Figure 18, blue)** and potential mechanotransducers **(Figure 18, red)**. As we used a cGKI pulldown antibody for immunoprecipitation, cGKI was highly enriched compared to the negative control, roughly in an 8-fold manner **(Figure 18)**. This indicates that the immunoprecipitation of cGKI was effective and thus provides a basis for the further analysis of interacting proteins. The significant enrichment of known cGKI interactors (IRAG and IP_3R) [82, 134] in the positive eluates compared to the negative control additionally substantiates the effectiveness of our Co-IP method. Furthermore, the sarcoplasmic/endoplasmic reticulum calcium ATPase (SERCA), an enzyme transporting calcium ions out of the cytosol, was also enriched in the eluates **(Figure 18)**. As for potential mechanotransducers, several integrins were also significantly enriched in our positive Co-IP, including integrin α_6, α_2, α_{IIb}, β_1 **(Figure 18, red)**. Integrins not only are essential for platelet activation, but they have also been described to play a role in mechanotransduction in endothelial cells and platelets [43, 44, 49]. Due to them playing a significant role in platelet physiology, magnified by the fact that several commercially available drugs target this receptor, we primarily chose to put our focus on the fibrinogen receptor (integrin $\alpha_{IIb}\beta_3$). Furthermore, we also decided to include the significantly enriched β_1 subunit of the collagen receptor ($\alpha_2\beta_1$) in our study. Both receptors presented themselves as suitable candidates for transducing mechanical stimuli into a biochemical signal connected to cGMP signaling. Although the significant enrichment of integrin α_6 (part of the laminin receptor $\alpha_6\beta_1$) was not further regarded in this study, it should not be ignored in future investigations.

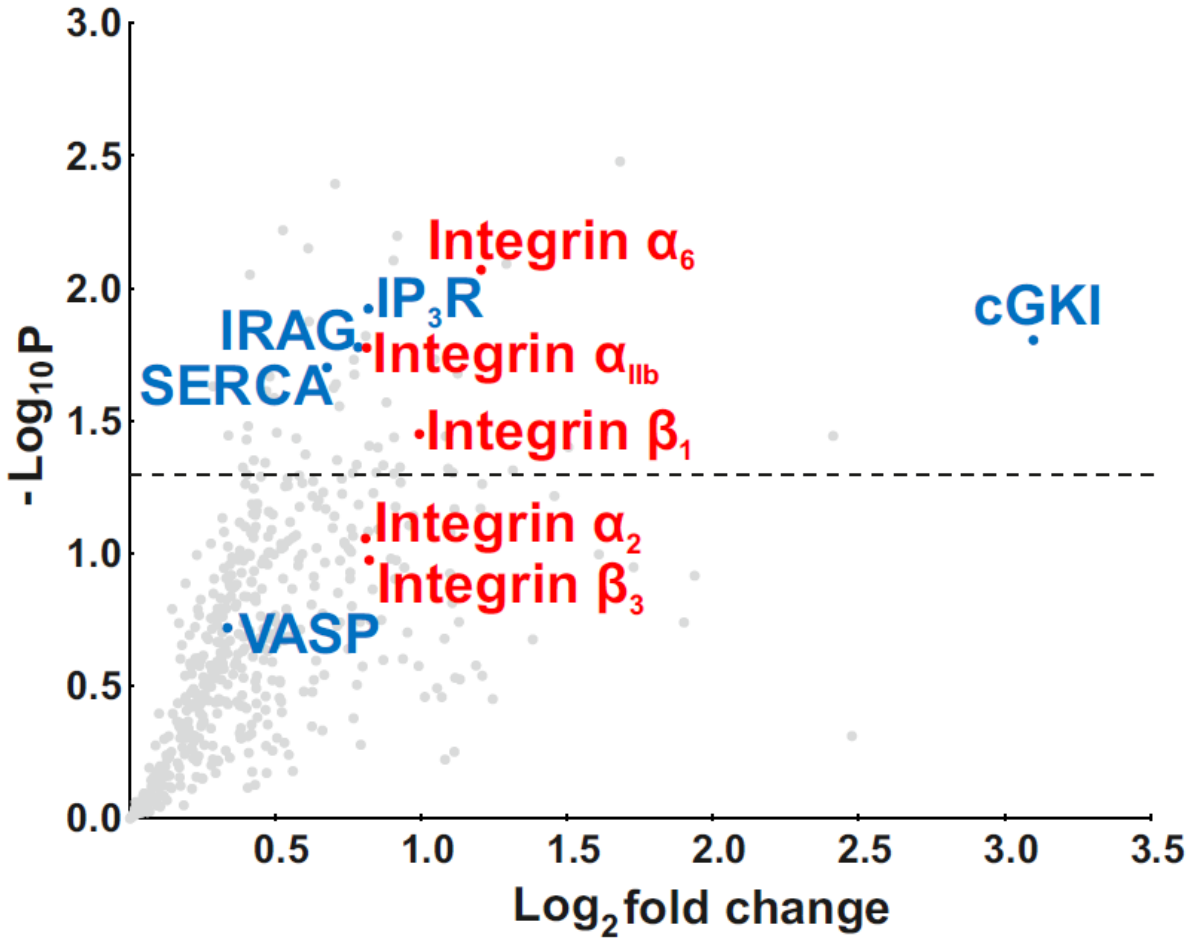

Figure 18. Volcano plot of MS data of cGKI Co-IPs of human platelet membranes.

Volcano plot showing all identified proteins (gray dots) enriched (higher amount on average) in the positive cGKI Co-IP compared to the negative IP control. Platelet membrane isolates from n=4 individuals with duplicates of both positive and negative Co-IP were used in the mass spectrometric analysis (performed by AG Sickmann, ISAS, Dortmund). The Log_2 fold change shown on the X-axis depicts the enrichment of the respective protein compared to the negative control. The Y-axis indicates the statistical significance of the respective enrichment. Components of cGMP signaling are marked in blue, while the integrins are colored red. The dotted line (at y=1.3) shows statistical significance with p=0.05 after calculation via paired student's *t*-test.

When tested for their intraplatelet localization, each of the three integrins was almost exclusively found in the membrane fraction with a small amount of integrin α_{IIb} detected in the cytosol **(Figure 19A)**. To confirm the MS data, we looked for the integrins in the eluates of the cGKI Co-IPs by Western Blotting **(Figure 19B)**. All three integrins were detected in the eluate of the positive Co-IP along with cGKI and NO-GCβ_1. Only integrin α_{IIb} was found to bind to the column unspecifically to a small extent, as seen in the negative Co-IP control **(Figure 19B**, "Eluate no AB"**)**. SERCA was also enriched in the membrane fraction **(Figure 19A)**. The positive cGKI Co-IP of SERCA which was detected by MS was also confirmed by Western Blot analysis (data not shown).

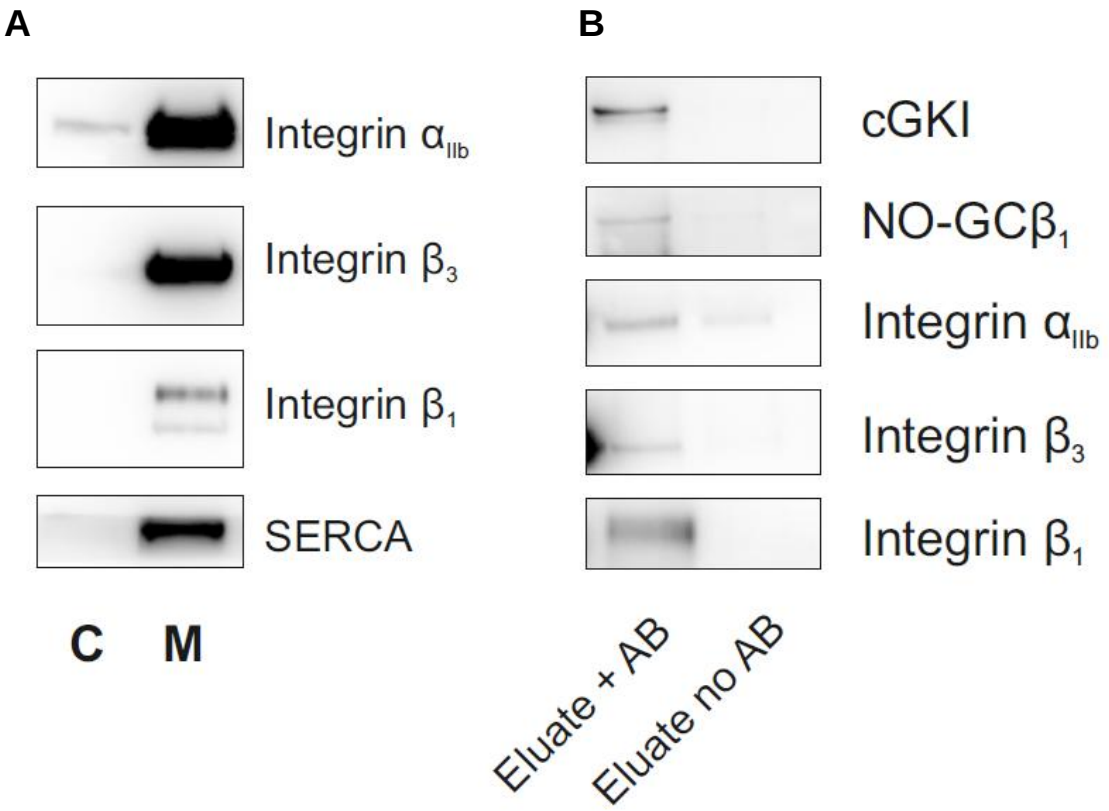

Figure 19. Integrins co-immunoprecipitate with cGKI in the membrane fraction of human platelets.

(A) Fractionated human platelet samples were tested for the presence of integrin α_{IIb}, β_1 and β_3 as well as SERCA in cytosolic (C) and membrane (M) fractions by Western Blotting after they were identified by MS. Loaded were equal volume fractions (29 µl) of the final dilution (375 µl) of cytosolic and membrane fractions gained from the preparation of platelets out of 15 ml whole blood **(B)** Membrane fraction Co-IP of cGKI, NO-GCβ_1 integrin α_{IIb}, β_1 and β_3 using a cGKI pulldown antibody (AB). Loaded were 50% of the entire eluates. All blots are representative for n=3 experiments.

Hence, we identified several proteins interacting with cGKI at the membrane of human platelets, including already described interactors such as IRAG and IP_3R [82, 134]. Several integrins were also enriched in the cGKI Co-IP samples and these might prove to be the missing link which can transduce the mechanical stimulus of shear stress into a biochemical cGMP signal, as they have already been described to be important mechanotransducers in platelets and other cells.

3.4 Blocking of integrin α_{IIb}, β_3 and β_1 attenuates the shear-dependent cGMP response in thrombi *ex vivo*

To further investigate a possible interaction between cGMP signaling and the different integrins, we examined whether a functional link between these two components exists. Our approach was to block or inhibit integrins and then assess whether the cGMP readout was subsequently altered. Using the FRET-based cGMP biosensor cGi500 [136, 137], cGMP level changes can be observed in real-time in any cell, including platelets and whole thrombi, also under flow conditions. With this tool, a change in cGMP signaling in thrombi with and without modified integrin signaling can be compared. This could provide hints to whether integrins are connected to cGMP signaling.

In this specific experimental setup, we checked whether blocking the integrins α_{IIb}, β_1 and β_3 and the respective heterodimer $\alpha_{IIb}\beta_3$ on pre-formed thrombi with different antibodies and drugs in a flow chamber setup alters the strength of the measured shear-dependent cGMP signal *ex vivo*. Murine whole blood expressing a FRET-based cGMP biosensor [136, 137] was perfused through a collagen-coated flow chamber to form thrombi. These were then treated with different antibodies targeting the α_{IIb}, β_1 and β_3 integrins alone or the fibrinogen receptor $\alpha_{IIb}\beta_3$. The latter was targeted with a blocking antibody (JON/A) that solely binds the activated form of the receptor. In addition, we used the drug Tirofiban, a small molecule integrin $\alpha_{IIb}\beta_3$ antagonist. After the incubation period, cGMP signaling in the thrombi was induced via application of DEA/NO under flow conditions and the cGMP response was analyzed in form of a FRET ratio trace of CFP/YFP emissions (F480/F535) **(Figure 20)**. The control FRET traces of vehicle-treated thrombi showed that 150 nM DEA/NO induced reliable cGMP signals **(Figure 20A, black trace)**. The clear separation of the CFP (blue) and YFP (yellow) single traces excludes the possibility of artifacts. A maximum peak height of the cGMP signal based on the ratio change was reached between a ratio increase of 25% – 30% **(Figure 20A)**. At this point, most probably, most sensor molecules have bound cGMP. Cessation of flow was followed by an immediate drop of the cGMP concentration to baseline levels in spite of the presence of DEA/NO, an observation already described in a previous study [139]. Resuming the perfusion and therefore flow conditions re-ignited cGMP generation back to the level of the initial peak **(Figure 20A)**.

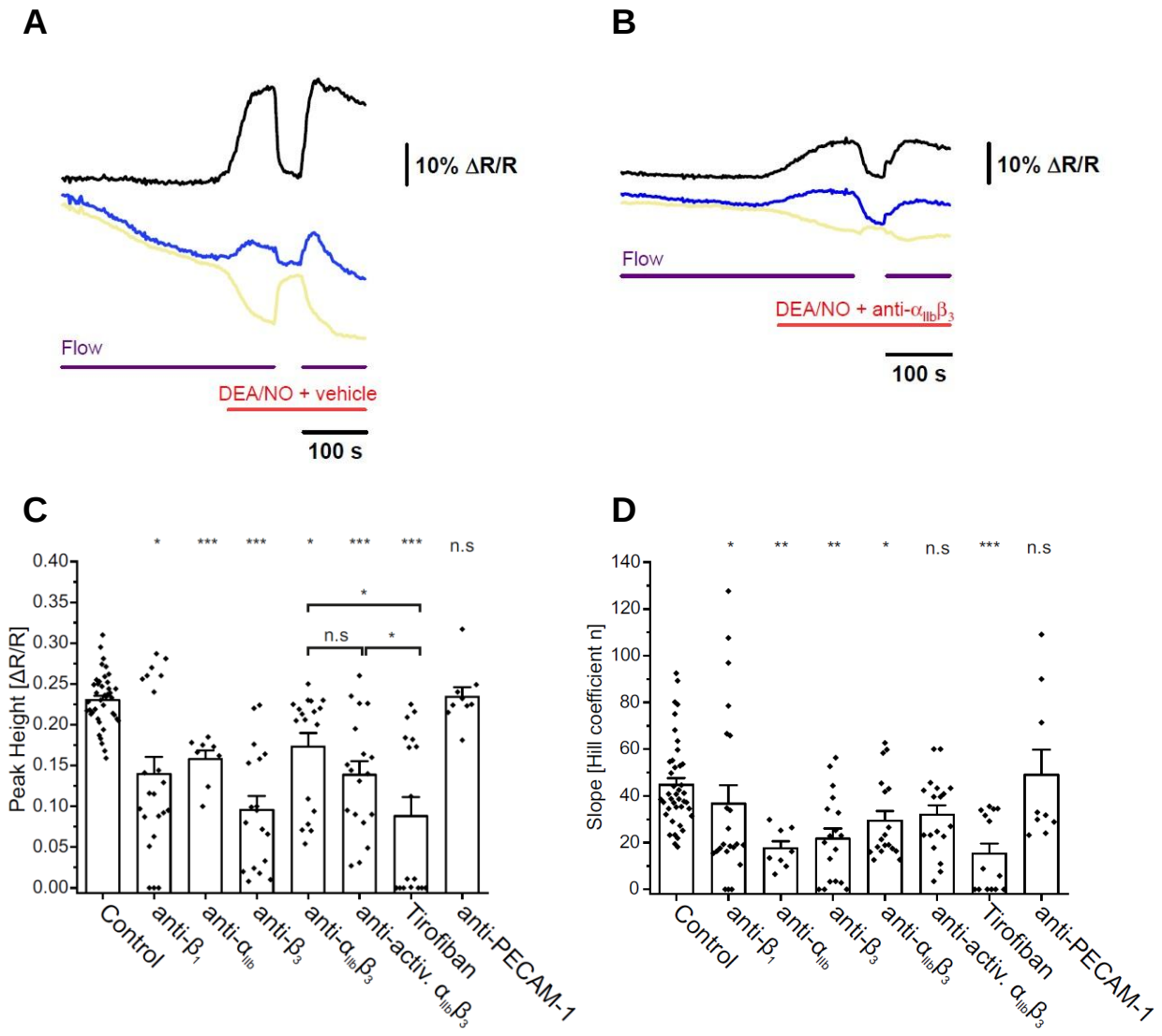

Figure 20. Blocking of integrin $\alpha_{IIb}\beta_3$ and β_1 attenuates cGMP response *ex vivo*.

Murine platelet thrombi of transgenic mice expressing the FRET-based cGi500 biosensor (Genotype: R26-cGi500(L1) +/L1 or L1/L1) were generated in a flow chamber coated with collagen with a shear rate of 500/s. Formed thrombi were then treated with antibodies targeting integrins α_{IIb}, β_1 and β_3, the activated form of $\alpha_{IIb}\beta_3$, and PECAM-1, Tirofiban, or vehicle control (see Table 11). After incubation for 20 min at room temperature, cGMP generation was induced with 150 nM DEA/NO. The respective antibody or drug used in the pre-treatment was then again applied together with DEA/NO at a shear rate of 1000/s. **(A)** – **(B)** Indicated are representative FRET traces of control **(A)** and treated **(B)** thrombi. FRET traces recorded and analyzed included the CFP emission (F_{480}) in blue, YFP emission (F_{535}) in yellow and CFP/YFP emission ratio (F_{480}/F_{535}) in black. The ratio of the emissions was normalized to average baseline signals and is depicted as a ratio change ΔR/R and thereby represents relative cGMP level changes. The flow was halted after cGMP levels reached the peak ratio (gap in purple line). The cGMP ratio trace was then fitted as a sigmoidal curve starting from the baseline up to the point of flow cessation. Peak height and slope of the fitted curves were then determined to gauge the strength of the cGMP signal (see also section 2.4.3 and **Figure 10**). Three different thrombi were recorded and evaluated per measurement and treatment. Also depicted is the quantification of both the peak height **(C)** and slope **(D)** of control and treated thrombi. All data is presented as mean + SEM. Statistical significance was determined by first testing for distribution and variances. For non-normally distributed data, the Mann-Whitney *U*-test was used and for normally distributed data the student's *t*-test (equal variances) or Welch's *t*-test (unequal variances) was performed with Bonferroni correction. Asterisks denote the statistical significance comparing to the control condition, with * = p≤0.05; ** = p≤0.01; *** = p≤0.001; n.s. = not significant.

Treating the thrombi with integrin-targeting antibodies or drugs led to a change in the average shear-dependent cGMP response after DEA/NO treatment, as depicted in a representative trace **(Figure 20B)**. While the flow-dependency of the cGMP signal was observed also in the treated thrombi, the peak height and rate of cGMP increase seemed to be altered in the treated thrombi, with the separation of both CFP and YFP traces still pointing towards a reliable signal **(Figure 20B-D)**. Interestingly, treatment of thrombi did not lead to weaker cGMP signals in all cases. In fact, about one half of the measured treated thrombi did not show a change in peak height compared to the respective control thrombi **(Figure 20C)**. The apparent bimodal distribution of data points can be explained by a limitation of our experimental setup, specifically of our cGMP sensor. At high cGMP levels, a saturation of all sensor molecules might occur in both control and treated thrombi, which could mask a possible cGMP-inhibiting effect of blocking the integrins. Despite this limitation and still including all this data in the evaluation, a significant decrease of both the peak height **(Figure 20C)** and the rate of cGMP increase depicted by the slope of the ratio curve **(Figure 20D)** was seen in thrombi treated with antibodies targeting the different integrins compared to the vehicle controls. Using anti-PECAM-1, an antibody not targeting integrins, there was no difference of cGMP signals compared to the control condition, supporting the notion that the attenuation of shear-dependent cGMP signals observed in this experimental setup was indeed linked to blocking of the investigated integrins **(Figure 20C-D)**.

In summary, we showed that mechanosensitive cGMP signaling (“mechano-cGMP”) is attenuated when targeting specific integrins with antibodies or drugs, supporting a functional link between integrins and shear-dependent cGMP signaling. As prominent mechanotransducers, these integrins might thus prove to be the missing link responsible for sensing and transducing shear stress into a biochemical cGMP signal.

3.5 Pharmacological stimulation of platelets with Riociguat drives thrombus dissolution *in vivo*

While understanding the mechanistic basis of mechano-cGMP in platelets might prove to be essential for a future development of an optimized anti-thrombotic drug, considering already developed cGMP-modulating drugs, the pharmacological relevance of mechano-cGMP has yet to be studied in great detail. Targeting other cell types, the cGMP signaling pathway has already successfully proven to be a highly druggable target with many clinically used drugs. For instance, Sildenafil and Riociguat increase cGMP levels to treat different disorders like erectile dysfunction and pulmonary hypertension, respectively [11, 53]. Despite the evident efficacy of these drugs, the exact pharmacological effect of cGMP drugs, whether they are NO-GC stimulators, activators or PDE inhibitors, has not been studied in detail in platelets. Some studies have suggested that cGMP-elevating compounds could act as effective platelet inhibitors under certain conditions [162, 163], but a lot of work remains to potentially establish the cGMP signaling pathway as a convenient target for anti-platelet therapy. One potential advantage of targeting cGMP signaling in platelets to limit thrombosis is its shear-dependency [139], which would limit thrombus growth only under high shear conditions and not in the initial vessel-sealing aggregation phase that happens under low shear stress. Therefore, drugs that activate the mechanosensitive cGMP system should bypass the side-effect of increased bleeding risk, which comes with clinically used drugs targeting platelet activation pathways.

To analyze the pharmacological relevance of cGMP signaling in platelets, we decided to check whether the NO-GC stimulator Riociguat affects thrombus formation in an *in vivo* cremaster model. Platelet-specific Pf4-Cre-recombined cGi500 sensor mice were used to distinguish platelets from other cells. This mouse model allows for a precise visualization of thrombus formation in real-time in an anesthetized mouse, with non-recombined cells expressing the red mTomato fluorophore. Thrombus formation was observed and analyzed after superfusion of either vehicle control (Krebs working solution+DMSO) or 10 µM Riociguat added to the Krebs Buffer working solution superfusate in the same mouse. After a laser-induced injury of an arterial vessel wall, formed thrombi seemed to dissolve faster under Riociguat superfusion compared to the control condition **(Figure 21A)**.

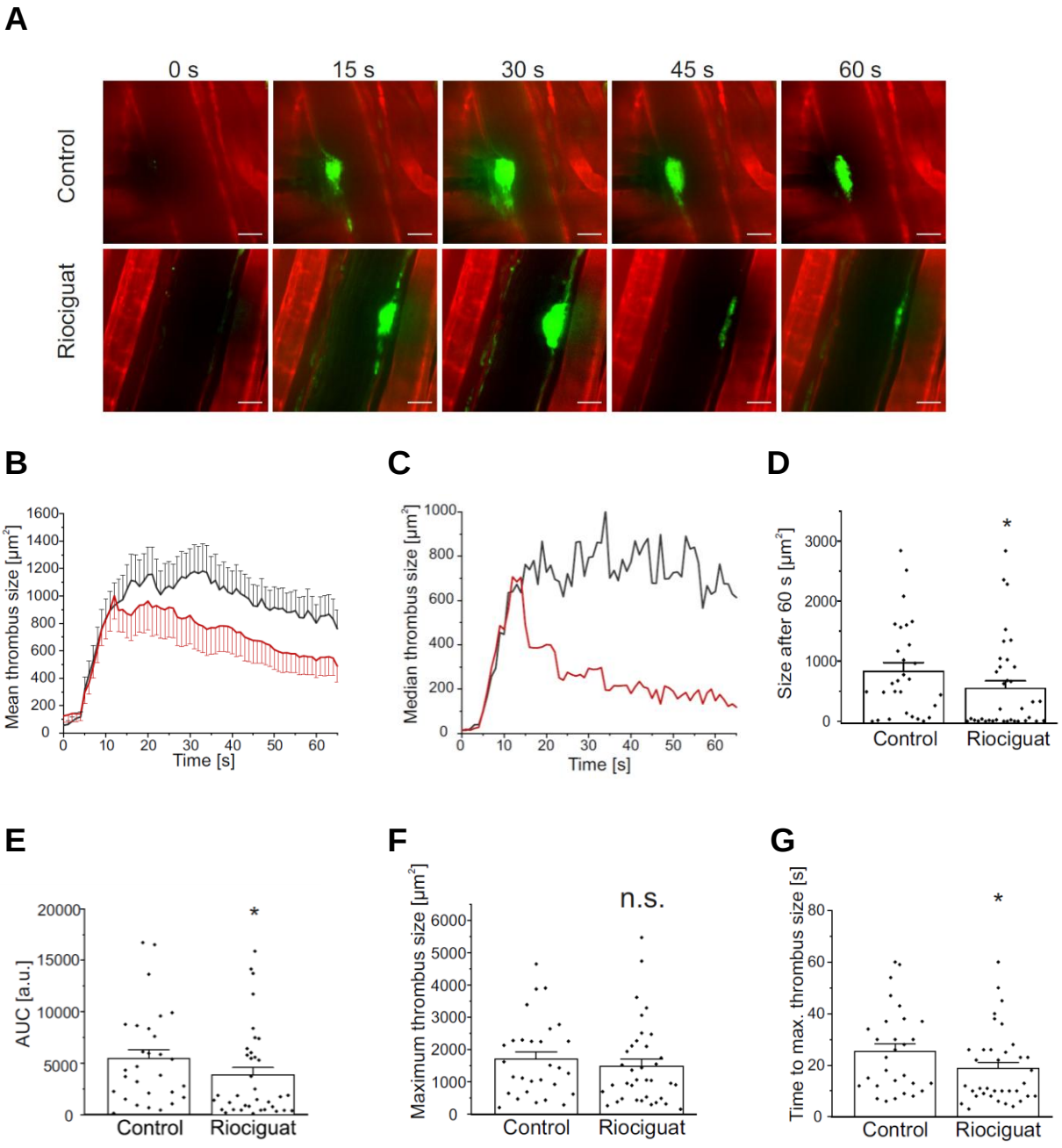

Figure 21. Riociguat drives thrombus dissolution *in vivo*.

Platelet-specific heterozygous NO-GC control male mice (n=8) (age: 52-68 weeks) (Genotype: R26-mT/cGi500-L2$^{fl/fl}$; Pf4-Cre$^{tg/+}$; NO-GC$\beta_1{}^{+/fl}$) expressing the cGi500 biosensor in Pf4-Cre-recombined platelets and megakaryocytes and the mTomato fluorophore in non-recombined cells were used for *in vivo* analysis of thrombus formation. The prepared cremaster of each mouse was superfused with either vehicle control (Krebs Buffer +DMSO) or 10 µM Riociguat added to the superfusate. An injury of an arterial vessel wall (diameter of vessel approx. 30-60 µm) was induced for 5 s at the beginning of each measurement by a laser to prompt thrombus formation. For the control condition, n=29 thrombi were analyzed, while n=36 thrombi were evaluated under Riociguat treatment from n=8 mice. **(A)** Time lapse images of representative control and Riociguat-treated thrombi after injury done 5 s into the measurement (indicated here as 0 s). Platelets expressing the cGi500 sensor are depicted in green, while non-recombined mTomato-expressing cells are shown in red. Scale bars represent 25 µm. Mean values (± SEM) **(B)** and median value **(C)** over time of all analyzed thrombi generated under control (black trace) and Riociguat (red trace) conditions. Thrombi were further analyzed regarding their size at the 60 s time point **(D)**, the area under the curve **(E)**, their maximum size **(F),** and the time to reach their maximum size **(G),** with each data point representing one thrombus. All data is represented as mean + SEM. Statistical significance was determined with Mann-Whitney U-test. Asterisks denote the statistical significance comparing to the control condition, with * = p≤0.05; n.s. = not significant.

Looking at both the mean and median curve of the thrombus area over time **(Figure 21B-C)**, Riociguat treatment (red curves) led to a faster reduction of thrombus size after reaching its maximum size around 5 s after vessel injury (corresponding to 10 s on the x-axis) compared to thrombi generated under control conditions (black curves). It is important to note that significantly more thrombi were less stable under Riociguat superfusion compared to the control **(Figure 22)**, with many thrombi almost completely breaking off within a second after reaching their maximum size. This factor weighs in more when regarding the median thrombus size curve **(Figure 21C)**, as the upper quantile of persistent larger remaining thrombi still contribute more to the mean value **(Figure 21B)**. Therefore, thrombus dissolution looks more drastic looking at the median curve **(Figure 21C)**, compared to the mean thrombus size over time **(Figure 21B)**. After 60 s, the average thrombus size was significantly smaller under Riociguat superfusion **(Figure 21D)**. Thrombi formed under vehicle control superfusion were roughly 50% larger on average at this time point. Riociguat superfusion also led to a significant reduction of the area under the curve (AUC) of the respective thrombus area curves, a value which serves as an indication of the thrombogenicity in total **(Figure 21E)**. Although there was no significant difference in maximum thrombus size comparing control and Riociguat treatment conditions **(Figure 21F)**, the time to reach the maximum thrombus size under control conditions was significantly higher **(Figure 21G)**, with thrombi under Riociguat superfusion reaching their maximum size at around 20 s, while control thrombi reached a slightly larger size after about 25 s **(Figure 21G)**. Despite this observation, the initial growth of the thrombus within the first 5 s after injury looks almost identical, judging by the slope of both the mean and median thrombus area curves **(Figure 21B-C)**.

Under superfusion with Riociguat, the thrombi seemed to dissolve faster compared to the control condition. This prompted us to specifically focus on the thrombus persistence under each condition **(Figure 22)**. For these analyses, each thrombus was normalized to its maximum size in order to solely visualize the relative changes in thrombus size over the duration of 60 s. We split the entire duration into two phases: the initial 30 s of thrombus formation and the following 30 s as a measure of thrombus persistence. By determining the AUC of each phase, we sought to investigate whether Riociguat treatment leads to a decrease in thrombus persistence.

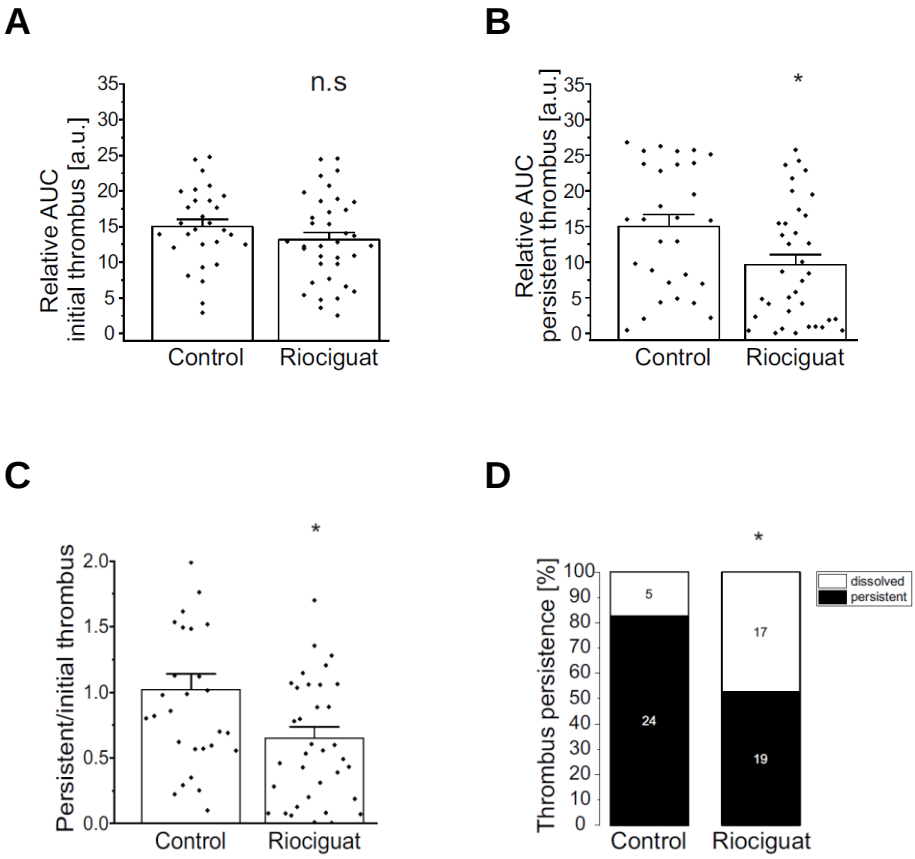

Figure 22. Thrombus persistence is decreased by Riociguat treatment.

Representation of the persistence of thrombi during the first 60 s under control condition or Riociguat superfusion (10 µM in the superfusate). Each thrombus growth profile was first normalized to the respective maximum thrombus size (which was set to 1 a.u.). The AUC of the normalized curves was then determined for two different time periods: The first 30 s of thrombus formation (initial thrombus) **(A)** and at the following 30 s (persistent thrombus) **(B)**. The ratio of both time windows is depicted in **(C)**. Amount of persistent and dissolved thrombi **(D)**. If the AUC value of the latter time window (persistent thrombus) reached at least half (50%) of the first time window (initial thrombus), the thrombus was defined as "persistent", while a value below 50% classified it as "dissolved". Statistical significance was determined with student's *t*-test for **(A)**, Mann-Whitney *U*-test for **(B)** – **(C)** and χ^2 test for **(D)**. All data is represented as mean + SEM. Asterisks denote the statistical significance comparing to the control condition, with * = p≤0.05; n.s. = not significant.

Despite many thrombi dissolving almost completely already after roughly 1 s after reaching their maximum size (data not shown), Riociguat treatment did not lead to a significant reduction in the thrombus size compared to the control in the initial 30 s time period **(Figure 22A)**. When looking at the later time window, however, a significant decrease in the AUC value of the thrombi formed under Riociguat superfusion was observed **(Figure 22B)**, while thrombi formed under control conditions persisted for a longer time with a greater AUC **(Figure 22A)**. In relation, Riociguat treatment led to a significant decrease of the ratio of persistent over initial thrombus **(Figure 22C)**. This observation implies that after the initial 30 s, Riociguat led to a faster dissolution of the thrombi, stabilizing them at a smaller size.

When applying the criterion that a thrombus is persistent if half of the AUC value is still reached in the later persistence phase compared to the initial aggregation phase, about 80% of thrombi formed under control conditions fell under the category of being persistent **(Figure 22D)**. Riociguat treatment, however, led to roughly 50% of the thrombi fulfilling this criterion, indicating that pharmacological stimulation with Riociguat decreased the number of persistent thrombi. Supporting this assessment are the previous observations that Riociguat treatment led to a significantly lower average thrombus size at the time point of 60 s **(Figure 21D)** and that it did not influence the initial build up to the maximum thrombus size **(Figure 21F)**. In this experimental model, the first 30 s seemed to be paramount for the initial growth of the thrombus, while from this time point on, pharmacological intervention with Riociguat promoted the dissolution of the thrombus after it has reached its maximum size.

Thus, our *in vivo* analysis of the NO-GC stimulator Riociguat underlines the pharmacological relevance of targeting cGMP signaling in platelets. Thrombi formed under Riociguat treatment did not show noticeable differences compared to control thrombi with respect to the initial phase of thrombus buildup. After this phase, treatment with Riociguat led to a faster dissolution of thrombi, leading to less thrombogenicity overall. This could be therapeutically valuable, as stimulating cGMP signaling with Riociguat apparently led to a faster dissolution of the thrombus, but only after the initial injury of the vessel wall has been sealed.

4. Discussion

4.1 Intraplatelet localization of cGMP signaling pathway components in platelets

Based on the results of a previous study by Wen et al. [139] which showed that cGMP signaling in platelets is shear-dependent, we first sought to identify a mechanotransducer sensing shear stress in platelets and how this is connected to the cGMP signaling pathway. Since this mechanotransducer was most likely localized at the platelet plasma membrane, our hypothesis predicted the existence of a cGMP signaling complex at the membrane where shear stress is perceived **(Figure 8)**.

To test this hypothesis, we first separated a human platelet lysate into a cytosolic and membrane fraction. Judging by the enrichment of the membrane marker PECAM-1 in the membrane fraction and the cytosolic marker GAPDH in the cytosol, the fractionation process seemed efficient **(Figure 14)**. Furthermore, when taking the analysis of the localization of the different integrins into consideration, membrane proteins were highly enriched in our membrane preparation **(Figure 19A),** which speaks for the efficiency of our platelet fractionation protocol. Very low amounts of residual GAPDH were found in the membrane fraction (**Figure 14-16**) speaking for either a less than fully efficient separation or for the assumption that this enzyme is also, at least in part and contrary to common belief, situated at the membrane. The latter conjecture is supported by a similar study which also describes the presence of GAPDH in human platelet membrane fractions [160].

To test the hypothesis that cGMP signaling components localize to the platelet membrane, we checked for the presence of NO-GC, cGKI, VASP and PDE5 in the membrane fraction via Western Blot analysis. We observed all of the mentioned proteins at the membrane, albeit in different relative quantities as compared to their respective cytosolic abundance **(Figure 14-15)**. While both cGKI and VASP were roughly equally situated in the membrane and cytosolic fractions, PDE5 was highly enriched in the cytosolic fraction, in roughly about a 5-fold manner compared to the membrane abundance **(Figure 15)**. Despite the approximately three times higher presence in the cytosol, platelet NO-GC β_1 was also found in the membrane fraction **(Figure 15)**. Previous analysis of platelet membrane fractions also supports the

validity of this observation. Lewandrowski et al., using a mass spectrometric analysis of enriched platelet plasma membranes, detected VASP, PDE5 and the β_1 subunit of NO-GC as platelet membrane proteins [160]. It has to be mentioned that cGKI was not discovered in the mentioned study, but this could be due to technical limitations of the detection conditions in the mass spectrometric analysis of the cGKI fragments. Taking this into consideration, an analysis of specific proteins via Western Blot might be more sensitive in some cases. Another possibility of differing results could be varying experimental setups and/or conditions. For example, Zabel et al. [150] showed the presence of NO-GC in the membrane fraction of human platelets, while a fractionation of murine platelets in the study of Wen et al. [139] showed the membrane localization of both NO-GC and cGKI. In the latter study, the relative localization of both cGKI and NO-GC seemed more membrane-oriented in murine platelets compared to the human counterpart. Here, the analysis of murine platelets showed an about 3-fold higher relative presence of NO-GC and a roughly 6-fold higher abundance of cGKI in the membrane compared to the cytosolic fraction [139]. While also taking the difference in size between human and murine platelets into consideration, this observation might also speak for an even greater abundance and importance of membrane compartmented cGMP signaling in murine compared to human platelets. In our study, neither stimulation of cGMP signaling in the platelets with DEA/NO nor subjection to shear stress via vortexing or the combination of DEA/NO and vortexing altered the intraplatelet localization of the analyzed cGMP signaling components cGKI, NO-GC, PDE5 and VASP **(Figure 15)**. It hast to be noted that in this specific experimental setup, the chosen concentration of DEA/NO, was already sufficient to induce VASP phosphorylation even in the absence of shear stress **(Figure 15A)**. Therefore, the repetition of this experiment with a lower concentration of DEA/NO might give better insights. A further limitation is the form of the applied shear stress, which, under vortexing conditions consists of a turbulent flow in a reaction tube, which contrasts with the laminar flow applied in a flow chamber. Guaranteeing the full absence of shear stress in the respective tested condition is also difficult, as the preparation procedure itself contains steps that possibly expose the platelets to shear stress. Nevertheless, the tested proteins might be present at the membrane already at baseline conditions in resting platelets, which could suffice for a NO- and shear-induced generation of cGMP. Nevertheless, one should not completely exclude the possibility that cGMP signaling components might

localize more to the membrane upon NO stimulation and exposure to shear stress. For instance, Zabel et al. described a calcium-dependent translocation of NO-GC to the membrane fraction upon platelet activation [150]. In our experimental setup, however, time passing between treatment application and the lysis of the platelets as well as the form of the applied shear stress might be major limitations. In this case, a different experimental setup tailored specifically for this scientific question might help in unraveling the exact mechanism on how NO induces cGMP signals in platelets and how this is connected to shear stress. Furthermore, unlike Zabel et al. [150], we did not investigate activated, but rather resting platelets. Using the same experimental approach on platelets after they have been activated (i.e. via aggregometer) and checking whether the results differ compared to resting platelets could therefore be warranted.

Taking the results of our study and previously published data into consideration, we found that cGMP signaling proteins were not only principally present in the membrane fraction of human platelets, but also surprisingly found there in a relatively high abundance, which would support the existence of a membrane-associated cGMP signaling complex in platelets.

4.2 Interaction of cGMP signaling pathway components at the platelet membrane

By enriching membrane proteins, we hoped to visualize protein interactions connected to cGMP signaling specifically occurring only in this platelet compartment compared to the cytosolic compartment. Particularly, using a Co-IP approach, we first determined whether NO-GC interacts with cGKI either in the cytosol and/or at the platelet membrane. Unfortunately, an initial attempt to establish the only available NO-GC antibody at that time (self-made) as a pulldown antibody did not yield positive results (data not shown). We therefore decided to continue with a self-made antibody targeting cGKI for Co-IPs [151]. We did not observe a Co-IP of NO-GC with cGKI in the cytosolic fraction but strikingly, NO-GC was detected in the Co-IP eluates of the membrane fraction **(Figure 16)**. This not only demonstrates that NO-GC specifically interacts with cGKI at the platelet membrane, but also supports the notion that pre-enriching membrane proteins is a necessary procedure to see this interaction, as a

potential dilution of the membrane fraction with non-interacting cytosolic proteins in a complete lysate would possibly obscure a membrane-specific interaction. Considering the lack of a specific interaction between NO-GC and cGKI in the cytosolic platelet fraction, the initially hypothesized model has to be modified, as a direct interaction between NO-GC and cGKI at the membrane therefore also becomes more unlikely. The results rather support the idea of a larger signaling complex specifically at the platelet membrane, with membrane-bound proteins serving as the framework where NO-GC and cGKI bind to and therefore are present in close proximity, but do not bind directly to each other (see chapter 5, **Figure 23**).

Previously, Wilson et al. also used a Co-IP approach to identify a cGMP signaling complex in the membrane fraction of human platelets comprising cGKI, PDE5 and IP_3R [134]. We also tested whether PDE5 was co-immunoprecipitated with cGKI in the membrane fraction, but could not detect an interaction of these two enzymes (data not shown). Furthermore, we also observed in our experiments that the localization of PDE5 was largely confined to the cytosolic fraction, whereas Wilson et al. detected and co-immunoprecipitated it from the membrane fraction. Despite these seemingly contradictory findings, a direct comparison of these experiments is severely complicated by the fact that different non-commercially available, self-made antibodies were used in the studies as well as deviating Co-IP conditions. In our study, despite several optimization attempts, the efficiency of the cGKI immunoprecipitation was limited to a small fraction of the input protein amount **(Figure 16)**. This could be due to the pulldown antibody not being highly suitable in this experimental setup or due to suboptimal Co-IP conditions. Testing the bead efficiency with different antibodies could also help to determine the cause for the low IP efficiency. As we observed a Co-IP of NO-GC with cGKI despite the low efficiency, it can be assumed that a higher IP efficiency would lead not only to a higher yield of co-immunoprecipitated interacting proteins, but the NO-GC-cGKI interaction would probably become more visible. Therefore, further optimization of the procedure specifically for the investigated proteins is warranted. Specifically, testing the ideal conditions where the membrane proteins are solubilized but protein interactions remain intact would help to identify cGMP signaling protein interactions more robustly. Furthermore, the reverse IP using an NO-GC pulldown antibody to detect cGKI in the co-immunoprecipitate would also strengthen the validity of the results,

which would also include optimizing the Co-IP conditions for another antibody. In fact, recently released commercially available antibodies targeting NO-GC (Abcam, Cayman) could be a good start to further strengthen the observation that cGKI and NO-GC are present in a signaling complex at the platelet membrane. Using a VASP antibody can also be taken into consideration, although, due to the protein size overlapping with the size of IgGs heavy chain, an analysis with a Western Blot approach becomes remains difficult.

Nevertheless, despite the low IP efficiency, we were able to detect an interaction of cGKI with NO-GC specifically at the membrane of platelets, supporting the idea of a cGMP signaling complex consisting of at least NO-GC, cGKI and a membrane-specific protein connecting them. Integrins might play a key role in this regard, as we also observed a Co-IP of integrin α_{IIb}, β_3 and β_1 with cGKI in our mass spectrometric and Western Blot analyses **(Figure 18-19)**. How exactly a mechanotransducer sensing and transducing the shear stress is involved in this regard remains to be determined.

4.3 Mass spectrometric analysis of cGKI interactors in platelets

In an approach that analyzes possible cGKI interactors at a larger scale, in collaboration with AG Sickmann, we checked the entire cGKI immunoprecipitation from the platelet membrane fraction for proteins interacting with cGKI using MS (see 2.10). With this approach, we sought to detect suitable candidates which could link the sensing and transduction of mechanical shear forces to the cGMP signaling pathway. Looking at the silver staining of both membrane cGKI Co-IPs and control IPs, a plethora of proteins were detected in the immunoprecipitates **(Figure 17)**. As in large, the pattern of protein bands on the silver-stained gel did not differ between the cGKI co-immunoprecipitates and the control IPs, it can be assumed that most of the proteins detected bind unspecifically to the column and are therefore also present in the cGKI Co-IPs. This is a phenomenon generally accepted when using a Co-IP approach, as it is next to impossible to specifically pull down only the proteins that interact with the immunoprecipitated bait considering the large amount of different proteins and interactions in the input lysate or fraction. Proteins that are commonly unspecifically co-immunoprecipitated have also been analyzed from a large set of

MS data and have been listed in a repository [164]. Some of the detected proteins in our mass spectrometric analysis were also found in this repository (for example keratin) and were therefore not considered **(Appendix, red)**. A requirement for a high enrichment of specific protein interactions would also be a higher IP efficiency, which, as observed in the analysis of the Co-IP (see 4.2), did not reach ideal levels in our experimental setup. However, as the (unspecific) band pattern of proteins on the silver-stained gel was highly similar across all samples, a mass spectrometric analysis was possible. Had this not been the case, the requirement for a statistically robust analysis of the co-immunoprecipitates would not have been fullfilled. The sensitivity of the silver staining was also insufficient to detect enriched proteins in the positive IP samples, as beside the enriched (unbound) antibody at around 54 kDa, other enriched proteins were not visible in any other size range **(Figure 17)**. Nevertheless, by using the negative control IPs as a background measurement ruling out unspecific binders, only the proteins enriched in the cGKI Co-IPs could be identified as possible interaction partners in the mass spectrometric analysis.

The immunoprecipitation of cGKI itself was clearly observed in the mass spectrometric analysis (**Figure 18**), despite the relatively low IP efficiency **(Figure 16B)**. This provided the basis for further analysis of co-immunoprecipitates. In their membrane-based Co-IP studies of platelets, Wilson et al. [134] described the Co-IP of cGKI, PDE5, IP_3R and IRAG via Western Blot analysis using different antibodies against cGKI (Stressgen) and PDE5 (self-made) in their study compared to ours. They suggest a compartment-specific regulation of PDE5 via cGKI in the membrane fraction, associated in a complex which also includes IP_3R and IRAG. Both of these proteins are known to be cGKI targets and regulators of intracellular calcium release which is vital for platelet activation [82]. We also observed the enrichment of IP_3R and IRAG, substantiating our Co-IP approach (**Figure 18**) as we pulled down known cGKI interactors. We also confirmed the observation from Wilson et al. that cGKI acts in a membrane compartment-specific manner. Despite this, in our case and in contrast to Wilson et al., neither a Western Blot analysis of the Co-IPs (data not shown), nor the mass spectrometric analysis **(Figure 18, Appendix)** showed a Co-IP of PDE5. This can be attributed to the fact that different cGKI antibodies as well as Co-IP protocols were used in these two studies, as these differences can influence the final results greatly. The presence of the downstream phosphorylation target of

cGKI, VASP, was detected in the MS analysis of the Co-IPs, but it was not enriched in a significant manner, suggesting that VASP is not localized to the cGMP signaling complex at the platelet membrane. It has to be mentioned that while we did detect NO-GC in the cGKI co-immunoprecipitate in the Western Blot analysis **(Figure 16)**, the mass spectrometric analysis did not recognize any NO-GC fragments in the membrane Co-IPs **(Figure 18, Appendix)**. This could be due to suboptimal ionization conditions or the detection method for the respective fragments. The Western Blot analysis seems to be more sensitive when looking specifically at the NO-GC-cGKI interaction. Another reason might be the addition of a non-denaturating solubilization buffer to the freshly fractionated membrane samples for Western Blot analysis. This buffer was not added in the MS as it would be detrimental to this measurement. Detecting the interaction of cGKI and NO-GC could therefore be dependent on the solubilization level of the membrane fraction as well as the detergents used. To confirm this, the cGKI Co-IP eluates of non-solubilized membrane fractions (no addition of NP40) should also be tested for the presence of NO-GC by Western Blotting.

The seemingly contradictory findings also highlight the importance of using many experimental approaches to investigate and validate results, especially when looking at interactions with a large biochemical complexity. In this regard, an important experiment would therefore be to analyze an NO-GC Co-IP and test it for the presence of cGKI fragments by MS.

Strikingly, several proteins associated with vesicle trafficking, such as TAO3, SNAP23 and actin-related protein 2/3 complex were found highly enriched in the cGKI co-immunoprecipitates **(Appendix)**. This finding might implicate cGKI as an important mediator in the regulation of vesicle trafficking in platelets and warrant further research. To date, only cGKII has been described to regulate synaptic vesicle recycling in cerebellar granule cells [165]. Despite their high enrichment, as it was unlikely that that these proteins are key regulators of mechanotransduction, we focused on other candidates for mechanotransducers, which were also enriched in the cGKI co-immunoprecipitates.

When looking for potential mechanotransducers, the list of enriched interactors of cGKI included several integrins, including integrin α_6, α_{IIb}, β_1, α_2 and β_3 **(Figure 18)**. These have been described in the literature as potential mechanotransducers in

endothelial cells and in platelets [43-45, 49, 51]. Since these integrins are very abundant in platelets and also play an important role in platelet physiology, we put our focus on the $\alpha_{IIb}\beta_3$ fibrinogen receptor and integrin β_1 as potential mechanotransducers. In platelets, the mechanosensing properties of integrin β_3 and the entire $\alpha_{IIb}\beta_3$ receptor have already been described [49, 51], albeit in an aggregation-promoting manner. This does NOT exclude the possibility that the cGMP signaling pathway could make use of the shear-sensing properties of these integrins in order to inhibit platelet aggregation. From our observation that integrins are co-immunoprecipitated with cGKI, we therefore hypothesized a cGMP signaling complex at the platelet membrane with integrins possibly sensing and transducing shear forces which eventually leads to an intraplatelet cGMP response. Both cGKI and NO-GC as intracellular proteins would presumably bind the cytoplasmatic tail of the integrin receptor, thereby associating to the inner leaflet of the plasma membrane. We also speculate that other, yet-to-be-identified proteins are part of this signalosome at the platelet membrane and that platelets relay the mechano-cGMP signal in this manner. In the future, a suitable NO-GC antibody could be used to not only validate cGKI-NO-GC-integrin interactions by Co-IP, but also to confirm proteins identified in the mass spectrometric analysis in both NO-GC and cGKI pulldowns of platelet membrane fractions. This might give further clues as to which proteins are present in the membrane-associated cGMP signaling complex. Another approach would be the use of the different integrin antibodies for Co-IPs to strengthen the hypothesis of a membrane-situated signaling complex.

Another protein which was enriched in the cGKI immunoprecipitates was the SERCA **(Figure 18)**. This enzyme is a calcium ATPase with the function to transport calcium from the cytosol into the ER. SERCA is inhibited by phospholamban which, in an unphosphorylated state, reduces calcium uptake into the ER [166]. It has been described that both the cAMP-dependent protein kinase as well as the cGKI can phosphorylate phospholamban thereby relieving SERCA inhibition [166, 167]. Since an increased calcium concentration in the cytoplasm is necessary for platelet activation, higher SERCA activity would lead to an inhibition of platelet activation. It is known that cGMP regulates calcium influx via IRAG and IP_3R [85]. Our data suggests that the cGMP signaling pathway also seems to be involved in regulating calcium influx into the ER via SERCA. This would therefore be another mechanism of

negative regulation of platelet activity through cGMP, as relieving SERCA inhibition would lead to the removal of calcium from the cytosol.

4.4 Functional analysis of a possible mechanosensitive interplay between integrins and cGMP signaling

To further investigate whether the identified integrins are functionally linked to shear-dependent cGMP signaling in platelets, we used a transgenic cGMP sensor mouse line to test whether inhibiting integrins alters the mechanosensitive cGMP signal. In this approach, pre-formed thrombi in a flow chamber were incubated with antibodies targeting integrins α_{IIb}, β_3 and β_1 as well as different forms of the heterodimer $\alpha_{IIb}\beta_3$ in order to inhibit them. Then, a cGMP response was elicited with DEA/NO under flow conditions (see 2.4).

In sum, thrombi treated with integrin targeting antibodies or the drug Tirofiban, which binds the fibrinogen binding site of integrin $\alpha_{IIb}\beta_3$, showed a significantly reduced cGMP response as measured by peak height and slope of the FRET ratio curves **(Figure 20)**. These findings support the hypothesis that not only an interaction between these integrins cGKI, and NO-GC takes place, but a functional connection exists. Control values for peak height and slope were consistent across all measurements and the cGMP resonse after treatment with an antibody targeting PECAM-1 did not differ from the control. Therefore, the downregulation of mechanosensitive cGMP signaling in this experimental setup seems to be specifically attained when blocking either single integrin subunits or the dimeric fibrinogen receptor $\alpha_{IIb}\beta_3$ with specific antibodies or Tirofiban **(Figure 20)**. While the lower peak height in the treated thrombi indicates that less cGMP was generated in total, the decreased slope shows a decreased “on-rate” of cGMP generation. Interestingly, both antibodies used against integrin $\alpha_{IIb}\beta_3$ as well as Tirofiban are known to bind to the receptor’s fibrinogen binding site, indicating that this region could be important for mechanotransduction.

From an experimental standpoint, although our transgenic mice allow for a live measurement of cGMP signals, several limitations have to be considered in this specific experimental setup. For one, the data in many integrin-inhibited FRET measurements were not normally distributed. Beside integrin α_{IIb}, the data showed

two populations per measurement with one having peak height and slope values in the rage of the control and another population with clearly attenuated cGMP signals **(Figure 20C-D)**. This is especially noticeable looking at the peak height values after integrin β_1 or Tirofiban treatment **(Figure 20C)**. The apparent bimodal dirstibution of data points can be explained, at least in part, by the saturation of the cGi500 sensor molecules at high cGMP concentrations. Using a concentration of 150 nM DEA/NO, a clear cGMP signal in every control thrombus was generated and many of these cGMP peaks reached the point of sensor saturation, as the ratio trace abruptly reached and maintained a peak value above which a higher signal level did not seem to be reachable. In other words, the saturated cGMP peaks looked like it was “cut off”. It has to be assumed that the real cGMP levels went beyond the point of saturation of the sensor in these measurements, which would lead to a gross discrepancy in cGMP signal strength measured as compared actual cGMP levels. Therefore, the cGMP concentrations measured in our experiments probably underestimated the true cGMP response in the thrombus. A potential difference between control condition compared to the integrin-inhibited thrombi could therefore be masked by the limitation of the saturated sensor molecules: Although the responses in both conditions show the same peak height at the point of saturation, the concentration of cGMP might still be higher in the control condition. However this difference would remain undetected. Lower concentrations of DEA/NO were also tested in this experimental setup, but they did not elicit a reliable cGMP response in all control thrombi (data not shown), while a titration of DEA/NO for each measurement would change the variables and therefore comparability between measurements. Despite this limitation and including all the potentially saturated measurements, a significant reduction in cGMP response was observable in thrombi where integrin α_{IIb}, β_3 and β_1 were inhibited. These results further strengthen the hypothesis that integrin signaling is functionally linked to the shear-dependent cGMP signaling pathway.

Another point of debate is how the antibodies possibly alter the capability of the integrins to detect shear stress and how they lead to a reduction in the cGMP response. The basic idea was to block the extracellular domains of the integrins with antibodies to diminish their shear sensing capabilities. A similar experiment concerning a crosstalk of integrin and cGMP signaling in VSMCs has been

performed in a study of Weinmeister et al., in which integrin β_3 blocking antibodies were used to inhibit cGKI-induced adhesion of VSMCs [168]. In the Weinmeister et al. study [168], cGMP signaling increased integrin activity, acting in an “inside-out” manner. In our study, as no permeabilization of the thrombi was performed, it has to be assumed that the antibodies against integrin α_{IIb}, β_3 and β_1 bind an extracellular part of the receptor, since our data shows inhibition of cGMP signaling in all of the integrin-inhibited measurements **(Figure 20)**. Therefore, we deduce that in our case, cGMP is regulated in an “outside-in” mechanism. But, taking together the results from both studies, a bidirectional interaction between integrins and the cGMP signaling pathway seems to be taking place.

At this point, it has to be noted that the experimental setup could benefit from optimization. For instance, a functional evaluation and validation that the integrins are bound by the applied antibodies in the chamber was not carried out prior to the measurements. Therefore, it cannot be excluded that in some preparations, the applied antibodies might not have effectively bound and blocked the intended target. The efficacy of Tirofiban was tested and confirmed prior to the experiments (data not shown), but similar experiments should be performed with the other applied antibodies. Additionally, interindividual differences of cGMP responses in platelets resulting from different preparations from different mice of varying sex and age cannot be excluded. Furthermore, a specific concentration of applied DEA/NO might elicit a different strength of response in different preparations. However, it has to be mentioned that the peak height and slope of control thrombi showed consistent (maximum) values across all measurements, although potential differences of DEA/NO responsiveness might be masked by sensor saturation.

Details as to where the antibodies exactly bind could be important information to analyze the exact role of the respective integrins in mechanotransduction. The inhibition of cGMP signaling using antibodies and the drug Tirofiban against the fibrinogen receptor domain of integrin $\alpha_{IIb}\beta_3$ also supports the hypothesis that the shear sensing capabilities of the integrins lie in this part of the receptor. We further tried to decipher whether the activation state of integrin $\alpha_{IIb}\beta_3$ plays a role in mechano-cGMP transduction. Integrin $\alpha_{IIb}\beta_3$ can either take up a bent, low affinity, inactive form or in an extended, activated, high affinity form [169]. Both the JON/A and integrin $\alpha_{IIb}\beta_3$ blocking antibody solely bind the activated form of the receptor

[170]. We observed no significant difference in the mechano-cGMP-inhibiting properties of these two antibodies **(Figure 20C)**. Tirofiban is a small molecule drug with an Arg-Gly-Asp (RGD) site which can bind the $\alpha_{IIb}\beta_3$ receptor in both the inactive, as well as the active form [169, 171-173]. Tirofiban significantly reduced the peak height of the cGMP ratio trace compared to the general integrin $\alpha_{IIb}\beta_3$ blocking antibody as well as JON/A **(Figure 20C)**. We therefore assume that the site on the inactive integrin recognizing the RGD sequence might be of great importance for mechano-cGMP transduction. Nevertheless, drawing a clear conclusion as to whether integrin activation is required for a mechano-cGMP signal is not possible in this case, as all of the tested antibodies against the single integrin subunits might bind the activated form of the receptor and not exclusively the inactive form. In fact, as blocking all of the investigated integrins including integrin α_{IIb}, β_3 and β_1 with antibodies and Tirofiban led to an inhibition of the shear- and NO-induced cGMP response, pinpointing a specific mechanotransducing integrin specifically to the cGMP signaling cascade is difficult using only the observations from this experiment. To study the mechanosensing properties of the integrins, it could be beneficial to mutate specific functional domains of the receptor in order to find an effect on the shear sensing capabilities as well as an exact connection to the cGMP signaling pathway components cGKI and NO-GC. For this, altering the cytoplasmic domain of the integrin receptors in order to prevent adapter proteins as well as cGKI and NO-GC from binding the integrin, hereby preventing the generation of a cGMP signal, could be a good approach. The primary sequences of the cytoplasmic domains of β-integrins are generally well conserved and consists of 40-60 amino acids [174]. A lot of previous work has already been put into identifying integrin cytoplasmic domain-binding proteins and protein interactions in this domain are pivotal in mediating integrin-induced intracellular signaling [175]. Some studies have even effectively analyzed signaling pathways connected to the cytoplasmatic domain of integrin $\alpha_{IIb}\beta_3$ [176, 177]. Nevertheless, focusing on this domain could give us more insight into the exact mechanistic background of whether or how cGMP signaling components bind the mechanosensing integrins directly and whether a membrane-associated cGMP signaling complex which includes integrins leads to a shear-dependent, NO-induced inhibition of platelet aggregation.

4.5 The pharmacological relevance of mechano-cGMP in platelets

Numerous advances have been made in the field of cGMP research that have led to the approval of several cGMP-elevating drugs to treat different diseases, underlining the pharmacological potential of the cGMP signaling pathway in general. These drugs include NO-GC stimulators and activators, and PDE inhibitors, each used with different clinical indications. In our study, we looked to investigate the therapeutic potential of targeting cGMP signaling in platelets in order to potentially minimize the risk to develop thrombosis. For this, in an *in vivo* cremaster model of laser-induced thrombosis, we checked whether application of the NO-GC stimulator Riociguat, combined with endogenous NO supply, alters thrombus formation and stability (see 2.11). At this point it has to be meintioned that ignoring the supply of NO, for example in *ex vivo* or *in vitro* experiments involving Riociguat, could be detrimental. NO might be required for a Riociguat-induced effect on platelets or work synergistically in conjuction with the drug.

From our observations, the initial thrombus growth in the first approx. 15 s after vessel injury was not altered in Riociguat treated compared to control thrombi **(Figure 21A-C)**. Additionally, no significant difference in maximum thrombus size between the two conditions was observed **(Figure 21F)**. These results implicate that Riociguat does not affect the important initial phase of sealing the rupture in the vessel which keeps hemostasis intact, therefore circumventing a possible bleeding side-effect. In our experimental setup, in general, the lesions were apparently sealed during the initial thrombus formation phase (roughly first 15-20 s), as no bleeding into the surrounding tissue was observable and the blood flow remained constant **(Figure 21A)**. Interestingly, our data suggests that Riociguat drives thrombus dissolution after the initial thrombus growth phase **(Figure 21A-C)**. One minute after thrombus induction, the mean size of Riociguat treated thrombi was significantly reduced compared to the control, as well as the area under the curve portraying the total thrombogenicity during this time frame **(Figure 21D-E)**. Moreover, while roughly half of the thrombi (19 out of 36) treated with Riociguat began to dissolve almost immediately after reaching their maximum size, this phenomenon was only observed in 5 out of 29 control thrombi **(Figure 22D)**. Comparing the time frame of thrombus development in our *in vivo* measurement to the one published by Wen et al. [139], there also seems to be a discrepancy. While thrombi reached their maximum size at

around 30 s in our study, the time to maximum thrombus size in the publication of Wen et al. was roughly doubled [139]. This could be due to a general difference in vessels chosen for the laser-induced injury as well as the criteria applied to include only the more stable thrombi in the analysis. On the other hand, in their *in vivo* cremaster measurements, Salles et al. show a thrombus development as well as time to maximum thrombus size comparable to our study [178].

Furthermore, some limitations of our experimental setup should also be considered. First, while it could also have advantages like eliminating interindividual variances, measuring both the control and Riociguat conditions in one mouse could also have disadvantages. For one, triggering thrombus formation several times in a row at different sites of the same vessel could change subsequent thrombus formation. A time-dependent effect on thrombus growth can also not be completely excluded. Control measurements, meaning repetitively inducing thrombi over a longer time period without any treatments to rule out this time-dependent effect were not done as the presence of Riociguat eliminated this possibility as soon as it was applied. In order to solve the limiting factors of the long measurement duration as well as the, the measurement of both conditions in the same mouse, respective platelet-specific NO-GC knockout mice, as it was done in the study of Wen et al. [139], could act as important control, since Riociguat treatment should not affect platelets devoid of NO-GC. Another possible pitfall is the application method of Riociguat, namely in the buffer used for superfusion of the cremaster. As an important control, the application and presence of Riociguat should be confirmed. While the superfusion of drugs can be performed in a simplistic way, it can be difficult to determine whether the substance really reaches the vessels in entirety or which drug concentration is reached in a measured thrombus and produces an effect. Since cGMP sensor mice were used, a measurement of cGMP level changes in the thrombi could have been a good validation method for the efficacy of Riociguat in our experiments. This was sadly not possible in our experimental setup, as the measurement of further wavelengths (in this case for CFP) was limited by the acquisition settings. Different application methods could also be a possible option to investigate the effect of Riociguat on thrombus growth. Oral administration (gavage) of Riociguat would lead to a more systemic application and would mimic the human situation in a more realistic way. A tail vein injection could also be a viable alternative for systemic drug

delivery. Another suggested improvement for the experiment is the measurement duration. Most of our measurements were stopped after 60 s, as most of the Riociguat treated thrombi were already completely dissolved. It would be advisable to prolong the measurement despite the lack of thrombi in order to gain a longer time frame of thrombus development in the more stable control thrombi and to gain more options for comparison.

Despite the limitations discussed above, our data shows that Riociguat has an effect on thrombus growth *in vivo*. Compared to control thrombi, Riociguat treatment led to a faster dissolution of thrombi and stabilization at a smaller size without altering the initial phase of thrombus formation. Considering this pharmacological effect of Riociguat, targeting mechanosensitive cGMP signaling in platelets could be beneficial to induce an anti-thrombotic effect without an increased bleeding risk, as the initial thrombus aggregation phase is not hampered by the drug.

5. Summary and outlook

Previous work has discovered that NO-induced cGMP generation in platelets is shear-dependent. In this study, we made several interesting observations regarding a potential mechanosensitive cGMP signaling complex at the platelet plasma membrane. Our findings suggest that integrins might act as mechanotransducers sensing the shear forces and relaying them into an intracellular, biochemical cGMP signal **(Figure 23)**. A cGMP signaling complex consisting of a transmembrane integrin such as α_{IIb}, β_3 or β_1 as well as cGKI and NO-GC binding the cytoplasmatic tail of the integrins would respond to a combination of shear stress and NO by generating cGMP, leading to an inhibition of platelet aggregation. Further validation of this model would include performing and optimizing a Co-IP using antibodies against NO-GC and the different integrins with subsequent mass spectrometric analysis to confirm the presence and composition of the membrane-bound cGMP signaling complex.

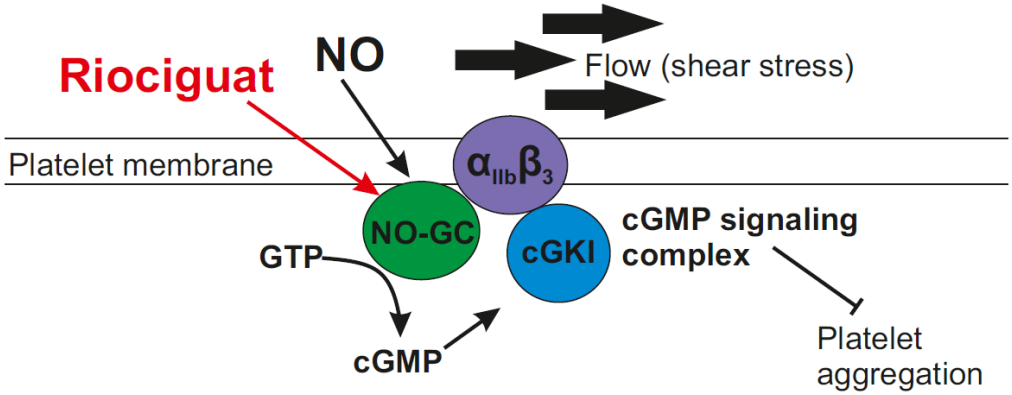

Figure 23: Model of a shear-sensitive cGMP signaling complex at the platelet plasma membrane.

In our working model, we hypothesize a cGMP signaling complex at the platelet plasma membrane which locally responds to NO and shear stress by producing cGMP. The generation of cGMP in platelets is dependent on the binding of NO to the NO-GC (green) as well as the presence of shear stress, which is sensed by a mechanotransducer, possibly integrin $\alpha_{IIb}\beta_3$ (purple) or $\alpha_2\beta_1$. Both the NO-GC and cGKI (blue), and presumably other, yet to be identified proteins form a complex around the cytoplasmatic domain of the integrin mechanotransducer. Once generated by NO-GC, cGMP activates cGKI which phosphorylates substrate proteins further downstream (not shown) leading to the inhibition of platelet aggregation. Activation of the mechanosensitive cGMP signaling complex, e.g. by the NO-GC stimulator Riociguat, limits the overgrowth of the thrombus in a shear-dependent manner.

Another method to visualize this signaling complex could also be an immunofluorescence staining of both cGKI and NO-GC in platelets. High resolution microscopy to detect a potential co-localization of NO-GC and cGKI as well as the different integrins at the platelet membrane would greatly support the data which was generated using rather biochemical methods. Furthermore, as this signaling complex also likely consists of further adapter proteins, their identification is also crucial to unravel the mechanosensitive cGMP signaling mechanism. To show a functional relevance, one could use a murine model in which the cytoplasmic domain of the integrins is mutated in platelets, which could therefore possibly prohibit the formation of a signaling complex. However, it is important to note that platelet aggregation cannot be inhibited completely, as it is a prerequisite for our experimental setup. Furthermore, combined with our transgenic cGMP sensor mouse line, one could analyze whether NO- and shear-dependent cGMP generation is changed at the platelet membrane. Integrin mutant mice have been successfully used in previous studies to investigate different research questions [176, 177]. In humans, patients suffering from Glanzmann's thrombasthenia express a very low amount of integrin $\alpha_{IIb}\beta_3$, resulting in a severe bleeding phenotype. While the live measurement of cGMP level changes in humans is not possible like in the transgenic mouse line

expressing the cGMP biosensor, using live calcium measurements as an indirect marker for cGMP changes might be a possible alternative [139].

As our preliminary data shows [139], cGMP generation in VSMCs also seems to be shear-dependent. It would therefore be interesting to check whether the mechanosensitive cGMP signaling complex detected in platelets in the present study also exists in other cell types. Nevertheless, we are just at the beginning of unraveling the mechanosensitive aspect of cGMP signaling, which could play a major role in many types of cells.

Previous studies have linked defective NO-dependent cGMP signaling to an increased risk to develop cardiovascular diseases [56-58]. The study by Erdmann et al. [56] described that dysfunctional NO-dependent cGMP signaling in platelets increases the risk of myocardial infarction, possibly due to accelerated thrombus formation. Our data is in line with this conjecture and suggests that their described phenotype might be, in fact, due to defective mechano-cGMP signaling in platelets. It has been proposed that pharmacological stimulation of NO-mediated cGMP signaling might be a viable treatment option to reduce the risk of cardiovascular diseases [56, 57]. Our *in vivo* data supports this assessment, as exposing thrombi to the NO-GC stimulator Riociguat led to a faster dissolution of thrombi and stabilization at a smaller size. Because this would theoretically reduce the risk of thrombosis, we conclude that the cGMP signaling pathway might indeed be a sensible pharmacological target to prevent cardiovascular diseases.

Additionally, our findings imply that cGMP-stimulating drugs could have a further advantage when comparing them to current anti-thrombotics. Since mechanistically, the NO-cGMP pathway negatively regulates platelet aggregation in a shear-dependent manner, the initial thrombus growth sealing the lesion in the vessel is not limited by cGMP due to low shear stress. Because of this, the possible side effect of an increased bleeding risk can be circumvented. Thus, a possible anti-thrombotic effect of PDE inhibitors like Sildenafil, Tadalafil or NO-GC stimulators and activators like Vericiguat and Cinaciguat should be looked at in the future. Testing the potential of these drugs to limit thrombosis in experimental approaches such as the *in vivo* cremaster model or the $FeCl_3$ model might therefore pave the way to eventually establish cGMP modulators as premier anti-thrombotics.

6. Appendix

6.1 MS protein list

PSMs are the so-called peptide spectrum matches, specifically the number of MS/MS spectra which clearly resulted in a peptide identification (the number of PSMs of given protein roughly correlates with the certainty of identification and quantification). Log2SumNormAbundance gives the Logarithm of the summed peptide feature intensities (MS level) of a given protein after normalization to the total intensity of the respective sample. Log2Ratio gives the logarithm of the ratio of a sample vs. the respective control which results in a symmetric data distribution around zero with values >0 indicating an enrichment. Shown in green are the control samples with their respective positive IP counterpart in orange (for example control 1.1 and sample 1.1). P-values were calculated using a Student's *t*-test for the Log2SumNormAbundance. Crossed out peptides are contaminants in the sample, while peptides marked in red are listed in the CRAPome [164]. All significantly enriched proteins are written in black, while proteins enriched in a statistically non-significant manner ($p<0.05$) are gray.

Uniprot Accession	Protein Description	# PSMs	# Unique Peptides	Log2SumNormAbundance: F17: Control, 1, 1	Log2SumNormAbundance: F20: Control, 2, 2	Log2SumNormAbundance: F21: Control, 3, 2	Log2SumNormAbundance: F24: Control, 3, 3	Log2SumNormAbundance: F25: Control, 4, 1	Log2SumNormAbundance: F31: Control, 2, 1	Log2SumNormAbundance: F18: Sample, 1, 1	Log2SumNormAbundance: F19: Sample, 2, 2	Log2SumNormAbundance: F22: Sample, 3, 2	Log2SumNormAbundance: F23: Sample, 3, 3	Log2SumNormAbundance: F26: Sample, 4, 1	Log2SumNormAbundance: F32: Sample, 2, 1	t.test logInt	Log2Ratio1.1	Log2Ratio2.2	Log2Ratio3.2	Log2Ratio3.3	Log2Ratio4.1	Log2Ratio2.1	Mean Log2Ratio
O95721	Synaptosomal-associated protein 29 OS=Homo sapiens GN=SNAP29 PE=1 SV=1	6	3	14.1	14.7	13.9	15.4	16.1	14.2	19.4	18.9	18.9	17.9	17.2	17.7	0.003	5.3	4.2	5.0	2.5	1.2	3.5	3.6
P04040	Catalase OS=Homo sapiens GN=CAT PE=1 SV=3	9	3	17.4	17.4	17.0	15.3	15.3	12.8	18.1	19.0	18.7	16.7	16.8	15.9	0.003	0.7	1.6	1.7	1.4	1.6	3.1	1.7
Q9H2K8	Serine/threonine-protein kinase TAO3 OS=Homo sapiens GN=TAOK3 PE=1 SV=2	14	3	16.0	17.4	17.1	16.3	17.4	16.0	16.9	17.9	18.0	17.0	17.5	17.2	0.004	0.9	0.6	0.8	0.7	0.1	1.1	0.7
Q14764	Major vault protein OS=Homo sapiens GN=MVP PE=1 SV=4	31	11	20.0	19.1	18.8	18.4	15.9	18.5	20.4	19.4	19.8	18.6	16.4	19.2	0.006	0.5	0.3	1.0	0.2	0.5	0.7	0.5
Q96HS1	Serine/threonine-protein phosphatase PGAM5, mitochondrial OS=Homo sapiens GN=PGAM5 PE=1 SV=2	9	2	17.5	17.8	17.2	16.1	17.3	15.7	18.4	18.5	18.9	17.1	17.5	16.7	0.006	0.9	0.7	1.7	1.0	0.2	1.0	0.9
Q16181	Septin-7 OS=Homo sapiens GN=SEPT7 PE=1 SV=2	41	10	17.8	20.0	19.6	18.9	19.4	19.8	18.6	20.0	20.6	19.6	19.7	20.6	0.007	0.8	0.0	1.0	0.7	0.4	0.8	0.6
Q15833	Syntaxin-binding protein 2 OS=Homo sapiens GN=STXBP2 PE=1 SV=2	112	14	19.8	21.4	20.8	20.8	20.8	18.5	20.9	21.7	22.6	21.3	21.4	19.6	0.008	1.1	0.3	1.7	0.5	0.7	1.1	0.9
Q15149	Plectin OS=Homo sapiens GN=PLEC PE=1 SV=3	1550	239	25.8	27.5	24.3	22.8	24.0	24.2	27.3	27.8	26.7	24.6	24.9	25.3	0.008	1.4	0.3	2.4	1.7	0.9	1.0	1.3
P23229	Integrin alpha-6 OS=Homo sapiens GN=ITGA6 PE=1 SV=5	68	10	17.7	21.0	19.5	19.9	20.5	18.3	18.4	21.9	22.0	21.1	21.7	19.0	0.009	0.7	0.9	2.6	1.2	1.2	0.7	1.2
P01042	Kininogen-1 OS=Homo sapiens GN=KNG1 PE=1 SV=2	27	6	19.1	19.6	18.4	16.7	17.3	16.0	19.3	19.7	19.2	17.3	17.9	16.3	0.009	0.2	0.1	0.7	0.5	0.5	0.3	0.4
~~P98171~~	~~Rho GTPase-activating protein 4 OS=Homo sapiens GN=ARHGAP4 PE=1 SV=2~~	~~2~~	~~2~~	~~18.7~~	~~18.7~~	~~18.5~~	~~17.9~~	~~17.9~~	~~17.3~~	~~17.9~~	~~18.8~~	~~17.7~~	~~17.0~~	~~16.9~~	~~15.9~~	~~0.012~~	~~-0.8~~	~~0.1~~	~~-0.8~~	~~-0.9~~	~~-1.1~~	~~-1.4~~	~~-0.8~~
Q14571	Inositol 1,4,5-trisphosphate receptor type 2 OS=Homo sapiens GN=ITPR2 PE=1 SV=2	15	3	15.8	17.3	16.9	14.3	16.7	15.9	16.9	18.1	18.0	15.7	17.1	15.9	0.012	1.1	0.8	1.1	1.4	0.4	0.0	0.8
P08567	Pleckstrin OS=Homo sapiens GN=PLEK PE=1 SV=3	26	5	18.4	19.9	19.6	19.8	19.2	18.6	19.3	20.1	20.8	19.9	19.8	19.3	0.013	0.9	0.2	1.2	0.2	0.6	0.6	0.6
P10809	60 kDa heat shock protein, mitochondrial OS=Homo sapiens GN=HSPD1 PE=1 SV=2	74	12	19.1	21.0	19.8	19.8	20.6	17.5	19.6	21.9	21.5	20.0	21.1	18.6	0.015	0.4	0.9	1.7	0.2	0.6	1.1	0.8
Q13976	cGMP-dependent protein kinase 1 OS=Homo sapiens GN=PRKG1 PE=1 SV=3	16	5	14.3	18.0	16.7	14.9	15.3	NA	20.1	19.2	20.0	18.0	17.4	14.8	0.016	5.8	1.2	3.4	3.1	2.1	#####	3.1
~~Q13177~~	~~Serine/threonine-protein kinase PAK 2 OS=Homo sapiens GN=PAK2 PE=1 SV=3~~	~~4~~	~~2~~	~~15.4~~	~~16.7~~	~~NA~~	~~16.0~~	~~NA~~	~~14.8~~	~~NA~~	~~16.1~~	~~17.7~~	~~15.5~~	~~NA~~	~~14.4~~	~~0.017~~	~~#####~~	~~-0.6~~	~~#####~~	~~-0.5~~	~~#####~~	~~-0.4~~	~~-0.5~~
Q9Y6F6	Protein MRVI1 OS=Homo sapiens GN=MRVI1 PE=1 SV=2	84	19	20.6	22.8	21.4	19.4	20.6	18.9	21.3	23.0	23.1	20.0	20.9	20.1	0.017	0.7	0.2	1.7	0.6	0.3	1.2	0.8
P08514	Integrin alpha-IIb OS=Homo sapiens GN=ITGA2B PE=1 SV=3	1020	42	24.9	26.5	25.6	25.7	26.2	24.0	25.2	27.2	27.5	26.2	27.0	24.6	0.017	0.3	0.7	1.9	0.6	0.8	0.6	0.8
Q5SW79	Centrosomal protein of 170 kDa OS=Homo sapiens GN=CEP170 PE=1 SV=1	7	3	16.5	16.2	17.3	17.1	16.0	16.2	17.4	18.4	18.6	17.0	16.9	17.1	0.019	1.0	2.2	1.3	-0.1	1.0	0.9	1.0
Q14203	Dynactin subunit 1 OS=Homo sapiens GN=DCTN1 PE=1 SV=3	50	15	18.4	20.3	19.4	19.4	18.9	18.0	19.0	20.5	21.2	19.9	19.6	18.8	0.019	0.6	0.2	1.8	0.5	0.7	0.8	0.8
Q93084	Sarcoplasmic/endoplasmic reticulum calcium ATPase 3 OS=Homo sapiens GN=ATP2A3 PE=1 SV=2	234	14	21.5	23.4	22.4	20.6	22.4	20.2	22.4	23.6	24.0	21.1	22.9	20.6	0.020	0.9	0.2	1.5	0.4	0.6	0.4	0.7
O43920	NADH dehydrogenase [ubiquinone] iron-sulfur protein 5 OS=Homo sapiens GN=NDUFS5 PE=1 SV=3	4	3	13.4	16.5	NA	NA	16.3	11.2	14.2	17.2	16.6	13.7	17.7	12.9	0.021	0.7	0.7	####	####	1.4	1.7	1.1
Q9UHQ9	NADH-cytochrome b5 reductase 1 OS=Homo sapiens GN=CYB5R1 PE=1 SV=1	6	3	16.0	16.7	16.0	14.5	16.5	NA	16.6	17.3	17.6	15.2	16.8	12.5	0.021	0.7	0.5	1.6	0.7	0.4	#####	0.8
P31146	Coronin-1A OS=Homo sapiens GN=CORO1A PE=1 SV=4	148	18	21.7	23.1	22.7	21.8	22.1	20.6	22.0	23.4	23.8	22.1	22.3	21.3	0.022	0.3	0.3	1.1	0.3	0.2	0.7	0.5
P04217	Alpha-1B-glycoprotein OS=Homo sapiens GN=A1BG PE=1 SV=4	21	4	17.6	19.0	18.4	18.1	17.8	NA	18.2	19.5	19.9	18.5	18.2	16.1	0.023	0.6	0.6	1.5	0.4	0.4	#####	0.7
P56202	Cathepsin W OS=Homo sapiens GN=CTSW PE=1 SV=2	11	3	17.2	19.3	17.5	15.9	17.9	16.3	17.8	19.2	17.9	16.3	18.1	16.5	0.023	0.6	0.0	0.4	0.4	0.1	0.2	0.3
P38646	Stress-70 protein, mitochondrial OS=Homo sapiens GN=HSPA9 PE=1 SV=2	36	8	17.7	20.0	18.3	17.7	18.8	16.3	17.7	20.4	19.7	18.0	19.7	17.4	0.024	0.0	0.4	1.5	0.3	0.8	1.1	0.7
P01876	Immunoglobulin heavy constant alpha 1 OS=Homo sapiens GN=IGHA1 PE=1 SV=2	190	4	22.6	22.5	22.3	21.3	20.8	20.2	22.9	22.7	23.4	21.6	21.1	20.8	0.024	0.4	0.2	1.1	0.2	0.2	0.6	0.5
Q14141	Septin-6 OS=Homo sapiens GN=SEPT6 PE=1 SV=4	63	5	17.0	19.2	18.9	18.3	18.2	17.6	17.4	19.4	19.8	18.6	18.3	18.5	0.026	0.4	0.2	0.9	0.3	0.1	0.9	0.5
P22694	cAMP-dependent protein kinase catalytic subunit beta OS=Homo sapiens GN=PRKACB PE=1 SV=2	34	4	18.3	20.2	19.4	19.4	18.9	16.9	19.0	20.3	20.4	19.5	19.1	17.7	0.026	0.8	0.1	1.0	0.1	0.2	0.7	0.5
P0DMV8	Heat shock 70 kDa protein 1A OS=Homo sapiens GN=HSPA1A PE=1 SV=1	115	5	16.0	19.5	17.6	17.8	17.6	16.7	16.9	19.4	19.7	18.4	18.4	17.6	0.027	0.9	-0.1	2.1	0.6	0.8	0.9	0.9
Q13586	Stromal interaction molecule 1 OS=Homo sapiens GN=STIM1 PE=1 SV=3	45	8	18.0	21.4	19.2	18.1	19.7	17.6	18.4	21.7	21.0	18.4	20.4	18.5	0.028	0.4	0.3	1.8	0.3	0.7	0.9	0.7
P35611	Alpha-adducin OS=Homo sapiens GN=ADD1 PE=1 SV=2	135	15	20.2	22.1	21.7	21.6	21.1	20.1	20.7	22.4	22.7	21.6	21.2	20.6	0.033	0.5	0.3	1.0	0.0	0.2	0.5	0.4
Q53GL0	Pleckstrin homology domain-containing family O member 1 OS=Homo sapiens GN=PLEKHO1 PE=1 SV=2	20	6	18.5	19.2	18.4	18.7	17.6	17.4	18.4	20.0	19.4	18.8	18.3	17.9	0.035	-0.1	0.8	1.0	0.1	0.7	0.5	0.5
Q8N1G4	Leucine-rich repeat-containing protein 47 OS=Homo sapiens GN=LRRC47 PE=1 SV=1	3	2	13.1	16.3	16.2	14.9	15.0	NA	15.1	17.5	16.5	15.2	16.0	14.6	0.035	2.0	1.2	0.3	0.3	1.1	#####	1.0
P13645	Keratin, type I cytoskeletal 10 OS=Homo sapiens GN=KRT10 PE=1 SV=6	1239	36	26.3	25.8	26.3	25.8	25.0	24.3	27.0	26.1	26.5	26.1	24.9	24.9	0.036	0.7	0.3	0.2	0.3	-0.1	0.7	0.3
O15143	Actin-related protein 2/3 complex subunit 1B OS=Homo sapiens GN=ARPC1B PE=1 SV=3	63	7	20.4	21.6	20.0	18.2	19.8	17.5	25.1	21.9	24.3	18.6	23.6	18.5	0.036	4.7	0.2	4.3	0.4	3.8	1.0	2.4
Q13561	Dynactin subunit 2 OS=Homo sapiens GN=DCTN2 PE=1 SV=4	30	5	18.4	19.7	19.3	19.1	18.9	15.9	19.1	20.2	20.8	19.5	19.5	18.8	0.036	0.7	0.6	1.5	0.4	0.6	2.8	1.1

P05556	Integrin beta-1 OS=Homo sapiens GN=ITGB1 PE=1 SV=2	79	8	18.8	22.0	20.3	20.3	21.2	19.2	19.0	22.6	22.7	21.1	22.4	19.6	0.037	0.1	0.6	2.3	0.8	1.1	0.4	0.9
Q12913	Receptor-type tyrosine-protein phosphatase eta OS=Homo sapiens GN=PTPRJ PE=1 SV=3	89	17	20.0	22.2	21.3	20.7	21.3	18.2	20.5	22.5	22.8	21.0	21.6	18.6	0.037	0.5	0.3	1.6	0.3	0.3	0.5	0.6
Q9H939	Proline-serine-threonine phosphatase-interacting protein 2 OS=Homo sapiens GN=PSTPIP2 PE=1 SV=4	13	4	18.1	18.9	18.4	18.5	18.3	17.9	18.6	19.4	19.3	18.4	18.7	18.1	0.037	0.5	0.5	0.9	-0.1	0.4	0.2	0.4
O00194	Ras-related protein Rab-27B OS=Homo sapiens GN=RAB27B PE=1 SV=4	52	6	19.3	20.9	20.0	18.9	19.8	17.7	20.6	20.8	21.8	19.2	20.0	19.0	0.039	1.3	0.0	1.8	0.4	0.2	1.3	0.8
~~P30740~~	~~Leukocyte elastase inhibitor OS=Homo sapiens GN=SERPINB1 PE=1 SV=1~~	~~12~~	~~3~~	~~NA~~	~~NA~~	~~15.9~~	~~15.5~~	~~15.5~~	~~NA~~	~~NA~~	~~NA~~	~~NA~~	~~14.0~~	~~14.0~~	~~NA~~	~~0.040~~	~~####~~	~~#####~~	~~####~~	~~-0.6~~	~~-0.7~~	~~#####~~	~~-0.6~~
Q9Y5X1	Sorting nexin-9 OS=Homo sapiens GN=SNX9 PE=1 SV=1	3	2	15.8	15.8	14.9	14.1	14.9	NA	16.5	NA	17.4	16.2	15.8	15.7	0.040	0.7	#####	2.4	2.0	0.9	#####	1.5
P25705	ATP synthase subunit alpha, mitochondrial OS=Homo sapiens GN=ATP5A1 PE=1 SV=1	104	11	20.0	22.1	20.5	19.6	21.1	18.3	20.3	22.5	22.8	20.2	21.8	19.1	0.040	0.3	0.4	2.4	0.6	0.7	0.7	0.8
P16284	Platelet endothelial cell adhesion molecule OS=Homo sapiens GN=PECAM1 PE=1 SV=1	79	16	20.2	22.7	21.0	20.4	21.6	19.4	20.5	22.9	22.6	20.7	22.4	19.7	0.042	0.3	0.2	1.6	0.3	0.8	0.3	0.6
Q96FZ7	Charged multivesicular body protein 6 OS=Homo sapiens GN=CHMP6 PE=1 SV=3	8	2	14.9	16.5	16.0	15.8	16.6	12.8	15.4	16.8	17.8	16.0	16.8	14.1	0.044	0.4	0.3	1.8	0.2	0.3	1.3	0.7
P26038	Moesin OS=Homo sapiens GN=MSN PE=1 SV=3	136	26	21.1	21.4	21.3	20.9	21.1	20.0	21.3	21.7	22.4	21.0	21.3	20.7	0.045	0.1	0.3	1.1	0.1	0.2	0.7	0.4
Q8NG06	E3 ubiquitin-protein ligase TRIM58 OS=Homo sapiens GN=TRIM58 PE=2 SV=2	45	8	19.1	20.8	20.1	19.2	19.9	16.4	19.8	20.9	21.2	19.2	20.1	17.2	0.046	0.6	0.1	1.1	0.0	0.2	0.8	0.5
O75558	Syntaxin-11 OS=Homo sapiens GN=STX11 PE=1 SV=1	84	9	18.0	21.3	20.0	19.6	20.1	15.3	18.5	22.0	22.0	20.0	20.0	16.3	0.046	0.6	0.7	2.0	0.5	-0.1	1.1	0.8
~~Q9HBI1~~	~~Beta-parvin OS=Homo sapiens GN=PARVB PE=1 SV=1~~	~~52~~	~~4~~	~~18.0~~	~~20.7~~	~~20.2~~	~~20.6~~	~~10.5~~	~~16.1~~	~~17.0~~	~~20.2~~	~~20.0~~	~~20.1~~	~~19.0~~	~~14.6~~	~~0.046~~	~~-0.1~~	~~-0.5~~	~~-0.2~~	~~-0.4~~	~~-0.6~~	~~-1.5~~	~~-0.5~~
P30101	Protein disulfide-isomerase A3 OS=Homo sapiens GN=PDIA3 PE=1 SV=4	18	5	17.4	19.5	17.5	17.1	18.2	15.5	17.3	20.3	19.7	17.5	19.0	16.7	0.047	-0.1	0.7	2.2	0.4	0.7	1.3	0.9
Q16799	Reticulon-1 OS=Homo sapiens GN=RTN1 PE=1 SV=1	11	2	15.9	17.7	16.5	15.7	17.2	12.3	16.1	18.4	18.3	16.0	17.5	14.5	0.047	0.2	0.7	1.8	0.3	0.3	2.2	0.9
O00116	Alkyldihydroxyacetonephosphate synthase, peroxisomal OS=Homo sapiens GN=AGPS PE=1 SV=1	12	3	17.6	18.5	17.8	17.1	18.0	NA	17.8	18.7	18.7	17.6	18.2	11.2	0.047	0.2	0.1	0.9	0.4	0.3	#####	0.4
Q9H3N1	Thioredoxin-related transmembrane protein 1 OS=Homo sapiens GN=TMX1 PE=1 SV=1	11	2	15.7	18.9	16.5	15.2	17.8	15.2	15.9	18.6	19.1	16.6	18.9	16.6	0.048	0.2	-0.3	2.6	1.4	1.1	1.5	1.1
Q9Y624	Junctional adhesion molecule A OS=Homo sapiens GN=F11R PE=1 SV=1	18	3	15.4	19.3	16.7	17.4	18.5	15.3	15.5	20.2	20.4	18.3	19.7	16.4	0.049	0.0	0.9	3.7	0.9	1.2	1.1	1.3
P14625	Endoplasmin OS=Homo sapiens GN=HSP90B1 PE=1 SV=1	6	2	16.4	17.9	15.6	16.6	16.4	15.6	16.9	18.4	18.0	16.7	17.3	16.4	0.050	0.5	0.4	2.4	0.1	0.9	0.8	0.8
Q08722	Leukocyte surface antigen CD47 OS=Homo sapiens GN=CD47 PE=1 SV=1	13	2	NA	17.7	16.3	16.8	17.2	NA	15.1	18.2	18.4	17.4	18.3	13.0	0.050	####	0.5	2.1	0.6	1.2	#####	1.1
P53621	Coatomer subunit alpha OS=Homo sapiens GN=COPA PE=1 SV=2	12	4	16.1	17.7	16.6	17.0	16.7	14.9	17.4	17.8	18.5	17.0	17.1	15.8	0.050	1.3	0.1	1.8	0.0	0.4	0.9	0.8
O14672	Disintegrin and metalloproteinase domain-containing protein 10 OS=Homo sapiens GN=ADAM10 PE=1 SV=1	8	2	16.7	18.6	17.3	17.3	17.7	NA	17.3	19.0	19.5	17.9	18.5	16.5	0.050	0.6	0.4	2.2	0.6	0.8	#####	0.9
Q9NXH8	Torsin-4A OS=Homo sapiens GN=TOR4A PE=1 SV=2	54	5	19.9	21.3	20.4	19.8	20.4	19.6	20.9	21.5	21.2	19.7	20.6	19.9	0.050	0.9	0.2	0.8	0.0	0.2	0.3	0.4
P61952	Guanine nucleotide-binding protein G(I)/G(S)/G(O) subunit gamma-11 OS=Homo sapiens GN=GNG11 PE=1 SV=1	44	5	19.5	21.9	20.3	20.7	21.3	19.3	19.6	22.2	22.0	21.1	21.8	19.8	0.051	0.1	0.4	1.7	0.4	0.5	0.5	0.6
Q96RT1	Erbin OS=Homo sapiens GN=ERBIN PE=1 SV=2	6	2	16.1	18.2	17.2	16.4	17.3	15.8	17.1	18.3	18.2	16.8	17.3	16.1	0.051	1.0	0.1	1.0	0.3	0.0	0.3	0.4
P11171	Protein 4.1 OS=Homo sapiens GN=EPB41 PE=1 SV=4	140	17	19.0	21.9	21.0	22.1	19.8	20.1	20.0	21.8	22.0	22.3	20.0	21.2	0.052	0.9	-0.1	1.0	0.2	0.2	1.0	0.5
P61769	Beta-2-microglobulin OS=Homo sapiens GN=B2M PE=1 SV=1	46	3	20.8	22.7	20.7	20.4	21.0	20.5	21.7	23.0	22.6	21.1	21.6	20.3	0.052	0.9	0.3	1.9	0.8	0.7	-0.2	0.7
Q14677	Clathrin interactor 1 OS=Homo sapiens GN=CLINT1 PE=1 SV=1	92	14	18.9	22.3	21.3	20.8	20.9	18.5	19.6	22.5	23.0	21.0	21.0	19.5	0.053	0.8	0.2	1.6	0.2	0.0	1.0	0.6
P27824	Calnexin OS=Homo sapiens GN=CANX PE=1 SV=2	28	6	16.1	19.8	17.2	17.2	18.7	16.1	16.6	20.2	19.9	17.4	19.4	17.1	0.054	0.5	0.4	2.7	0.2	0.7	1.0	0.9
Q14643	Inositol 1,4,5-trisphosphate receptor type 1 OS=Homo sapiens GN=ITPR1 PE=1 SV=3	30	7	18.6	20.1	19.1	17.4	18.8	16.5	19.4	20.1	20.2	17.3	19.1	17.7	0.054	0.9	0.1	1.2	-0.1	0.3	1.3	0.6
P22695	Cytochrome b-c1 complex subunit 2, mitochondrial OS=Homo sapiens GN=UQCRC2 PE=1 SV=3	10	2	15.9	17.2	16.1	15.1	17.5	12.1	15.5	18.3	18.2	16.0	18.0	15.0	0.055	-0.4	1.1	2.1	0.9	0.5	2.9	1.2
Q16891	MICOS complex subunit MIC60 OS=Homo sapiens GN=IMMT PE=1 SV=1	187	29	22.2	23.8	22.3	20.7	21.9	20.7	22.8	23.6	23.3	21.1	22.1	21.0	0.055	0.5	-0.1	1.0	0.4	0.2	0.3	0.4
P14543	Nidogen-1 OS=Homo sapiens GN=NID1 PE=1 SV=3	32	8	19.9	21.6	20.3	19.4	19.5	18.0	20.3	21.7	21.5	19.6	19.7	19.3	0.056	0.4	0.0	1.1	0.2	0.2	1.3	0.5
Q14247	Src substrate cortactin OS=Homo sapiens GN=CTTN PE=1 SV=2	552	41	24.4	25.6	24.7	24.2	24.5	22.1	25.6	25.6	25.5	24.3	24.6	23.2	0.056	1.2	-0.1	0.8	0.1	0.2	1.1	0.5
P38606	V-type proton ATPase catalytic subunit A OS=Homo sapiens GN=ATP6V1A PE=1 SV=2	13	2	16.4	17.2	17.4	17.5	16.0	15.2	16.5	17.5	18.3	17.4	17.0	15.6	0.057	0.1	0.3	0.9	-0.1	0.9	0.3	0.4
P11234	Ras-related protein Ral-B OS=Homo sapiens GN=RALB PE=1 SV=1	20	5	18.4	20.0	19.3	18.9	19.7	17.7	18.6	20.1	21.2	19.4	20.6	18.2	0.059	0.2	0.1	1.9	0.4	0.8	0.5	0.7
P63010	AP-2 complex subunit beta OS=Homo sapiens GN=AP2B1 PE=1 SV=1	16	2	17.6	16.6	18.6	18.5	18.0	16.0	18.3	18.7	19.4	18.3	18.2	17.4	0.059	0.7	2.1	0.8	-0.2	0.2	1.5	0.8
Q9Y2Q0	Phospholipid-transporting ATPase IA OS=Homo sapiens GN=ATP8A1 PE=1 SV=1	9	2	15.6	NA	16.5	16.6	17.7	14.6	15.5	17.7	17.8	17.0	18.4	16.0	0.060	-0.1	#####	1.3	0.4	0.7	1.4	0.7
O43815	Striatin OS=Homo sapiens GN=STRN PE=1 SV=4	14	3	14.6	18.1	16.9	12.9	17.5	NA	15.3	19.1	19.2	16.1	17.5	14.1	0.061	0.7	1.0	2.3	3.1	0.0	#####	1.5
Q99961	Endophilin-A2 OS=Homo sapiens GN=SH3GL1 PE=1 SV=1	10	2	17.3	18.2	18.0	17.8	17.7	16.3	18.4	18.6	19.2	17.5	17.9	17.5	0.061	1.1	0.3	1.2	-0.3	0.2	1.2	0.6
P20674	Cytochrome c oxidase subunit 5A, mitochondrial OS=Homo sapiens GN=COX5A PE=1 SV=2	16	4	17.9	20.6	18.6	18.2	20.3	16.5	18.1	20.9	20.4	18.8	20.3	17.6	0.063	0.2	0.3	1.7	0.6	0.0	1.1	0.6
P19367	Hexokinase-1 OS=Homo sapiens GN=HK1 PE=1 SV=3	5	2	15.1	17.2	16.0	15.9	16.7	14.0	15.3	17.4	17.3	16.1	17.3	14.1	0.065	0.2	0.3	1.3	0.1	0.5	0.1	0.4
Q9Y4D1	Disheveled-associated activator of morphogenesis 1 OS=Homo sapiens GN=DAAM1 PE=1 SV=2	110	19	21.0	23.0	20.9	20.0	20.8	19.5	21.3	23.1	22.2	20.1	21.0	20.0	0.065	0.4	0.0	1.2	0.2	0.2	0.6	0.4
P26641	Elongation factor 1-gamma OS=Homo sapiens GN=EEF1G PE=1 SV=3	14	3	17.0	16.1	18.3	18.4	17.7	NA	18.2	17.5	19.4	18.3	17.9	13.2	0.066	1.2	1.4	1.2	-0.1	0.2	#####	0.8
Q8NBX0	Saccharopine dehydrogenase-like oxidoreductase OS=Homo sapiens GN=SCCPDH PE=1 SV=1	3	2	16.1	18.1	16.4	14.8	17.1	NA	16.1	18.6	17.9	15.2	17.9	NA	0.066	0.0	0.5	1.5	0.4	0.7	#####	0.6
Q8NE71	ATP-binding cassette sub-family F member 1 OS=Homo sapiens GN=ABCF1 PE=1 SV=2	8	4	16.5	NA	17.3	16.8	16.6	14.8	17.1	16.1	17.6	17.0	16.9	16.3	0.067	0.6	#####	0.3	0.2	0.3	1.5	0.6
P28482	Mitogen-activated protein kinase 1 OS=Homo sapiens GN=MAPK1 PE=1 SV=3	5	2	15.7	16.8	16.3	15.3	16.7	13.5	17.0	16.5	17.6	16.6	16.5	15.6	0.067	1.3	-0.3	1.2	1.4	-0.2	2.1	0.9
P41091	Eukaryotic translation initiation factor 2 subunit 3 OS=Homo sapiens GN=EIF2S3 PE=1 SV=3	20	4	16.9	18.6	18.4	18.2	18.1	15.3	19.5	19.4	19.4	18.2	18.0	18.1	0.068	2.6	0.8	1.0	0.1	-0.2	2.9	1.2
Q01518	Adenylyl cyclase-associated protein 1 OS=Homo sapiens GN=CAP1 PE=1 SV=5	79	11	19.0	20.7	20.9	21.0	20.6	17.1	19.6	20.7	22.2	21.1	20.9	18.8	0.068	0.6	-0.1	1.3	0.1	0.3	1.7	0.7
P00387	NADH-cytochrome b5 reductase 3 OS=Homo sapiens GN=CYB5R3 PE=1 SV=3	18	3	NA	19.4	NA	16.1	18.7	13.4	17.2	19.8	19.5	17.0	19.6	15.7	0.068	####	0.4	####	0.8	0.9	2.3	1.1
P11142	Heat shock cognate 71 kDa protein OS=Homo sapiens GN=HSPA8 PE=1 SV=1	232	16	20.2	22.6	21.7	21.4	21.0	19.8	20.9	22.6	22.9	21.5	21.2	20.1	0.069	0.8	0.0	1.2	0.1	0.3	0.3	0.4

P61224	Ras-related protein Rap-1b OS=Homo sapiens GN=RAP1B PE=1 SV=1	207	12	23.0	23.9	23.7	23.5	23.8	22.8	23.4	24.1	25.1	23.6	24.3	22.9	0.070	0.4	0.2	1.4	0.2	0.5	0.1	0.5
Q9H7D0	Dedicator of cytokinesis protein 5 OS=Homo sapiens GN=DOCK5 PE=1 SV=3	2	2	16.7	16.1	16.5	16.0	16.7	16.4	16.8	16.8	17.7	16.1	16.7	16.7	0.071	0.1	0.7	1.2	0.1	0.1	0.3	0.4
Q9H425	Uncharacterized protein C1orf198 OS=Homo sapiens GN=C1orf198 PE=1 SV=1	55	11	19.6	21.7	19.9	19.0	20.0	17.5	19.3	22.1	21.1	19.6	20.2	18.4	0.071	-0.3	0.4	1.2	0.5	0.2	0.9	0.5
P02671	Fibrinogen alpha chain OS=Homo sapiens GN=FGA PE=1 SV=2	1568	47	25.6	26.5	25.9	25.3	26.2	23.9	25.9	26.7	27.3	25.4	26.4	24.3	0.072	0.2	0.2	1.4	0.1	0.2	0.4	0.4
Q14165	Malectin OS=Homo sapiens GN=MLEC PE=1 SV=1	21	2	16.6	18.6	16.4	15.6	17.9	NA	17.1	19.5	18.9	16.2	18.3	15.0	0.072	0.5	0.9	2.5	0.6	0.4	#####	1.0
Q9NV96	Cell cycle control protein 50A OS=Homo sapiens GN=TMEM30A PE=1 SV=1	10	2	16.1	18.3	17.3	16.5	17.8	NA	15.9	18.8	19.0	17.2	18.5	16.7	0.072	-0.1	0.5	1.7	0.7	0.8	#####	0.7
P06396	Gelsolin OS=Homo sapiens GN=GSN PE=1 SV=1	740	34	26.6	26.6	26.0	25.2	25.5	24.9	27.0	26.7	27.0	25.2	25.7	25.1	0.074	0.3	0.1	1.0	0.0	0.2	0.2	0.3
P51148	Ras-related protein Rab-5C OS=Homo sapiens GN=RAB5C PE=1 SV=2	8	2	17.3	17.4	17.3	16.6	16.2	16.4	18.2	17.2	18.7	17.0	17.2	16.2	0.076	0.9	-0.1	1.3	0.4	1.0	-0.1	0.5
P27105	Erythrocyte band 7 integral membrane protein OS=Homo sapiens GN=STOM PE=1 SV=3	702	15	23.4	25.7	24.9	24.2	24.7	22.7	24.1	25.9	26.0	24.3	24.9	22.7	0.076	0.7	0.2	1.1	0.0	0.3	0.0	0.4
Q8N699	Myc target protein 1 OS=Homo sapiens GN=MYCT1 PE=1 SV=1	24	5	17.2	20.2	17.9	17.5	18.2	15.8	18.3	20.5	20.7	17.9	18.1	17.1	0.078	1.0	0.3	2.8	0.4	-0.1	1.3	1.0
Q9BR76	Coronin-1B OS=Homo sapiens GN=CORO1B PE=1 SV=1	103	9	19.6	21.4	20.3	19.9	19.8	19.5	20.1	21.5	21.4	19.8	20.3	19.7	0.079	0.5	0.1	1.1	-0.1	0.5	0.3	0.4
Q0ZGT2	Nexilin OS=Homo sapiens GN=NEXN PE=1 SV=1	1370	70	25.3	27.1	25.2	24.7	25.1	23.9	25.6	27.1	26.5	24.9	25.2	24.6	0.079	0.3	0.0	1.2	0.2	0.1	0.8	0.4
Q93050	V-type proton ATPase 116 kDa subunit a isoform 1 OS=Homo sapiens GN=ATP6V0A1 PE=1 SV=3	11	3	16.9	18.3	17.3	16.4	17.0	14.7	17.8	18.2	18.9	16.6	17.8	NA	0.080	0.9	0.0	1.6	0.2	0.8	#####	0.7
P22061	Protein-L-isoaspartate(D-aspartate) O-methyltransferase OS=Homo sapiens GN=PCMT1 PE=1 SV=4	7	2	16.8	17.6	17.3	17.5	17.1	15.8	17.1	19.8	18.6	17.5	17.4	16.3	0.081	0.2	2.2	1.4	0.0	0.3	0.4	0.8
P23219	Prostaglandin G/H synthase 1 OS=Homo sapiens GN=PTGS1 PE=1 SV=2	12	3	15.8	19.5	16.8	15.4	17.5	NA	16.7	19.6	19.0	15.9	18.0	12.2	0.081	0.9	0.1	2.2	0.5	0.5	#####	0.9
P62937	Peptidyl-prolyl cis-trans isomerase A OS=Homo sapiens GN=PPIA PE=1 SV=2	171	9	21.0	24.5	22.0	21.1	22.3	19.9	21.3	24.5	23.5	21.4	23.0	20.2	0.081	0.2	0.0	1.5	0.3	0.7	0.2	0.5
P50402	Emerin OS=Homo sapiens GN=EMD PE=1 SV=1	83	11	21.6	23.3	21.6	19.6	20.9	19.4	22.2	23.3	22.8	19.6	21.1	19.8	0.082	0.6	0.0	1.3	0.0	0.3	0.4	0.4
P43304	Glycerol-3-phosphate dehydrogenase, mitochondrial OS=Homo sapiens GN=GPD2 PE=1 SV=3	45	5	19.9	21.2	20.6	19.2	20.8	15.8	20.5	21.7	22.1	19.1	21.0	18.2	0.083	0.5	0.5	1.5	-0.1	0.2	2.4	0.8
Q86WR7	Proline and serine-rich protein 2 OS=Homo sapiens GN=PROSER2 PE=1 SV=2	25	3	18.2	19.6	18.0	17.2	18.3	17.9	18.2	19.9	19.0	17.3	18.5	18.3	0.083	0.0	0.2	1.0	0.1	0.2	0.4	0.3
P21926	CD9 antigen OS=Homo sapiens GN=CD9 PE=1 SV=4	30	3	17.1	19.9	18.1	18.6	20.0	17.4	18.8	20.6	21.1	19.6	20.9	16.6	0.084	1.7	0.7	3.0	1.0	0.9	-0.8	1.1
O60496	Docking protein 2 OS=Homo sapiens GN=DOK2 PE=1 SV=2	12	3	17.7	19.3	18.2	18.0	18.0	NA	18.0	19.6	19.3	18.3	18.2	16.9	0.084	0.2	0.3	1.1	0.2	0.2	#####	0.4
P09486	SPARC OS=Homo sapiens GN=SPARC PE=1 SV=1	12	2	15.5	20.6	18.9	18.7	19.2	NA	16.1	20.8	20.4	19.0	19.5	NA	0.085	0.6	0.2	1.5	0.3	0.2	#####	0.6
Q8WWA1	Transmembrane protein 40 OS=Homo sapiens GN=TMEM40 PE=1 SV=2	13	2	18.7	20.5	19.0	17.4	18.9	15.0	19.0	20.8	20.6	17.4	19.1	17.2	0.086	0.4	0.3	1.5	0.1	0.1	2.2	0.8
P40197	Platelet glycoprotein V OS=Homo sapiens GN=GP5 PE=1 SV=1	60	8	21.1	22.8	20.8	20.1	21.4	18.9	21.2	22.9	22.3	20.2	22.0	19.6	0.086	0.0	0.1	1.4	0.0	0.6	0.6	0.5
P01861	Immunoglobulin heavy constant gamma 4 OS=Homo sapiens GN=IGHG4 PE=1 SV=1	561	5	20.0	19.6	19.9	18.5	21.3	16.4	20.5	19.6	20.9	18.6	21.4	18.0	0.087	0.5	0.0	1.0	0.1	0.1	1.6	0.6
P07948	Tyrosine-protein kinase Lyn OS=Homo sapiens GN=LYN PE=1 SV=3	102	10	20.2	21.5	20.9	20.5	20.5	18.7	21.1	21.6	22.0	20.5	20.4	19.1	0.087	1.0	0.1	1.1	0.1	0.0	0.4	0.4
P17301	Integrin alpha-2 OS=Homo sapiens GN=ITGA2 PE=1 SV=1	19	4	17.8	19.6	17.9	17.8	18.5	17.0	17.9	19.5	20.3	18.7	19.5	17.3	0.088	0.1	0.0	2.5	1.0	1.1	0.3	0.8
Q9H4G4	Golgi-associated plant pathogenesis-related protein 1 OS=Homo sapiens GN=GLIPR2 PE=1 SV=3	38	3	18.3	20.0	19.6	20.3	19.5	17.4	19.2	19.6	20.6	20.2	20.0	18.6	0.090	0.9	-0.4	1.0	-0.1	0.5	1.2	0.5
P01709	Immunoglobulin lambda variable 2-8 OS=Homo sapiens GN=IGLV2-8 PE=1 SV=2	7	2	19.4	20.2	19.2	17.6	18.0	15.8	20.6	19.8	19.7	18.1	18.3	18.0	0.091	1.2	-0.4	0.6	0.5	0.4	2.1	0.7
P27987	Inositol-trisphosphate 3-kinase B OS=Homo sapiens GN=ITPKB PE=1 SV=5	35	7	19.0	20.6	19.1	17.1	18.6	17.0	18.8	20.7	19.9	17.4	18.9	17.5	0.092	-0.2	0.1	0.8	0.3	0.3	0.5	0.3
Q6ZU35	Uncharacterized protein KIAA1211 OS=Homo sapiens GN=KIAA1211 PE=1 SV=3	98	15	20.4	22.4	20.0	18.3	19.8	17.9	20.5	22.4	21.3	18.6	19.9	19.2	0.092	0.1	0.0	1.3	0.3	0.1	1.3	0.5
P18433	Receptor-type tyrosine-protein phosphatase alpha OS=Homo sapiens GN=PTPRA PE=1 SV=2	12	3	16.3	17.6	16.4	16.9	17.4	15.9	17.1	17.8	18.7	16.9	17.4	16.9	0.092	0.9	0.2	2.3	0.0	0.1	1.0	0.7
Q7L576	Cytoplasmic FMR1-interacting protein 1 OS=Homo sapiens GN=CYFIP1 PE=1 SV=1	65	9	19.6	19.4	20.3	20.0	20.1	18.0	20.5	19.7	20.9	20.1	19.9	18.2	0.094	0.9	0.4	0.7	0.1	-0.2	0.2	0.3
Q9Y6M1	Insulin-like growth factor 2 mRNA-binding protein 2 OS=Homo sapiens GN=IGF2BP2 PE=1 SV=2	23	3	18.2	17.0	17.5	17.1	17.2	16.6	18.1	18.3	18.4	17.2	17.1	17.6	0.095	-0.1	1.3	0.9	0.1	-0.1	1.0	0.5
P11021	78 kDa glucose-regulated protein OS=Homo sapiens GN=HSPA5 PE=1 SV=2	83	13	18.3	21.2	20.0	19.2	19.4	NA	18.3	21.7	21.7	19.6	20.0	15.7	0.095	0.0	0.5	1.7	0.4	0.5	#####	0.6
Q96C24	Synaptotagmin-like protein 4 OS=Homo sapiens GN=SYTL4 PE=1 SV=2	78	14	19.5	22.0	20.5	19.9	20.4	19.6	19.7	22.3	22.3	20.2	20.8	19.8	0.096	0.2	0.3	1.8	0.3	0.3	0.2	0.5
P42566	Epidermal growth factor receptor substrate 15 OS=Homo sapiens GN=EPS15 PE=1 SV=2	16	3	16.3	18.9	18.4	18.3	17.5	15.2	16.7	19.0	19.7	18.4	17.8	17.5	0.096	0.4	0.1	1.4	0.1	0.2	2.3	0.7
Q05682	Caldesmon OS=Homo sapiens GN=CALD1 PE=1 SV=3	1930	69	26.0	28.4	26.2	25.2	26.5	24.4	26.1	28.4	27.4	25.4	26.5	25.1	0.097	0.1	0.1	1.2	0.2	0.0	0.7	0.4
Q92930	Ras-related protein Rab-8B OS=Homo sapiens GN=RAB8B PE=1 SV=2	12	2	17.0	17.4	16.8	16.4	16.9	NA	16.9	18.2	18.9	17.0	17.3	15.8	0.099	0.0	0.8	2.1	0.6	0.4	#####	0.8
P01009	Alpha-1-antitrypsin OS=Homo sapiens GN=SERPINA1 PE=1 SV=3	18	5	18.8	20.1	19.1	18.8	18.0	15.9	18.9	20.2	19.9	18.5	18.9	17.2	0.099	0.1	0.1	0.7	-0.2	0.9	1.3	0.5
O14617	AP-3 complex subunit delta-1 OS=Homo sapiens GN=AP3D1 PE=1 SV=1	53	5	20.0	20.8	19.6	19.9	20.0	18.4	20.5	20.8	20.9	19.9	20.0	19.5	0.100	0.5	0.0	1.2	0.0	0.0	1.1	0.5
Q13347	Eukaryotic translation initiation factor 3 subunit I OS=Homo sapiens GN=EIF3I PE=1 SV=1	22	5	19.7	19.6	18.1	17.9	17.4	18.2	20.4	19.6	18.2	18.1	17.5	19.5	0.100	0.7	0.0	0.2	0.2	0.1	1.3	0.4
P61026	Ras-related protein Rab-10 OS=Homo sapiens GN=RAB10 PE=1 SV=1	31	3	18.7	20.2	19.4	19.3	20.2	19.3	19.8	20.6	21.1	19.6	20.8	18.9	0.100	1.0	0.3	1.7	0.2	0.7	-0.4	0.6
O15127	Secretory carrier-associated membrane protein 2 OS=Homo sapiens GN=SCAMP2 PE=1 SV=2	8	2	NA	16.9	14.2	14.6	16.3	NA	15.3	17.8	17.9	15.4	17.3	NA	0.101	#####	0.9	3.7	0.9	0.9	#####	1.6
P07947	Tyrosine-protein kinase Yes OS=Homo sapiens GN=YES1 PE=1 SV=3	101	2	18.0	19.1	19.2	18.9	18.1	16.5	19.1	19.2	19.5	18.6	18.6	17.8	0.101	1.1	0.1	0.3	-0.3	0.4	1.3	0.5
O75190	DnaJ homolog subfamily B member 6 OS=Homo sapiens GN=DNAJB6 PE=1 SV=2	28	3	15.7	18.0	17.8	17.3	17.8	16.7	16.3	18.7	18.9	17.3	18.1	16.4	0.101	0.7	0.7	1.1	0.0	0.3	-0.3	0.4
Q8TEA8	D-aminoacyl-tRNA deacylase 1 OS=Homo sapiens GN=DTD1 PE=1 SV=2	32	3	20.1	20.2	20.0	19.7	19.3	19.6	20.3	20.2	20.8	19.8	19.6	19.9	0.101	0.1	0.0	0.7	0.0	0.3	0.2	0.2
O75563	Src kinase-associated phosphoprotein 2 OS=Homo sapiens GN=SKAP2 PE=1 SV=1	187	12	21.9	23.6	22.1	21.1	21.8	20.4	22.7	23.4	22.9	21.1	21.8	21.3	0.102	0.7	-0.2	0.8	0.0	0.0	0.9	0.4
P21281	V-type proton ATPase subunit B, brain isoform OS=Homo sapiens GN=ATP6V1B2 PE=1 SV=3	16	5	17.0	18.8	18.5	18.7	18.3	17.3	17.7	19.0	19.7	18.5	18.4	17.6	0.102	0.7	0.2	1.3	-0.2	0.1	0.3	0.4
Q6PJW8	Consortin OS=Homo sapiens GN=CNST PE=1 SV=3	44	9	19.5	21.9	20.3	18.5	20.1	18.2	19.5	21.9	21.5	18.7	20.3	18.7	0.103	0.0	0.0	1.2	0.2	0.3	0.5	0.3
Q13423	NAD(P) transhydrogenase, mitochondrial OS=Homo sapiens GN=NNT PE=1 SV=3	43	11	17.4	20.4	18.1	17.7	20.5	16.8	17.5	21.1	21.2	18.4	21.1	16.9	0.105	0.1	0.6	3.1	0.7	0.7	0.1	0.9

P01624	Immunoglobulin kappa variable 3-15 OS=Homo sapiens GN=IGKV3-15 PE=1 SV=2	57	2	21.8	21.1	20.8	19.7	19.6	NA	22.7	21.5	21.7	19.5	19.8	19.3	0.105	0.9	0.4	1.0	-0.2	0.2	#####	0.5
Q16762	Thiosulfate sulfurtransferase OS=Homo sapiens GN=TST PE=1 SV=4	15	3	17.0	19.8	17.7	16.6	18.1	14.3	17.3	19.9	19.5	16.5	18.5	15.4	0.105	0.3	0.1	1.8	-0.1	0.3	1.1	0.6
Q9UHB6	LIM domain and actin-binding protein 1 OS=Homo sapiens GN=LIMA1 PE=1 SV=1	122	18	21.3	23.1	21.4	20.3	21.0	20.2	21.6	23.1	22.7	20.5	21.1	20.6	0.105	0.3	0.0	1.3	0.2	0.1	0.4	0.4
P02679	Fibrinogen gamma chain OS=Homo sapiens GN=FGG PE=1 SV=3	651	25	24.4	25.1	24.9	24.1	25.0	22.7	25.2	25.2	25.9	24.0	25.2	22.9	0.106	0.8	0.2	1.0	-0.2	0.2	0.2	0.4
P05106	Integrin beta-3 OS=Homo sapiens GN=ITGB3 PE=1 SV=2	597	24	22.3	25.4	24.0	24.2	25.0	22.5	23.0	26.1	26.5	24.9	26.0	21.8	0.106	0.7	0.7	2.5	0.7	1.0	-0.7	0.8
Q12792	Twinfilin-1 OS=Homo sapiens GN=TWF1 PE=1 SV=3	5	2	17.1	16.8	16.8	16.9	16.0	13.9	17.3	17.0	17.4	17.1	17.1	17.0	0.106	0.2	0.2	0.6	0.2	1.2	3.1	0.9
O43561	Linker for activation of T-cells family member 1 OS=Homo sapiens GN=LAT PE=1 SV=1	27	3	17.8	19.8	19.4	19.5	19.0	18.2	17.8	20.4	20.5	19.2	19.5	18.6	0.106	0.0	0.6	1.1	-0.3	0.5	0.4	0.4
Q9BY44	Eukaryotic translation initiation factor 2A OS=Homo sapiens GN=EIF2A PE=1 SV=3	9	2	17.3	18.0	16.9	16.7	17.1	14.1	17.8	18.6	18.2	16.3	17.0	16.2	0.106	0.6	0.6	1.4	-0.3	0.0	2.1	0.7
P16615	Sarcoplasmic/endoplasmic reticulum calcium ATPase 2 OS=Homo sapiens GN=ATP2A2 PE=1 SV=1	79	4	16.9	19.6	18.8	17.2	18.7	13.6	17.3	19.7	20.0	17.1	19.0	15.7	0.108	0.4	0.1	1.2	-0.1	0.3	2.1	0.7
O00161	Synaptosomal-associated protein 23 OS=Homo sapiens GN=SNAP23 PE=1 SV=1	93	8	20.9	22.6	21.3	21.1	21.4	19.5	20.8	22.8	22.7	21.6	21.4	20.2	0.109	-0.1	0.2	1.4	0.5	0.0	0.7	0.5
P02751	Fibronectin OS=Homo sapiens GN=FN1 PE=1 SV=4	92	13	20.5	21.3	20.0	19.2	20.0	18.0	20.8	21.3	21.2	19.2	20.3	18.3	0.110	0.4	0.0	1.2	0.0	0.3	0.3	0.3
P53396	ATP-citrate synthase OS=Homo sapiens GN=ACLY PE=1 SV=3	7	2	13.6	15.7	15.9	16.0	16.0	NA	NA	16.2	17.0	16.2	16.1	14.0	0.110	####	0.5	1.0	0.2	0.1	#####	0.5
Q9NR12	PDZ and LIM domain protein 7 OS=Homo sapiens GN=PDLIM7 PE=1 SV=1	142	13	22.4	24.7	22.5	20.4	21.8	19.9	22.6	24.9	23.9	20.5	21.7	21.4	0.111	0.3	0.2	1.4	0.1	-0.1	1.6	0.6
P31930	Cytochrome b-c1 complex subunit 1, mitochondrial OS=Homo sapiens GN=UQCRC1 PE=1 SV=3	8	3	13.7	NA	14.7	NA	17.1	15.8	16.6	17.6	17.6	13.7	18.3	15.5	0.113	3.0	#####	2.9	####	1.3	-0.3	1.7
Q9P1Z2	Calcium-binding and coiled-coil domain-containing protein 1 OS=Homo sapiens GN=CALCOCO1 PE=1 SV=2	6	3	14.9	16.8	15.8	16.3	16.2	14.7	NA	18.0	17.8	16.7	15.7	16.5	0.113	####	1.1	1.9	0.3	-0.5	1.8	0.9
O95866	Megakaryocyte and platelet inhibitory receptor G6b OS=Homo sapiens GN=MPIG6B PE=1 SV=1	38	3	20.5	22.0	20.7	20.1	20.5	18.9	21.1	22.0	21.6	19.9	20.7	19.4	0.114	0.6	0.0	0.9	-0.2	0.2	0.5	0.3
Q15404	Ras suppressor protein 1 OS=Homo sapiens GN=RSU1 PE=1 SV=3	287	18	22.9	23.8	22.9	23.7	22.6	23.1	23.4	24.2	24.3	23.6	23.2	23.0	0.116	0.5	0.4	1.4	-0.1	0.6	-0.2	0.4
Q9BV40	Vesicle-associated membrane protein 8 OS=Homo sapiens GN=VAMP8 PE=1 SV=1	5	2	16.1	18.0	16.7	16.5	17.1	NA	16.6	18.3	18.9	16.5	17.7	15.9	0.118	0.5	0.4	2.2	0.0	0.6	#####	0.8
P62993	Growth factor receptor-bound protein 2 OS=Homo sapiens GN=GRB2 PE=1 SV=1	18	4	17.5	18.5	18.4	18.4	18.0	16.5	18.1	19.2	19.4	18.3	17.7	17.0	0.118	0.6	0.7	1.0	-0.1	-0.3	0.5	0.4
P11169	Solute carrier family 2, facilitated glucose transporter member 3 OS=Homo sapiens GN=SLC2A3 PE=1 SV=1	76	7	19.3	21.6	18.5	18.4	20.9	18.6	19.1	22.5	22.2	19.6	21.9	18.4	0.119	-0.2	0.9	3.7	1.2	1.1	-0.2	1.1
Q08379	Golgin subfamily A member 2 OS=Homo sapiens GN=GOLGA2 PE=1 SV=3	16	8	17.9	19.8	17.9	17.3	18.1	17.7	18.2	19.6	19.0	17.4	18.4	18.3	0.121	0.3	-0.2	1.1	0.1	0.3	0.6	0.3
Q01433	AMP deaminase 2 OS=Homo sapiens GN=AMPD2 PE=1 SV=2	12	2	17.2	18.1	17.8	17.1	17.3	17.9	16.7	18.6	18.5	17.9	17.7	18.2	0.121	-0.5	0.5	0.7	0.8	0.3	0.3	0.3
P48047	ATP synthase subunit O, mitochondrial OS=Homo sapiens GN=ATP5O PE=1 SV=1	3	2	13.3	15.1	14.0	13.8	14.7	NA	13.6	18.4	18.7	13.0	16.9	15.4	0.121	0.3	3.2	4.7	-0.7	2.2	#####	1.9
Q9Y5S2	Serine/threonine-protein kinase MRCK beta OS=Homo sapiens GN=CDC42BPB PE=1 SV=2	79	17	19.8	21.4	19.9	19.3	19.9	17.9	20.0	21.4	21.7	19.7	19.8	19.4	0.122	0.1	0.0	1.9	0.5	-0.1	1.5	0.6
Q9BRP8	Partner of Y14 and mago OS=Homo sapiens GN=PYM1 PE=1 SV=1	58	9	20.7	21.2	20.3	19.7	20.0	20.3	20.7	21.2	21.4	20.0	20.0	20.7	0.124	0.0	0.1	1.1	0.3	-0.1	0.5	0.3
P53814	Smoothelin OS=Homo sapiens GN=SMTN PE=1 SV=7	195	25	22.0	23.5	21.2	19.5	21.2	18.5	21.9	23.7	22.4	19.7	21.2	20.1	0.124	-0.1	0.3	1.2	0.2	0.0	1.6	0.5
P12259	Coagulation factor V OS=Homo sapiens GN=F5 PE=1 SV=4	783	51	24.4	25.9	24.6	23.9	24.3	23.7	24.9	25.7	25.5	23.9	24.5	24.0	0.125	0.5	-0.2	0.9	0.1	0.2	0.3	0.3
Q99623	Prohibitin-2 OS=Homo sapiens GN=PHB2 PE=1 SV=2	20	3	18.1	19.2	18.3	15.0	17.4	16.8	18.7	18.2	20.1	16.5	18.4	17.5	0.125	0.6	-1.0	1.8	1.5	1.0	0.6	0.8
P13073	Cytochrome c oxidase subunit 4 isoform 1, mitochondrial OS=Homo sapiens GN=COX4I1 PE=1 SV=1	29	4	17.5	20.6	18.2	17.4	19.9	NA	17.6	20.7	20.9	18.2	20.7	17.1	0.125	0.1	0.1	2.7	0.8	0.8	#####	0.9
P10124	Serglycin OS=Homo sapiens GN=SRGN PE=1 SV=3	22	2	18.2	20.6	19.1	18.8	18.9	NA	18.4	20.8	20.4	18.9	19.2	16.9	0.127	0.2	0.2	1.3	0.1	0.3	#####	0.4
Q13884	Beta-1-syntrophin OS=Homo sapiens GN=SNTB1 PE=1 SV=3	59	9	19.7	21.8	20.0	17.7	19.7	18.1	19.8	22.0	21.4	18.5	19.8	18.0	0.128	0.1	0.1	1.4	0.8	0.1	-0.1	0.4
Q9UI10	Translation initiation factor eIF-2B subunit delta OS=Homo sapiens GN=EIF2B4 PE=1 SV=2	19	2	17.5	18.6	17.9	17.8	17.3	17.4	17.9	18.9	18.5	17.9	17.4	17.2	0.130	0.4	0.3	0.5	0.0	0.1	-0.2	0.2
P07093	Glia-derived nexin OS=Homo sapiens GN=SERPINE2 PE=1 SV=1	16	3	18.3	18.5	18.3	17.7	17.6	17.2	19.1	18.3	19.3	17.6	18.4	17.2	0.131	0.7	-0.1	1.0	-0.1	0.7	0.0	0.4
Q9ULV4	Coronin-1C OS=Homo sapiens GN=CORO1C PE=1 SV=1	760	33	24.9	26.4	25.0	24.7	25.0	24.9	25.1	26.5	26.3	24.9	25.2	25.0	0.131	0.3	0.1	1.3	0.2	0.2	0.1	0.3
P17987	T-complex protein 1 subunit alpha OS=Homo sapiens GN=TCP1 PE=1 SV=1	15	6	18.7	18.7	19.1	19.6	18.6	16.2	19.2	18.8	19.8	19.7	18.7	18.5	0.133	0.5	0.1	0.7	0.1	0.1	2.3	0.6
Q9UJW0	Dynactin subunit 4 OS=Homo sapiens GN=DCTN4 PE=1 SV=1	7	2	16.5	17.7	17.3	17.0	17.3	NA	17.5	17.5	17.9	17.3	17.5	14.0	0.134	0.9	-0.2	0.6	0.3	0.2	#####	0.4
P02649	Apolipoprotein E OS=Homo sapiens GN=APOE PE=1 SV=1	13	4	19.4	18.9	17.2	15.5	17.3	16.9	19.2	19.1	18.0	16.6	17.3	17.1	0.134	-0.2	0.2	0.7	1.1	0.0	0.2	0.3
Q99719	Septin-5 OS=Homo sapiens GN=SEPT5 PE=1 SV=1	14	6	16.0	17.0	17.1	17.4	17.4	18.7	16.5	18.2	18.3	17.3	17.1	18.8	0.136	0.5	1.2	1.2	-0.1	-0.2	0.1	0.5
P45880	Voltage-dependent anion-selective channel protein 2 OS=Homo sapiens GN=VDAC2 PE=1 SV=2	67	5	19.2	21.7	20.7	19.6	20.9	18.1	20.4	22.2	22.4	19.5	21.3	17.9	0.136	1.2	0.5	1.7	-0.1	0.4	-0.3	0.6
P55160	Nck-associated protein 1-like OS=Homo sapiens GN=NCKAP1L PE=1 SV=3	10	2	15.5	16.6	15.6	16.3	15.8	NA	16.8	NA	17.3	16.0	16.5	14.7	0.137	1.3	#####	1.6	-0.2	0.6	#####	0.8
P61586	Transforming protein RhoA OS=Homo sapiens GN=RHOA PE=1 SV=1	40	5	20.0	21.5	20.1	20.4	20.4	16.7	19.9	21.7	21.9	20.1	20.8	18.9	0.141	-0.1	0.2	1.8	-0.3	0.5	2.1	0.7
Q99439	Calponin-2 OS=Homo sapiens GN=CNN2 PE=1 SV=4	97	11	20.4	22.3	21.2	20.6	20.5	19.2	20.8	22.4	22.1	20.9	20.8	18.9	0.142	0.4	0.1	0.9	0.3	0.3	-0.3	0.3
Q08495	Dematin OS=Homo sapiens GN=DMTN PE=1 SV=3	170	16	21.8	23.5	22.1	21.8	21.5	20.6	21.8	23.5	23.3	21.9	21.7	21.1	0.145	0.0	0.1	1.3	0.1	0.1	0.5	0.3
P37802	Transgelin-2 OS=Homo sapiens GN=TAGLN2 PE=1 SV=3	51	6	19.8	20.7	20.1	19.5	19.6	18.7	20.0	20.8	21.3	19.7	19.3	19.5	0.145	0.2	0.1	1.3	0.2	-0.2	0.8	0.4
O15144	Actin-related protein 2/3 complex subunit 2 OS=Homo sapiens GN=ARPC2 PE=1 SV=1	35	5	19.6	20.1	18.9	17.3	18.9	16.6	20.9	19.8	19.7	17.7	18.8	17.1	0.145	1.4	-0.4	0.7	0.4	-0.1	0.5	0.4
Q9NS28	Regulator of G-protein signaling 18 OS=Homo sapiens GN=RGS18 PE=1 SV=1	32	7	19.0	19.8	17.9	17.7	18.2	17.1	18.6	19.7	18.8	18.3	18.6	18.0	0.146	-0.4	-0.2	1.0	0.6	0.5	1.0	0.4
Q7Z2W4	Zinc finger CCCH-type antiviral protein 1 OS=Homo sapiens GN=ZC3HAV1 PE=1 SV=3	34	7	18.5	19.9	19.1	18.9	19.0	16.8	18.5	20.1	20.0	18.7	19.1	17.7	0.147	0.0	0.2	0.9	-0.2	0.2	0.8	0.3
Q93008	Probable ubiquitin carboxyl-terminal hydrolase FAF-X OS=Homo sapiens GN=USP9X PE=1 SV=3	3	2	NA	NA	NA	15.7	15.8	15.4	15.8	NA	NA	15.5	15.1	13.9	0.148	####	#####	####	-0.2	-0.7	-1.4	-0.8
P41240	Tyrosine-protein kinase CSK OS=Homo sapiens GN=CSK PE=1 SV=1	13	3	17.4	18.5	17.7	18.2	17.6	15.9	18.0	18.0	18.6	18.1	18.2	17.1	0.149	0.6	-0.5	0.9	-0.1	0.6	1.2	0.4
Q13576	Ras GTPase-activating-like protein IQGAP2 OS=Homo sapiens GN=IQGAP2 PE=1 SV=4	161	31	23.6	24.8	23.3	22.4	23.0	22.0	24.0	24.7	24.5	22.4	23.0	22.4	0.149	0.4	-0.1	1.2	0.1	0.0	0.5	0.3
O95810	Caveolae-associated protein 2 OS=Homo sapiens GN=CAVIN2 PE=1 SV=3	1465	46	26.0	26.9	26.7	26.4	25.6	26.3	26.5	26.8	27.5	26.5	25.7	26.3	0.149	0.5	-0.1	0.8	0.1	0.1	0.0	0.2

P40227	T-complex protein 1 subunit zeta OS=Homo sapiens GN=CCT6A PE=1 SV=3	20	6	17.0	18.0	18.3	18.3	17.6	16.2	17.6	17.8	19.6	18.1	17.7	17.2	0.151	0.6	-0.2	1.3	-0.2	0.2	1.0	0.4
Q14BN4	Sarcolemmal membrane-associated protein OS=Homo sapiens GN=SLMAP PE=1 SV=1	34	8	17.7	19.9	18.7	17.3	18.5	12.2	18.1	20.3	19.8	17.6	18.6	16.6	0.154	0.4	0.4	1.1	0.3	0.1	4.3	1.1
Q86WI1	Fibrocystin-L OS=Homo sapiens GN=PKHD1L1 PE=2 SV=2	22	6	18.9	19.6	19.2	20.0	19.2	19.3	19.4	19.5	20.0	19.8	19.3	20.5	0.155	0.5	-0.1	0.8	-0.2	0.1	1.2	0.4
P00747	Plasminogen OS=Homo sapiens GN=PLG PE=1 SV=2	5	2	16.7	18.1	16.6	15.2	16.7	NA	17.9	17.4	17.9	16.0	17.1	15.1	0.156	1.3	-0.6	1.3	0.8	0.4	#####	0.6
P09622	Dihydrolipoyl dehydrogenase, mitochondrial OS=Homo sapiens GN=DLD PE=1 SV=2	2	2	15.6	NA	14.8	13.7	15.4	14.7	15.7	16.9	16.8	14.8	16.4	14.2	0.158	0.1	#####	2.1	1.1	1.0	-0.5	0.8
Q96HC4	PDZ and LIM domain protein 5 OS=Homo sapiens GN=PDLIM5 PE=1 SV=5	89	9	18.9	22.2	20.5	19.3	19.7	17.4	19.0	22.3	21.9	19.4	19.9	17.6	0.159	0.1	0.0	1.4	0.1	0.2	0.2	0.4
Q92686	Neurogranin OS=Homo sapiens GN=NRGN PE=1 SV=1	27	3	19.5	21.0	19.7	19.4	20.3	19.0	19.5	21.2	20.6	19.3	20.5	20.0	0.161	-0.1	0.1	0.8	-0.1	0.1	1.0	0.3
Q7L7X3	Serine/threonine-protein kinase TAO1 OS=Homo sapiens GN=TAOK1 PE=1 SV=1	11	2	17.1	17.4	17.3	17.1	16.7	17.3	17.1	17.9	18.4	16.8	17.1	17.6	0.161	0.0	0.6	1.1	-0.3	0.3	0.2	0.3
Q9UBW5	Bridging integrator 2 OS=Homo sapiens GN=BIN2 PE=1 SV=3	193	15	21.3	22.7	22.4	22.3	21.7	21.6	21.5	22.7	23.6	22.4	22.0	21.6	0.161	0.2	0.0	1.2	0.1	0.3	0.0	0.3
Q92614	Unconventional myosin-XVIIIa OS=Homo sapiens GN=MYO18A PE=1 SV=3	82	16	24.2	23.9	24.0	23.4	23.3	22.4	24.1	24.4	24.3	23.4	23.4	22.4	0.162	-0.1	0.5	0.3	0.0	0.0	0.1	0.1
Q9H2D6	TRIO and F-actin-binding protein OS=Homo sapiens GN=TRIOBP PE=1 SV=3	13	2	17.1	17.6	16.5	15.7	16.7	14.8	17.3	18.1	17.2	15.5	16.5	15.8	0.162	0.2	0.5	0.7	-0.2	-0.2	1.0	0.3
Q86UT6	NLR family member X1 OS=Homo sapiens GN=NLRX1 PE=1 SV=1	10	4	14.4	18.0	17.4	16.3	17.1	13.1	16.0	18.4	17.9	15.9	17.7	NA	0.162	1.6	0.4	0.5	-0.3	0.6	#####	0.5
P11277	Spectrin beta chain, erythrocytic OS=Homo sapiens GN=SPTB PE=1 SV=5	484	62	21.6	23.7	22.9	24.5	21.4	23.5	21.9	23.6	23.6	24.5	21.4	24.1	0.162	0.3	-0.1	0.7	0.0	0.0	0.6	0.2
P00488	Coagulation factor XIII A chain OS=Homo sapiens GN=F13A1 PE=1 SV=4	5	3	15.0	17.4	16.5	17.0	15.7	16.8	16.7	17.9	18.4	16.6	16.4	16.4	0.169	1.7	0.4	2.0	-0.4	0.7	-0.4	0.7
P21333	Filamin-A OS=Homo sapiens GN=FLNA PE=1 SV=4	14198	245	30.3	32.0	30.6	29.4	30.0	28.9	30.6	32.0	31.8	29.4	30.2	29.0	0.170	0.3	0.0	1.2	0.0	0.2	0.1	0.3
P16157	Ankyrin-1 OS=Homo sapiens GN=ANK1 PE=1 SV=3	244	41	18.7	22.0	21.4	23.3	19.0	21.8	19.3	21.8	22.1	23.3	19.0	22.1	0.171	0.6	-0.2	0.7	0.0	0.0	0.3	0.2
P02533	Keratin, type I cytoskeletal 14 OS=Homo sapiens GN=KRT14 PE=1 SV=4	391	4	20.6	21.5	20.6	19.9	19.6	17.9	21.7	21.1	21.2	21.0	19.1	19.0	0.171	1.1	-0.4	0.6	1.1	-0.5	1.1	0.5
P04275	von Willebrand factor OS=Homo sapiens GN=VWF PE=1 SV=4	345	31	23.0	25.2	23.3	21.9	23.7	21.4	23.5	24.9	24.0	21.8	23.9	22.2	0.172	0.5	-0.3	0.7	-0.1	0.1	0.8	0.3
Q86YZ3	Hornerin OS=Homo sapiens GN=HRNR PE=1 SV=2	70	7	17.9	17.0	18.0	16.2	17.2	17.4	18.3	18.3	17.8	17.4	17.6	17.1	0.172	0.4	1.3	-0.2	1.1	0.4	-0.4	0.4
Q14847	LIM and SH3 domain protein 1 OS=Homo sapiens GN=LASP1 PE=1 SV=2	169	14	21.3	23.8	22.3	22.0	22.3	20.8	21.5	23.7	23.6	22.1	22.5	21.0	0.173	0.2	-0.1	1.3	0.1	0.2	0.2	0.3
Q92974	Rho guanine nucleotide exchange factor 2 OS=Homo sapiens GN=ARHGEF2 PE=1 SV=4	19	4	17.6	18.5	17.7	17.5	17.6	18.1	17.8	18.4	18.9	17.7	17.8	18.1	0.175	0.2	0.0	1.1	0.2	0.3	-0.1	0.3
P42356	Phosphatidylinositol 4-kinase alpha OS=Homo sapiens GN=PI4KA PE=1 SV=4	5	2	16.5	17.5	17.4	16.9	16.5	13.4	19.8	17.6	18.0	17.1	16.2	14.7	0.178	3.4	0.1	0.6	0.2	-0.4	1.3	0.9
P49757	Protein numb homolog OS=Homo sapiens GN=NUMB PE=1 SV=2	4	2	NA	17.1	15.7	16.6	16.3	NA	NA	18.1	17.7	16.3	16.9	15.5	0.179	####	1.0	2.0	-0.3	0.6	#####	0.8
O94919	Endonuclease domain-containing 1 protein OS=Homo sapiens GN=ENDOD1 PE=1 SV=2	64	7	19.2	21.0	20.0	18.7	20.2	17.6	19.3	21.4	22.0	19.1	20.8	17.2	0.181	0.1	0.4	1.9	0.4	0.6	-0.4	0.5
Q9BSJ8	Extended synaptotagmin-1 OS=Homo sapiens GN=ESYT1 PE=1 SV=1	15	4	17.3	19.5	17.9	16.6	18.3	14.2	17.7	20.1	19.9	15.9	18.3	16.8	0.181	0.3	0.6	2.0	-0.7	0.0	2.6	0.8
P51149	Ras-related protein Rab-7a OS=Homo sapiens GN=RAB7A PE=1 SV=1	2	2	14.3	17.6	14.8	15.0	16.2	NA	15.3	16.8	18.3	16.2	17.1	15.8	0.181	0.9	-0.9	3.5	1.2	0.9	#####	1.1
P02749	Beta-2-glycoprotein 1 OS=Homo sapiens GN=APOH PE=1 SV=3	12	2	17.6	19.3	NA	NA	17.5	16.9	17.3	20.5	18.6	15.5	19.1	17.3	0.182	-0.3	1.2	####	####	1.6	0.4	0.7
P30491	HLA class I histocompatibility antigen, B-53 alpha chain OS=Homo sapiens GN=HLA-B PE=1 SV=1	177	3	NA	NA	16.5	14.9	NA	NA	NA	NA	19.0	16.3	NA	NA	0.182	####	#####	2.5	1.3	####	#####	1.9
P35527	Keratin, type I cytoskeletal 9 OS=Homo sapiens GN=KRT9 PE=1 SV=3	981	32	25.2	25.6	25.4	23.9	24.4	24.9	26.1	25.9	25.6	25.2	24.4	24.6	0.183	0.9	0.2	0.2	1.3	0.0	-0.3	0.4
P01859	Immunoglobulin heavy constant gamma 2 OS=Homo sapiens GN=IGHG2 PE=1 SV=2	1097	5	24.7	24.0	24.2	23.2	23.1	22.7	25.0	24.1	24.8	23.2	23.1	22.6	0.183	0.3	0.1	0.6	0.1	0.1	-0.1	0.2
O15117	FYN-binding protein 1 OS=Homo sapiens GN=FYB1 PE=1 SV=2	568	28	23.3	25.7	24.1	23.3	23.8	23.4	23.7	25.7	25.4	23.3	23.8	23.5	0.186	0.4	0.0	1.2	0.0	0.0	0.1	0.3
P63000	Ras-related C3 botulinum toxin substrate 1 OS=Homo sapiens GN=RAC1 PE=1 SV=1	120	3	18.5	20.7	19.2	19.2	19.7	NA	18.9	20.7	21.6	19.2	20.4	18.6	0.188	0.5	0.0	2.4	0.0	0.6	#####	0.7
Q9Y6C2	EMILIN-1 OS=Homo sapiens GN=EMILIN1 PE=1 SV=3	479	35	23.7	26.2	23.9	22.8	23.5	23.1	23.7	26.3	24.8	22.8	23.6	23.4	0.189	-0.1	0.0	0.9	0.0	0.1	0.3	0.2
P50552	Vasodilator-stimulated phosphoprotein OS=Homo sapiens GN=VASP PE=1 SV=3	200	18	21.1	23.1	21.8	21.6	21.9	20.3	21.1	23.3	23.2	21.5	22.2	20.5	0.191	0.0	0.2	1.4	-0.1	0.3	0.1	0.3
P14618	Pyruvate kinase PKM OS=Homo sapiens GN=PKM PE=1 SV=4	71	15	19.6	21.2	21.4	22.2	21.0	17.8	20.1	21.5	22.4	21.9	21.3	17.8	0.192	0.4	0.3	1.0	-0.3	0.3	0.0	0.3
Q92619	Rho GTPase-activating protein 45 OS=Homo sapiens GN=ARHGAP45 PE=1 SV=2	19	5	17.7	17.3	18.2	18.8	18.5	16.8	18.1	19.2	19.0	18.4	18.4	17.2	0.192	0.4	1.9	0.8	-0.5	0.0	0.4	0.5
O95292	Vesicle-associated membrane protein-associated protein B/C OS=Homo sapiens GN=VAPB PE=1 SV=3	7	2	17.0	19.1	17.8	16.5	17.5	NA	16.7	19.5	19.3	16.8	17.9	16.2	0.193	-0.3	0.3	1.5	0.4	0.4	#####	0.5
Q13813	Spectrin alpha chain, non-erythrocytic 1 OS=Homo sapiens GN=SPTAN1 PE=1 SV=3	131	27	20.8	22.1	21.7	20.4	20.6	18.4	21.1	22.0	22.8	20.5	20.5	20.1	0.194	0.3	-0.2	1.1	0.1	-0.2	1.7	0.5
Q70J99	Protein unc-13 homolog D OS=Homo sapiens GN=UNC13D PE=1 SV=1	32	6	18.2	19.5	17.4	18.5	18.8	16.6	18.2	19.7	19.7	18.5	18.7	17.8	0.194	-0.1	0.2	2.3	0.0	-0.1	1.1	0.6
P00738	Haptoglobin OS=Homo sapiens GN=HP PE=1 SV=1	23	6	19.9	20.6	19.3	17.4	17.4	16.9	20.0	19.9	19.9	18.2	17.8	18.2	0.196	0.1	-0.6	0.6	0.7	0.4	1.4	0.4
P15153	Ras-related C3 botulinum toxin substrate 2 OS=Homo sapiens GN=RAC2 PE=1 SV=1	97	4	15.0	19.5	17.7	17.7	17.3	18.2	18.2	19.4	20.2	17.7	18.2	17.4	0.199	3.2	-0.2	2.5	0.0	1.0	-0.8	1.0
P13647	Keratin, type II cytoskeletal 5 OS=Homo sapiens GN=KRT5 PE=1 SV=3	233	16	21.9	22.1	21.8	20.8	20.4	20.6	22.8	22.0	22.0	21.9	20.4	20.6	0.199	0.9	-0.2	0.2	1.1	0.0	0.0	0.3
Q14162	Scavenger receptor class F member 1 OS=Homo sapiens GN=SCARF1 PE=1 SV=3	11	3	18.2	20.1	18.1	16.7	17.4	NA	18.4	20.0	19.4	16.9	17.6	15.8	0.201	0.2	0.0	1.3	0.1	0.2	#####	0.4
P60953	Cell division control protein 42 homolog OS=Homo sapiens GN=CDC42 PE=1 SV=2	55	5	19.6	20.9	19.5	18.6	19.9	19.2	19.4	21.1	21.4	19.1	20.8	18.9	0.201	-0.2	0.2	1.9	0.5	0.9	-0.3	0.5
P10644	cAMP-dependent protein kinase type I-alpha regulatory subunit OS=Homo sapiens GN=PRKAR1A PE=1 SV=1	175	13	21.0	23.0	22.3	22.3	21.6	20.7	21.1	22.9	23.2	22.4	21.7	20.9	0.203	0.1	-0.1	0.9	0.1	0.1	0.2	0.2
P61981	14-3-3 protein gamma OS=Homo sapiens GN=YWHAG PE=1 SV=2	180	5	19.5	21.3	20.2	19.2	19.7	16.7	19.9	21.0	21.0	19.4	19.5	17.2	0.205	0.5	-0.3	0.8	0.2	-0.2	0.5	0.3
Q9Y251	Heparanase OS=Homo sapiens GN=HPSE PE=1 SV=2	22	3	19.2	19.3	19.1	19.0	18.8	16.1	19.9	19.1	20.1	18.6	18.8	18.2	0.206	0.7	-0.2	1.0	-0.4	0.1	2.1	0.5
Q8IZD0	Sterile alpha motif domain-containing protein 14 OS=Homo sapiens GN=SAMD14 PE=2 SV=2	53	8	19.0	19.9	18.8	19.0	18.9	17.3	19.0	19.9	19.7	18.9	19.0	18.8	0.206	0.0	0.0	0.9	-0.1	0.1	1.5	0.4
P51572	B-cell receptor-associated protein 31 OS=Homo sapiens GN=BCAP31 PE=1 SV=3	51	9	20.9	22.6	20.2	19.5	21.3	20.0	21.1	22.4	22.2	19.8	21.6	20.2	0.209	0.2	-0.2	1.9	0.3	0.3	0.1	0.4
Q00059	Transcription factor A, mitochondrial OS=Homo sapiens GN=TFAM PE=1 SV=1	23	5	18.7	20.3	19.1	18.0	18.8	15.8	18.9	20.4	19.8	17.9	18.8	17.8	0.209	0.2	0.1	0.7	-0.1	0.0	2.0	0.5
Q15084	Protein disulfide-isomerase A6 OS=Homo sapiens GN=PDIA6 PE=1 SV=1	9	4	16.4	18.5	16.2	16.7	17.2	14.7	16.1	18.8	18.3	17.0	17.2	15.3	0.210	-0.3	0.3	2.1	0.3	0.0	0.6	0.5
O60674	Tyrosine-protein kinase JAK2 OS=Homo sapiens GN=JAK2 PE=1 SV=2	6	2	16.2	17.2	16.5	16.3	16.2	10.6	16.3	17.4	17.3	16.6	16.5	15.3	0.210	0.1	0.2	0.8	0.3	0.3	4.8	1.1

Q14766	Latent-transforming growth factor beta-binding protein 1 OS=Homo sapiens GN=LTBP1 PE=1 SV=4	448	25	23.8	25.8	23.6	22.5	23.4	22.4	23.8	25.9	24.8	22.6	23.6	22.4	0.211	0.0	0.1	1.2	0.1	0.3	0.0	0.3
Q9BUL8	Programmed cell death protein 10 OS=Homo sapiens GN=PDCD10 PE=1 SV=1	3	2	17.4	16.2	17.6	17.6	NA	NA	17.0	19.8	19.4	18.0	16.9	16.3	0.211	-0.4	3.6	1.8	0.5	####	#####	1.4
Q86YW5	Trem-like transcript 1 protein OS=Homo sapiens GN=TREML1 PE=1 SV=2	17	3	19.6	21.1	19.3	18.4	19.5	17.0	18.8	21.5	21.1	18.4	20.3	18.0	0.213	-0.8	0.4	1.8	0.0	0.8	1.0	0.5
Q9BZL4	Protein phosphatase 1 regulatory subunit 12C OS=Homo sapiens GN=PPP1R12C PE=1 SV=1	20	8	18.5	19.8	18.2	16.6	18.4	16.6	18.5	19.8	19.5	17.5	18.2	16.7	0.213	0.0	0.0	1.3	0.8	-0.2	0.2	0.3
P02776	Platelet factor 4 OS=Homo sapiens GN=PF4 PE=1 SV=2	1070	3	20.7	22.1	20.9	19.7	20.4	20.8	19.9	20.9	21.5	20.4	19.5	18.1	0.214	-0.7	-1.2	0.5	0.6	-0.9	-2.8	-0.7
O43182	Rho GTPase-activating protein 6 OS=Homo sapiens GN=ARHGAP6 PE=1 SV=3	46	10	18.3	20.0	19.1	19.7	18.8	16.9	18.1	20.1	20.3	19.5	19.2	17.3	0.216	-0.1	0.2	1.2	-0.2	0.3	0.4	0.3
Q15555	Microtubule-associated protein RP/EB family member 2 OS=Homo sapiens GN=MAPRE2 PE=1 SV=1	66	7	18.4	19.8	19.1	18.9	18.6	18.3	18.5	19.4	20.2	18.9	19.2	18.8	0.216	0.1	-0.4	1.1	0.0	0.6	0.5	0.3
O00264	Membrane-associated progesterone receptor component 1 OS=Homo sapiens GN=PGRMC1 PE=1 SV=3	11	3	16.4	19.4	18.1	15.6	18.3	16.2	16.4	19.2	20.1	16.2	19.2	16.0	0.219	0.0	-0.2	2.0	0.7	0.9	-0.3	0.5
P0DOY3	Immunoglobulin lambda constant 3 OS=Homo sapiens GN=IGLC3 PE=1 SV=1	749	7	25.6	24.6	24.3	23.0	23.1	22.9	25.9	24.5	25.0	23.1	22.9	23.0	0.222	0.3	-0.1	0.7	0.1	-0.2	0.1	0.2
Q9UJU6	Drebrin-like protein OS=Homo sapiens GN=DBNL PE=1 SV=1	156	16	20.8	22.4	21.1	20.5	20.9	18.6	20.7	22.3	22.4	20.5	21.1	19.4	0.227	-0.1	-0.2	1.3	0.0	0.2	0.8	0.3
Q5T4S7	E3 ubiquitin-protein ligase UBR4 OS=Homo sapiens GN=UBR4 PE=1 SV=1	14	5	16.7	17.7	18.1	18.2	17.7	16.3	16.9	17.7	19.6	18.0	17.5	17.4	0.228	0.2	0.0	1.4	-0.3	-0.1	1.1	0.4
Q8H4X1	Regulator of cell cycle RGCC OS=Homo sapiens GN=RGCC PE=1 SV=1	25	3	16.8	20.1	17.9	17.9	18.6	13.9	16.4	20.1	19.1	18.1	18.6	15.6	0.228	-0.3	0.0	1.2	0.2	0.0	1.7	0.5
Q9Y2L6	FERM domain-containing protein 4B OS=Homo sapiens GN=FRMD4B PE=1 SV=4	8	3	14.9	17.4	14.8	14.4	15.4	15.8	14.6	16.1	16.2	16.9	16.9	16.4	0.229	-0.3	-1.2	1.5	2.4	1.5	0.6	0.7
P62873	Guanine nucleotide-binding protein G(I)/G(S)/G(T) subunit beta-1 OS=Homo sapiens GN=GNB1 PE=1 SV=3	52	3	19.1	20.3	19.5	19.5	19.7	19.2	20.8	20.4	20.8	19.6	20.1	18.6	0.233	1.7	0.1	1.2	0.1	0.3	-0.6	0.5
P10646	Tissue factor pathway inhibitor OS=Homo sapiens GN=TFPI PE=1 SV=1	14	4	17.4	19.2	18.0	17.5	18.2	NA	18.2	18.8	19.2	17.7	18.3	14.2	0.234	0.9	-0.4	1.2	0.1	0.1	#####	0.4
Q5D862	Filaggrin-2 OS=Homo sapiens GN=FLG2 PE=1 SV=1	19	4	17.2	NA	15.0	15.9	15.8	16.7	15.6	13.8	14.3	16.6	15.6	15.8	0.236	-1.6	#####	-0.6	0.7	-0.3	-0.8	-0.5
Q99832	T-complex protein 1 subunit eta OS=Homo sapiens GN=CCT7 PE=1 SV=2	35	6	18.8	18.6	19.4	19.3	18.6	17.1	19.4	18.4	20.1	19.3	18.3	18.2	0.237	0.6	-0.2	0.7	0.0	-0.3	1.1	0.3
Q8N5K1	CDGSH iron-sulfur domain-containing protein 2 OS=Homo sapiens GN=CISD2 PE=1 SV=1	9	2	17.9	18.6	17.7	16.1	17.7	16.6	18.3	18.5	19.0	15.6	18.3	16.7	0.238	0.4	0.0	1.3	-0.4	0.6	0.1	0.3
Q05209	Tyrosine-protein phosphatase non-receptor type 12 OS=Homo sapiens GN=PTPN12 PE=1 SV=3	45	8	18.3	20.3	19.6	19.3	19.2	NA	18.3	20.6	21.0	19.5	19.2	17.4	0.240	0.0	0.3	1.4	0.3	-0.1	#####	0.4
P51659	Peroxisomal multifunctional enzyme type 2 OS=Homo sapiens GN=HSD17B4 PE=1 SV=3	277	29	22.5	23.3	22.6	21.9	21.8	21.2	23.4	23.1	23.3	21.8	22.1	21.2	0.243	0.9	-0.3	0.7	-0.1	0.3	0.0	0.3
Q15942	Zyxin OS=Homo sapiens GN=ZYX PE=1 SV=1	438	15	22.9	25.8	23.7	23.7	23.9	23.0	22.6	26.0	25.6	24.0	24.3	22.9	0.245	-0.2	0.2	1.9	0.4	0.4	-0.1	0.4
O75116	Rho-associated protein kinase 2 OS=Homo sapiens GN=ROCK2 PE=1 SV=4	109	13	20.1	21.5	20.6	20.9	20.5	18.8	20.3	21.2	21.7	20.7	20.6	19.8	0.248	0.2	-0.3	1.1	-0.2	0.1	1.0	0.3
B9A064	Immunoglobulin lambda-like polypeptide 5 OS=Homo sapiens GN=IGLL5 PE=2 SV=2	475	7	23.4	22.7	22.5	21.5	21.7	21.7	24.2	22.7	23.3	21.6	21.7	21.4	0.249	0.7	0.0	0.8	0.1	0.0	-0.3	0.2
Q9NYL9	Tropomodulin-3 OS=Homo sapiens GN=TMOD3 PE=1 SV=1	310	14	23.5	25.0	23.2	22.4	23.4	21.9	23.4	25.1	24.3	22.5	23.3	22.1	0.249	0.0	0.1	1.0	0.1	-0.1	0.2	0.2
P10909	Clusterin OS=Homo sapiens GN=CLU PE=1 SV=1	333	17	23.2	25.4	23.9	22.8	23.8	22.2	23.3	25.4	24.7	22.9	23.7	22.3	0.250	0.1	0.0	0.8	0.1	-0.1	0.1	0.2
Q63ZY3	KN motif and ankyrin repeat domain-containing protein 2 OS=Homo sapiens GN=KANK2 PE=1 SV=1	5	2	16.5	18.4	16.7	NA	16.6	12.0	16.3	18.6	17.8	15.5	16.7	15.6	0.250	-0.2	0.2	1.1	####	0.1	3.6	0.9
Q92556	Engulfment and cell motility protein 1 OS=Homo sapiens GN=ELMO1 PE=1 SV=2	6	2	18.1	18.8	17.2	17.6	18.3	17.0	17.8	19.1	19.1	17.7	18.1	18.1	0.252	-0.3	0.3	1.9	0.0	-0.2	1.1	0.5
P01137	Transforming growth factor beta-1 OS=Homo sapiens GN=TGFB1 PE=1 SV=2	190	13	21.9	23.5	22.2	21.1	21.9	20.3	22.4	23.7	23.1	21.2	21.9	19.9	0.252	0.6	0.2	0.9	0.1	0.0	-0.4	0.2
Q9NX63	MICOS complex subunit MIC19 OS=Homo sapiens GN=CHCHD3 PE=1 SV=1	52	7	20.7	22.0	20.8	19.2	20.2	14.9	21.1	22.0	21.9	19.2	19.9	19.0	0.252	0.4	0.0	1.1	0.0	-0.3	4.1	0.9
P61978	Heterogeneous nuclear ribonucleoprotein K OS=Homo sapiens GN=HNRNPK PE=1 SV=1	10	2	15.5	17.3	16.4	16.6	16.3	13.1	16.7	16.9	NA	16.5	16.5	15.3	0.254	1.2	-0.4	####	-0.1	0.3	2.2	0.6
O00159	Unconventional myosin-Ic OS=Homo sapiens GN=MYO1C PE=1 SV=4	89	13	21.4	22.3	21.9	21.2	21.4	20.6	22.3	22.3	22.9	21.4	21.5	20.1	0.256	0.9	0.1	1.0	0.1	0.1	-0.5	0.3
P50148	Guanine nucleotide-binding protein G(q) subunit alpha OS=Homo sapiens GN=GNAQ PE=1 SV=4	81	7	19.8	21.6	20.4	19.6	20.5	19.4	19.4	21.7	22.1	20.0	20.6	19.6	0.256	-0.3	0.1	1.7	0.4	0.1	0.2	0.4
Q9Y2J2	Band 4.1-like protein 3 OS=Homo sapiens GN=EPB41L3 PE=1 SV=2	35	2	17.4	18.3	17.4	16.9	16.7	14.7	17.7	18.4	17.6	16.7	16.9	17.1	0.256	0.3	0.1	0.2	-0.2	0.1	2.4	0.5
Q99501	GAS2-like protein 1 OS=Homo sapiens GN=GAS2L1 PE=1 SV=2	39	7	18.2	21.2	19.1	18.6	19.4	16.7	18.7	21.2	20.5	18.3	19.5	16.8	0.260	0.5	0.0	1.4	-0.3	0.1	0.2	0.3
P68366	Tubulin alpha-4A chain OS=Homo sapiens GN=TUBA4A PE=1 SV=1	400	7	21.1	22.0	22.0	22.3	21.5	20.6	21.8	21.8	22.5	22.1	21.7	20.8	0.260	0.7	-0.3	0.6	-0.2	0.2	0.2	0.2
P98194	Calcium-transporting ATPase type 2C member 1 OS=Homo sapiens GN=ATP2C1 PE=1 SV=3	12	3	16.2	17.7	16.8	16.6	17.1	15.5	17.2	17.2	18.1	16.8	17.6	15.2	0.263	0.9	-0.5	1.3	0.2	0.5	-0.3	0.4
Q3YEC7	Rab-like protein 6 OS=Homo sapiens GN=RABL6 PE=1 SV=2	31	6	18.8	20.0	19.4	19.4	18.9	18.0	18.8	19.9	20.5	19.3	18.7	18.9	0.264	0.1	-0.1	1.1	-0.1	-0.1	0.9	0.3
O75955	Flotillin-1 OS=Homo sapiens GN=FLOT1 PE=1 SV=3	116	17	20.6	21.7	21.4	20.7	21.1	18.8	20.7	21.5	22.5	20.7	21.1	19.5	0.264	0.1	-0.3	1.2	0.0	0.0	0.7	0.3
P15924	Desmoplakin OS=Homo sapiens GN=DSP PE=1 SV=3	4	2	14.9	15.6	14.6	13.0	NA	15.9	16.7	NA	15.6	16.0	13.9	14.8	0.265	1.8	#####	1.1	3.0	####	-1.1	1.2
Q16643	Drebrin OS=Homo sapiens GN=DBN1 PE=1 SV=4	924	40	23.6	26.1	23.6	22.9	23.5	23.1	23.8	26.0	25.1	23.1	23.4	23.4	0.265	0.1	-0.2	1.5	0.1	-0.1	0.4	0.3
Q14152	Eukaryotic translation initiation factor 3 subunit A OS=Homo sapiens GN=EIF3A PE=1 SV=1	58	19	20.4	20.6	18.8	19.0	19.2	19.8	21.2	20.7	19.1	18.7	19.0	20.5	0.265	0.8	0.1	0.3	-0.3	-0.2	0.7	0.2
P10606	Cytochrome c oxidase subunit 5B, mitochondrial OS=Homo sapiens GN=COX5B PE=1 SV=2	8	3	13.6	18.4	15.8	14.4	17.7	NA	NA	18.7	18.9	15.4	17.3	NA	0.266	####	0.3	3.0	1.0	-0.3	#####	1.0
P13747	HLA class I histocompatibility antigen, alpha chain E OS=Homo sapiens GN=HLA-E PE=1 SV=3	32	2	15.3	17.4	15.5	13.0	17.0	12.7	NA	18.0	17.8	NA	17.9	12.1	0.267	####	0.6	2.3	####	0.9	-0.5	0.8
Q13201	Multimerin-1 OS=Homo sapiens GN=MMRN1 PE=1 SV=3	2362	73	26.6	28.5	26.7	25.8	26.5	26.1	26.9	28.4	27.7	25.8	26.5	26.2	0.268	0.3	-0.1	1.0	0.0	0.0	0.1	0.2
P02768	Serum albumin OS=Homo sapiens GN=ALB PE=1 SV=2	86	16	20.9	22.0	20.9	20.5	20.3	20.4	21.9	22.3	22.2	20.6	20.8	19.6	0.270	1.1	0.3	1.3	0.0	0.5	-0.8	0.4
P09493	Tropomyosin alpha-1 chain OS=Homo sapiens GN=TPM1 PE=1 SV=2	900	17	23.7	26.0	24.0	22.6	23.5	21.4	24.1	26.5	25.3	22.6	22.9	21.7	0.272	0.5	0.5	1.3	0.0	-0.6	0.3	0.3
Q01082	Spectrin beta chain, non-erythrocytic 1 OS=Homo sapiens GN=SPTBN1 PE=1 SV=2	203	30	21.4	22.5	22.0	20.9	21.2	19.7	21.3	22.4	23.2	21.0	21.1	20.7	0.274	-0.1	-0.1	1.2	0.0	-0.1	1.0	0.3
A0A0B4J1V0	Immunoglobulin heavy variable 3-15 OS=Homo sapiens GN=IGHV3-15 PE=3 SV=1	33	5	20.6	19.7	19.4	18.1	18.3	17.6	21.9	19.9	19.8	17.9	18.3	17.6	0.277	1.4	0.2	0.4	-0.2	0.0	0.0	0.3
P47756	F-actin-capping protein subunit beta OS=Homo sapiens GN=CAPZB PE=1 SV=4	384	19	24.0	25.2	24.2	23.2	23.3	22.8	24.5	25.1	25.2	23.2	23.1	22.9	0.285	0.5	-0.1	1.0	0.0	-0.2	0.1	0.2
P04085	Platelet-derived growth factor subunit A OS=Homo sapiens GN=PDGFA PE=1 SV=1	23	3	19.5	19.8	19.4	19.3	18.7	16.2	19.5	19.8	20.1	19.2	18.7	17.9	0.286	0.0	0.0	0.7	-0.1	-0.1	1.7	0.4

Q9UIB8	SLAM family member 5 OS=Homo sapiens GN=CD84 PE=1 SV=1	16	4	16.9	19.5	17.2	16.6	17.3	NA	16.3	19.6	19.8	17.2	18.0	NA	0.287	-0.6	0.0	2.6	0.6	0.7	#####	0.7
P02730	Band 3 anion transport protein OS=Homo sapiens GN=SLC4A1 PE=1 SV=3	66	10	15.1	19.7	19.1	21.6	18.0	21.0	21.2	19.5	20.6	21.9	17.8	20.9	0.289	6.1	-0.2	1.5	0.3	-0.3	-0.2	1.2
P02549	Spectrin alpha chain, erythrocytic 1 OS=Homo sapiens GN=SPTA1 PE=1 SV=5	593	87	22.5	24.2	23.5	24.9	21.2	23.4	22.5	23.8	24.1	25.0	21.4	24.1	0.289	0.1	-0.4	0.6	0.1	0.1	0.7	0.2
P04004	Vitronectin OS=Homo sapiens GN=VTN PE=1 SV=1	14	4	18.6	19.9	18.3	17.4	18.3	NA	19.1	20.3	20.1	17.3	18.0	16.8	0.290	0.4	0.4	1.8	-0.1	-0.3	#####	0.4
P50851	Lipopolysaccharide-responsive and beige-like anchor protein OS=Homo sapiens GN=LRBA PE=1 SV=4	16	10	17.1	19.5	18.9	19.4	18.9	17.3	17.9	19.5	20.0	19.0	18.7	17.6	0.291	0.9	0.0	1.1	-0.4	-0.1	0.3	0.3
Q96SB3	Neurabin-2 OS=Homo sapiens GN=PPP1R9B PE=1 SV=2	64	17	21.0	23.3	21.0	19.3	20.9	19.4	21.0	23.0	22.0	19.4	20.9	20.2	0.293	0.0	-0.4	1.0	0.1	0.0	0.7	0.3
P06753	Tropomyosin alpha-3 chain OS=Homo sapiens GN=TPM3 PE=1 SV=2	822	9	23.3	25.0	23.0	22.1	22.7	20.7	23.3	25.4	24.4	22.0	22.0	21.9	0.294	0.0	0.4	1.4	0.0	-0.7	1.3	0.4
P01127	Platelet-derived growth factor subunit B OS=Homo sapiens GN=PDGFB PE=1 SV=1	18	3	18.6	19.5	18.6	18.6	18.6	12.3	18.8	19.6	19.3	18.5	18.6	18.1	0.295	0.2	0.1	0.7	-0.1	0.0	5.8	1.1
Q9P270	SLAIN motif-containing protein 2 OS=Homo sapiens GN=SLAIN2 PE=1 SV=2	22	2	17.2	19.0	18.1	18.4	18.0	16.5	16.9	19.0	19.4	18.1	18.1	17.3	0.296	-0.2	0.1	1.3	-0.3	0.1	0.8	0.3
Q86UE4	Protein LYRIC OS=Homo sapiens GN=MTDH PE=1 SV=2	85	15	19.9	22.1	20.1	18.9	19.7	17.6	20.2	22.0	21.4	18.7	19.9	17.7	0.298	0.3	-0.1	1.3	-0.2	0.2	0.1	0.3
Q4KMP7	TBC1 domain family member 10B OS=Homo sapiens GN=TBC1D10B PE=1 SV=3	2	2	NA	16.4	15.6	15.9	16.5	13.2	14.6	NA	NA	16.4	16.6	15.9	0.299	####	#####	####	0.6	0.1	2.7	1.1
P02675	Fibrinogen beta chain OS=Homo sapiens GN=FGB PE=1 SV=2	781	30	24.0	25.2	24.6	23.7	25.0	22.9	24.3	25.4	26.2	23.6	24.9	22.7	0.299	0.3	0.3	1.6	-0.1	-0.1	-0.1	0.3
O15400	Syntaxin-7 OS=Homo sapiens GN=STX7 PE=1 SV=4	3	2	15.3	16.8	15.9	14.8	15.8	12.3	14.2	17.8	18.0	15.8	16.0	NA	0.300	-1.1	1.0	2.1	1.0	0.2	#####	0.6
P78559	Microtubule-associated protein 1A OS=Homo sapiens GN=MAP1A PE=1 SV=6	12	4	17.1	18.7	17.3	17.1	17.3	15.9	17.9	18.3	18.1	18.1	19.1	14.9	0.301	0.7	-0.4	0.8	1.1	1.8	-1.0	0.5
Q9ULL4	Plexin-B3 OS=Homo sapiens GN=PLXNB3 PE=1 SV=2	2	2	NA	NA	15.9	16.0	15.4	13.8	NA	16.6	17.1	16.1	15.5	NA	0.302	####	#####	1.3	0.1	0.2	#####	0.5
Q12912	Lymphoid-restricted membrane protein OS=Homo sapiens GN=LRMP PE=1 SV=3	34	2	25.4	25.8	25.4	25.1	25.0	21.5	25.5	25.9	25.6	24.9	25.2	23.8	0.304	0.1	0.1	0.2	-0.2	0.1	2.3	0.4
P07384	Calpain-1 catalytic subunit OS=Homo sapiens GN=CAPN1 PE=1 SV=1	15	3	17.2	17.8	18.0	18.0	18.3	13.5	17.9	17.1	18.5	17.8	18.6	16.0	0.307	0.7	-0.7	0.5	-0.2	0.3	2.5	0.5
Q15365	Poly(rC)-binding protein 1 OS=Homo sapiens GN=PCBP1 PE=1 SV=2	51	3	19.1	19.7	18.7	19.2	18.3	19.0	19.3	19.7	20.1	19.3	18.4	18.7	0.310	0.3	0.0	1.3	0.1	0.1	-0.4	0.3
A4UGR9	Xin actin-binding repeat-containing protein 2 OS=Homo sapiens GN=XIRP2 PE=1 SV=2	4	2	14.7	15.5	13.6	NA	14.6	NA	NA	16.0	NA	14.1	14.7	18.5	0.312	####	0.5	####	####	0.2	#####	0.3
Q15389	Angiopoietin-1 OS=Homo sapiens GN=ANGPT1 PE=1 SV=2	12	3	16.9	18.7	16.4	16.2	17.2	15.9	17.6	18.7	17.4	16.6	16.9	15.5	0.312	0.8	0.0	1.1	0.4	-0.3	-0.3	0.3
P18859	ATP synthase-coupling factor 6, mitochondrial OS=Homo sapiens GN=ATP5J PE=1 SV=1	3	3	NA	16.7	NA	14.1	16.2	NA	NA	18.2	15.6	13.7	17.4	NA	0.313	####	1.5	####	-0.4	1.2	#####	0.8
Q12846	Syntaxin-4 OS=Homo sapiens GN=STX4 PE=1 SV=2	8	2	17.7	18.6	17.5	16.8	17.3	15.8	17.7	18.0	18.4	17.1	18.0	16.1	0.313	-0.1	-0.6	0.9	0.3	0.7	0.2	0.3
O00151	PDZ and LIM domain protein 1 OS=Homo sapiens GN=PDLIM1 PE=1 SV=4	387	16	23.0	25.1	23.8	22.6	23.6	22.0	23.0	25.2	25.3	22.7	23.7	21.8	0.318	0.0	0.1	1.5	0.1	0.2	-0.2	0.3
O15145	Actin-related protein 2/3 complex subunit 3 OS=Homo sapiens GN=ARPC3 PE=1 SV=3	39	3	20.7	21.1	19.5	18.6	19.8	19.0	21.6	20.8	20.6	18.5	19.8	18.9	0.320	0.9	-0.3	1.1	0.0	0.0	-0.1	0.3
P46976	Glycogenin-1 OS=Homo sapiens GN=GYG1 PE=1 SV=4	2	2	NA	NA	17.5	17.8	14.2	NA	NA	NA	18.8	17.4	16.6	14.3	0.322	####	#####	1.2	-0.4	2.3	#####	1.1
Q9P0L0	Vesicle-associated membrane protein-associated protein A OS=Homo sapiens GN=VAPA PE=1 SV=3	55	7	18.4	21.0	18.7	17.1	18.2	15.3	19.1	20.8	20.7	16.5	18.2	15.9	0.323	0.8	-0.2	2.1	-0.6	0.0	0.7	0.4
Q14254	Flotillin-2 OS=Homo sapiens GN=FLOT2 PE=1 SV=2	65	11	20.9	21.6	20.9	19.7	20.2	18.0	21.3	21.2	21.8	19.7	20.0	18.4	0.324	0.4	-0.4	0.9	0.1	-0.1	0.4	0.2
P61106	Ras-related protein Rab-14 OS=Homo sapiens GN=RAB14 PE=1 SV=4	12	3	12.4	18.8	16.8	15.3	15.9	NA	NA	18.1	18.6	16.2	16.3	NA	0.332	####	-0.7	1.8	0.9	0.4	#####	0.6
Q14008	Cytoskeleton-associated protein 5 OS=Homo sapiens GN=CKAP5 PE=1 SV=3	12	4	15.9	18.7	17.4	17.5	16.6	12.6	15.7	18.4	18.9	17.5	16.2	15.8	0.333	-0.2	-0.3	1.5	0.0	-0.3	3.2	0.6
P19823	Inter-alpha-trypsin inhibitor heavy chain H2 OS=Homo sapiens GN=ITIH2 PE=1 SV=2	3	3	17.3	17.1	16.0	15.5	15.8	13.0	17.5	16.8	16.0	16.6	15.7	13.4	0.334	0.2	-0.3	0.0	1.1	-0.1	0.4	0.2
P12931	Proto-oncogene tyrosine-protein kinase Src OS=Homo sapiens GN=SRC PE=1 SV=3	226	8	20.7	22.7	22.4	22.0	21.7	20.6	21.5	22.5	23.1	21.8	22.0	20.4	0.334	0.9	-0.2	0.7	-0.2	0.3	-0.2	0.2
P01024	Complement C3 OS=Homo sapiens GN=C3 PE=1 SV=2	43	6	19.5	19.3	18.4	17.4	17.7	17.2	19.5	19.0	19.2	16.6	17.4	15.1	0.335	0.1	-0.3	0.8	-0.7	-0.3	-2.0	-0.4
Q9Y2Q3	Glutathione S-transferase kappa 1 OS=Homo sapiens GN=GSTK1 PE=1 SV=3	13	3	16.0	18.3	NA	17.1	16.8	17.3	17.1	14.9	18.7	16.8	16.5	16.1	0.336	1.1	-3.4	####	-0.3	-0.3	-1.2	-0.8
P35579	Myosin-9 OS=Homo sapiens GN=MYH9 PE=1 SV=4	18225	281	30.0	31.5	30.0	29.3	29.8	29.2	30.4	31.5	31.2	29.2	29.7	29.0	0.336	0.4	-0.1	1.2	0.0	-0.1	-0.1	0.2
P07203	Glutathione peroxidase 1 OS=Homo sapiens GN=GPX1 PE=1 SV=4	29	3	18.7	19.2	18.9	17.9	18.5	16.3	19.2	18.9	20.2	18.0	18.2	16.7	0.340	0.5	-0.3	1.3	0.0	-0.3	0.3	0.3
O95425	Supervillin OS=Homo sapiens GN=SVIL PE=1 SV=2	38	12	17.4	18.9	18.5	16.3	19.4	14.1	17.2	19.2	19.4	15.9	19.0	16.1	0.343	-0.2	0.3	0.9	-0.3	-0.3	1.9	0.4
Q9Y6E0	Serine/threonine-protein kinase 24 OS=Homo sapiens GN=STK24 PE=1 SV=1	2	2	16.5	19.0	17.0	16.8	16.6	NA	16.6	18.8	19.2	16.7	16.9	15.5	0.346	0.1	-0.2	2.2	0.0	0.3	#####	0.5
Q96AP7	Endothelial cell-selective adhesion molecule OS=Homo sapiens GN=ESAM PE=1 SV=1	8	3	14.4	18.7	14.4	14.1	16.6	NA	13.3	18.8	19.0	14.9	17.1	14.2	0.348	-1.0	0.2	4.6	0.7	0.6	#####	1.0
P23284	Peptidyl-prolyl cis-trans isomerase B OS=Homo sapiens GN=PPIB PE=1 SV=2	440	20	23.7	24.8	24.1	23.7	23.4	23.3	24.5	24.7	24.8	23.6	23.6	23.0	0.348	0.8	-0.1	0.6	0.0	0.2	-0.4	0.2
P08670	Vimentin OS=Homo sapiens GN=VIM PE=1 SV=4	24	12	19.0	21.7	18.5	16.1	18.5	10.5	19.1	21.4	19.8	15.8	18.1	16.5	0.348	0.1	-0.3	1.3	-0.3	-0.4	6.1	1.1
O43150	Arf-GAP with SH3 domain, ANK repeat and PH domain-containing protein 2 OS=Homo sapiens GN=ASAP2 PE=1 SV=3	4	2	15.7	18.0	16.0	16.1	16.0	14.3	NA	17.4	18.1	16.1	16.0	15.4	0.351	####	-0.6	2.1	-0.1	0.0	1.1	0.5
P48735	Isocitrate dehydrogenase [NADP], mitochondrial OS=Homo sapiens GN=IDH2 PE=1 SV=2	13	2	17.3	18.8	17.6	17.1	18.4	15.9	17.8	19.1	19.0	16.7	19.0	15.4	0.354	0.4	0.4	1.4	-0.4	0.6	-0.6	0.3
Q4KMQ2	Anoctamin-6 OS=Homo sapiens GN=ANO6 PE=1 SV=2	2	2	14.0	16.1	14.8	NA	15.4	NA	NA	15.4	17.8	15.9	16.8	12.8	0.354	####	-0.6	2.9	####	1.4	#####	1.2
Q9UDY2	Tight junction protein ZO-2 OS=Homo sapiens GN=TJP2 PE=1 SV=2	54	10	18.6	21.6	19.6	18.9	19.3	19.4	19.1	21.6	20.9	18.8	19.2	19.2	0.355	0.5	0.0	1.3	0.0	-0.1	-0.2	0.2
P09496	Clathrin light chain A OS=Homo sapiens GN=CLTA PE=1 SV=1	64	5	21.8	23.7	21.9	21.9	22.2	21.4	21.8	23.6	23.3	22.1	22.0	21.5	0.356	0.0	-0.1	1.4	0.2	-0.2	0.1	0.2
Q9UEY8	Gamma-adducin OS=Homo sapiens GN=ADD3 PE=1 SV=1	55	9	19.5	20.8	20.6	20.1	19.9	19.5	20.1	20.6	21.5	20.1	19.9	19.4	0.356	0.6	-0.3	0.9	0.0	0.0	-0.1	0.2
P68871	Hemoglobin subunit beta OS=Homo sapiens GN=HBB PE=1 SV=2	165	5	20.8	22.2	21.2	23.6	20.4	20.3	20.3	22.5	22.5	23.5	20.6	20.7	0.357	-0.6	0.3	1.2	-0.2	0.3	0.4	0.2
P0C7P3	Protein SLFN14 OS=Homo sapiens GN=SLFN14 PE=1 SV=2	18	8	19.0	19.3	18.5	18.8	18.4	18.4	19.6	19.0	18.5	17.5	18.3	17.9	0.357	0.6	-0.3	0.0	-1.3	-0.1	-0.5	-0.3
P46939	Utrophin OS=Homo sapiens GN=UTRN PE=1 SV=2	72	17	20.2	22.2	20.4	18.6	19.9	17.8	20.5	22.0	21.5	18.3	19.7	18.8	0.359	0.3	-0.2	1.2	-0.3	-0.2	0.9	0.3
P49411	Elongation factor Tu, mitochondrial OS=Homo sapiens GN=TUFM PE=1 SV=2	38	8	19.1	20.8	19.8	19.8	20.4	17.4	19.8	21.0	21.0	18.7	20.7	17.9	0.359	0.7	0.2	1.2	-1.1	0.3	0.5	0.3
O14974	Protein phosphatase 1 regulatory subunit 12A OS=Homo sapiens GN=PPP1R12A PE=1 SV=1	154	22	21.0	23.5	21.7	20.2	21.4	18.8	21.2	23.5	22.6	20.2	21.0	19.5	0.360	0.1	0.0	0.8	-0.1	-0.4	0.7	0.2
P06576	ATP synthase subunit beta, mitochondrial OS=Homo sapiens GN=ATP5B PE=1 SV=3	74	10	19.5	21.7	20.3	19.8	21.0	18.8	19.3	21.8	21.8	20.1	21.7	18.2	0.360	-0.2	0.2	1.6	0.3	0.7	-0.6	0.3

Q8IYJ2	Uncharacterized protein C10orf67, mitochondrial OS=Homo sapiens GN=C10orf67 PE=2 SV=3	4	2	15.1	16.5	15.4	14.1	14.9	15.4	15.3	16.1	16.0	13.7	15.3	16.5	0.361	0.3	-0.4	0.6	-0.4	0.4	1.0	0.2
O75947	ATP synthase subunit d, mitochondrial OS=Homo sapiens GN=ATP5H PE=1 SV=3	2	2	15.2	NA	15.5	NA	15.4	NA	14.9	17.1	16.8	NA	15.9	14.4	0.362	-0.2	#####	1.3	####	0.5	#####	0.5
Q7Z434	Mitochondrial antiviral-signaling protein OS=Homo sapiens GN=MAVS PE=1 SV=2	61	9	17.0	21.5	19.2	17.7	18.8	17.3	17.6	21.3	21.0	17.7	18.9	16.9	0.362	0.6	-0.2	1.8	0.1	0.1	-0.4	0.3
P33176	Kinesin-1 heavy chain OS=Homo sapiens GN=KIF5B PE=1 SV=1	17	4	16.5	16.8	16.1	17.8	16.9	15.8	16.5	16.8	18.2	17.8	16.6	16.3	0.362	-0.1	-0.1	2.1	0.0	-0.3	0.4	0.4
Q9NQ75	Cas scaffolding protein family member 4 OS=Homo sapiens GN=CASS4 PE=1 SV=2	29	5	18.0	19.9	18.7	18.5	18.2	14.4	17.9	20.0	20.1	18.5	18.1	14.6	0.363	-0.1	0.1	1.4	-0.1	-0.1	0.2	0.2
P35612	Beta-adducin OS=Homo sapiens GN=ADD2 PE=1 SV=3	18	3	16.8	18.5	17.9	19.1	17.8	18.1	17.1	19.4	19.0	18.3	17.6	18.5	0.366	0.3	0.9	1.1	-0.8	-0.2	0.4	0.3
Q14554	Protein disulfide-isomerase A5 OS=Homo sapiens GN=PDIA5 PE=1 SV=1	82	11	21.3	21.0	20.6	19.8	21.2	20.3	22.1	21.0	21.1	20.0	21.1	20.0	0.367	0.8	0.0	0.5	0.2	-0.1	-0.3	0.2
Q9NVA2	Septin-11 OS=Homo sapiens GN=SEPT11 PE=1 SV=3	53	7	16.1	16.7	17.1	16.3	16.7	18.5	16.9	17.2	15.7	16.7	17.0	20.5	0.368	0.9	0.5	-1.4	0.4	0.3	1.9	0.4
O75592	E3 ubiquitin-protein ligase MYCBP2 OS=Homo sapiens GN=MYCBP2 PE=1 SV=3	33	9	17.8	18.6	19.0	19.0	18.6	18.2	19.0	18.4	19.4	18.8	18.8	18.0	0.369	1.2	-0.2	0.4	-0.1	0.2	-0.2	0.2
Q8H2G2	STE20-like serine/threonine-protein kinase OS=Homo sapiens GN=SLK PE=1 SV=1	13	6	18.7	20.7	18.7	18.2	19.3	16.9	19.5	20.0	19.5	17.9	19.3	18.4	0.370	0.8	-0.7	0.8	-0.3	0.0	1.5	0.3
P50990	T-complex protein 1 subunit theta OS=Homo sapiens GN=CCT8 PE=1 SV=4	18	5	18.6	19.4	19.6	19.7	18.8	17.3	19.9	19.1	20.0	19.5	18.7	17.8	0.371	1.3	-0.3	0.4	-0.2	-0.2	0.5	0.2
O43312	Metastasis suppressor protein 1 OS=Homo sapiens GN=MTSS1 PE=1 SV=2	58	6	18.6	20.0	19.0	18.9	18.6	18.7	18.6	20.1	20.2	19.1	18.1	19.0	0.371	-0.1	0.2	1.2	0.2	-0.5	0.3	0.2
Q00610	Clathrin heavy chain 1 OS=Homo sapiens GN=CLTC PE=1 SV=5	204	21	21.3	23.1	22.8	22.2	21.9	20.6	21.9	23.0	23.9	22.1	22.0	20.4	0.372	0.6	-0.1	1.0	-0.1	0.1	-0.3	0.2
Q5M775	Cytospin-B OS=Homo sapiens GN=SPECC1 PE=1 SV=1	13	5	17.8	20.0	18.5	17.6	18.1	16.2	16.6	20.1	20.0	17.8	18.5	17.5	0.375	-1.2	0.2	1.5	0.2	0.4	1.3	0.4
P51153	Ras-related protein Rab-13 OS=Homo sapiens GN=RAB13 PE=1 SV=1	28	3	15.4	18.3	16.9	16.5	16.9	13.4	15.8	18.3	18.8	16.1	17.1	NA	0.376	0.4	0.0	1.9	-0.4	0.1	#####	0.4
P02647	Apolipoprotein A-I OS=Homo sapiens GN=APOA1 PE=1 SV=1	8	2	17.2	18.4	16.2	15.5	16.6	16.1	16.9	18.6	16.9	16.5	16.1	16.4	0.378	-0.3	0.2	0.7	0.9	-0.5	0.3	0.2
P48059	LIM and senescent cell antigen-like-containing domain protein 1 OS=Homo sapiens GN=LIMS1 PE=1 SV=4	64	5	20.7	21.4	21.0	21.3	20.4	21.5	21.4	20.4	20.8	21.0	20.6	20.2	0.378	0.7	-1.0	-0.2	-0.2	0.2	-1.3	-0.3
P09497	Clathrin light chain B OS=Homo sapiens GN=CLTB PE=1 SV=1	36	7	17.4	20.0	18.8	18.2	18.9	16.2	17.6	19.6	19.3	18.1	18.8	17.5	0.379	0.1	-0.5	0.5	0.0	-0.1	1.2	0.2
P63104	14-3-3 protein zeta/delta OS=Homo sapiens GN=YWHAZ PE=1 SV=1	432	15	23.5	25.2	23.8	22.7	23.4	21.9	23.6	24.7	24.8	23.0	23.4	22.2	0.380	0.1	-0.5	1.1	0.3	0.0	0.3	0.2
Q9NZN3	EH domain-containing protein 3 OS=Homo sapiens GN=EHD3 PE=1 SV=2	38	5	17.7	18.7	17.7	18.5	17.9	15.2	17.4	18.7	19.6	17.9	17.9	16.6	0.384	-0.3	0.0	2.0	-0.6	0.1	1.4	0.4
Q99683	Mitogen-activated protein kinase kinase kinase 5 OS=Homo sapiens GN=MAP3K5 PE=1 SV=1	5	2	14.3	17.8	16.2	17.1	16.8	15.2	16.2	17.7	17.9	16.7	15.7	16.1	0.389	1.9	-0.1	1.7	-0.4	-1.1	0.8	0.5
P12814	Alpha-actinin-1 OS=Homo sapiens GN=ACTN1 PE=1 SV=2	2286	46	26.1	27.7	26.5	24.9	26.1	24.8	26.3	27.6	27.7	25.0	26.1	24.8	0.391	0.2	-0.2	1.2	0.0	0.0	-0.1	0.2
Q5T447	E3 ubiquitin-protein ligase HECTD3 OS=Homo sapiens GN=HECTD3 PE=1 SV=1	14	2	17.0	19.2	18.4	18.5	17.7	15.6	14.1	16.8	19.3	18.3	16.1	17.5	0.392	-2.9	-2.4	0.9	-0.2	-1.6	1.9	-0.7
O95260	Arginyl-tRNA--protein transferase 1 OS=Homo sapiens GN=ATE1 PE=1 SV=2	4	2	13.5	16.1	14.8	15.6	15.0	14.9	15.9	15.6	17.0	15.1	14.9	14.5	0.397	2.4	-0.5	2.2	-0.5	-0.1	-0.3	0.5
Q14644	Ras GTPase-activating protein 3 OS=Homo sapiens GN=RASA3 PE=1 SV=3	153	20	21.5	22.8	22.0	21.7	21.6	20.7	22.7	22.4	22.8	21.6	21.5	20.6	0.399	1.2	-0.4	0.9	-0.1	-0.1	0.0	0.2
Q9Y613	FH1/FH2 domain-containing protein 1 OS=Homo sapiens GN=FHOD1 PE=1 SV=3	195	19	20.5	22.3	21.0	21.5	20.6	19.1	20.8	22.1	22.4	21.5	20.4	19.1	0.400	0.3	-0.2	1.5	0.1	-0.2	0.0	0.2
P68371	Tubulin beta-4B chain OS=Homo sapiens GN=TUBB4B PE=1 SV=1	513	4	20.4	22.0	21.5	21.2	21.1	20.8	21.5	22.2	22.9	21.0	20.8	20.3	0.401	1.1	0.2	1.5	-0.2	-0.3	-0.5	0.3
P01591	Immunoglobulin J chain OS=Homo sapiens GN=JCHAIN PE=1 SV=4	30	3	22.3	22.2	21.4	20.2	20.3	20.7	22.3	22.2	22.0	20.3	20.1	20.9	0.402	0.0	0.0	0.6	0.1	-0.2	0.2	0.1
Q06830	Peroxiredoxin-1 OS=Homo sapiens GN=PRDX1 PE=1 SV=1	60	3	18.5	20.4	18.9	18.9	19.1	18.4	19.3	20.0	19.3	19.0	19.3	18.3	0.402	0.8	-0.4	0.4	0.0	0.2	-0.1	0.1
P13501	C-C motif chemokine 5 OS=Homo sapiens GN=CCL5 PE=1 SV=3	299	7	24.0	24.6	23.8	23.6	23.4	23.6	24.5	25.0	25.1	23.8	23.4	22.8	0.411	0.5	0.4	1.3	0.2	-0.1	-0.8	0.2
Q9Y2A7	Nck-associated protein 1 OS=Homo sapiens GN=NCKAP1 PE=1 SV=1	12	2	15.2	13.5	13.7	17.0	17.3	17.3	17.5	13.8	NA	16.9	17.4	16.8	0.415	2.3	0.2	####	-0.1	0.1	-0.4	0.4
Q5JSL3	Dedicator of cytokinesis protein 11 OS=Homo sapiens GN=DOCK11 PE=1 SV=2	6	3	16.2	16.6	NA	18.6	18.9	16.0	18.6	19.6	NA	18.6	18.8	14.5	0.418	2.4	3.0	####	0.0	-0.1	-1.5	0.8
Q6WCQ1	Myosin phosphatase Rho-interacting protein OS=Homo sapiens GN=MPRIP PE=1 SV=3	29	10	18.1	21.2	18.6	15.3	17.9	17.6	18.3	21.2	19.9	13.8	17.1	15.8	0.423	0.2	0.0	1.3	-1.4	-0.8	-1.8	-0.4
P04264	Keratin, type II cytoskeletal 1 OS=Homo sapiens GN=KRT1 PE=1 SV=6	1663	51	26.5	26.4	26.7	25.4	25.4	25.8	27.0	26.7	26.8	26.2	25.0	25.4	0.430	0.5	0.3	0.2	0.8	-0.4	-0.3	0.2
P07996	Thrombospondin-1 OS=Homo sapiens GN=THBS1 PE=1 SV=2	2600	58	27.0	28.8	27.8	27.6	27.6	27.0	27.9	28.5	28.7	27.4	27.7	26.7	0.430	0.9	-0.3	0.9	-0.1	0.1	-0.3	0.2
Q9ULH1	Arf-GAP with SH3 domain, ANK repeat and PH domain-containing protein 1 OS=Homo sapiens GN=ASAP1 PE=1 SV=4	5	3	15.3	18.0	16.8	16.2	16.1	NA	NA	18.0	17.9	16.2	16.0	NA	0.431	####	0.0	1.1	0.0	-0.1	#####	0.3
Q9BZF9	Uveal autoantigen with coiled-coil domains and ankyrin repeats OS=Homo sapiens GN=UACA PE=1 SV=2	23	7	18.9	20.6	17.1	15.7	16.4	16.3	18.7	20.0	17.6	15.9	17.1	16.8	0.435	-0.2	-0.6	0.5	0.2	0.6	0.5	0.2
Q9UKE5	TRAF2 and NCK-interacting protein kinase OS=Homo sapiens GN=TNIK PE=1 SV=1	9	3	15.4	17.0	17.8	16.7	16.4	NA	14.0	16.6	17.9	17.1	16.4	15.6	0.436	-1.4	-0.4	0.1	0.4	0.0	#####	-0.3
Q13045	Protein flightless-1 homolog OS=Homo sapiens GN=FLII PE=1 SV=2	98	11	20.5	22.3	20.6	19.2	20.2	18.7	21.4	22.1	22.0	19.0	20.2	18.4	0.436	0.8	-0.3	1.4	-0.1	0.0	-0.3	0.2
Q6IAA8	Ragulator complex protein LAMTOR1 OS=Homo sapiens GN=LAMTOR1 PE=1 SV=2	5	3	17.2	18.7	17.4	16.6	17.3	NA	17.6	18.4	19.8	17.2	16.5	13.8	0.442	0.3	-0.3	2.4	0.7	-0.8	#####	0.5
Q00013	55 kDa erythrocyte membrane protein OS=Homo sapiens GN=MPP1 PE=1 SV=2	11	5	16.5	17.4	17.4	17.7	17.1	16.6	17.9	18.3	19.2	16.2	17.5	16.1	0.442	1.4	0.9	1.8	-1.5	0.3	-0.4	0.4
P16671	Platelet glycoprotein 4 OS=Homo sapiens GN=CD36 PE=1 SV=2	165	9	21.5	22.3	22.5	22.4	21.7	21.1	22.3	22.0	23.4	22.5	22.0	20.6	0.443	0.7	-0.3	0.8	0.0	0.3	-0.5	0.2
Q27J81	Inverted formin-2 OS=Homo sapiens GN=INF2 PE=1 SV=2	266	23	21.2	23.5	21.8	21.5	21.9	21.2	21.4	23.3	23.0	21.5	21.9	21.0	0.445	0.2	-0.2	1.2	0.0	0.0	-0.2	0.2
P04406	Glyceraldehyde-3-phosphate dehydrogenase OS=Homo sapiens GN=GAPDH PE=1 SV=3	391	19	22.7	24.9	24.1	23.9	23.9	23.5	23.3	25.1	25.3	24.0	24.1	22.5	0.448	0.6	0.3	1.3	0.1	0.2	-1.0	0.2
Q7L591	Docking protein 3 OS=Homo sapiens GN=DOK3 PE=1 SV=2	31	6	18.8	20.4	18.9	19.1	18.7	17.6	18.9	20.2	20.1	18.9	18.9	17.6	0.449	0.0	-0.2	1.2	-0.2	0.1	0.1	0.2
Q05655	Protein kinase C delta type OS=Homo sapiens GN=PRKCD PE=1 SV=2	9	3	14.7	16.4	15.6	15.5	16.0	15.4	15.4	17.8	18.6	16.3	16.5	12.7	0.449	0.7	1.4	3.0	0.8	0.5	-2.7	0.6
Q15019	Septin-2 OS=Homo sapiens GN=SEPT2 PE=1 SV=1	28	5	16.2	18.6	17.8	17.7	17.0	19.8	17.1	17.8	19.9	17.9	17.7	18.9	0.456	0.9	-0.8	2.2	0.2	0.8	-0.9	0.4
O43294	Transforming growth factor beta-1-induced transcript 1 protein OS=Homo sapiens GN=TGFB1I1 PE=1 SV=2	51	3	14.1	18.6	17.2	16.7	17.4	NA	14.4	18.5	18.7	16.8	16.8	11.0	0.457	0.4	0.0	1.5	0.1	-0.6	#####	0.3
Q9Y608	Leucine-rich repeat flightless-interacting protein 2 OS=Homo sapiens GN=LRRFIP2 PE=1 SV=1	194	21	21.4	23.9	21.7	20.0	21.7	19.3	21.2	23.8	23.0	19.9	21.4	19.9	0.458	-0.2	-0.1	1.3	-0.1	-0.3	0.6	0.2
P05023	Sodium/potassium-transporting ATPase subunit alpha-1 OS=Homo sapiens GN=ATP1A1 PE=1 SV=1	11	5	NA	18.3	17.2	17.2	17.7	11.8	15.7	17.4	18.5	16.8	17.4	15.4	0.465	####	-0.9	1.3	-0.3	-0.4	3.6	0.7
P62191	26S proteasome regulatory subunit 4 OS=Homo sapiens GN=PSMC1 PE=1 SV=1	3	2	14.8	NA	16.3	16.8	15.6	NA	14.7	15.7	17.1	16.9	15.5	15.6	0.466	-0.1	#####	0.8	0.2	-0.1	#####	0.2

O95674	Phosphatidate cytidylyltransferase 2 OS=Homo sapiens GN=CDS2 PE=1 SV=1	10	2	12.3	17.3	16.3	15.9	16.9	NA	NA	17.5	17.9	15.4	17.0	NA	0.477	####	0.2	1.7	-0.5	0.1	#####	0.4
Q8NF50	Dedicator of cytokinesis protein 8 OS=Homo sapiens GN=DOCK8 PE=1 SV=3	9	6	19.8	20.3	20.8	20.7	19.3	15.0	19.8	19.8	21.3	20.5	19.0	18.1	0.478	0.0	-0.5	0.5	-0.2	-0.3	3.0	0.4
Q13459	Unconventional myosin-IXb OS=Homo sapiens GN=MYO9B PE=1 SV=3	3	2	16.0	17.7	16.2	15.7	14.4	16.1	15.5	17.4	17.2	15.7	15.4	16.1	0.479	-0.6	-0.3	1.0	0.0	1.0	0.0	0.2
Q8N392	Rho GTPase-activating protein 18 OS=Homo sapiens GN=ARHGAP18 PE=1 SV=3	13	3	17.9	18.6	17.1	17.9	17.1	16.5	17.6	17.9	18.3	17.9	17.4	17.2	0.486	-0.4	-0.7	1.2	0.1	0.4	0.8	0.2
Q15836	Vesicle-associated membrane protein 3 OS=Homo sapiens GN=VAMP3 PE=1 SV=3	3	2	NA	15.1	12.8	NA	NA	NA	NA	15.2	17.7	NA	NA	NA	0.488	####	0.1	4.9	####	####	#####	2.5
P67936	Tropomyosin alpha-4 chain OS=Homo sapiens GN=TPM4 PE=1 SV=3	1249	21	24.9	26.2	24.5	23.5	24.1	23.3	25.0	26.6	25.7	23.5	23.4	23.4	0.488	0.1	0.4	1.2	0.0	-0.7	0.1	0.2
P47755	F-actin-capping protein subunit alpha-2 OS=Homo sapiens GN=CAPZA2 PE=1 SV=3	146	6	20.5	21.7	20.9	20.3	20.0	20.2	21.1	21.2	21.4	20.2	20.3	20.3	0.489	0.6	-0.6	0.5	-0.1	0.3	0.1	0.1
P61421	V-type proton ATPase subunit d 1 OS=Homo sapiens GN=ATP6V0D1 PE=1 SV=1	3	2	15.7	17.2	15.5	13.4	14.7	NA	16.9	16.2	NA	14.3	15.3	13.4	0.490	1.2	-1.1	####	0.9	0.6	#####	0.4
P16452	Erythrocyte membrane protein band 4.2 OS=Homo sapiens GN=EPB42 PE=1 SV=3	11	4	12.1	16.6	16.6	17.6	15.9	16.7	15.2	17.9	17.5	17.9	14.3	15.7	0.496	3.1	1.3	0.9	0.3	-1.6	-1.0	0.5
Q9Y2X7	ARF GTPase-activating protein GIT1 OS=Homo sapiens GN=GIT1 PE=1 SV=2	27	8	18.2	19.8	18.1	19.0	18.5	18.0	18.2	19.3	19.8	18.6	18.5	18.6	0.497	0.0	-0.5	1.7	-0.3	0.0	0.6	0.2
P35609	Alpha-actinin-2 OS=Homo sapiens GN=ACTN2 PE=1 SV=1	267	2	18.9	21.1	19.7	17.4	19.2	16.6	19.5	21.0	20.9	17.4	19.0	16.3	0.497	0.6	-0.1	1.1	-0.1	-0.2	-0.3	0.2
P00390	Glutathione reductase, mitochondrial OS=Homo sapiens GN=GSR PE=1 SV=2	6	2	14.5	16.3	16.9	16.7	16.5	NA	16.5	16.4	17.9	16.4	15.7	13.9	0.497	2.0	0.1	1.0	-0.4	-0.8	#####	0.4
P62263	40S ribosomal protein S14 OS=Homo sapiens GN=RPS14 PE=1 SV=3	2	2	16.3	15.0	NA	14.5	16.2	16.3	16.8	17.2	NA	14.8	15.9	15.5	0.497	0.5	2.2	####	0.3	-0.3	-0.9	0.4
P18206	Vinculin OS=Homo sapiens GN=VCL PE=1 SV=4	318	38	22.7	23.3	22.5	22.7	23.4	21.4	22.6	23.5	24.0	22.6	23.5	21.1	0.498	-0.2	0.1	1.5	-0.1	0.1	-0.2	0.2
P35908	Keratin, type II cytoskeletal 2 epidermal OS=Homo sapiens GN=KRT2 PE=1 SV=2	957	36	24.8	23.7	24.3	23.6	23.4	22.8	25.2	24.2	24.6	23.5	22.8	23.0	0.502	0.4	0.5	0.3	-0.1	-0.6	0.2	0.1
O00429	Dynamin-1-like protein OS=Homo sapiens GN=DNM1L PE=1 SV=2	13	6	17.4	19.3	17.9	18.7	18.1	17.7	17.3	18.7	18.7	18.3	17.8	17.3	0.502	-0.1	-0.6	0.8	-0.3	-0.3	-0.4	-0.1
Q9H479	Fructosamine-3-kinase OS=Homo sapiens GN=FN3K PE=1 SV=1	22	5	17.9	19.0	16.4	17.0	18.5	16.0	17.9	18.1	17.3	17.3	18.4	17.2	0.513	0.0	-0.9	0.8	0.3	-0.2	1.2	0.2
Q6ZVM7	TOM1-like protein 2 OS=Homo sapiens GN=TOM1L2 PE=1 SV=1	4	2	14.9	17.6	NA	14.0	14.1	NA	13.7	17.5	17.3	15.3	16.2	13.0	0.517	-1.2	-0.1	####	1.3	2.1	#####	0.5
Q9UNF1	Melanoma-associated antigen D2 OS=Homo sapiens GN=MAGED2 PE=1 SV=2	8	5	16.0	17.5	16.2	16.7	16.5	15.2	15.6	17.7	17.1	16.3	16.3	13.9	0.519	-0.4	0.1	0.9	-0.4	-0.2	-1.3	-0.2
P10314	HLA class I histocompatibility antigen, A-32 alpha chain OS=Homo sapiens GN=HLA-A PE=1 SV=2	308	3	NA	18.6	16.7	15.4	NA	NA	NA	18.9	19.5	14.7	11.7	16.6	0.527	####	0.3	2.8	-0.7	####	#####	0.8
P04792	Heat shock protein beta-1 OS=Homo sapiens GN=HSPB1 PE=1 SV=2	76	10	18.5	21.3	19.8	21.3	18.1	19.8	18.3	21.2	21.7	20.7	18.8	19.7	0.528	-0.2	-0.1	1.9	-0.7	0.7	-0.2	0.3
P49748	Very long-chain specific acyl-CoA dehydrogenase, mitochondrial OS=Homo sapiens GN=ACADVL PE=1 SV=1	15	4	17.4	17.5	17.7	16.9	17.7	NA	17.7	17.7	17.4	16.8	18.0	15.8	0.530	0.4	0.2	-0.3	-0.1	0.3	#####	0.1
Q9NTJ5	Phosphatidylinositide phosphatase SAC1 OS=Homo sapiens GN=SACM1L PE=1 SV=2	9	2	16.5	NA	NA	15.1	17.6	15.3	NA	NA	17.2	15.7	18.3	14.9	0.531	####	#####	####	0.6	0.7	-0.5	0.3
Q7LDG7	RAS guanyl-releasing protein 2 OS=Homo sapiens GN=RASGRP2 PE=1 SV=1	16	4	13.3	19.8	18.1	17.4	17.9	14.5	16.5	19.4	20.0	16.7	16.6	14.6	0.532	3.1	-0.3	1.9	-0.7	-1.4	0.1	0.5
P31946	14-3-3 protein beta/alpha OS=Homo sapiens GN=YWHAB PE=1 SV=3	138	3	18.5	20.8	19.0	18.6	19.5	17.7	18.6	20.4	20.5	18.7	19.3	17.5	0.539	0.1	-0.4	1.5	0.2	-0.1	-0.2	0.2
Q14156	Protein EFR3 homolog A OS=Homo sapiens GN=EFR3A PE=1 SV=2	5	2	16.6	17.6	17.5	16.6	16.3	NA	17.6	17.5	18.3	15.9	16.4	13.5	0.540	1.0	0.0	0.8	-0.8	0.1	#####	0.2
P05198	Eukaryotic translation initiation factor 2 subunit 1 OS=Homo sapiens GN=EIF2S1 PE=1 SV=3	57	4	20.4	20.4	20.0	19.8	19.2	18.4	20.5	20.0	20.8	19.5	18.7	20.0	0.551	0.1	-0.4	0.8	-0.3	-0.4	1.6	0.2
P01780	Immunoglobulin heavy variable 3-7 OS=Homo sapiens GN=IGHV3-7 PE=1 SV=2	34	2	18.6	16.9	17.8	15.6	15.2	16.7	20.9	15.7	18.1	16.2	16.0	15.8	0.554	2.3	-1.2	0.3	0.7	0.8	-0.8	0.3
Q96A65	Exocyst complex component 4 OS=Homo sapiens GN=EXOC4 PE=1 SV=1	3	2	16.3	15.9	15.6	15.9	15.8	15.9	19.2	15.7	18.5	14.9	14.8	15.3	0.554	2.9	-0.2	2.9	-1.0	-1.0	-0.6	0.5
Q9UJC5	SH3 domain-binding glutamic acid-rich-like protein 2 OS=Homo sapiens GN=SH3BGRL2 PE=1 SV=2	3	2	NA	18.8	13.9	11.8	13.4	NA	16.4	16.7	16.8	14.2	NA	NA	0.560	####	-2.1	2.9	2.5	####	#####	1.1
P55209	Nucleosome assembly protein 1-like 1 OS=Homo sapiens GN=NAP1L1 PE=1 SV=1	18	3	17.3	19.2	18.3	18.1	17.5	19.0	17.9	19.1	19.1	17.9	17.9	18.3	0.560	0.6	-0.1	0.8	-0.2	0.5	-0.7	0.1
P05534	HLA class I histocompatibility antigen, A-24 alpha chain OS=Homo sapiens GN=HLA-A PE=1 SV=2	240	7	12.2	15.0	20.2	19.5	19.7	13.0	NA	13.0	21.8	19.9	20.4	14.4	0.565	####	-2.0	1.6	0.4	0.7	1.3	0.4
P16109	P-selectin OS=Homo sapiens GN=SELP PE=1 SV=3	9	2	16.5	17.5	17.0	16.5	17.0	14.9	16.9	17.2	17.3	16.0	17.1	14.2	0.567	0.4	-0.2	0.3	-0.6	0.1	-0.7	-0.1
P07359	Platelet glycoprotein Ib alpha chain OS=Homo sapiens GN=GP1BA PE=1 SV=2	584	19	24.6	27.1	25.5	24.5	25.2	24.2	26.0	26.9	26.4	24.2	25.2	23.6	0.572	1.3	-0.2	0.9	-0.2	-0.1	-0.6	0.2
P02538	Keratin, type II cytoskeletal 6A OS=Homo sapiens GN=KRT6A PE=1 SV=3	202	5	17.1	19.5	17.2	NA	NA	16.7	19.2	18.8	NA	NA	NA	17.0	0.574	2.1	-0.7	####	####	####	0.3	0.5
P46109	Crk-like protein OS=Homo sapiens GN=CRKL PE=1 SV=1	8	3	15.9	18.1	16.4	16.8	16.9	NA	15.6	18.1	18.0	15.5	15.2	15.0	0.576	-0.3	0.1	1.6	-1.3	-1.7	#####	-0.3
Q15746	Myosin light chain kinase, smooth muscle OS=Homo sapiens GN=MYLK PE=1 SV=4	49	9	19.5	21.5	19.5	18.3	19.3	18.0	19.6	21.1	20.6	18.1	19.4	18.1	0.577	0.1	-0.4	1.1	-0.2	0.1	0.1	0.1
P21291	Cysteine and glycine-rich protein 1 OS=Homo sapiens GN=CSRP1 PE=1 SV=3	75	5	17.9	20.2	18.5	17.3	18.5	19.2	18.1	20.2	20.4	17.5	18.7	18.1	0.581	0.3	-0.1	2.0	0.1	0.1	-1.1	0.2
Q9NRL3	Striatin-4 OS=Homo sapiens GN=STRN4 PE=1 SV=2	12	3	16.4	18.9	17.7	16.4	17.6	14.6	16.4	19.0	18.5	16.3	17.9	11.6	0.581	0.0	0.1	0.7	-0.1	0.3	-3.0	-0.3
P20042	Eukaryotic translation initiation factor 2 subunit 2 OS=Homo sapiens GN=EIF2S2 PE=1 SV=2	16	7	18.0	18.9	17.9	17.9	17.3	18.4	19.0	18.5	18.6	17.9	17.4	17.9	0.586	1.0	-0.4	0.6	0.0	0.1	-0.4	0.1
Q9UPN3	Microtubule-actin cross-linking factor 1, isoforms 1/2/3/5 OS=Homo sapiens GN=MACF1 PE=1 SV=4	46	11	17.7	20.8	19.1	18.0	19.2	17.2	16.5	20.5	19.9	17.5	18.8	17.7	0.589	-1.2	-0.3	0.9	-0.5	-0.4	0.5	-0.2
O14791	Apolipoprotein L1 OS=Homo sapiens GN=APOL1 PE=1 SV=5	6	2	17.9	NA	16.0	15.1	15.1	13.3	17.8	16.5	17.2	NA	14.0	14.7	0.590	-0.1	#####	1.2	####	-1.0	1.4	0.3
Q8IZP0	Abl interactor 1 OS=Homo sapiens GN=ABI1 PE=1 SV=4	15	3	17.4	19.2	18.6	18.0	18.4	NA	16.4	19.3	20.0	18.5	18.6	15.5	0.592	-1.0	0.1	1.4	0.4	0.2	#####	0.2
Q9BW04	Specifically androgen-regulated gene protein OS=Homo sapiens GN=SARG PE=1 SV=2	19	4	16.2	19.4	17.1	17.1	17.2	16.3	15.5	18.8	19.7	17.2	17.4	16.5	0.598	-0.8	-0.6	2.7	0.1	0.2	0.2	0.3
Q9Y4I1	Unconventional myosin-Va OS=Homo sapiens GN=MYO5A PE=1 SV=2	71	14	20.6	21.4	19.6	18.8	20.3	17.8	21.0	21.4	20.6	18.2	20.3	17.9	0.599	0.4	-0.1	1.0	-0.6	0.0	0.0	0.1
A0A0B4J1X5	Immunoglobulin heavy variable 3-74 OS=Homo sapiens GN=IGHV3-74 PE=3 SV=1	16	2	16.0	NA	NA	15.3	NA	NA	18.6	NA	NA	14.9	14.1	14.6	0.599	2.6	#####	####	-0.4	####	#####	1.1
Q5T5U3	Rho GTPase-activating protein 21 OS=Homo sapiens GN=ARHGAP21 PE=1 SV=1	11	6	16.0	18.9	16.7	NA	15.7	13.9	NA	18.3	18.4	NA	15.3	14.4	0.603	####	-0.6	1.7	####	-0.4	0.4	0.3
Q9Y5K6	CD2-associated protein OS=Homo sapiens GN=CD2AP PE=1 SV=1	12	5	17.2	19.5	18.2	17.7	18.2	12.6	17.5	19.2	18.9	17.2	17.1	15.3	0.608	0.2	-0.2	0.7	-0.6	-1.1	2.8	0.3
Q13642	Four and a half LIM domains protein 1 OS=Homo sapiens GN=FHL1 PE=1 SV=4	7	2	17.5	19.5	17.9	17.9	17.7	15.5	19.3	18.8	17.2	17.5	17.9	16.7	0.608	1.8	-0.7	-0.7	-0.4	0.2	1.2	0.2
P69905	Hemoglobin subunit alpha OS=Homo sapiens GN=HBA1 PE=1 SV=2	85	4	21.2	22.0	21.0	23.2	20.1	21.4	20.6	22.3	22.5	23.1	20.2	21.0	0.617	-0.5	0.3	1.6	-0.1	0.1	-0.4	0.2
Q9BRZ2	E3 ubiquitin-protein ligase TRIM56 OS=Homo sapiens GN=TRIM56 PE=1 SV=3	4	2	16.4	NA	NA	13.8	NA	15.0	NA	NA	NA	13.9	14.4	14.3	0.626	####	#####	####	0.1	####	-0.7	-0.3
Q8IVB4	Sodium/hydrogen exchanger 9 OS=Homo sapiens GN=SLC9A9 PE=1 SV=1	9	3	15.1	18.4	16.7	NA	16.6	13.4	15.5	17.9	18.4	NA	16.1	NA	0.629	0.4	-0.5	1.7	####	-0.5	#####	0.3
Q9UJZ1	Stomatin-like protein 2, mitochondrial OS=Homo sapiens GN=STOML2 PE=1 SV=1	6	2	17.4	17.9	17.3	14.5	16.2	NA	16.8	18.1	17.6	NA	15.8	15.1	0.629	-0.7	0.2	0.3	####	-0.4	#####	-0.1

P50991	T-complex protein 1 subunit delta OS=Homo sapiens GN=CCT4 PE=1 SV=4	19	6	18.0	18.3	19.1	19.4	18.8	18.2	18.1	18.0	20.1	19.3	18.4	18.3	0.634	0.1	-0.3	1.0	0.0	-0.3	0.1	0.1
Q13418	Integrin-linked protein kinase OS=Homo sapiens GN=ILK PE=1 SV=2	490	25	23.5	24.4	24.0	24.6	23.8	23.6	24.2	24.1	24.9	24.3	24.1	23.1	0.636	0.7	-0.3	0.9	-0.4	0.3	-0.5	0.1
P14770	Platelet glycoprotein IX OS=Homo sapiens GN=GP9 PE=1 SV=3	149	5	22.4	25.6	23.8	22.2	23.3	21.6	22.8	25.3	25.0	22.2	23.2	21.1	0.636	0.5	-0.2	1.1	0.0	-0.1	-0.5	0.1
P78371	T-complex protein 1 subunit beta OS=Homo sapiens GN=CCT2 PE=1 SV=4	30	7	18.5	19.1	19.7	19.9	18.7	18.6	18.9	17.8	20.3	19.7	18.4	18.4	0.637	0.5	-1.4	0.7	-0.1	-0.3	-0.2	-0.1
P61158	Actin-related protein 3 OS=Homo sapiens GN=ACTR3 PE=1 SV=3	33	9	19.5	20.7	19.1	18.2	19.2	17.8	20.9	20.7	20.2	17.6	19.0	17.3	0.640	1.4	0.0	1.0	-0.6	-0.3	-0.6	0.2
P29350	Tyrosine-protein phosphatase non-receptor type 6 OS=Homo sapiens GN=PTPN6 PE=1 SV=1	100	14	20.0	21.5	21.0	20.8	20.1	21.0	20.5	21.2	21.4	20.8	20.3	20.8	0.643	0.4	-0.3	0.4	-0.1	0.2	-0.3	0.1
Q9Y6W5	Wiskott-Aldrich syndrome protein family member 2 OS=Homo sapiens GN=WASF2 PE=1 SV=3	27	4	16.5	18.8	18.0	17.9	17.9	17.0	16.0	18.9	19.3	17.8	17.4	15.7	0.656	-0.5	0.1	1.3	-0.1	-0.5	-1.3	-0.2
Q9Y277	Voltage-dependent anion-selective channel protein 3 OS=Homo sapiens GN=VDAC3 PE=1 SV=1	33	8	18.3	20.4	19.8	19.2	20.4	20.2	19.6	20.8	20.7	18.8	20.6	15.1	0.658	1.3	0.4	1.0	-0.4	0.2	-5.1	-0.5
P54577	Tyrosine--tRNA ligase, cytoplasmic OS=Homo sapiens GN=YARS PE=1 SV=4	2	2	14.2	17.0	NA	16.0	NA	15.7	16.9	NA	NA	16.0	NA	14.7	0.662	2.7	#####	####	-0.1	####	-0.9	0.6
Q8TD55	Pleckstrin homology domain-containing family O member 2 OS=Homo sapiens GN=PLEKHO2 PE=1 SV=1	3	2	16.4	17.6	16.9	16.9	16.9	16.5	16.8	17.8	17.6	16.9	16.9	15.8	0.664	0.5	0.2	0.7	0.0	0.0	-0.8	0.1
O43707	Alpha-actinin-4 OS=Homo sapiens GN=ACTN4 PE=1 SV=2	974	32	22.2	24.6	23.1	21.0	22.6	20.3	22.1	24.3	24.2	21.0	22.5	20.2	0.664	0.0	-0.2	1.2	-0.1	-0.1	-0.2	0.1
P61247	40S ribosomal protein S3a OS=Homo sapiens GN=RPS3A PE=1 SV=2	4	2	15.0	12.2	14.6	13.5	15.1	12.6	14.9	15.6	11.4	13.9	15.3	14.5	0.666	-0.1	3.4	-3.3	0.3	0.2	1.9	0.4
O60313	Dynamin-like 120 kDa protein, mitochondrial OS=Homo sapiens GN=OPA1 PE=1 SV=3	6	3	13.0	16.2	15.6	14.1	14.5	13.4	15.9	16.4	13.6	NA	15.4	NA	0.673	2.8	0.2	-2.0	####	0.9	#####	0.5
P05546	Heparin cofactor 2 OS=Homo sapiens GN=SERPIND1 PE=1 SV=3	7	2	17.8	16.8	14.7	NA	14.7	14.0	18.9	15.2	15.4	14.6	NA	15.0	0.673	1.0	-1.6	0.7	####	####	1.0	0.3
P23528	Cofilin-1 OS=Homo sapiens GN=CFL1 PE=1 SV=3	229	8	22.0	23.6	22.5	22.7	22.2	21.6	22.0	22.9	23.5	22.7	22.1	21.8	0.685	0.1	-0.6	0.9	0.0	-0.1	0.2	0.1
Q04917	14-3-3 protein eta OS=Homo sapiens GN=YWHAH PE=1 SV=4	174	8	19.4	20.1	19.6	18.7	18.9	17.1	20.1	19.4	20.1	18.2	18.7	18.1	0.685	0.7	-0.8	0.6	-0.5	-0.2	1.0	0.1
P07437	Tubulin beta chain OS=Homo sapiens GN=TUBB PE=1 SV=2	596	5	20.5	21.9	21.6	21.7	21.3	21.3	21.1	21.9	23.1	21.3	21.2	20.5	0.689	0.6	0.0	1.4	-0.3	-0.1	-0.8	0.1
P06241	Tyrosine-protein kinase Fyn OS=Homo sapiens GN=FYN PE=1 SV=3	78	2	NA	17.5	16.2	16.8	15.2	15.3	17.3	14.9	17.5	16.7	16.6	13.6	0.689	####	-2.7	1.3	-0.2	1.5	-1.7	-0.4
P49368	T-complex protein 1 subunit gamma OS=Homo sapiens GN=CCT3 PE=1 SV=4	21	6	15.9	17.3	18.3	19.0	18.1	NA	15.8	17.7	19.4	18.5	17.9	NA	0.695	-0.1	0.3	1.1	-0.5	-0.2	#####	0.1
Q8IZ83	Aldehyde dehydrogenase family 16 member A1 OS=Homo sapiens GN=ALDH16A1 PE=1 SV=2	6	2	14.7	NA	16.4	16.1	14.5	12.1	NA	NA	17.4	15.4	13.8	13.4	0.696	####	#####	1.0	-0.7	-0.6	1.3	0.2
P52907	F-actin-capping protein subunit alpha-1 OS=Homo sapiens GN=CAPZA1 PE=1 SV=3	251	10	21.9	23.5	22.5	21.4	21.7	21.3	22.3	23.4	23.3	21.3	21.7	20.7	0.697	0.5	-0.1	0.8	-0.1	0.0	-0.5	0.1
Q92572	AP-3 complex subunit sigma-1 OS=Homo sapiens GN=AP3S1 PE=1 SV=1	26	3	20.8	20.2	20.2	19.9	19.3	20.7	20.8	19.6	21.0	20.0	19.2	20.1	0.699	0.0	-0.6	0.8	0.1	-0.1	-0.6	-0.1
O00203	AP-3 complex subunit beta-1 OS=Homo sapiens GN=AP3B1 PE=1 SV=3	32	9	19.1	19.2	19.7	19.7	19.2	18.4	21.1	19.2	20.2	19.4	18.4	17.9	0.699	2.1	0.0	0.5	-0.3	-0.7	-0.5	0.2
P62258	14-3-3 protein epsilon OS=Homo sapiens GN=YWHAE PE=1 SV=1	99	10	20.1	21.7	20.5	19.5	20.2	17.5	20.6	21.0	21.5	19.5	19.7	17.9	0.704	0.5	-0.7	1.0	0.0	-0.5	0.4	0.1
P19013	Keratin, type II cytoskeletal 4 OS=Homo sapiens GN=KRT4 PE=1 SV=4	50	4	18.8	19.8	18.4	15.7	18.3	18.8	18.8	19.2	19.3	18.6	17.2	18.0	0.704	0.0	-0.6	1.0	2.9	-1.1	-0.8	0.2
Q00577	Transcriptional activator protein Pur-alpha OS=Homo sapiens GN=PURA PE=1 SV=2	14	2	16.8	17.1	13.4	14.5	14.8	15.0	16.7	15.8	16.6	14.1	14.9	15.2	0.707	-0.1	-1.3	3.2	-0.5	0.0	0.2	0.2
Q96MK2	RIPOR family member 3 OS=Homo sapiens GN=RIPOR3 PE=1 SV=4	13	3	17.2	19.2	17.8	17.1	17.7	16.0	17.3	18.9	19.0	17.2	17.4	14.4	0.711	0.1	-0.3	1.2	0.1	-0.3	-1.6	-0.1
Q32MZ4	Leucine-rich repeat flightless-interacting protein 1 OS=Homo sapiens GN=LRRFIP1 PE=1 SV=2	44	6	18.7	20.2	19.8	18.7	19.3	19.3	18.4	21.1	19.6	19.0	19.2	19.1	0.717	-0.3	0.9	-0.2	0.3	-0.1	-0.3	0.1
Q8NE86	Calcium uniporter protein, mitochondrial OS=Homo sapiens GN=MCU PE=1 SV=1	9	2	16.8	18.3	17.2	16.4	17.6	15.7	17.6	17.6	18.0	16.9	17.6	13.1	0.726	0.8	-0.7	0.9	0.5	0.0	-2.6	-0.2
P01834	Immunoglobulin kappa constant OS=Homo sapiens GN=IGKC PE=1 SV=2	1146	14	26.2	26.0	25.3	24.1	23.8	24.9	26.7	25.8	26.3	24.0	23.8	24.3	0.729	0.6	-0.3	0.9	-0.2	0.0	-0.6	0.1
P07951	Tropomyosin beta chain OS=Homo sapiens GN=TPM2 PE=1 SV=1	649	6	20.4	22.3	19.8	18.6	19.0	18.5	20.2	22.4	20.9	18.4	18.4	18.8	0.732	-0.2	0.2	1.1	-0.2	-0.6	0.3	0.1
P00403	Cytochrome c oxidase subunit 2 OS=Homo sapiens GN=MT-CO2 PE=1 SV=1	2	2	14.2	17.4	14.1	14.4	16.4	13.8	NA	15.6	18.0	NA	16.5	13.5	0.746	####	-1.9	3.8	####	0.0	-0.3	0.4
P59998	Actin-related protein 2/3 complex subunit 4 OS=Homo sapiens GN=ARPC4 PE=1 SV=3	27	3	20.0	20.1	18.5	16.9	17.6	16.3	20.5	18.7	19.4	17.0	17.5	17.0	0.751	0.5	-1.4	0.9	0.1	-0.1	0.7	0.1
P04843	Dolichyl-diphosphooligosaccharide--protein glycosyltransferase subunit 1 OS=Homo sapiens GN=RPN1 PE=1 SV=1	16	3	16.1	18.3	16.6	15.8	17.2	17.0	16.5	18.5	18.6	15.4	17.8	15.2	0.751	0.4	0.2	2.1	-0.4	0.5	-1.8	0.2
O75083	WD repeat-containing protein 1 OS=Homo sapiens GN=WDR1 PE=1 SV=4	26	4	18.0	20.1	19.2	19.0	18.9	17.6	17.8	20.7	20.1	18.4	19.3	17.0	0.755	-0.2	0.6	0.9	-0.6	0.4	-0.6	0.1
Q15067	Peroxisomal acyl-coenzyme A oxidase 1 OS=Homo sapiens GN=ACOX1 PE=1 SV=3	4	2	16.7	17.2	16.7	16.6	16.8	16.2	17.4	16.9	17.5	16.5	16.9	15.5	0.757	0.7	-0.3	0.7	-0.1	0.2	-0.7	0.1
P29692	Elongation factor 1-delta OS=Homo sapiens GN=EEF1D PE=1 SV=5	11	2	16.6	16.5	17.5	17.7	17.1	NA	17.0	17.3	18.3	17.7	15.7	13.4	0.758	0.4	0.7	0.9	0.1	-1.4	#####	0.1
Q562R1	Beta-actin-like protein 2 OS=Homo sapiens GN=ACTBL2 PE=1 SV=2	4241	4	16.7	21.6	20.4	18.8	20.1	18.8	17.4	21.3	21.3	19.1	18.9	17.8	0.762	0.7	-0.4	0.9	0.3	-1.2	-1.0	-0.1
P60660	Myosin light polypeptide 6 OS=Homo sapiens GN=MYL6 PE=1 SV=2	1017	13	27.1	28.0	26.4	25.5	26.0	24.4	27.0	27.2	27.4	25.7	25.4	25.4	0.764	-0.1	-0.8	0.9	0.2	-0.6	1.0	0.1
Q96BS2	Calcineurin B homologous protein 3 OS=Homo sapiens GN=TESC PE=1 SV=3	3	2	13.8	16.6	14.7	14.7	15.1	12.3	NA	15.9	16.1	NA	NA	NA	0.765	####	-0.6	1.4	####	####	#####	0.4
O75410	Transforming acidic coiled-coil-containing protein 1 OS=Homo sapiens GN=TACC1 PE=1 SV=2	5	3	NA	18.1	16.5	14.8	17.3	15.7	15.0	17.5	18.1	14.6	16.6	16.4	0.768	####	-0.7	1.6	-0.2	-0.8	0.7	0.1
O76074	cGMP-specific 3',5'-cyclic phosphodiesterase OS=Homo sapiens GN=PDE5A PE=1 SV=2	6	2	15.5	17.0	16.4	16.9	16.2	16.5	NA	14.3	17.5	17.2	16.4	16.5	0.769	####	-2.7	1.1	0.3	0.2	0.0	-0.2
P60228	Eukaryotic translation initiation factor 3 subunit E OS=Homo sapiens GN=EIF3E PE=1 SV=1	9	4	18.7	17.4	17.1	15.1	14.1	16.6	19.3	15.0	17.3	NA	15.2	18.1	0.772	0.6	-2.4	0.2	####	1.1	1.6	0.2
Q13464	Rho-associated protein kinase 1 OS=Homo sapiens GN=ROCK1 PE=1 SV=1	18	4	17.1	17.5	16.6	17.9	17.8	16.6	15.7	17.4	17.6	17.0	17.5	17.4	0.784	-1.4	0.0	1.0	-0.8	-0.3	0.8	-0.1
P48426	Phosphatidylinositol 5-phosphate 4-kinase type-2 alpha OS=Homo sapiens GN=PIP4K2A PE=1 SV=2	112	10	19.2	20.6	19.8	19.6	19.1	19.0	20.0	20.5	20.2	19.4	18.6	18.8	0.803	0.8	-0.1	0.4	-0.2	-0.4	-0.2	0.0
P19086	Guanine nucleotide-binding protein G(z) subunit alpha OS=Homo sapiens GN=GNAZ PE=2 SV=3	18	4	14.7	18.2	17.4	17.5	17.3	16.2	17.7	16.8	18.9	17.4	17.2	11.4	0.803	3.0	-1.3	1.5	0.0	-0.1	-4.8	-0.3
Q9NY65	Tubulin alpha-8 chain OS=Homo sapiens GN=TUBA8 PE=1 SV=1	237	2	18.1	18.7	18.6	19.1	18.2	18.9	19.1	17.9	19.2	18.8	18.7	18.4	0.806	0.9	-0.8	0.6	-0.3	0.5	-0.5	0.1
O43866	CD5 antigen-like OS=Homo sapiens GN=CD5L PE=1 SV=1	14	3	17.5	17.6	16.3	15.1	15.3	16.0	17.8	17.0	17.2	14.9	15.5	15.0	0.809	0.3	-0.5	0.8	-0.2	0.1	-1.0	-0.1
P04114	Apolipoprotein B-100 OS=Homo sapiens GN=APOB PE=1 SV=2	21	10	18.9	18.9	17.7	17.2	19.0	14.7	19.4	20.1	18.0	16.8	17.3	15.6	0.816	0.5	1.2	0.2	-0.4	-1.7	0.9	0.1
P61160	Actin-related protein 2 OS=Homo sapiens GN=ACTR2 PE=1 SV=1	24	6	18.7	19.3	17.7	16.9	17.8	17.5	19.7	19.0	18.4	16.4	18.0	16.7	0.817	1.1	-0.3	0.7	-0.4	0.2	-0.8	0.1

Q9BX10	GTP-binding protein 2 OS=Homo sapiens GN=GTPBP2 PE=1 SV=1	6	3	NA	16.4	15.6	15.9	14.4	15.1	NA	15.7	16.6	16.5	15.3	13.9	0.818	#####	-0.7	1.0	0.6	0.9	-1.2	0.1
O00139	Kinesin-like protein KIF2A OS=Homo sapiens GN=KIF2A PE=1 SV=3	121	16	21.7	22.3	21.4	21.5	21.5	21.6	22.1	22.0	22.2	21.3	21.6	21.2	0.819	0.4	-0.4	0.8	-0.2	0.1	-0.4	0.0
P81605	Dermcidin OS=Homo sapiens GN=DCD PE=1 SV=2	6	2	15.8	18.4	18.1	17.9	17.2	NA	15.3	19.2	18.2	17.3	17.1	14.9	0.821	-0.5	0.8	0.1	-0.6	-0.1	#####	-0.1
P01871	Immunoglobulin heavy constant mu OS=Homo sapiens GN=IGHM PE=1 SV=4	624	23	25.3	24.9	24.4	23.1	23.0	23.2	26.2	24.4	24.6	22.9	22.9	23.0	0.824	0.9	-0.5	0.2	-0.1	-0.1	-0.2	0.0
Q8N9U0	Tandem C2 domains nuclear protein OS=Homo sapiens GN=TC2N PE=1 SV=2	15	3	16.6	21.7	17.6	17.7	18.4	NA	16.9	20.2	19.1	17.3	19.0	16.3	0.826	0.3	-1.5	1.5	-0.4	0.6	#####	0.1
O95782	AP-2 complex subunit alpha-1 OS=Homo sapiens GN=AP2A1 PE=1 SV=3	21	3	21.1	19.3	19.1	18.6	18.4	18.1	19.2	19.6	20.2	18.7	18.6	17.8	0.828	-1.9	0.3	1.0	0.1	0.3	-0.3	-0.1
P01891	HLA class I histocompatibility antigen, A-68 alpha chain OS=Homo sapiens GN=HLA-A PE=1 SV=4	210	5	NA	20.9	NA	14.1	14.0	18.1	NA	21.9	NA	NA	13.5	17.1	0.828	#####	1.0	#####	#####	-0.5	-0.9	-0.1
Q9P2E9	Ribosome-binding protein 1 OS=Homo sapiens GN=RRBP1 PE=1 SV=4	41	7	19.2	18.8	18.4	17.7	18.2	17.8	18.3	19.2	18.7	17.1	18.5	18.5	0.830	-0.8	0.4	0.3	-0.6	0.3	0.7	0.1
P14317	Hematopoietic lineage cell-specific protein OS=Homo sapiens GN=HCLS1 PE=1 SV=3	6	2	15.3	16.4	NA	NA	14.5	12.4	14.7	16.6	15.7	14.4	14.6	NA	0.830	-0.6	0.2	#####	#####	0.2	#####	-0.1
P07814	Bifunctional glutamate/proline--tRNA ligase OS=Homo sapiens GN=EPRS PE=1 SV=5	14	4	18.1	17.4	16.5	17.0	15.8	17.0	18.6	17.4	17.5	15.5	NA	17.5	0.840	0.5	0.0	1.0	-1.5	#####	0.5	0.1
Q02413	Desmoglein-1 OS=Homo sapiens GN=DSG1 PE=1 SV=2	2	2	15.7	16.1	15.6	14.5	15.3	15.1	NA	15.4	16.2	15.4	14.1	NA	0.846	#####	-0.7	0.6	0.9	-1.2	#####	-0.1
Q14344	Guanine nucleotide-binding protein subunit alpha-13 OS=Homo sapiens GN=GNA13 PE=1 SV=2	81	5	20.3	22.1	21.6	21.3	21.2	20.0	21.3	21.9	22.4	21.4	21.4	18.5	0.847	1.0	-0.1	0.8	0.1	0.3	-1.5	0.1
P60709	Actin, cytoplasmic 1 OS=Homo sapiens GN=ACTB PE=1 SV=1	14225	21	29.0	30.1	29.1	28.2	28.5	28.3	29.9	29.7	29.7	28.1	28.5	27.6	0.852	0.9	-0.3	0.6	-0.1	0.0	-0.7	0.0
O43149	Zinc finger ZZ-type and EF-hand domain-containing protein 1 OS=Homo sapiens GN=ZZEF1 PE=1 SV=6	12	5	15.5	15.4	18.0	18.0	17.0	17.0	15.2	17.0	17.6	17.5	16.7	16.6	0.852	-0.4	1.6	-0.4	-0.5	-0.3	-0.5	-0.1
P48643	T-complex protein 1 subunit epsilon OS=Homo sapiens GN=CCT5 PE=1 SV=1	6	3	17.3	NA	17.8	18.2	17.3	17.6	17.2	16.6	18.6	17.9	16.7	NA	0.852	-0.1	#####	0.8	-0.3	-0.6	#####	-0.1
O60763	General vesicular transport factor p115 OS=Homo sapiens GN=USO1 PE=1 SV=2	4	2	16.2	NA	15.7	16.4	15.8	14.7	14.7	NA	17.7	16.1	15.0	15.9	0.853	-1.5	#####	2.0	-0.3	-0.8	1.3	0.1
P13224	Platelet glycoprotein Ib beta chain OS=Homo sapiens GN=GP1BB PE=1 SV=1	328	8	24.2	27.1	25.2	24.1	24.8	23.9	25.7	26.5	26.1	24.0	24.7	22.8	0.855	1.5	-0.7	0.9	-0.1	-0.1	-1.1	0.1
Q96T51	RUN and FYVE domain-containing protein 1 OS=Homo sapiens GN=RUFY1 PE=1 SV=2	12	2	15.2	17.3	15.9	16.3	16.3	16.4	15.9	16.7	17.4	16.5	15.7	15.7	0.858	0.7	-0.7	1.5	0.3	-0.6	-0.7	0.1
P18054	Arachidonate 12-lipoxygenase, 12S-type OS=Homo sapiens GN=ALOX12 PE=1 SV=4	26	5	17.4	20.1	19.9	19.6	19.6	17.5	17.9	20.0	20.1	19.3	19.4	17.6	0.865	0.5	-0.1	0.2	-0.3	-0.2	0.1	0.0
Q8YHK3	CD109 antigen OS=Homo sapiens GN=CD109 PE=1 SV=2	10	3	16.8	18.2	17.7	17.4	16.5	16.4	17.9	16.9	18.4	17.3	16.5	15.7	0.876	1.1	-1.4	0.8	-0.2	0.0	-0.7	-0.1
Q9Y490	Talin-1 OS=Homo sapiens GN=TLN1 PE=1 SV=3	5061	168	27.0	28.6	27.1	27.7	27.4	27.0	26.7	28.4	28.4	27.4	27.5	26.6	0.880	-0.3	-0.2	1.4	-0.3	0.1	-0.4	0.0
Q9Y2T2	AP-3 complex subunit mu-1 OS=Homo sapiens GN=AP3M1 PE=1 SV=1	5	3	16.7	16.5	16.7	17.3	17.2	16.4	19.4	14.3	17.3	16.9	16.6	15.5	0.889	2.8	-2.2	0.7	-0.4	-0.5	-0.9	-0.1
P19827	Inter-alpha-trypsin inhibitor heavy chain H1 OS=Homo sapiens GN=ITIH1 PE=1 SV=3	2	2	17.5	16.4	13.9	13.9	14.1	11.2	16.6	NA	NA	NA	NA	12.4	0.890	-0.9	#####	####	####	####	1.2	0.2
Q9Y3I0	tRNA-splicing ligase RtcB homolog OS=Homo sapiens GN=RTCB PE=1 SV=1	5	2	16.0	17.3	15.0	15.8	15.7	13.7	15.6	17.1	17.0	15.9	15.3	13.1	0.892	-0.4	-0.2	1.9	0.1	-0.4	-0.6	0.1
O43306	Adenylate cyclase type 6 OS=Homo sapiens GN=ADCY6 PE=1 SV=2	4	2	16.8	18.1	15.8	14.1	15.2	NA	17.0	16.8	18.4	14.0	14.4	16.8	0.893	0.2	-1.2	2.5	-0.2	-0.8	#####	0.1
P04899	Guanine nucleotide-binding protein G(i) subunit alpha-2 OS=Homo sapiens GN=GNAI2 PE=1 SV=3	162	9	19.9	22.3	21.9	21.7	21.4	20.3	20.2	22.0	22.8	21.6	21.4	19.4	0.895	0.3	-0.3	0.9	-0.1	-0.1	-0.9	0.0
P30273	High affinity immunoglobulin epsilon receptor subunit gamma OS=Homo sapiens GN=FCER1G PE=1 SV=1	4	2	19.0	18.6	16.6	17.2	16.9	16.0	19.1	15.5	19.6	17.6	17.2	15.9	0.901	0.2	-3.1	3.0	0.4	0.3	-0.2	0.1
Q86UX7	Fermitin family homolog 3 OS=Homo sapiens GN=FERMT3 PE=1 SV=1	318	20	22.4	24.1	23.2	23.9	23.0	23.1	23.4	23.9	24.6	23.3	23.2	21.8	0.902	0.9	-0.3	1.4	-0.6	0.2	-1.3	0.1
O75427	Leucine-rich repeat and calponin homology domain-containing protein 4 OS=Homo sapiens GN=LRCH4 PE=1 SV=2	10	2	14.8	18.6	16.9	15.5	16.3	NA	13.5	18.8	18.6	15.4	16.1	14.9	0.905	-1.3	0.2	1.7	-0.1	-0.2	#####	0.1
Q6IBS0	Twinfilin-2 OS=Homo sapiens GN=TWF2 PE=1 SV=2	50	8	20.4	22.0	20.7	20.2	20.6	20.6	20.5	21.7	21.5	20.2	20.4	20.2	0.918	0.1	-0.3	0.8	0.0	-0.2	-0.3	0.0
O60610	Protein diaphanous homolog 1 OS=Homo sapiens GN=DIAPH1 PE=1 SV=2	24	8	18.7	19.4	19.2	19.4	18.6	18.7	18.4	19.6	20.4	19.3	18.5	18.0	0.924	-0.3	0.1	1.2	0.0	-0.1	-0.7	0.0
P24844	Myosin regulatory light polypeptide 9 OS=Homo sapiens GN=MYL9 PE=1 SV=4	470	8	23.2	25.6	23.5	23.1	23.7	22.5	23.2	25.5	24.5	23.0	23.8	21.4	0.928	0.1	-0.2	0.9	-0.1	0.1	-1.1	0.0
P02766	Transthyretin OS=Homo sapiens GN=TTR PE=1 SV=1	10	2	17.0	19.6	16.8	15.6	16.3	NA	16.6	19.4	17.5	15.4	16.4	15.7	0.928	-0.4	-0.1	0.7	-0.2	0.2	#####	0.0
Q96C19	EF-hand domain-containing protein D2 OS=Homo sapiens GN=EFHD2 PE=1 SV=1	5	2	16.9	18.0	16.8	NA	NA	NA	16.8	17.5	17.3	16.4	13.7	15.3	0.930	-0.1	-0.5	0.5	####	####	#####	0.0
Q9Y262	Eukaryotic translation initiation factor 3 subunit L OS=Homo sapiens GN=EIF3L PE=1 SV=1	7	3	18.2	17.3	16.2	16.9	16.1	17.6	18.9	16.5	17.9	16.8	15.3	17.1	0.935	0.8	-0.9	1.7	-0.1	-0.8	-0.5	0.0
P42345	Serine/threonine-protein kinase mTOR OS=Homo sapiens GN=MTOR PE=1 SV=1	4	2	NA	17.6	NA	16.3	13.1	15.9	NA	NA	16.2	15.0	14.6	16.0	0.941	####	#####	####	-1.3	1.5	0.0	0.1
P55036	26S proteasome non-ATPase regulatory subunit 4 OS=Homo sapiens GN=PSMD4 PE=1 SV=1	2	2	15.2	NA	15.2	16.1	15.3	NA	13.2	NA	16.5	16.0	16.5	15.0	0.943	-2.1	#####	1.2	-0.1	1.2	#####	0.1
P01857	Immunoglobulin heavy constant gamma 1 OS=Homo sapiens GN=IGHG1 PE=1 SV=1	1298	8	25.9	26.3	25.4	24.3	23.7	25.3	27.3	26.0	26.5	24.1	23.5	23.8	0.943	1.3	-0.4	1.1	-0.2	-0.2	-1.5	0.0
P10599	Thioredoxin OS=Homo sapiens GN=TXN PE=1 SV=3	5	2	15.6	16.2	16.6	16.5	16.2	15.5	17.5	15.9	17.7	16.5	13.9	14.9	0.945	1.9	-0.3	1.1	0.0	-2.4	-0.6	0.0
P98172	Ephrin-B1 OS=Homo sapiens GN=EFNB1 PE=1 SV=1	18	3	16.1	19.4	18.0	17.6	17.8	13.8	13.5	19.6	19.2	17.4	18.0	15.2	0.949	-2.6	0.2	1.3	-0.2	0.2	1.4	0.0
P08779	Keratin, type I cytoskeletal 16 OS=Homo sapiens GN=KRT16 PE=1 SV=4	373	9	19.2	22.3	19.8	19.3	18.6	18.1	21.0	21.2	19.7	20.0	17.4	18.1	0.955	1.8	-1.1	-0.1	0.7	-1.1	0.0	0.0
Q04759	Protein kinase C theta type OS=Homo sapiens GN=PRKCQ PE=1 SV=3	2	2	14.3	16.5	14.7	15.0	16.1	13.9	NA	16.5	16.7	14.8	15.0	13.1	0.960	####	0.0	2.0	-0.2	-1.1	-0.9	0.0
Q8ZNJ1	Neurobeachin-like protein 2 OS=Homo sapiens GN=NBEAL2 PE=1 SV=2	6	2	16.7	17.2	16.9	16.9	NA	16.2	17.2	NA	17.7	16.7	16.0	15.1	0.960	0.5	#####	0.9	-0.2	####	-1.1	0.0
Q96CW1	AP-2 complex subunit mu OS=Homo sapiens GN=AP2M1 PE=1 SV=2	5	3	16.8	17.2	17.7	17.7	17.7	17.5	18.0	15.9	18.6	17.5	18.2	16.6	0.971	1.2	-1.3	0.8	-0.2	0.5	-0.9	0.0
Q9H4B7	Tubulin beta-1 chain OS=Homo sapiens GN=TUBB1 PE=1 SV=1	954	18	24.0	24.8	24.4	24.6	24.1	23.9	24.5	24.4	25.2	24.4	24.1	23.2	0.971	0.5	-0.4	0.8	-0.2	0.1	-0.7	0.0
Q17RC7	Exocyst complex component 3-like protein 4 OS=Homo sapiens GN=EXOC3L4 PE=1 SV=2	13	4	16.8	20.2	18.6	18.1	18.2	16.5	16.7	20.1	20.3	17.4	17.2	16.7	0.982	-0.1	-0.1	1.7	-0.6	-0.9	0.2	0.0
P36957	Dihydrolipoyllysine-residue succinyltransferase component of 2-oxoglutarate dehydrogenase complex, mitochondrial OS=Homo sapiens GN=DLST PE=1 SV=4	14	4	16.4	18.9	18.0	17.6	18.3	17.5	17.1	19.3	19.4	17.3	18.7	14.7	0.986	0.8	0.4	1.4	-0.3	0.4	-2.8	0.0
P29144	Tripeptidyl-peptidase 2 OS=Homo sapiens GN=TPP2 PE=1 SV=4	9	2	NA	17.6	17.0	16.2	16.2	16.0	13.8	15.5	18.3	16.5	16.4	16.1	0.991	####	-2.1	1.3	0.3	0.2	0.2	0.0
P02775	Platelet basic protein OS=Homo sapiens GN=PPBP PE=1 SV=3	904	14	26.1	26.9	27.5	27.0	25.5	24.9	26.7	26.7	28.1	26.8	25.4	24.2	0.993	0.6	-0.3	0.6	-0.1	-0.1	-0.8	0.0
P27816	Microtubule-associated protein 4 OS=Homo sapiens GN=MAP4 PE=1 SV=3	4	2	14.3	17.0	14.8	16.6	15.8	15.0	NA	17.3	15.8	14.8	15.8	15.4	0.994	####	0.3	1.0	-1.7	0.1	0.4	0.0
P27708	CAD protein OS=Homo sapiens GN=CAD PE=1 SV=3	7	2	15.5	16.0	16.7	15.2	16.9	16.5	17.0	16.2	17.5	16.5	14.0	15.5	1.000	1.5	0.1	0.8	1.3	-2.8	-0.9	0.0

7. References

1. Machlus, K.R., J.N. Thon, and J.E. Italiano, Jr., *Interpreting the developmental dance of the megakaryocyte: a review of the cellular and molecular processes mediating platelet formation.* Br J Haematol, 2014. **165**(2): p. 227-36.

2. Kaushansky, K., *Historical review: megakaryopoiesis and thrombopoiesis.* Blood, 2008. **111**(3): p. 981-6.

3. Franco, A.T., A. Corken, and J. Ware, *Platelets at the interface of thrombosis, inflammation, and cancer.* Blood, 2015. **126**(5): p. 582-8.

4. Huo, Y. and K.F. Ley, *Role of platelets in the development of atherosclerosis.* Trends Cardiovasc Med, 2004. **14**(1): p. 18-22.

5. Weber, C., *Platelets and chemokines in atherosclerosis: partners in crime.* Circ Res, 2005. **96**(6): p. 612-6.

6. Yun, S.H., et al., *Platelet activation: The mechanisms and potential biomarkers.* Biomed Res Int, 2016. **2016**: p. 9060143.

7. Furie, B. and B.C. Furie, *Mechanisms of thrombus formation.* N Engl J Med, 2008. **359**(9): p. 938-49.

8. Ruggeri, Z.M., *Platelet adhesion under flow.* Microcirculation, 2009. **16**(1): p. 58-83.

9. Ruggeri, Z.M., *Old concepts and new developments in the study of platelet aggregation.* J Clin Invest, 2000. **105**(6): p. 699-701.

10. Stegner, D. and B. Nieswandt, *Platelet receptor signaling in thrombus formation.* J Mol Med (Berl), 2011. **89**(2): p. 109-21.

11. Wen, L., S. Feil, and R. Feil, *cGMP signaling in platelets*, in *Platelets, Haemostasis and Inflammation*. 2017, Springer. p. 231-252.

12. Eberl, D.F., R.W. Hardy, and M.J. Kernan, *Genetically similar transduction mechanisms for touch and hearing in Drosophila.* J Neurosci, 2000. **20**(16): p. 5981-8.

13. Burger, E.H. and J. Klein-Nulend, *Mechanotransduction in bone--role of the lacuno-canalicular network.* FASEB J, 1999. **13 Suppl**: p. S101-12.

14. Wirtz, H.R. and L.G. Dobbs, *The effects of mechanical forces on lung functions.* Respir Physiol, 2000. **119**(1): p. 1-17.

15. Serluca, F.C., I.A. Drummond, and M.C. Fishman, *Endothelial signaling in kidney morphogenesis: a role for hemodynamic forces.* Curr Biol, 2002. **12**(6): p. 492-7.

16. Orr, A.W., et al., *Mechanisms of mechanotransduction.* Dev Cell, 2006. **10**(1): p. 11-20.

17. Jaalouk, D.E. and J. Lammerding, *Mechanotransduction gone awry.* Nat Rev Mol Cell Biol, 2009. **10**(1): p. 63-73.

18. Cunningham, K.S. and A.I. Gotlieb, *The role of shear stress in the pathogenesis of atherosclerosis.* Lab Invest, 2005. **85**(1): p. 9-23.

19. Gimbrone, M.A., Jr., et al., *Endothelial dysfunction, hemodynamic forces, and atherogenesis.* Ann N Y Acad Sci, 2000. **902**: p. 230-9; discussion 239-40.

20. Garcia-Cardena, G., et al., *Biomechanical activation of vascular endothelium as a determinant of its functional phenotype.* Proc Natl Acad Sci U S A, 2001. **98**(8): p. 4478-85.

21. Haga, J.H., Y.S. Li, and S. Chien, *Molecular basis of the effects of mechanical stretch on vascular smooth muscle cells.* J Biomech, 2007. **40**(5): p. 947-60.

22. Hahn, C. and M.A. Schwartz, *Mechanotransduction in vascular physiology and atherogenesis.* Nat Rev Mol Cell Biol, 2009. **10**(1): p. 53-62.

23. Resnick, N., et al., *Fluid shear stress and the vascular endothelium: for better and for worse.* Prog Biophys Mol Biol, 2003. **81**(3): p. 177-99.

24. Shi, Z.D. and J.M. Tarbell, *Fluid flow mechanotransduction in vascular smooth muscle cells and fibroblasts.* Ann Biomed Eng, 2011. **39**(6): p. 1608-19.

25. Tarbell, J.M., S.I. Simon, and F.R. Curry, *Mechanosensing at the vascular interface.* Annu Rev Biomed Eng, 2014. **16**: p. 505-32.

26. Kano, Y., K. Katoh, and K. Fujiwara, *Lateral zone of cell-cell adhesion as the major fluid shear stress-related signal transduction site.* Circ Res, 2000. **86**(4): p. 425-33.

27. Fujiwara, K., et al., *Is PECAM-1 a mechanoresponsive molecule?* Cell Struct Funct, 2001. **26**(1): p. 11-7.

28. Shay-Salit, A., et al., *VEGF receptor 2 and the adherens junction as a mechanical transducer in vascular endothelial cells.* Proc Natl Acad Sci U S A, 2002. **99**(14): p. 9462-7.

29. Ohno, M., et al., *Fluid shear stress induces endothelial transforming growth factor beta-1 transcription and production. Modulation by potassium channel blockade.* J Clin Invest, 1995. **95**(3): p. 1363-9.

30. Uematsu, M., et al., *Regulation of endothelial cell nitric oxide synthase mRNA expression by shear stress.* Am J Physiol, 1995. **269**(6 Pt 1): p. C1371-8.

31. Karaman, S. and K. Alitalo, *ORAI1 controls the unique adjustment of lymphatics to fluid flow.* Circ Res, 2017. **120**(9): p. 1373-1375.

32. Katsumi, A., et al., *Integrins in mechanotransduction.* J Biol Chem, 2004. **279**(13): p. 12001-4.

33. Rizzo, V., et al., *In situ flow activates endothelial nitric oxide synthase in luminal caveolae of endothelium with rapid caveolin dissociation and calmodulin association.* J Biol Chem, 1998. **273**(52): p. 34724-9.

34. Gudi, S., J.P. Nolan, and J.A. Frangos, *Modulation of GTPase activity of G proteins by fluid shear stress and phospholipid composition.* Proc Natl Acad Sci U S A, 1998. **95**(5): p. 2515-9.

35. Lam, R.M. and A.T. Chesler, *Shear elegance: A novel screen uncovers a mechanosensitive GPCR.* J Gen Physiol, 2018. **150**(7): p. 907-910.

36. Xu, J., et al., *GPR68 Senses Flow and Is Essential for Vascular Physiology.* Cell, 2018. **173**(3): p. 762-775 e16.

37. Imberti, B., et al., *Shear stress-induced cytoskeleton rearrangement mediates NF-kappaB-dependent endothelial expression of ICAM-1.* Microvasc Res, 2000. **60**(2): p. 182-8.

38. Knudsen, H.L. and J.A. Frangos, *Role of cytoskeleton in shear stress-induced endothelial nitric oxide production.* Am J Physiol, 1997. **273**(1 Pt 2): p. H347-55.

39. Zeng, Y., et al., *The role of endothelial surface glycocalyx in mechanosensing and transduction.* Adv Exp Med Biol, 2018. **1097**: p. 1-27.

40. Shattil, S.J. and P.J. Newman, *Integrins: dynamic scaffolds for adhesion and signaling in platelets.* Blood, 2004. **104**(6): p. 1606-15.

41. Hynes, R.O., *Integrins: bidirectional, allosteric signaling machines.* Cell, 2002. **110**(6): p. 673-87.

42. Nieswandt, B., D. Varga-Szabo, and M. Elvers, *Integrins in platelet activation.* J Thromb Haemost, 2009. **7 Suppl 1**: p. 206-9.

43. Tzima, E., et al., *Activation of integrins in endothelial cells by fluid shear stress mediates Rho-dependent cytoskeletal alignment.* EMBO J, 2001. **20**(17): p. 4639-47.

44. Tzima, E., et al., *A mechanosensory complex that mediates the endothelial cell response to fluid shear stress.* Nature, 2005. **437**(7057): p. 426-31.

45. Wang, L., et al., *Integrin-YAP/TAZ-JNK cascade mediates atheroprotective effect of unidirectional shear flow.* Nature, 2016. **540**(7634): p. 579-582.

46. Bhatt, D.L. and E.J. Topol, *Scientific and therapeutic advances in antiplatelet therapy.* Nat Rev Drug Discov, 2003. **2**(1): p. 15-28.

47. Coller, B.S., *Anti-GPIIb/IIIa drugs: current strategies and future directions.* Thromb Haemost, 2001. **86**(1): p. 427-43.

48. Estevez, B. and X. Du, *New concepts and mechanisms of platelet activation signaling.* Physiology (Bethesda), 2017. **32**(2): p. 162-177.

49. Pang, A., et al., *Shear-induced integrin signaling in platelet phosphatidylserine exposure, microvesicle release, and coagulation.* Blood, 2018. **132**(5): p. 533-543.

50. Ye, F., C. Kim, and M.H. Ginsberg, *Molecular mechanism of inside-out integrin regulation.* J Thromb Haemost, 2011. **9 Suppl 1**: p. 20-25.

51. Chen, Y., et al., *An integrin alphaIIbbeta3 intermediate affinity state mediates biomechanical platelet aggregation.* Nat Mater, 2019. **18**(7): p. 760-769.

52. Ashman, D.F., et al., *Isolation of adenosine 3', 5'-monophosphate and guanosine 3', 5'-monophosphate from rat urine.* Biochem Biophys Res Commun, 1963. **11**: p. 330-4.

53. Kemp-Harper, B. and R. Feil, *Meeting report: cGMP matters.* Sci Signal, 2008. **1**(9): p. pe12.

54. Hofmann, F., *The cGMP system: components and function.* Biol Chem, 2020. **401**(4): p. 447-469.

55. Ehret, G.B., et al., *Genetic variants in novel pathways influence blood pressure and cardiovascular disease risk.* Nature, 2011. **478**(7367): p. 103-9.

56. Erdmann, J., et al., *Dysfunctional nitric oxide signalling increases risk of myocardial infarction.* Nature, 2013. **504**(7480): p. 432-6.

57. Emdin, C.A., et al., *Phenotypic consequences of a genetic predisposition to enhanced nitric oxide signaling.* Circulation, 2018. **137**(3): p. 222-232.

58. Kessler, T., et al., *Functional characterization of the GUCY1A3 coronary artery disease risk locus.* Circulation, 2017. **136**(5): p. 476-489.

59. Feil, R. and B. Kemp-Harper, *cGMP signalling: from bench to bedside. Conference on cGMP generators, effectors and therapeutic implications.* EMBO Rep, 2006. **7**(2): p. 149-53.

60. Alderton, W.K., C.E. Cooper, and R.G. Knowles, *Nitric oxide synthases: structure, function and inhibition.* Biochem J, 2001. **357**(Pt 3): p. 593-615.

61. Moncada, S. and E.A. Higgs, *Nitric oxide and the vascular endothelium.* Handb Exp Pharmacol, 2006(176 Pt 1): p. 213-54.

62. Bredt, D.S. and S.H. Snyder, *Isolation of nitric oxide synthetase, a calmodulin-requiring enzyme.* Proc Natl Acad Sci U S A, 1990. **87**(2): p. 682-5.

63. Forstermann, U., et al., *Nitric oxide synthase isozymes. Characterization, purification, molecular cloning, and functions.* Hypertension, 1994. **23**(6 Pt 2): p. 1121-31.

64. Biel, M., et al., *Structure and function of cyclic nucleotide-gated channels.* Rev Physiol Biochem Pharmacol, 1999. **135**: p. 151-71.

65. Smolenski, A., *Novel roles of cAMP/cGMP-dependent signaling in platelets.* J Thromb Haemost, 2012. **10**(2): p. 167-76.

66. Sandner, P., et al., *Soluble guanylate cyclase stimulators and activators.* Handb Exp Pharmacol, 2019.

67. Moncada, S., E.A. Higgs, and J.R. Vane, *Human arterial and venous tissues generate prostacyclin (prostaglandin x), a potent inhibitor of platelet aggregation.* Lancet, 1977. **1**(8001): p. 18-20.

68. Mellion, B.T., et al., *Inhibition of human platelet aggregation by S-nitrosothiols. Heme-dependent activation of soluble guanylate cyclase and stimulation of cyclic GMP accumulation.* Mol Pharmacol, 1983. **23**(3): p. 653-64.

69. Mellion, B.T., et al., *Evidence for the inhibitory role of guanosine 3', 5'-monophosphate in ADP-induced human platelet aggregation in the presence of nitric oxide and related vasodilators.* Blood, 1981. **57**(5): p. 946-55.

70. Makhoul, S., et al., *Effects of the NO/soluble guanylate cyclase/cGMP system on the functions of human platelets.* Nitric Oxide, 2018. **76**: p. 71-80.

71. Walter, U. and S. Gambaryan, *cGMP and cGMP-dependent protein kinase in platelets and blood cells.* Handb Exp Pharmacol, 2009(191): p. 533-48.

72. Schwarz, U.R., U. Walter, and M. Eigenthaler, *Taming platelets with cyclic nucleotides.* Biochem Pharmacol, 2001. **62**(9): p. 1153-61.

73. Haslam, R.J., N.T. Dickinson, and E.K. Jang, *Cyclic nucleotides and phosphodiesterases in platelets.* Thromb Haemost, 1999. **82**(2): p. 412-23.

74. Rondina, M.T. and A.S. Weyrich, *Targeting phosphodiesterases in anti-platelet therapy.* Handb Exp Pharmacol, 2012(210): p. 225-38.

75. Mullershausen, F., et al., *Rapid nitric oxide-induced desensitization of the cGMP response is caused by increased activity of phosphodiesterase type 5 paralleled by phosphorylation of the enzyme.* J Cell Biol, 2001. **155**(2): p. 271-8.

76. Zaccolo, M. and M.A. Movsesian, *cAMP and cGMP signaling cross-talk: role of phosphodiesterases and implications for cardiac pathophysiology.* Circ Res, 2007. **100**(11): p. 1569-78.

77. Sager, G., *Cyclic GMP transporters.* Neurochem Int, 2004. **45**(6): p. 865-73.

78. Jedlitschky, G., et al., *The nucleotide transporter MRP4 (ABCC4) is highly expressed in human platelets and present in dense granules, indicating a role in mediator storage.* Blood, 2004. **104**(12): p. 3603-10.

79. Borgognone, A. and F.M. Pulcinelli, *Reduction of cAMP and cGMP inhibitory effects in human platelets by MRP4-mediated transport.* Thromb Haemost, 2012. **108**(5): p. 955-62.

80. Wu, X.B., et al., *Efflux of cyclic GMP from activated human platelets.* Mol Pharmacol, 1993. **43**(4): p. 564-8.

81. Rius, M., J. Hummel-Eisenbeiss, and D. Keppler, *ATP-dependent transport of leukotrienes B4 and C4 by the multidrug resistance protein ABCC4 (MRP4).* J Pharmacol Exp Ther, 2008. **324**(1): p. 86-94.

82. Antl, M., et al., *IRAG mediates NO/cGMP-dependent inhibition of platelet aggregation and thrombus formation.* Blood, 2007. **109**(2): p. 552-9.

83. Massberg, S., et al., *Enhanced in vivo platelet adhesion in vasodilator-stimulated phosphoprotein (VASP)-deficient mice.* Blood, 2004. **103**(1): p. 136-42.

84. Geiselhoringer, A., et al., *IRAG is essential for relaxation of receptor-triggered smooth muscle contraction by cGMP kinase.* EMBO J, 2004. **23**(21): p. 4222-31.

85. Schlossmann, J., et al., *Regulation of intracellular calcium by a signalling complex of IRAG, IP3 receptor and cGMP kinase Ibeta.* Nature, 2000. **404**(6774): p. 197-201.

86. Halbrugge, M., et al., *Stoichiometric and reversible phosphorylation of a 46-kDa protein in human platelets in response to cGMP- and cAMP-elevating vasodilators.* J Biol Chem, 1990. **265**(6): p. 3088-93.

87. Benz, P.M., et al., *Cytoskeleton assembly at endothelial cell-cell contacts is regulated by alphaII-spectrin-VASP complexes.* J Cell Biol, 2008. **180**(1): p. 205-19.

88. Horstrup, K., et al., *Phosphorylation of focal adhesion vasodilator-stimulated phosphoprotein at Ser157 in intact human platelets correlates with fibrinogen receptor inhibition.* Eur J Biochem, 1994. **225**(1): p. 21-7.

89. Aszodi, A., et al., *The vasodilator-stimulated phosphoprotein (VASP) is involved in cGMP- and cAMP-mediated inhibition of agonist-induced platelet aggregation, but is dispensable for smooth muscle function.* EMBO J, 1999. **18**(1): p. 37-48.

90. Reinhard, M., T. Jarchau, and U. Walter, *Actin-based motility: stop and go with Ena/VASP proteins.* Trends Biochem Sci, 2001. **26**(4): p. 243-9.

91. Danielewski, O., J. Schultess, and A. Smolenski, *The NO/cGMP pathway inhibits Rap 1 activation in human platelets via cGMP-dependent protein kinase I.* Thromb Haemost, 2005. **93**(2): p. 319-25.

92. Hoffmeister, M., et al., *Cyclic nucleotide-dependent protein kinases inhibit binding of 14-3-3 to the GTPase-activating protein Rap1GAP2 in platelets.* J Biol Chem, 2008. **283**(4): p. 2297-306.

93. Chrzanowska-Wodnicka, M., et al., *Rap1b is required for normal platelet function and hemostasis in mice.* J Clin Invest, 2005. **115**(3): p. 680-7.

94. Gegenbauer, K., et al., *Regulator of G-protein signaling 18 integrates activating and inhibitory signaling in platelets.* Blood, 2012. **119**(16): p. 3799-807.

95. Nagy, Z., et al., *Cyclic nucleotide-dependent protein kinases target ARHGAP17 and ARHGEF6 complexes in platelets.* J Biol Chem, 2015. **290**(50): p. 29974-83.

96. Aslan, J.E. and O.J. McCarty, *Rho GTPases in platelet function.* J Thromb Haemost, 2013. **11**(1): p. 35-46.

97. Sauzeau, V., et al., *Cyclic GMP-dependent protein kinase signaling pathway inhibits RhoA-induced Ca2+ sensitization of contraction in vascular smooth muscle.* J Biol Chem, 2000. **275**(28): p. 21722-9.

98. Sawada, N., et al., *cGMP-dependent protein kinase phosphorylates and inactivates RhoA.* Biochem Biophys Res Commun, 2001. **280**(3): p. 798-805.

99. Aburima, A., et al., *cGMP signaling inhibits platelet shape change through regulation of the RhoA-Rho Kinase-MLC phosphatase signaling pathway.* J Thromb Haemost, 2017. **15**(8): p. 1668-1678.

100. Nishikawa, M., et al., *Phosphorylation of mammalian myosin light chain kinases by the catalytic subunit of cyclic AMP-dependent protein kinase and by cyclic GMP-dependent protein kinase.* J Biol Chem, 1984. **259**(13): p. 8429-36.

101. Chirkov, Y.Y., et al., *Antiplatelet effects of nitroglycerin in healthy subjects and in patients with stable angina pectoris.* J Cardiovasc Pharmacol, 1993. **21**(3): p. 384-9.

102. Stamler, J.S. and J. Loscalzo, *The antithrombotic effects of organic nitrates.* Trends Cardiovasc Med, 1991. **1**(8): p. 346-53.

103. Torfgard, K.E. and J. Ahlner, *Mechanisms of action of nitrates.* Cardiovasc Drugs Ther, 1994. **8**(5): p. 701-17.

104. Watanabe, H., et al., *Platelet cyclic GMP. A potentially useful indicator to evaluate the effects of nitroglycerin and nitrate tolerance.* Circulation, 1993. **88**(1): p. 29-36.

105. Li, Z., et al., *A stimulatory role for cGMP-dependent protein kinase in platelet activation.* Cell, 2003. **112**(1): p. 77-86.

106. Zhang, G., et al., *Biphasic roles for soluble guanylyl cyclase (sGC) in platelet activation.* Blood, 2011. **118**(13): p. 3670-9.

107. Gambaryan, S., A. Friebe, and U. Walter, *Does the NO/sGC/cGMP/PKG pathway play a stimulatory role in platelets?* Blood, 2012. **119**(22): p. 5335-6; author reply 5336-7.

108. Li, Z. and X. Du, *Response: yes, cGMP plays a stimulatory role in platelet activation.* Blood, 2012. **119**(22): p. 5336-5337.

109. Derbyshire, E.R. and M.A. Marletta, *Structure and regulation of soluble guanylate cyclase.* Annu Rev Biochem, 2012. **81**: p. 533-59.

110. Kamisaki, Y., et al., *Soluble guanylate cyclase from rat lung exists as a heterodimer.* J Biol Chem, 1986. **261**(16): p. 7236-41.

111. Mergia, E., et al., *Major occurrence of the new alpha2beta1 isoform of NO-sensitive guanylyl cyclase in brain.* Cell Signal, 2003. **15**(2): p. 189-95.

112. Harteneck, C., et al., *Molecular cloning and expression of a new alpha-subunit of soluble guanylyl cyclase. Interchangeability of the alpha-subunits of the enzyme.* FEBS Lett, 1991. **292**(1-2): p. 217-22.

113. Russwurm, M., et al., *Functional properties of a naturally occurring isoform of soluble guanylyl cyclase.* Biochem J, 1998. **335 (Pt 1)**: p. 125-30.

114. Budworth, J., et al., *Tissue distribution of the human soluble guanylate cyclases.* Biochem Biophys Res Commun, 1999. **263**(3): p. 696-701.

115. Friebe, A. and D. Koesling, *The function of NO-sensitive guanylyl cyclase: what we can learn from genetic mouse models.* Nitric Oxide, 2009. **21**(3-4): p. 149-56.

116. Yuen, P.S., L.R. Potter, and D.L. Garbers, *A new form of guanylyl cyclase is preferentially expressed in rat kidney.* Biochemistry, 1990. **29**(49): p. 10872-8.

117. Humbert, P., et al., *Purification of soluble guanylyl cyclase from bovine lung by a new immunoaffinity chromatographic method.* Eur J Biochem, 1990. **190**(2): p. 273-8.

118. Zhao, Y., et al., *Inhibition of soluble guanylate cyclase by ODQ.* Biochemistry, 2000. **39**(35): p. 10848-54.

119. Schrammel, A., et al., *Characterization of 1H-[1,2,4]oxadiazolo[4,3-a]quinoxalin-1-one as a heme-site inhibitor of nitric oxide-sensitive guanylyl cyclase.* Mol Pharmacol, 1996. **50**(1): p. 1-5.

120. Mergia, E., et al., *Spare guanylyl cyclase NO receptors ensure high NO sensitivity in the vascular system.* J Clin Invest, 2006. **116**(6): p. 1731-7.

121. Dangel, O., et al., *Nitric oxide-sensitive guanylyl cyclase is the only nitric oxide receptor mediating platelet inhibition.* J Thromb Haemost, 2010. **8**(6): p. 1343-52.

122. Thoonen, R., et al., *Cardiovascular and pharmacological implications of haem-deficient NO-unresponsive soluble guanylate cyclase knock-in mice.* Nat Commun, 2015. **6**: p. 8482.

123. Hanafy, K.A., J.S. Krumenacker, and F. Murad, *NO, nitrotyrosine, and cyclic GMP in signal transduction.* Med Sci Monit, 2001. **7**(4): p. 801-19.

124. Feil, R., et al., *Cyclic GMP-dependent protein kinases and the cardiovascular system: insights from genetically modified mice.* Circ Res, 2003. **93**(10): p. 907-16.

125. Pfeifer, A., et al., *Defective smooth muscle regulation in cGMP kinase I-deficient mice.* EMBO J, 1998. **17**(11): p. 3045-51.

126. Sausbier, M., et al., *Mechanisms of NO/cGMP-dependent vasorelaxation.* Circ Res, 2000. **87**(9): p. 825-30.

127. Massberg, S., et al., *Increased adhesion and aggregation of platelets lacking cyclic guanosine 3',5'-monophosphate kinase I.* J Exp Med, 1999. **189**(8): p. 1255-64.

128. Aicher, A., et al., *cGMP-dependent protein kinase I is crucial for angiogenesis and postnatal vasculogenesis.* PLoS One, 2009. **4**(3): p. e4879.

129. Wegener, J.W., et al., *cGMP-dependent protein kinase I mediates the negative inotropic effect of cGMP in the murine myocardium.* Circ Res, 2002. **90**(1): p. 18-20.

130. Kleppisch, T., et al., *Hippocampal cGMP-dependent protein kinase I supports an age- and protein synthesis-dependent component of long-term potentiation but is not essential for spatial reference and contextual memory.* J Neurosci, 2003. **23**(14): p. 6005-12.

131. Hofmann, F., et al., *cGMP regulated protein kinases (cGK).* Handb Exp Pharmacol, 2009(191): p. 137-62.

132. Hofmann, F., A. Ammendola, and J. Schlossmann, *Rising behind NO: cGMP-dependent protein kinases.* J Cell Sci, 2000. **113 (Pt 10)**: p. 1671-6.

133. Orstavik, S., et al., *Characterization of the human gene encoding the type I alpha and type I beta cGMP-dependent protein kinase (PRKG1).* Genomics, 1997. **42**(2): p. 311-8.

134. Wilson, L.S., et al., *Compartmentation and compartment-specific regulation of PDE5 by protein kinase G allows selective cGMP-mediated regulation of platelet functions.* Proc Natl Acad Sci U S A, 2008. **105**(36): p. 13650-5.

135. Greenwald, E.C., S. Mehta, and J. Zhang, *Genetically Encoded Fluorescent Biosensors Illuminate the Spatiotemporal Regulation of Signaling Networks.* Chem Rev, 2018. **118**(24): p. 11707-11794.

136. Russwurm, M., et al., *Design of fluorescence resonance energy transfer (FRET)-based cGMP indicators: a systematic approach.* Biochem J, 2007. **407**(1): p. 69-77.

137. Thunemann, M., et al., *Transgenic mice for cGMP imaging.* Circ Res, 2013. **113**(4): p. 365-71.

138. Förster, T., *Zwischenmolekulare Energiewanderung und Fluoreszenz.* Annalen der Physik, 1948. **437**(1-2): p. 55-75.

139. Wen, L., et al., *A shear-dependent NO-cGMP-cGKI cascade in platelets acts as an auto-regulatory brake of thrombosis.* Nat Commun, 2018. **9**(1): p. 4301.

140. Thunemann, M., et al., *Correlative intravital imaging of cGMP signals and vasodilation in mice.* Front Physiol, 2014. **5**: p. 394.

141. Feil, R., et al., *Regulation of Cre recombinase activity by mutated estrogen receptor ligand-binding domains.* Biochem Biophys Res Commun, 1997. **237**(3): p. 752-7.

142. Feil, R., et al., *Ligand-activated site-specific recombination in mice.* Proc Natl Acad Sci U S A, 1996. **93**(20): p. 10887-90.

143. Feil, S., N. Valtcheva, and R. Feil, *Inducible Cre mice.* Methods Mol Biol, 2009. **530**: p. 343-63.

144. Muzumdar, M.D., et al., *A global double-fluorescent Cre reporter mouse.* Genesis, 2007. **45**(9): p. 593-605.

145. Vogel, S., et al., *Platelet-derived HMGB1 is a critical mediator of thrombosis.* J Clin Invest, 2015. **125**(12): p. 4638-54.

146. Du, X., J.A. Marjanovic, and Z. Li, *On the roles of cGMP and glycoprotein Ib in platelet activation.* Blood, 2004. **103**(11): p. 4371-2; author reply 4372-3.

147. Nesbitt, W.S., et al., *A shear gradient-dependent platelet aggregation mechanism drives thrombus formation.* Nat Med, 2009. **15**(6): p. 665-73.

148. Westein, E., et al., *Atherosclerotic geometries exacerbate pathological thrombus formation poststenosis in a von Willebrand factor-dependent manner.* Proc Natl Acad Sci U S A, 2013. **110**(4): p. 1357-62.

149. Goto, S., et al., *Distinct mechanisms of platelet aggregation as a consequence of different shearing flow conditions.* J Clin Invest, 1998. **101**(2): p. 479-86.

150. Zabel, U., et al., *Calcium-dependent membrane association sensitizes soluble guanylyl cyclase to nitric oxide.* Nat Cell Biol, 2002. **4**(4): p. 307-11.

151. Valtcheva, N., et al., *The commonly used cGMP-dependent protein kinase type I (cGKI) inhibitor Rp-8-Br-PET-cGMPS can activate cGKI in vitro and in intact cells.* J Biol Chem, 2009. **284**(1): p. 556-62.

152. Sakariassen, K.S., L. Orning, and V.T. Turitto, *The impact of blood shear rate on arterial thrombus formation.* Future Sci OA, 2015. **1**(4): p. FSO30.

153. Schindelin, J., et al., *Fiji: an open-source platform for biological-image analysis.* Nat Methods, 2012. **9**(7): p. 676-82.

154. Burkhart, J.M., et al., *Systematic and quantitative comparison of digest efficiency and specificity reveals the impact of trypsin quality on MS-based proteomics.* J Proteomics, 2012. **75**(4): p. 1454-62.

155. Olsen, J.V., et al., *Parts per million mass accuracy on an Orbitrap mass spectrometer via lock mass injection into a C-trap.* Mol Cell Proteomics, 2005. **4**(12): p. 2010-21.

156. Kall, L., et al., *Semi-supervised learning for peptide identification from shotgun proteomics datasets.* Nat Methods, 2007. **4**(11): p. 923-5.

157. Falati, S., et al., *Real-time in vivo imaging of platelets, tissue factor and fibrin during arterial thrombus formation in the mouse.* Nat Med, 2002. **8**(10): p. 1175-81.

158. Dubois, C., et al., *Real-time in vivo imaging of platelets during thrombus formation.* Platelets, 2nd Edition, 2007: p. 611-626.

159. Wykes, V. and J. Garthwaite, *Membrane-association and the sensitivity of guanylyl cyclase-coupled receptors to nitric oxide.* Br J Pharmacol, 2004. **141**(7): p. 1087-90.

160. Lewandrowski, U., et al., *Platelet membrane proteomics: a novel repository for functional research.* Blood, 2009. **114**(1): p. e10-9.

161. Bagi, Z., et al., *PECAM-1 mediates NO-dependent dilation of arterioles to high temporal gradients of shear stress.* Arterioscler Thromb Vasc Biol, 2005. **25**(8): p. 1590-5.

162. Armstrong, P.C., et al., *Combination of cyclic nucleotide modulators with P2Y12 receptor antagonists as anti-platelet therapy.* J Thromb Haemost, 2020. **18**(7): p. 1705-1713.

163. Reiss, C., et al., *The sGC stimulator riociguat inhibits platelet function in washed platelets but not in whole blood.* Br J Pharmacol, 2015. **172**(21): p. 5199-210.

164. Mellacheruvu, D., et al., *The CRAPome: a contaminant repository for affinity purification-mass spectrometry data.* Nat Methods, 2013. **10**(8): p. 730-6.

165. Collado-Alsina, A., et al., *The regulation of synaptic vesicle recycling by cGMP-dependent protein kinase type II in cerebellar granule cells under strong and sustained stimulation.* J Neurosci, 2014. **34**(26): p. 8788-99.

166. Masterson, L.R., et al., *cAMP-dependent protein kinase A selects the excited state of the membrane substrate phospholamban.* J Mol Biol, 2011. **412**(2): p. 155-64.

167. Zhang, Q., et al., *Cyclic GMP signaling and regulation of SERCA activity during cardiac myocyte contraction.* Cell Calcium, 2005. **37**(3): p. 259-66.

168. Weinmeister, P., et al., *Cyclic guanosine monophosphate-dependent protein kinase I promotes adhesion of primary vascular smooth muscle cells.* Mol Biol Cell, 2008. **19**(10): p. 4434-41.

169. Armstrong, P.C. and K. Peter, *GPIIb/IIIa inhibitors: from bench to bedside and back to bench again.* Thromb Haemost, 2012. **107**(5): p. 808-14.

170. Bergmeier, W., et al., *Flow cytometric detection of activated mouse integrin alphaIIbbeta3 with a novel monoclonal antibody.* Cytometry, 2002. **48**(2): p. 80-6.

171. Calvete, J.J., *Clues for understanding the structure and function of a prototypic human integrin: the platelet glycoprotein IIb/IIIa complex.* Thromb Haemost, 1994. **72**(1): p. 1-15.

172. Topol, E.J., T.V. Byzova, and E.F. Plow, *Platelet GPIIb-IIIa blockers.* Lancet, 1999. **353**(9148): p. 227-31.

173. Zhu, J., et al., *Closed headpiece of integrin alphaIIbbeta3 and its complex with an alphaIIbbeta3-specific antagonist that does not induce opening.* Blood, 2010. **116**(23): p. 5050-9.

174. Sastry, S.K. and A.F. Horwitz, *Integrin cytoplasmic domains: mediators of cytoskeletal linkages and extra- and intracellular initiated transmembrane signaling.* Curr Opin Cell Biol, 1993. **5**(5): p. 819-31.

175. Liu, S., D.A. Calderwood, and M.H. Ginsberg, *Integrin cytoplasmic domain-binding proteins.* J Cell Sci, 2000. **113 (Pt 20)**: p. 3563-71.

176. Huang, J., et al., *Platelet integrin alphaIIbbeta3: signal transduction, regulation, and its therapeutic targeting.* J Hematol Oncol, 2019. **12**(1): p. 26.

177. Petrich, B.G., et al., *The antithrombotic potential of selective blockade of talin-dependent integrin alpha IIb beta 3 (platelet GPIIb-IIIa) activation.* J Clin Invest, 2007. **117**(8): p. 2250-9.

178. Salles, C., II, et al., *Vessel wall BAMBI contributes to hemostasis and thrombus stability.* Blood, 2014. **123**(18): p. 2873-81.